LABORATORY AND FIELD INVESTIGATIONS OF A VARIANT OF THE TWO-ELECTRODE D.C. RESISTIVITY ARRAY

BY

VICTOR MAKINDE
B.Sc, M.Sc (PHYSICS)

A THESIS SUBMITTED TO THE DEPARTMENT OF PHYSICS, AHMADU BELLO UNIVERSITY, ZARIA IN PARTIAL FULFILMENT OF THE REQUIREMENT FOR THE AWARD OF THE DEGREE OF DOCTOR OF PHILOSOPHY IN GEOPHYSICS

JANUARY, 1996

DECLARATION

The report presented in this thesis is the result of the original research work carried out by the author. The report has not been presented in whatever form to any other body, organization or institution other than Ahmadu Bello University, Zaria Nigeria for the purpose of the award of any degree. The work of others cited are duly acknowledged and referenced.

22/10/96

VICTOR MAKINDE

CERTIFICATION

This thesis entitled Laboratory and Field Investigations of a Variant of the Two-Electrode D.C. Resistivity Array by Victor Makinde meets the regulations governing the award of the degree of Doctor of Philosophy of Ahmadu Bello University, and is approved for its contributions to knowledge and literary presentation.

Prof. C.O. Ajayi
Chairman, Supervisory Committee

Date: 5/9/96

Dr. P. Sule
Member, Supervisory Committee

Date: 5/9/96

Prof. S.B. Ojo
Head of Department

Date: 22/10/96

Prof. J.Y. Olayemi
Dean, Postgraduate School

Date: 21/11/96

ACKNOWLEDGEMENT

I specially thank my major supervisor, Prof. C.O. Ajayi for suggesting this topic, providing the fundamental details and for handling the supervision of the work. I also thank Dr. P. Sule for carefully reading through this work.

My gratitude goes to the Head, Department of Physics, Prof. S.B. Ojo; the PG coordinator, Department of Physics, Dr. I.B. Osazuwa; and Dr. M.N. Umego for their roles and contributions to the completion of this work. Gratitude also goes to coursemates, and others in the department who were with us when gravitation felt different. I thank you all.

I thank all those who thoughtfully came to my aid during the course of this work. I thank Drs. B.W. Jimba, T.C. Akpa, A.O. Oyewale, Messrs. S.A. Alagbe, D.O. Akanni, G.A. Adewole, P.L. Adejumo, S. Osasona, L. Sule, B. Nwosu, O. Fagbemi, J. Adigun, S. Olatunji, and Super B; Madam 'Dupe, 'Foluke and SisterPio for their support in times of need. I thank Messrs B. Ojewole, D. Obafemi, S. Jayeoba, A. Onifade, B. Afolabi, K. Ibikunle, A. Obiniyi and all other friends including Capt. Funso Ampitan and family for their solid support. I thank `Freeman', Nuru, Taju, Bisir, Jibs, Tumbi and others not easily remembered.

The support and encouragement by my colleagues at work cannot be overlooked. I am most grateful.

I specially thank Prof. A.O. Ogungbile and the entire family for the parental support given me; so also do I thank Prof. V.B. Ogunlela and Dr. M.A.G. Akale for their support.

Finally, I thank God for His will for my life.

ABSTRACT

The present work has considered the application of a variant of the two-electrode array to the detection of, and prospecting for horizontal layerings within the earth. The mode of this two-electrode array makes use of only the two current electrodes without the potential electrodes. In its use, the electrode separation is varied by moving the two current electrodes equidistantly away from the sounding point. The result of this is that the current I, delivered by the power source through the earth also changes. The driving potential as indicated by the source voltage indicator was taken as the voltage developed across the section of the earth between the two current electrodes. In investigating the capability of this technique, called the C-C mode, in delineating horizontally-layered media, a laboratory experiment was set up. Different materials such as water - an electrolyte, lateritic clay, river sand and mixed-soil (a mixture of lateritic clay and river sand) were experimented for the one-layer (overburden) case. The experiment was conducted at various frequencies within the operating frequency range of the tank. All the frequencies used, including 0 Hz and 50 Hz, gave good alignment of the resisitivity point for all the materials and combinations used. The lateritic clay, river sand and mixed-soil were again variously combined to form two-layer and three-layer cases, all underlain by the non-conductive perspex as "basement". Graphs were plotted to show the variation of the "bulk resistivity" with the electrode separation (or its reciprocal). The most direct and easily interpretable results was given by the graph in which the "bulk resistivity" (b was plotted against the electrode separation

AB/2 on a log-linear scale. The accurate delineation of the layers in the laboratory investigation encouraged the initiation of the field study. The Kubanni River Basin was chosen as the field study area. The basin occupies the centre of the South-Eastern sector of the Zaria sheet (No. 102 S.W.) of the 1:50,000 sheet ordinances series of the Nigeria ordinances survey map, with an average area of about 150 km^2. It is underlain by Precambrian rocks of the Nigerian Basement Complex comprising mostly of older granites and biotite granite-gneiss overlain mostly by superficial deposits recognised by their brown cellular aspects. In carrying out the field investigations, thirty-one soundings were made in twenty-three stations using conventional Schlumberger VES method and the expanding C-C technique. Depth horizontal profilings were also carried out in one of the twenty-three stations and one other independent station using the Wenner array and the constant spacing C-C mode of the two-electrode array. Typical graphs as done for the laboratory model studies were plotted and deductions made. Results from the interpretation of the collected data using the C-C mode show that the depth to basement within the basin varied from about 7.9 m to about 36 m on the average. The result at each sounding location was compared with the interpreted result of the collected data using either the Schlumberger array or the Wenner array as the case may be. The layer delineation by the C-C mode agreed well with that delineated by the Schlumberger array. The C-C technique has delineated layers and has also given a good estimation of the layer thickness and an uncomplicated way of determining the surface layer resistivity.

TABLE OF CONTENTS

TITLE PAGE		i
DECLARATION		ii
CERTIFICATION		iii
ACKNOWLEDGEMENTS		iv
ABSTRACT		v
TABLE OF CONTENTS		vii
LIST OF TABLES		x
LIST OF FIGURES		xii
LIST OF APPENDICES		xvi
GLOSSARY OF TERMS		xvii
CHAPTER 1	INTRODUCTION	
1.1	Historical Background Of Electrical Prospecting	1
1.2	Fundamentals Of Prospecting With Direct Current	5
1.2.1	Electrical Conduction By Earth Materials	5
1.2.2	Factors Affecting the Resistivity of an Earth Material	9
1.2.3	Factors Affecting the Measurement of Earth Resistivity	15
1.3	D.C. Resisitivity Prospecting	17
1.4	The Existing Electrode Configurations And Their Principles	23
1.4.1	The Four-Electrode Configuration	23
1.4.2	The Three-Electrode Configuration	26
1.4.3	The Two-Electrode Configuration	27
1.4.4	Other Electrode Configurations	36
1.5	Aims Of The Present Work	36
1.6	Advantages Of The Proposed Two-electrode Method	38
CHAPTER 2	PRINCIPLE AND THEORY OF THE PROPOSED VARIANT OF THE TWO-ELECTRODE D.C. RESISTIVITY METHOD	
2.1	Principle of the Proposed Two-electrode Configuration (Method)	40

2.2 Assumptions Made In The Proposed Two-electrode Configuration 43

2.3 Theory Of The Proposed Two-electrode Method 45

2.3.1 The "Equivalent Cylinder" Approach 52

2.3.2 The "Specific Resistance" Approach 55

2.4 General Equations for Different Number Of Layers Using The Specific Resistance Approach 56

2.4.1 The n-layer Overburden Case 56

2.4.2 Typical Equations for Different Number Of Layers 59

CHAPTER 3 LABORATORY SCALE MODEL STUDIES

3.1 Introduction 62

3.2 Scaling Factor of the Model System 63

3.3 The Experimental Set-up 66

3.3.1 The Apparatus 66

3.3.2 Determination of the Tank Characteristics 70

3.3.3 Experimental Procedure 72

3.3.4 Sources of Error 79

3.3.5 Precautions Taken 81

3.4 Data Processing 89

3.5 Typical Model Data and Results 99

3.5.1 Two-layer Cases (Single Overburden) 100

3.5.2 Three-layer Cases 106

3.5.3 Four-layer Cases 112

3.5.4 Model Horizontal Profiling With The Two-Electrode Array 123

3.6 Deductions 128

CHAPTER 4 THE FIELD SURVEY

4.1 Instrumentation 131

4.1.1 Designing a Suitable Instrument 131

4.1.2 Instrument Used for the Field Work 136

4.2 The Field Work 137

4.2.1	The Choice of the Project (Field Test) Area	137
4.2.2	Geology of the Project Area	141
4.2.3	The Data Collection	144
4.3	Data Analysis and Interpretation	148
4.3.1	Treatment of Field Data obtained using the Proposed Method	148
4.3.2	Treatment of Field Data Obtained using the Schlumberger Array	150
4.4	Horizontal Profiling Results	154
4.4.1	Field Data obtained using the Proposed Method	154
4.4.2	Field Data obtained using the Wenner Array	159
4.5	Depth Sounding Results	160
4.5.1	Field Data obtained using the Proposed Method	160
4.5.2	Field Data obtained using the Schlumberger Array	163
4.6	Comparison of Depth to Basement Values obtained in the Kubanni Basin from This and Previous Works	163

CHAPTER 5 DEDUCTIONS AND CONCLUSIONS

5.1	Goals and Achievements of the Present Work	170
5.2	Comparison of Model Results (Between the Two-Electrode Array and the Model Values)	171
5.3	Comparison of Field Results (Of the Two-Electrode Array, the Wenner Array and the Schlumberger Array).	172
5.3.1	Horizontal Profiling	172
5.3.2	Vertical Profiling	174
5.4	Recommendations for Future Work	177
5.5	Conclusions	179
REFERENCES		187
APPENDICES		191

LIST OF TABLES

TABLE		
1.1(a)	Resistivities of rocks and ores	10
1.1(b)	Generalized resistivity ranges for rocks of different lithology and age.	16
3.1	Dimensions of scaling variables	65
3.2	Computed Resistivity Values using Wenner, Two-Electrode, Tube and Metre Bridge Methods.	89
3.3	Typical Model Data for Water over Perspex	100
3.4	Model Data for Lateritic Clay over Perspex	102
3.5	Model Data for River Sand over Perspex	104
3.6	Model Data for Lateritic Clay on River Sand on Perspex	106
3.7	Model Data for River Sand on Lateritic Clay on Perspex	110
3.8	Model Data for Lateritic Clay on Mixed-soil on River Sand on Perspex	113
3.9	Model Data for Lateritic Clay on River Sand on Lateritic Clay on Perspex	116
3.10	Model Data for Mixed-soil on Lateritic Clay on River Sand on Perspex	118
3.11	Model Data for River Sand on Mixed-soil on Lateritic Clay on Perspex	121
3.12	Horizontal Profiling with Wenner (a = 2cm)	126
3.13	Horizontal Profiling with Wenner (a = 5cm)	126
3.14	Horizontal Profiling with Two-Electrode Method (L = 2cm).	127
3.15	Horizontal Profiling with Two-Electrode Method (L = 5cm).	127

4.1	Typical Resistivity Values of Earth Materials in Basement	145
4.2	Horizontal Profiling Field Data with Two-Electrode Method NAERLS Profile 1	155
4.3	Horizontal Profiling Field Data with Two-Electrode Method NAERLS Profile 2	155
4.4	Horizontal Profiling Field Data with Two-Electrode Method A.B.U. Dam Site	155
4.5	Horizontal Profiling Field Data with Wenner Array NAERLS Profile 1	160
4.6	Horizontal Profiling Field Data with Wenner Array NAERLS Profile 2	160
4.7	Horizontal Profiling Field Data with Wenner Array A.B.U. Dam Site	160
5.1	Comparison of Results Between the Two-Electrode Array and the Model Values	173
5.2	Table Showing Summary of Results Between the Two-electrode and the Four-electrode Methods	175
5.3	Comparison of Top Layer Resistivity and Thickness Values Using the Hemispherical and the Near-Spherical Models, with the Schlumberger Array Result for the Field Study.	186

LIST OF FIGURES

FIGURE		
1.1	Average resistivity for groups of sedimentary rocks with similar characteristics	16
1.2	Field arrangement set-up for d.c. resistivity measurements.	19
1.3	Geoelectric section for horizontal beds	22
1.4	Some four-electrode arrays	25
1.5	Some three-electrode arrays	28
1.6	Types of resistivity profiling	30
1.7	Most frequently used arrays.	32
1.8	Some Other Electrode Arrangements	37
2.1	Simple circuit to verify Ohm's Law	41
2.2	Equipotential Lines and Flow Lines	46
2.3	Geometry for determining volume of earth trapped within a layer using the hemispherical model	47
2.4	Geometry for determining spherical cap volume	47
2.5	Geometry for determining volume of earth trapped within a layer using the near-spherical model	47
2.6	Earth layering at electrode spacing L_n [n-layer case of earth layering] -(hemispherical model)	57
3.1	Scale model tank apparatus	67
3.2	Graph of current I against frequency f used in determining the operating frequency	71
3.3	Graph of apparent resistivity of tank Water against frequency for Wenner array using different electrode spacings.	71
3.4	Graph of apparent resistivity of Lateritic Clay against frequency for Wenner array using different electrode spacings.	73
3.5	Graph of apparent resistivity of Mixed-soil against frequency for Wenner array using different electrode spacings.	73

3.6	Graph of apparent resistivity of River Sand against frequency for Wenner array using different electrode spacings.	74
3.7	Variation of bulk resistivity with frequency for Water. (Two-electrode methoÇL	74
3.8	Variation of bulk resistivity with frequency for Lateritic Clay. (Two-electrode method)	75
3.9	Variation of bulk resistivity with frequency for Mixed-soil. (Two-electrode method)	75
3.10	Variation of bulk resistivity with frequency for River Sand. (Two-electrode method)	76
3.11	Graph of Apparent Resistivity against Frequency (using Wenner Array) to show capacitative coupling effect	76
3.12	Relative Positions of Electrodes with respect to the Tank Walls for Wenner Configuration	82
3.13	Graph of resistivity against frequency for investigating the side tank wall effect	82
3.14	Graph of resistivity against A/Z for investigating the effect of the bottom of the tank wall.	84
3.15	Graph of resistivity against electrode spacing showing the value of water resistivity (for Wenner and Two-electrode Arrays).	86
3.16	Experimental setup for determining the actual resistivity values of samples used	86
3.17	Graph of resistivity against electrode spacing on log-linear scale for a four-layered earth model	95
3.18	Water in model tank	100
3.19	Graph of bulk resistivity against electrode spacing for water on perspex	101
3.20	Lateritic Clay in model tank	102
3.21	Graph of bulk resistivity against electrode spacing for lateritic clay on perspex	103
3.22	River Sand in model tank	104
3.23	Graph of bulk resistivity against electrode spacing for river sand on perspex	105
3.24	Lateritic Clay on River Sand in model tank	106
3.25(a)	Graph of normalised bulk resistivity against 1/L for Clay on River Sand on Basement	108

3.25(b) Graph of bulk resistivity against electrode spacing for Clay on River Sand on Basement 108

3.26 River Sand on Clay in model tank 110

3.27(a) Graph of normalised bulk resistivity against 1/L for river sand on clay on basement 111

3.27(b) Graph of bulk resistivity against electrode spacing for river sand on clay on basement 111

3.28 Clay on Mixed-soil on River Sand in model tank 113

3.29(a) Graph of normalised bulk resistivity against 1/L for Clay on Mixed-soil on River Sand on Basement 114

3.29(b) Graph of bulk resistivity against electrode spacing for Clay on Mixed-soil on River Sand on Basement 114

3.30 Clay on River Sand on Clay in Model Tank 116

3.31(a) Graph of normalised bulk resistivity against 1/L for Clay on River Sand on Clay on Basement 117

3.31(b) Graph of bulk resistivity against electrode spacing for Clay on River Sand on Clay on Basement 117

3.32 Mixed-soil on Clay on River Sand in Model Tank 118

3.33(a) Graph of normalised bulk resistivity against 1/L for Mixed-soil on Clay on River Sand on Basement 119

3.33(b) Graph of bulk resistivity against electrode spacing for Mixed-soil on Clay on River Sand on Basement 119

3.34 River Sand on Mixed-soil on Clay in Model Tank 121

3.35(a) Graph of normalised bulk resistivity against 1/L for River Sand on Mixed-soil on Clay on Basement 122

3.35(b) Graph of bulk resistivity against electrode spacing for River Sand on Mixed-soil on Clay on Basement 122

3.36 Earth Material Composition/Arrangement for Horizontal Profiling 124

3.37 Horizontal profiling with Two-electrode (L = 2 cm) and Wenner (a = 2cm). 125

3.38 Horizontal profiling with Two-electrode (L = 5 cm) and Wenner (a = 5cm). 125

3.39 Graph of bulk resistivity against electrode spacing showing results at 0 Hz, 40 Hz, and 50 Hz for water using the two-electrode method 130

4.1 Arrangement of the Field Equipment used for the Field Survey 135

4.2 Location Map of the Area under Study 138

4.3(a) Basement Geology of Kubanni Basin 140

4.3(b) The Geology of Parts of the Quarter Degree Sheets 101 and 102 (After McCurry 1970). 140

4.4 Simplified Geological Map of Nigeria 142

4.5 Interpreted Schlumberger Values for FCE, Zaria 153

4.6 Horizontal Profiling. NAERLS Profile 1 156

4.7 Horizontal Profiling. NAERLS Profile 2 156

4.8 Horizontal Profiling for ABU Dam 157

4.9 Graph of Bulk Resistivity Against Electrode Spacing for FCE Zaria, Using the Two-Electrode Method. 162

4.10(a) Depth to Basement (Overburden Thickness) Map Deduced From Electrical Resistivity Method Using the Two Electrode Superimposed on the Outcrop map of the Kubanni Basin 165

4.10(b) Depth to Basement (Overburden Thickness) Map Derived from Schlumberger Sounding Data (used in this work) Superimposed on the Outcrop map of the Kubanni Basin 166

4.10(c) Depth to Basement (Overburden Thickness) Map Superimposed on the Outcrop Map of the Basin (As obtained by Shemang, 1990) 167

4.10(d) Depth to Basement (Overburden Thickness) Map Superimposed on the Outcrop Map of the Basin (As obtained by Bajeh, 1992) 168

LIST OF APPENDICES

APPENDIX A1: Computed Model Slope Values Using The Two-electrode Method 191

APPENDIX A2: Computed Field Slope Values Using The Two-electrode Method 192

APPENDIX A3: Computed Model Resistivity Values Using The Two-electrode Method 195

APPENDIX A4: Computed Field Resistivity Values Using The Two-electrode Method 197

APPENDIX B1: Field Data Collected Using The Two-electrode Method 203

APPENDIX B2: Field Data Collected Using The Schlumberger Array 210

APPENDIX C1: Interpreted Vertical Electrical Sounding Field Data Using Two-electrode Method: (Graph Of Bulk Resistivity Against Electrode Spacing) 215

APPENDIX C2: Interpreted Vertical Electrical Sounding Field Data Using The Schlumberger Array: (Graph Of Apparent Resistivity Against AB/2) 221

APPENDIX C3: Graph Of Specific Resistance Against Electrode Spacing For The Laboratory Models (Using The Two-Electrode Method) 225

APPENDIX C4: Graph Of Specific Resistance Against Electrode Spacing For The Field Stations (Using The Two-electrode Method) 227

GLOSSARY OF TERMS

`Dot' system of arranging electrodes

- a system whereby the sharp ends of the electrodes are driven into the ground; in which case the electrodes stand vertically upright rather than lying horizontally on the side.

`Line' system of arranging electrodes

- a system whereby the electrodes are made to lie on their sides when driven into the ground.

Unfocussed system

- a system in which one of the two current electrodes serves as the feeder electrode and the other serves as the return electrode.

Focussed system

- a system in which all of the current electrodes serves as feeder electrodes toward/over the target; the return electrode(s) may be located at a very distant point away for it to be considered as being at infinity.

C-C mode

- the current-current mode of the two-electrode array in which only the two current electrodes are involved in the measurement.

`Mixed-soil'

- a mixture of lateritic clay and river sand in the ratio of one to three.

CHAPTER 1

INTRODUCTION

1.1 Historical Background Of Electrical Prospecting

Electrical prospecting is, according to Van Nostrand and Cook (1966), the art of measuring the electrical properties of rocks in the study of the structure and composition of those layers of the earth which are sufficiently shallow to be exploited by man. It involves the detection of surface effects produced by electric current flow in the ground. Some of the available electrical methods such as the self-potential and electromagnetic methods such as the telluric, the magnetotelluric and the AFMAG among others use naturally existing fields within the earth. The most prominent electrical prospecting methods such as the galvanic resistivity methods, however, like the seismic prospecting method, have the means of excitation under the control of the operator and are therefore not concerned with natural phenomena of the earth as with both gravity and magnetic techniques (Smith, 1955).

The electrical prospecting technique has gone through various stages of development but its continued development has been rather too slow; much slower than the developments in the other major geophysical techniques such as seismic, gravity and magnetics. This situation can be attributed to the fact that due to its limited depth of penetration, modern developments of electrical prospecting methods have been mainly for use in comparatively shallow formations and hence, they have been of more interest to the mining companies than to the oil industry.

The earliest recorded work in electrical prospecting is credited to Gray and Wheeler who made electrical studies of rocks and listed their electric conductivities in 1920 (Van Nostrand and Cook, 1966). Watson, in 1746 discovered independently that the ground is an electrical conductor. He also found that an electric current passed through the ground between two electrodes placed two miles (3.2 kilometres) apart fluctuated in an erratic manner different from when wire was used instead of the earth to complete the circuit (Van Nostrand and Cook, 1966).

Another important work is credited to R. W. Fox who, in 1830 in the copper mines of Cornwall, made the momentous discovery that there were natural electric currents associated with sulphide ore deposits. This forms the basis of the self-potential method. Other successful earlier workers, according to Van Nostrand and Cook (1966), include Henwood, Reich, W. Skey and A.C. Becquerel. Prominent also is Mattheucci whose name stands out in the early descriptions of telluric currents, and Carl Barus whose attempt in 1882 at eliminating the troublesome electrode effects led him to the invention of an ingenious nonpolarizing electrode as we know it today. The non-polarising electrode consisted of an amalgamated metal strip immersed in zinc sulphate solution. Also notable are R.C. Wells, Conrad Schlumberger, Louis Cagniard, Fred Brown, Leo Daft and Alfred Williams who in 1902 first suggested the use of potential difference observations rather than equipotential-line method for resistivity work. Daft and William devised a method whereby a low-frequency alternating current was impressed into the ground by means of electrodes, and the resulting current distribution was studied by means of a sensitive telephone receiver

connected to two search electrodes placed on the ground - a method known as the Daft-Williams method. McCollum and Logan in 1913, were the first to determine the resistivity of soil samples by compressing the sample into the shape of a cylinder and then applying the voltmeter - ammeter measurements to the flow of current through the sample. Of note is that McCollum designed a device for measuring the soil resistivity and current density in the earth surrounding pipes or other objects of interest; his electrode arrangement being an inverted Wenner system. Contributions were also recorded of Wenner, Ahlborn, H.R. Conklin, Sundberg, S.F. Kelly, A.S. Eve, D.A. Keys, C.A. Heiland, F.W. Lee, Weaver, and, Sharon and Sandberg (Van Nostrand and Cook, 1966).

Gish and Rooney in 1923 made two major contributions to the development of electrical prospecting methods. The first involved instrumentation of what is known as the Gish-Rooney double commutator equipment while their second contribution involved the development of an empirical method of interpretation that gave rise to "depth of penetration equals the electrode separation" rule. Gish is credited with giving the general requirements for measuring telluric currents. Crosby and Leonardon in 1928 applied electrical methods successfully to map bedrock topography at a proposed dam site on the upper Connecticut River in what was apparently the first engineering application of these methods in the U.S.. Pullen in 1929 made laboratory resistivity measurements by both a.c. and d.c. techniques on many cores mostly of metamorphic rocks. He is credited with finding out that:

-- resistivity measurements varied with time because of electrical polarization;

-- the rate of polarization differs in various rocks;

-- resistivity varies as a function of applied voltage and frequency;

-- water content greatly alters the resistivity of materials, and

-- the resistivity of an ore containing conducting minerals may be high if the ore minerals are disseminated.

Also of note is the work of Joyce and Boyer, Tagg, and J.H. Swartz (Van Nostrand and Cook, 1966).

In addition to the investigation in France and North America are the significant contributions made by the Scandinavians. Notable among these are Petersson and Wallin in 1906, Trustedt in 1904, Tegengen and Bodman in 1912, Bergstrom in 1913, Lundberg and Nathorst in 1918, Lowy and Leimback in 1910, K. Schilowsky in 1913 and Muenster who in 1907 in Norway, made the first discovery of a previously unknown ore deposit of commercial value with electrical prospecting methods. Of much importance is the work of Ambronn whose greatest contribution in 1926 was his text on the elements of geophysics which contains a comprehensive bibliography of papers on electrical methods to the year 1926. Also notable are Mueller, Fritsch and Belluigi; Petrowsky who in 1924 is credited with using the `dot system' of arranging electrodes; Skaryatin and Kleiman among others innumerable to mention (Van Nostrand and Cook, 1966).

The principal initiators of modern-day quantitative resistivity methods are Wenner and Schlumberger. Wenner is much noted for his clear statement of the theorem of

reciprocity as applied to his four-electrode measurement and also for his invention in 1915 of what is today designated as the Wenner configuration of electrodes - a configuration that, before the two-electrode method, was the best for horizontal earth resistivity profiling. C. Schlumberger on the other hand is most noted for the electric logging as well as what is known today as the four-electrode Schlumberger configuration which is most suitable for shallow vertical earth resistivity profiling otherwise known as the Vertical Electric-Depth Sounding, VES. Worthy of mention is Lee for his Lee configuration and the Lee partition method of 1930.

The measurement of earth resistance using the two-electrode configuration was first attempted by Fred Brown in 1833 (Rust, 1938). The method adopted by Fred Brown in his measurement is not adequately described in literature; hence not much can be said about Fred Brown's two-electrode resistivity measurement technique. The measurement of earth resistivity using the two-electrode configuration has long been abandoned and is only being revived of recent through the work of Apparao and Roy (1973).

1.2 Fundamentals Of Prospecting With Direct Current (D.C.)

1.2.1 Electrical conduction by earth materials

Electrical conduction in minerals may take place by electronic or ionic processes (Keller and Frischknecht, 1966). Rocks are not formed of minerals alone and the electrical properties of a rock are not necessarily

determined by the properties of the mineral constituents alone. Hence electronic (ohmic), electrolytic (ionic) and dielectric mode of conduction are possible in earth materials.

Electronic conduction is important in materials containing free electrons as in metallic conductors such as gold and copper and in semiconductors such as sulphide ore minerals. It is believed that the atoms in a metal such as the native metals are perfectly ordered hence there should be almost no resistance to the motion of electrons through the metal when an electric field is applied. In practice, imperfections in the crystal structure are always present and such imperfections interfere with the free movement of the valence electrons. The greater the number of such imperfections, the higher will be the resistivity of the metal (Keller and Frischknecht, 1966). Semiconductors are non-metallic materials in which conduction is by electron motion, but in which the conductivity is lower than that in true metals. The lower conductivity is not as a result of lower mobility of the electrons, but rather due to a lesser number of conduction electrons. The energy level of the conduction electrons must therefore be raised to an appreciable amount before the electrons are free to wander through the crystal lattice, as in the case of a metal. This energy is most commonly provided in the form of heat, so that in semiconductors, the number of conduction electrons increases with temperature (Keller and Frischknecht, 1966).

For most rocks near the earth's surface, conduction will be electrolytic, the conducting medium being an aqueous solution of common salts, distributed in a complicated manner through the pore structure of a rock. The resistivity of a water-bearing rock will depend on the

amount of water present, the salinity of this water and the way in which the water is distributed in the rock. When a salt goes into solution in water, the constituent ions in the solid salt separate and these ions are free to move around independently in the solution. When an electric field is applied across an electrolytic solution, cations will be accelerated towards the negative pole and anions to the positive pole. Once the ions have been accelerated by the electric field, a viscous drag force limits the velocity which is attained. This terminal velocity is defined as the mobility of an ion. Most rock-forming minerals can be considered as solid electrolytes, so far as conduction of current is concerned. Electrolytic conduction can take place in ionic bonded crystals. When an electric field is applied to an ionic bonded crystal structure, the force exerted on each ion by the field is small compared to the strength of the binding forces, so that in an ideal crystal, one would not expect any electrolysis, or conduction by ion movement to take place. However, crystals are not perfect and electrolysis does take place when an electric field is applied. The current flow is comparatively due to the electronic conduction and there is actual transport of materials usually resulting in chemical transformation. There are two important types of imperfection in crystals which aid in current conduction; inherent imperfections in crystal lattice (Schottky defects), and thermally induced imperfections (Frenkel's defects).

Electronic conduction mechanism is more important than electrolytic conduction through pore water in the following three cases:

-- where rock contains a high percentage of conducting minerals;

-- in completely frozen rocks or region; and

-- in rocks which lie sufficiently deep in the earth so that all the pore spaces are closed by overburden pressure.

Dielectric conduction occurs in poor conductors or insulators having very few free carriers or even none. In the presence of an external alternating electric field, there is a slight displacement between the atomic electrons and their nucleons. The slight separation of charges is called the Dielectric Polarization, P (electric dipole moment per unit volume). There are four mechanisms by which polarisation occurs, these are:

-- by displacement of electron orbit - (electric polarization);

-- by displacement of ions - (ionic polarization);

-- by reorientation of polar molecules - (molecular polarization); and

-- in conductors, when the charges are collected at the boundaries - (interfacial polarization).

Polarization is therefore as a result of changing electronic, ionic, molecular or interfacial polarization caused by the varying electric field. The changing polarization gives rise to the changing current, that is, the displacement current which is the mechanism for dielectric conduction. The important parameter in the dielectric conduction is the dielectric constant k (the specific inductive capacity of the medium). The dielectric

constant vary with water content. Displacement current are generally negligible in earth materials, since electrical methods generally use direct current or alternating current of low frequencies less than 3kHz.

1.2.2 Factors affecting the resistivity of an earth material

The electrical properties of a rock are not necessarily determined by the properties of the mineral constituents alone. Most rocks at the earth's surface are porous to a certain extent (Dobrin, 1976). The amount of current flow and hence the resistivity of a rock is therefore affected by a number of natural, geological and hydrogeological factors namely: the mineralogical composition, porosity and degree of water saturation of the rocks, mineralization of the water filling the pores, the structure and texture of the rocks, age of deposition and, temperature and pressure (Mares 1984). These factors directly affect the amount of current flow through the earth and consequently the earth resistivity.

Mineralogical Composition: As shown in table 1.1(a), the range of resistivities among rocks and rock materials is enormous. According to Dobrin (1976), in most rock materials, the porosity and the chemical content of the water filling the pore spaces are more important in controlling the rock resistivity than the conductivity of the mineral grains contained in the rock. The salinity of the water in the pores is probably the most critical factor determining the resistivity. When porous rocks, particularly those with large concentrations of magnetite

Table 1.1(a) Resistivities of rocks and ores *(After Mares, 1984)*

Rock, ore	Resistivity ϱ (Ωm)
Sedimentary rocks	
loams	10^{-1} to 10^{2}
clays	10 to 10^{2}
sands	10^{2} to 10^{4}
sands saturated with mineral water	10^{-1} to 10
sandstones	10^{2} to 10^{4}
limestones	10^{2} to 10^{4}
arenaceous marls	10 to 10^{2}
conglomerates	10 to 10^{4}
gypsum	10 to 10^{6}
Magmatic and metamorphosed rocks	
granite, syenite	10^{2} to 10^{5}
diabase, basalt, gabbro	10^{2} to 10^{3}
schists	10^{2} to 10^{4}
shales	10 to 10^{3}
quartzites	10^{3} to 10^{8}
marbles	10^{2} to 10^{9}
gneisses	10^{2} to 10^{4}
Ores	
chalcopyrite ore mineralization	10^{-4} to 10^{-1}
galena ore mineralization	10^{-2}
arsenopyrite ore mineralization	10^{-1}
haematite ore mineralization	10^{-1} to 10^{2}
chromite ore mineralization	10^{3}
wolframite ore mineralization	10^{3} to 10^{4}
antimonite ore mineralization	10^{3} to 10^{7}

or graphite, lie above the water table at shallow depths, or when they occur at such great depths that all pore spaces are closed by ambient pressure, the conduction through them takes place within the mineral grains themselves. Under these conditions, the resistivity of the rock will depend on the resistivity of the grains. When the pores are saturated with fluids, it will be controlled by the fluid resistivity as well (Collett and Katsube, 1973).

The most frequently occuring rock-forming minerals such as quartz, mica and feldspar, have high resistivity values ranging from 10^{12} to 10^{14} ohm-metre (Mares, 1984). This indicates that the principal rock-forming minerals are insulators and do not conduct electric current. The resistivity of most igneous, metamorphic and sedimentary rocks does not depend on the mineralogical composition but on porosity, the degree of water saturation and on the mineralization of the water filling the pores (Mares, 1984).

Porosity and, Degree of Water Saturation and Salinity:
The porosity of rocks varies from very small percentages in tectonically undisrupted crystalline rocks to tens of per cent in unconsolidated sediments. The water filling the pores is always mineralized and changes of mineralization affect the resistivity of rocks. The greater the salinity of the water, the smaller the resistivity of the rock. The resistivity of a water-bearing rock decreases with increasing water content. For a rock to conduct electricity, its pore spaces must be interconnected and filled with water. Since most of the resistance to current

flow is met in the connecting pores, a rock with a high ratio of storage pores to connecting pores will have a higher resistivity for the same porosity than a rock having a low ratio of storage pores to connecting pores (Mares, 1984).

According to Keller and Frischknecht (1966), a great deal of work has been done in correlating resistivity with water content for petroleum-bearing rocks. For these rocks, which are primarily porous sandstones and limestones, it has been observed that resistivity varies approximately as the inverse-square of the porosity when the rock is fully saturated with water. This observation has led to the widespread use of an empirical function which is known as Archie's law relating resistivity and porosity; it is written as

$$\rho = a\rho_w \, \phi^{-m} \, S^{-n} \qquad \ldots\ldots 1.1$$

where ρ - the bulk resistivity of the rock;

ρ_w - the resistivity of the water contained in the pore structure;

ϕ - the porosity expressed as a fraction per unit volume of rock;

S - the fraction of the pores containing water.

and a, m, and n are constants whose values are assigned arbitrarily to make the equation fit a particular group of measurements.

Usually, $n \approx 2$; $0.5 \leq a \leq 2.5$; $1.3 \leq m \leq 2.5$

Structure and Texture: In rocks containing minerals with first-order conductivity, such as sulphide ores,

graphitized and pyritized rocks, the resistivity is affected by their structure and texture (Mares, 1984). If the conducting ore minerals form isolated clusters, surrounded by non-conducting cement such as liquid magmatic Ni-Cu ore mineralization, the ore has a high resistivity and cannot be found by d.c. electric methods. In the opposite case, in which the conducting minerals form a continuous net interconnected throughout the whole body, such as in hydrothermal polymetallic ore mineralization, the ore has a low resistivity and ore bodies may therefore be prospected for successfully by d.c. electric methods (Mares, 1984). Well-sorted rocks usually have high resistivities while poorly-sorted rocks have lower resistivities. The finer the rock grain size, the lower is the resisitivity.

Temperature and Pressure: According to Keller and Frischknecht (1966), extreme ranges in temperature may affect the resistivity of a water-bearing rock markedly, particularly if the temperature is high enough to drive water out of the rock as steam or low enough to freeze the water in the pores of a rock. At moderate temperatures, a change in temperature changes the conductivity of a rock only in so far as the conductivity of the electrolyte in the rock is changed. The conductivity of aqueous electrolytes increases with increasing temperature since the viscosity of water is decreased, in turn increasing the mobility of the ions. The dependence of resistivity on temperature for either an electrolyte or a rock saturated with an electrolyte is given by the equation.

$$\rho_t = \frac{\rho_0}{1 + \alpha_t(t-0)} \qquad \ldots\ldots 1.2$$

where ρ_0 - the resistivity measured at a reference temperature 0°C;

ρ_t - the resistivity measured at the ambient temperature t;

and α_t - the temperature coefficient of resistivity; it has a value of about $0.025°C^{-1}$ for most electrolytes (Keller and Frischknecht, (1966).

It is of note, therefore, that

-- the resistivity of rocks decreases with increasing temperature;

-- because temperature increases with increasing depth, the resistivity of rocks also decreases with increasing depth of burial; and

-- the resistivity of rocks is high at extreme temperatures.

Most ground water contain salts in solution, the presence of which lowers the freezing point. Pressure affect the resistivity of rocks in a very complicated way most especially at sub-freezing temperatures. Pressure lowers the freezing point of water. Water adsorbed on grain surfaces is under great pressure and will not reorient into ice crystals until the temperature is considerably below the normal freezing point. Also, as some water does freeze, it attempts to occupy a greater volume than it has in the liquid state, further increasing the pressure on the unfrozen water (Keller and Frischknecht, 1966). Freezing can therefore be considered then as merely a reduction in the fraction of pore space which is saturated with water.

These two factors cause the freezing process in rocks to take place over an extended temperature range rather than at a single temperature. The higher the salinity of the pore water, the lower will be the temperature at which freezing first starts to take place, and the finer the

grain size, the broader will be the temperature range through which freezing continues. Hence pressure tends to increase the resistivity of rocks even at very low temperatures (Mares, 1984).

Age of Deposition: In water-bearing rocks, there is an indirect relationship between resisitivity and, lithology and geologic age, since these two factors tend to control the porosity or water storage capacity of a rock, and to a lesser extent, the salinity of the water contained in a rock (Keller and Frischknecht, 1966). Table 1.1(b) shows geologic age as it affects the resistivity of rocks while fig. 1.1 shows this in relation to measurements made around radio stations for sedimentary rocks with apparently similar lithologic characteristics having ages which cover the entire range of geologic time. These earth resistivity values are estimated from the rate of decay in field strength about a radio transmitter. Normally, one would expect a fairly uniform increase of resistivity with geological age because of the greater compaction associated with increasing thickness of overburden (Dobrin, 1976).

1.2.3 Factors affecting the measurement of earth resistivity

The measurement of earth resistivity is affected by three important factors namely: the topography of the ground, anisotropy of the ground and inhomogeneity of the ground.

According to Telford *et al.* (1976), resistivity measurements are strongly influenced by local variations in surface conductivity, caused by weathering and moisture content. Rugged topography will have a similar effect, since the current flow tend to follow the surface particularly if the shallow layers are somewhat conductive.

Table 1.1(b) Generalized resistivity ranges in ohm-metres for rocks of different lithology and age.(After Dobrin, 1976)

Age	Marine sedimentary rocks	Terrestrial sedimentary rocks	Extrusive rocks (basalt, rhyolite)	Intrusive rocks (granite, gabbro)	Chemical precipitates (limestone, salt)
Quaternary and Tertiary age	1–10	15–50	10–200	500–2000	50–5000
Mesozoic	5–20	25–100	20–500	500–2000	100–10,000
Carboniferous Paleozoic	10–40	50–300	50–1000	1000–5000	200–100,000
Early Paleozoic	40–200	100–500	100–2000	1000–5000	10,000–100,000
Precambrian	100–2000	300–5000	200–5000	5000–20,000	10,000–100,000

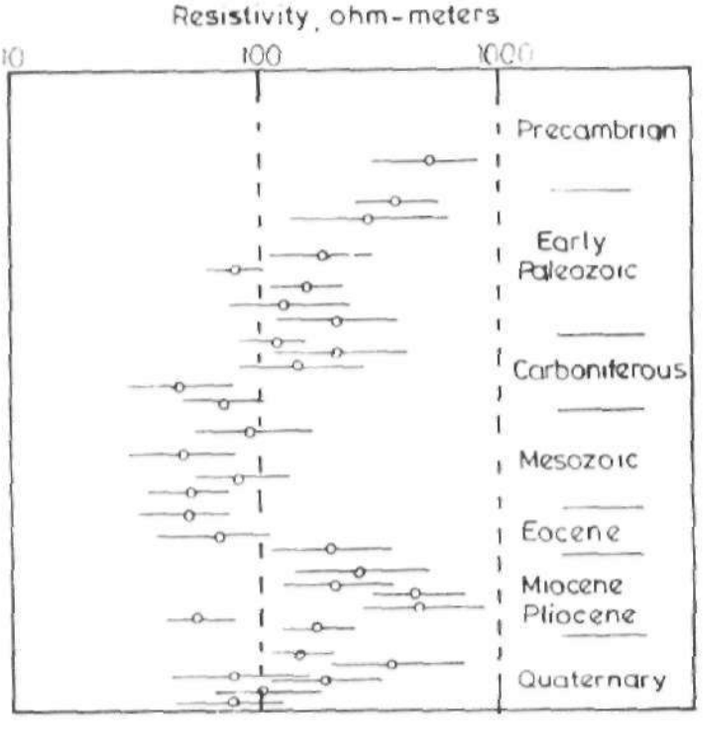


Figure 1.1 Average resistivity for groups of sedimentary rocks with similar characteristics (After Dobrin, 1976)

The equipotential surfaces are distorted as a result, producing false anomalies due to the topography alone. This effect may distort or mask a real anomaly. There is no method of isolating the topography effect in relation to d.c. electrical resistivity measurements (Mares, 1984).

The anisotropy of the ground whereby there is a preferred direction of current flow in the ground results in different current density components in different directions. This also makes the potential distribution to vary with direction. The end result is that the resistivity measured over horizontal beds is larger than the actual horizontal resistivity in the beds, but smaller than the vertical resistivity. If the beds have a steep dip and the measurement is made with a spread perpendicular to the strike, the apparent resistivity will be smaller than the true resistivity normal to the bedding, just the opposite to the result over horizontal layers; if the array is parallel to the strike of the dipping beds, the apparent resistivity will be too large (Telford *et al.*, 1976).

Inhomogeneity of the ground mainly results in a situation whereby both the current flow pattern and the potential curves are distorted at a plane surface. When a new layer of different resisitivity from the overlying layer is intercepted by a current flow line, depending on the relative resitivities of the two adjacent layers, the current flow lines are either flattened or bloated as they pass through the second layer (Dobrin, 1976).

1.3 D.C. Resisitivity Prospecting

Geoelectric d.c. methods are theoretically based on the theory of the stationary electric field sufficiently

described by the distribution of the current density, j which is dependent on the sources and resistivities of the medium.

In all conventional d.c. methods of prospecting, current is artifically passed into the ground and the energization effects of this current, both at the surface and within the ground are obtained through measurements of potential differences, potential, or through measurements of some other parameters that are directly related to these variables.

A resistivity instrument can be viewed as comprising of a current source (battery), a current meter (ammeter) and a voltage meter (voltmeter). These are connected, as shown in figure 1.2, to four electrodes inserted a few centimetres into the ground to make electrical contact. The current source causes a d.c. of amplitude, I to flow through the earth, entering at electrode C_1 and leaving at electrode C_2. The lines of current-flow through the earth are known to be three-dimensional (Mooney, 1980).

According to Keller and Frischknecht (1966), the simplest approach to the theoretical study of earth resistivity measurements is to consider first the case of a completely homogeneous isotropic earth. An equation giving the potential about a single point source of current can be developed from two basic considerations:

-- Ohm's law: $\bar{E} = \rho\bar{j}$ 1.3

where $\bar{E}$ - the potential gradient

$\bar{j}$ - the current density

and ρ - the resistivity of the medium

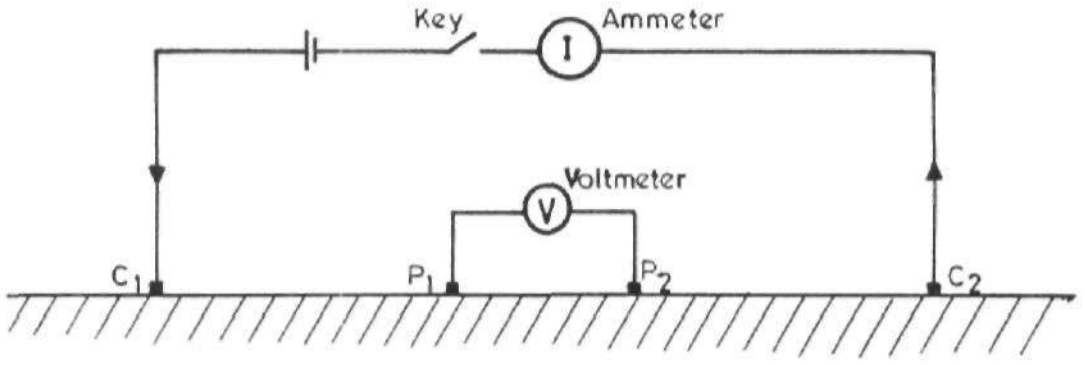


Figure 1.2 Field arrangement set-up for d.c. resistivity measurements.

-- The divergence condition: $\nabla \cdot \bar{j} = 0$ 1.4
which states that all the current going into a chunk of material must leave at the other side, unless there is a source or sink within the chunk. The divergence of the current density vector must be everywhere zero except at the current source.

It is noted that the electric field is the gradient of a scalar potential, that is,

$$\bar{E} = - \nabla U \qquad .....1.5$$

where U is in volts

Therefore, combining equations (1.3) and (1.4), we obtain Laplace's equation

$$\nabla \cdot \bar{j} = \frac{1}{\rho} \nabla \cdot E = - \frac{1}{\rho} \nabla^2 U = 0 \qquad .....1.6$$

The physical quantities measured in a field determination of resistivity are the current I, flowing between the two current electrodes, the difference in potential, ΔU, between two measuring points M and N, and the distances between the various electrodes. Thus, the applicable equation for the conventional earth resistivity measurement is:

$$\rho = K \frac{\Delta U}{I} \qquad .....1.7$$

where K is the geometric factor; it is dependent on the electrode configuration and has the dimension of length.

Equation (1.7) can be used to compute the true resistivity of the earth only if the earth is completely

homogeneous. On the contrary, the equation may be used as a definition for the apparent resistivity of the earth in a heterogeneous earth.

In d.c. electrical prospecting, the underlying idea is to delineate the earth into geoelectric and geologic sections. The geoelectric section differs from the geologic section in that boundaries between layers are determined by resistivity contrasts rather than by the combination of factors used by the geologists in establishing the boundaries between beds (Keller and Frischknecht, 1966). The electrical character of a rock is determined primarily by texture and water content. Boundaries in the geoelectric section coincide with boundaries in the geologic section only when there is a pronounced change in texture at such a boundary. A single named geologic unit may consist of several rocks with quite different textures and so, correspond to several units in the geoelectric section. The converse situation is also common, rocks covering a long period geologically may be uniform electrically, and all can be combined into a single unit in the geoelectric section (Keller and Frischknecht, 1966).

For a geoelectric section as shown in figure 1.3, the resisitivity ρ_h in the horizontal direction - a stack of beds effectively in parallel is:

$$\rho_h = \frac{\rho_1 \rho_2}{\rho_1(1-v) + \rho_2 v} \qquad \ldots\ldots 1.8$$

In the vertical direction, the beds are in series so that the vertical resistivity ρ_r is:

$$\rho_r = \rho_1 v + \rho_2(1-v) \qquad \ldots\ldots 1.9$$

where v - the fractional volume of layer with resistivity ρ_1 (Telford *et al.*, 1976).

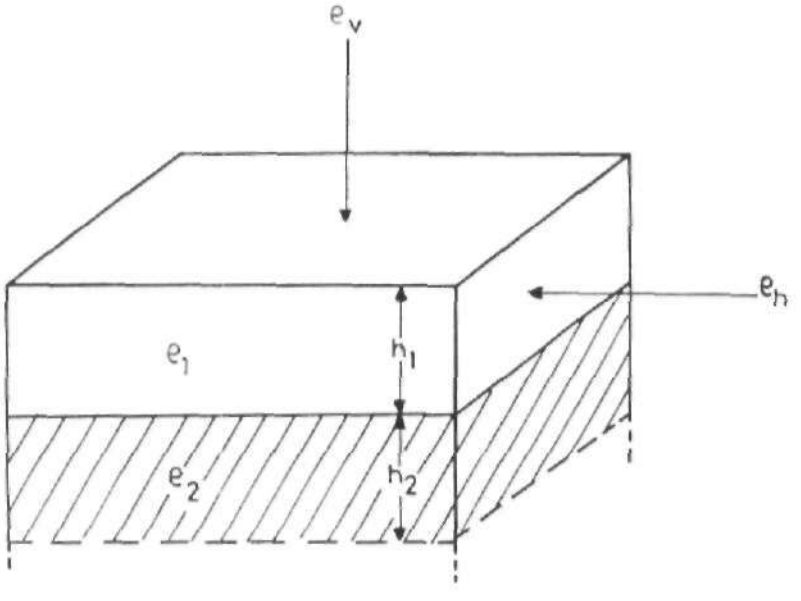


Figure 1.3 Geoelectric section for horizontal beds (After Telford *et al.*, 1976)

1.4 The Existing Electrode Configurations And Their Principles

Various electrode configurations have been successfully used to measure the resisitivities of earth materials. These configurations include the common four-electrode, three-electrode and tri-potential arrays. Others include the two-electrode, the five-electrode and the six-electrode differential arrays (Roy and Jain, 1973).

1.4.1 The four-electrode configuration

The four-electrode configuration is perhaps the most widely used configuration in field measurements. This configuration normally involves the use of two current electrodes to feed current into the ground and two potential electrodes to measure the potential difference between any two points in the vicinity of the current electrodes or along the line joining the current electrodes.

Common among these four-electrode configurations are the Wenner array, the Schlumberger array, the Asymmetrical Lee array, the Eltran, and the Dipole array.

The Wenner array is arranged such that the four electrodes are spaced along a line with equal interelectrode distances. Current is passed into the earth through the two outer electrodes, designated A and B, and the potential difference is measured between the two inner electrodes designated M and N. The Schlumberger electrode configuration consists of two current electrodes, A and B, and also two potential electrodes M and N, all along a straight line. The potential electrodes are placed symmetrically about the midpoint between A and B and are kept sufficiently close together so that the electric field

E between them can be considered constant. In practice, the separation between the potential electrodes M and N is always less than one-fifth of the separation between the current electrodes A and B, and is usually kept less than one-tenth of this separation (Van Nostrand and Cook, 1966).

The asymmetrical Lee configuration is obtained by removing the return current electrode to infinity in the Lee configuration. The electrodes are spaced along a straight line with each interelectrode separation between the potential electrodes (P_o,P_1,P_2) equal to half of the distance between the current electrode and the nearest potential electrode. The potential difference between P_o and P_1 and that between P_o and P_2 are measured.

The Eltran, also known as the linear dipole-dipole array, has the four electrodes spaced along a straight line with the current electrodes A and B, distinctly separated from the potential electrode connections M and N. The electrode separation between A and B is equal to the electrode separation between M and N. In the equally-spaced dipole-dipole array of electrodes used to minimize inductive coupling in induced polarization surveys, the interelectrode spacings are equal. In the unequally-spaced mode, the electrode spacing between the inner electrodes is an integral multiple of the current or potential electrodes' spacing. Figure 1.4 shows some of the common four-electrode arrays.

In computing the apparent resistivities from field measurements, the exact relative locations of the four electrodes is taken into account. The formular used for the computation of the apparent resistivity, ρ_a, is

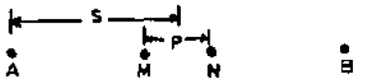
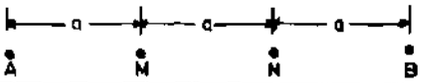
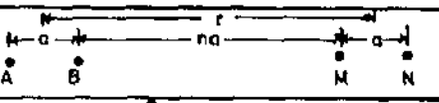
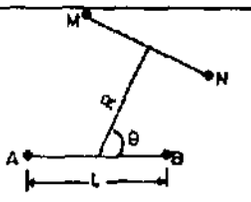
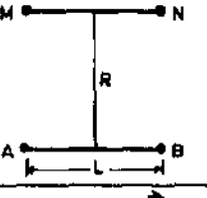
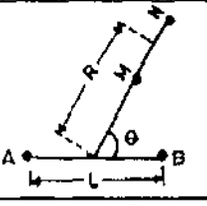
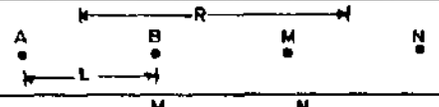
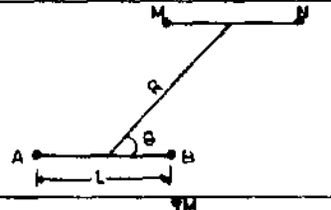
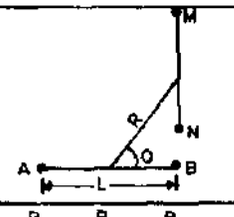
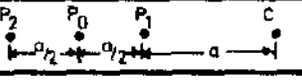
			LAYOUT	GEOMETRIC FACTOR, K
Dipole-Dipole	Schlumberger	S		$\pi\left(\frac{S}{P}^2 - \frac{P}{4}\right)$
	Wenner	W		$2\pi a$
	Eltran	E		$\pi\left(\frac{r^2}{a} - r\right)$
	Azimuthal	θ		$\frac{2\pi R^3}{L^2 \sin\theta}$
	Equatorial			$\frac{2\pi R^3}{L^2}$
	Radial	r		$\frac{\pi R^3}{L^2 \cos\theta}$
	Polar			$\frac{\pi R^3}{L^2}$
	Parallel	X		$\frac{2\pi R^3}{L^2} \cdot \frac{1}{3\cos^2\theta - 1}$
	Perpendicular	Y		$\frac{2\pi R^3}{2} \cdot \frac{1}{\sin\theta \cos\theta}$
	Asymmetrical Lee			$K_1 = 6\pi a$, $K_2 = 12\pi a$

Figure 1.4 Some four-electrode arrays (After Das and Ghosh, 1973)

$$\rho_a = \frac{K\Delta V}{I} \qquad \ldots\ldots 1.10$$

where ΔV - the potential difference between the potential electrodes;

I - the current passed into the ground

and K - the geometric factor, given by

$$K = \frac{2\pi}{\left[\frac{1}{AM} - \frac{1}{AM}\right] - \left[\frac{1}{BM} - \frac{1}{BM}\right]} \qquad \ldots\ldots 1.11$$

For the Wenner array, $K = 2\pi a$, implying that

$$\rho_a = 2\pi a \frac{\Delta V}{I} \qquad \ldots\ldots 1.12$$

For the symmetrical Schlumberger array,

$K = \pi(s^2/p - p/4)$, implying that

$$\rho_a = \pi\left[\frac{s^2}{p} - \frac{p}{4}\right]\frac{\Delta V}{I} \qquad \ldots\ldots 1.13$$

For the Asymmetrical Lee, two resistivities ρ_1 due to P_1P_0 and ρ_2 due to P_0P_2 are computed using the corresponding measured potentials V_{10} and V_{02} to give

$\rho_1 = 6\pi a\frac{V_{10}}{I}$ and $\rho_2 = 12\pi a\frac{V_{02}}{I}$ 1.14

1.4.2 The three-electrode configuration

The three-electrode configuration involves either the combination of one current electrode and two potential electrodes, or two current electrodes and one potential electrode with the uninvolved fourth electrode located at a point sufficiently far to approximate to infinity.

Common among this group is the Asymmetrical Wenner array (also called unsymmetrical method or the double equidistant probe method), the modified unipole, the pole-

dipole and the Lögn array (also known as the 'one-electrode' configuration) (Katsube and Collett, 1973). Figure 1.5 shows some of the common three-electrode arrays.

The underlying principle of the three-electrode arrays is the same as that of the four-electrode arrays. The relative position of the three electrodes is taken into account in computing the apparent resistivities from field measurements. For the Assymmetrical Wenner array,

$$\rho_a = 4\pi a \frac{\Delta V}{I} \qquad \ldots\ldots 1.15$$

For the Lögn configuration.

$$\rho_a = \frac{2\pi l^2}{a} \frac{\Delta V}{I} \qquad \ldots\ldots 1.16$$

1.4.3 The two-electrode configuration

The two electrode configuration can be configured in any of the following ways:

-- as an unfocused combination of one current electrode and one potential electrode with the other current and potential electrodes placed at sufficiently large distances away from the measuring environment so that they are considered to be conveniently at infinity. This is the combination worked on and reported by Apparao and Roy (1973), and Kumar (1974).

-- as a focused combination of two current electrodes in which the two current electrodes feed current

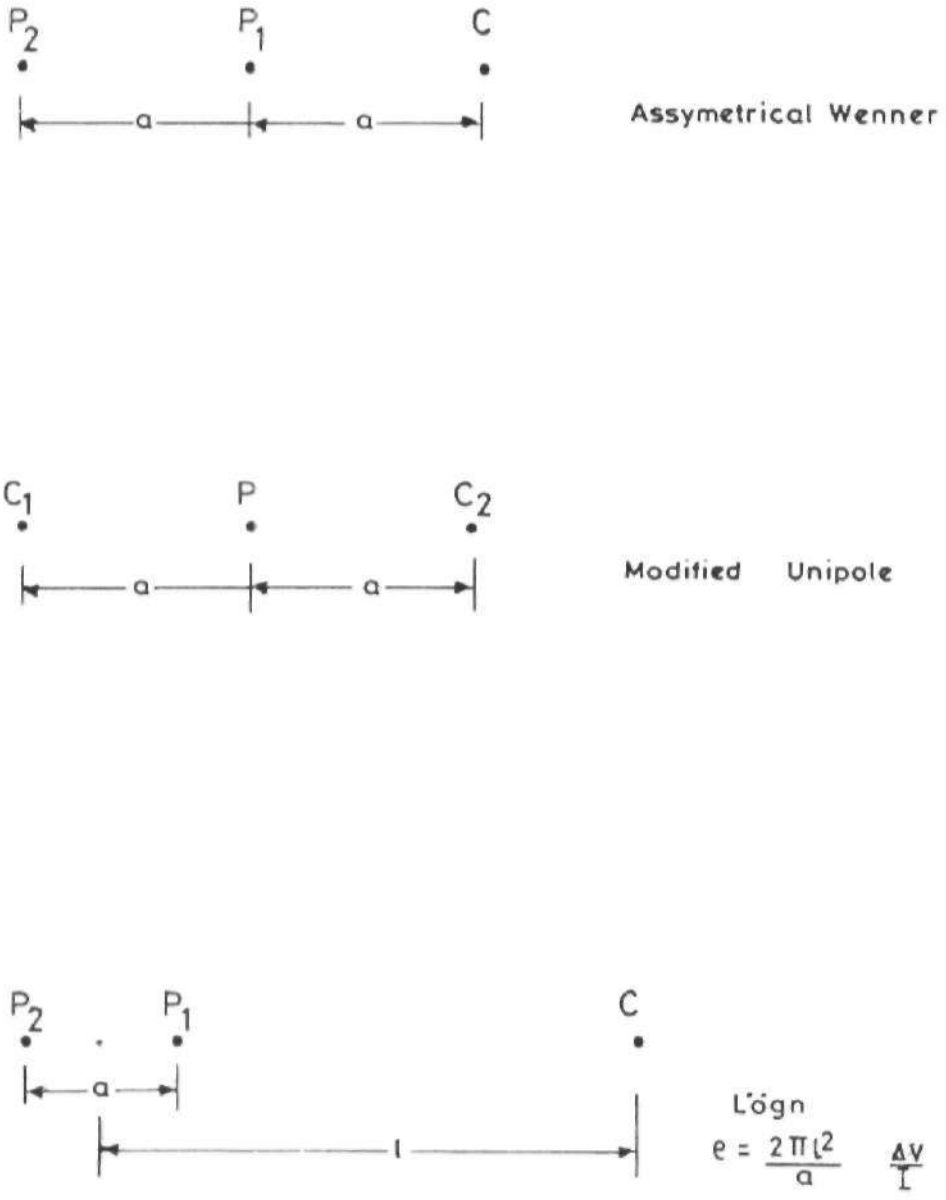


Figure. 1.5 Some three-electrode arrays
(After Van Nostrand and Cook, 1966)

into the ground with none acting as a current return electrode. This combination is reported by Gupta and Bhattacharya (1963) and, Brizzolari and Bernabini (1979).

-- as an unfocused combination of two current electrodes with a complete elimination of the potential electrodes. One of the current electrodes feed current into the ground, and the other current electrode acts as a current return electrode. This is the combination being proposed in this work.

A general outlay of the two-electrode, three electrode and four-electrode configurations as outlined by Mares (1984) is shown in figure 1.6 while figure 1.7 shows the most frequently used arrays.

It is known that as early as 1833, Fred Brown had proposed to find mineral deposits by the measurement of the resistance of the earth between two electrodes (Rust, 1938). Rust (1938) did not expantiate on the exact technique or theoretical basis of Fred Brown's adventure in the location of mineral deposits using two electrodes.

Apparao, *et al.* (1969) reported experimental initiatives using the mode of the two-electrode array having one current electrode and one potential electrode, with the other current and potential electrodes placed at "infinity". Apparao and Roy (1971), reported model experiments on surface prospecting of minerals by resistivity in-line profiling with Wenner, surface laterolog, unipole, modified unipole and two-electrode systems. The results show that, for conducting vein-type of targets, the simplest non-focused arrangement, namely, the

Types of resistivity profiling

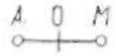
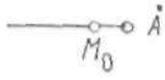
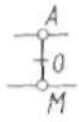
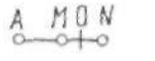
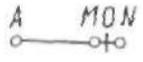
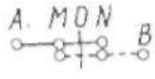
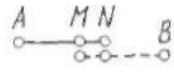
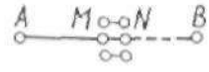
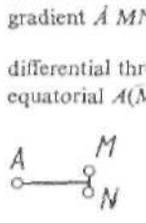
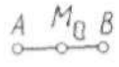
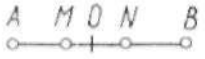
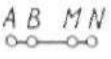
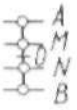
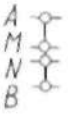
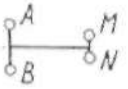
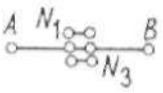
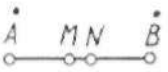
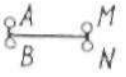
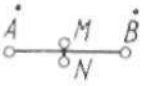
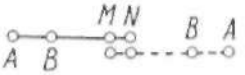
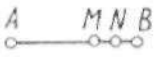
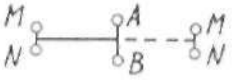
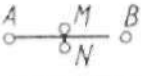
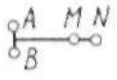
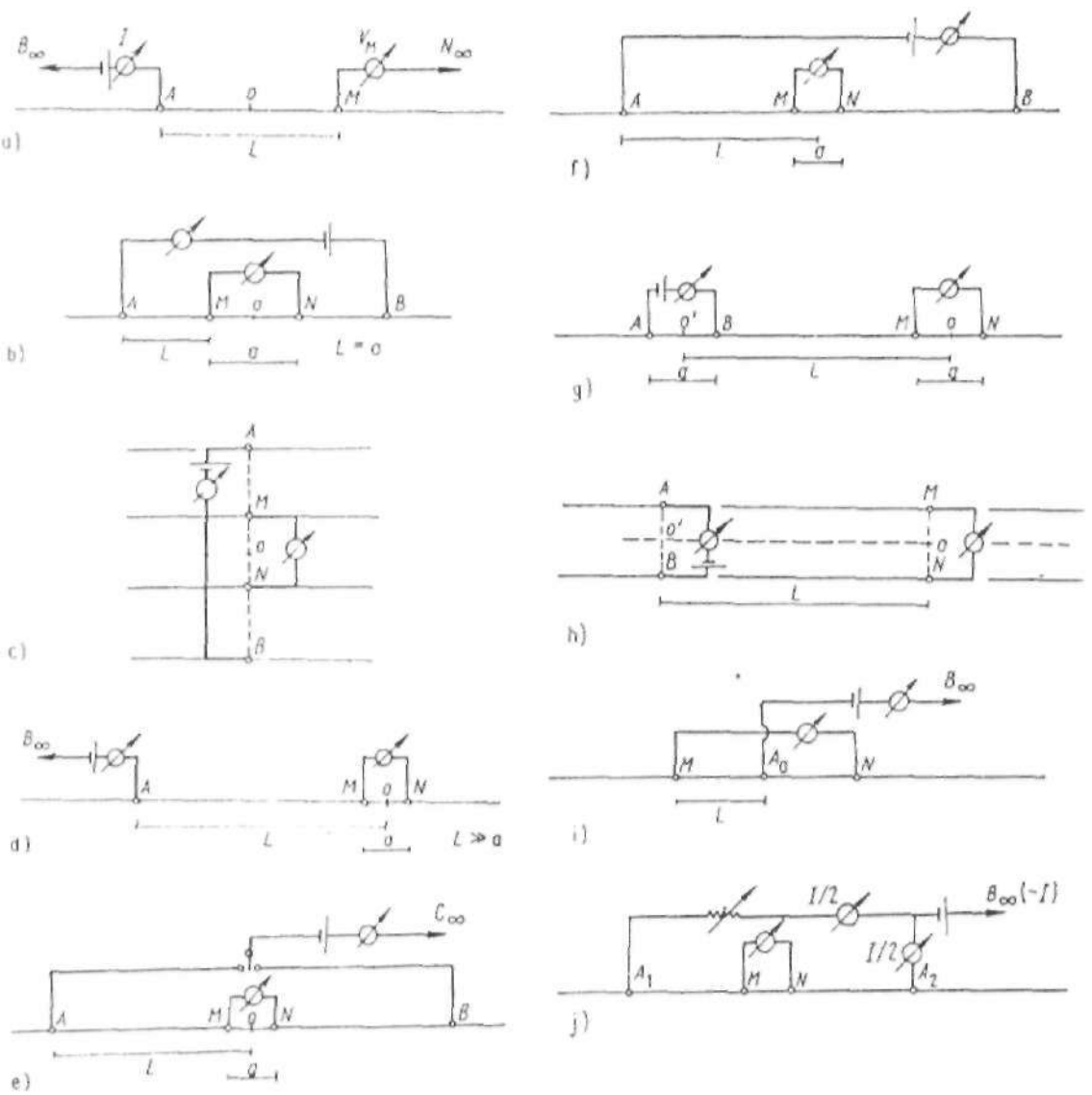
	Potential	Gradient	Dipole (+ with unequal dipoles)
two-electrode	potential *AM*  		
	potential with stable electrode *Á*  		
	potential with perpendicular array (*AM*)  		
three-electrode	three-electrode potential *AMN*  	three-electrode gradient *AMN*  	
	combined Wenner's *A MN, MN B*  	combined *A MN, MN B*  	
		combined parallel  	
		method of combined middle gradient *Á MN, MN B́*  	
	differential potential *AMB*  	differential three-electrode equatorial *A(MN)*	

Figure 1.6 Types of resistivity profiling (*After Mares, 1984*)

Figure 1.6 (continued)

four-electrode

Potential	Gradient	Dipole (* with unequal dipoles)
Wenner's profilling *AMNB* 	symmetrical (Schlumberger's) *A MN B* 	dipole (axial) $\overline{AB}\,MN$ 
Wenner's with perpendicular array (*AMNB*) 	symmetrical with perpendicular array (*A* $\overline{MN}$ *B*) 	dipole equatorial $(\overline{AB})\,(\overline{MN})$ 
	symmetrical parallel 	*) dipole axial 
	middle gradient method $\dot{A}\,\overline{MN}\,\dot{B}$ 	*) dipole equatorial 
	middle gradient method with perpendicular array ($\dot{A}\,MN\,\dot{B}$) 	*) dipole bilateral 
	asymmetric gradient $A\,\overline{MNB}$ 	*) dipole equatorial bilateral 
	differential gradient $A\,\overline{MN}\,A$ 	
	differential equatorial four-electrode $A\,(\overline{MN})\,B$ 	differential dipole $(\overline{AB})\,\overline{MN}$ 



a) potential, b) Wenner's; c) Wenner's profiling with perpendicular electrodes array; d) three-electrode gradient array; e) combined resistivity profiling; f) symmetrical (Schlumberger's) profiling; g) dipole axial array; h) dipole equatorial array; i) differential potential array; j) differential gradient array

A, B, C – current electrodes; *M, N* – measuring electrodes; *O* – recording point

Figure 1.7 Most frequently used arrays. (*After Mares, 1984*)

two-electrode system, gives the best response in regard to both shape and magnitude. Moreover, it was found that the two-electrode system had the greatest depth of investigation and the least resolution.

Apparao and Roy (1973) conducted field test of the two-electrode system by making resistivity profiling in three test areas namely Vajrakarur (Dist. Anantapur, Andhra Pradesh), Chitradurga (Dist, Chitradurga, Mysore) and Josiaralangalam (Dist. Madurai, Madras), for field experimentations over conducting targets. In the field tests, Wenner, Schlumberger, Modified Unipole and Two-electrode arrays were used. Profiling was done using a fixed value of electrode spacing.

From both the laboratory and field tests conducted, Apparao and Roy (1971, 1973) concluded that focusing does not improve the potentiality of an array, and that the unfocused two-electrode array had by far the largest depth of detection in the sense that it produced large anomalies with small spacings in comparison with other electrode arrays. The depth of investigation for the two-electrode array was found to be about 0.35L, where L is the distance of separation between the active current electrode and the active potential electrode (Roy and Apparao, 1971). In general, it was concluded that the two-electrode array had a lot of advantages over other arrays including that it had the least number of moving electrodes.

Gupta and Bhattacharya (1963), in investigating the effect of focusing on ground responses, concluded that focusing current lines towards the target or a higher current density in the region of the target may not apparently produce a correspondingly higher effect at the

receiving points on the ground surface. This finding was also confirmed by Apparao and Roy (1973) and, Brizollari and Bernabini (1979).

The above conclusion by Gupta and Bhattacharga (1963), Apparao and Roy (1971, 1973) made it very unnecessary to try to investigate any further the focused two-electrode arrangement as tried by Brizollari and Bernabini (1979).

Kumar (1974) made a simple analysis of the two-electrode array of Apparao and Roy (1971) and arrived at the apparent resistivity expression:

$$\rho_a = 2\pi L \frac{V}{I} \qquad \ldots\ldots 1.17$$

where L - the distance between the active current electrode and the active potential electrode,

and V - the potential at the positive potential electrode due to the positive current electrode.

It is of note that equation (1.17) is consistent with equations for the other earlier mentioned configurations in that the configuration factor also has the dimension of length.

The earlier mentioned conclusion by previous workers left the unfocussed arrangement using a combination of two current electrodes with no potential electrode as the only alternative to the arrangement used by Roy and Apparao (1971). The present work is devoted to this alternative electrode arrangement. The method considered in the present work does not separately measure the potential generated at

any point by the current distribution in the ground but rather employ the driving potential of the field equipment. A voltage source supplies a driving potential which drives current into the ground through one of the two current electrodes. The two current electrodes are separated by a distance L, and are such that one feeds current into the ground and the other makes a return to the voltage source. It is expected that a variation in the resistance of the ground, and hence its resistivity will be evidenced in the variation or change in the amount of current and voltage registered by the measuring instruments in the circuit. The current itself is expected to vary, not only as the electrode separation distance L is varied but also as the subsurface condition changes.

An electrode arrangement as is being considered here would consider the earth material between the two current electrodes as forming a cylinder or any other similar regular shape. By using the appropriate expression such as

$$R = \rho \frac{l}{A} \quad , \text{ and} \qquad \ldots\ldots 1.18a$$

$$R = \frac{V}{I} \qquad \ldots\ldots 1.18b$$

where A/l is the geometric factor, we hope to arrive at an expression such as

$$\rho = K \frac{V}{I} \qquad \ldots\ldots 1.19$$

where K has the dimension of length.

Equation (1.19) is the general expression for the apparent resistivity of a supposedly homogeneous earth through which

a current I flows and potential V is generated between the measuring electrodes.

According to Smythe (1950), the pattern of current flow in the earth is actually dependent on the nature of the interbedded planes. Although the above statement may be true, but for the purpose of this work, the pattern of current flow in the earth, known to actually depend on the nature of interbedded planes, is also considered hemispherical or near spherical.

1.4.4 Other electrode configurations

This class consists of the newly developed arrays such as the six-electrode Differential array of Zohdy (1969) and the relatively obscure ones such as the five-electrode Lee-partition tri-potential, resistolog array. Figure 1.8 shows a sketch of some of these electrode configurations.

1.5 Aims Of The Present Work

The present work has as its objective the investigation and possibly, development of a new non-conventional and simple electrical resistivity prospecting method which does not sacrifice accuracy.

The method is a non-conventional simple one in that only two movable electrodes are involved, and its development is based on Ohm's law. It is not commonly used because its pattern of operation does not follow the conventional four electrode arrays and that there is almost no basic interpetation procedure developed for the method as of now.

The investigation of the method would involve deriving basic resistivity expression(s) for the assumed geometry of

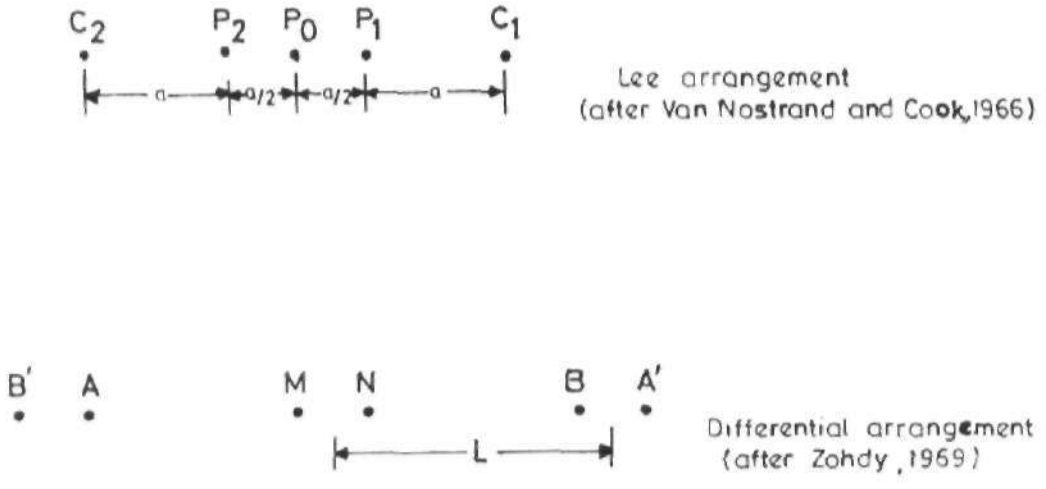


Figure 1.8 Some Other Electrode Arrangements

earth material and current flow pattern between the two current electrodes. Furthermore, horizontal profiling and vertical electrical sounding procedures would be performed on single and interbedded earth materials placed in a laboratory scale model tank. The results of the laboratory studies would be tried and cross-checked under field conditions in which horizontal and vertical profiling procedures would be performed on the real earth situation during a field work. Deductions and conclusions would then be drawn from the experiences of both the laboratory and the field studies to explain the behaviour of this variant of the two-electrode array in comparison with the Wenner and the Schlumberger arrays which would also be used in the field test for comparison purposes only. The accuracy of this array in determining layer resistivity value and most especially in the determination of layer thickness would be verified.

1.6 Advantages Of The Proposed Two-electrode Method

Due to its simple nature, it is envisaged that the proposed two-electrode method would have some basic advantages over the other conventional methods of electrical geophysical prospecting. The envisaged advantages of the proposed variant of the two-electrode d.c. resistivity array investigated in this work are:

- the method is easy to handle in the field in that its manpower requirement is low as only two or three people are needed for data collection (field work). Length measurements are also easy in that the electrode spacings are integral multiples of the metre. Hence, the method avoids measuring decimals (or fractions) of a metre as is normally required in the Schlumberger array;

- at the present stage of development, the underlying principle does not involve exotic mathematics such as complicated differentials and integrals; rather, the method is based on simple geometry;
- the method has a fewer number of moving electrodes during the field survey; the two current electrodes needed are the only ones moved at a time as against the four electrodes normally required for the Wenner and about two to four electrodes for the Schlumberger array; These two electrodes are moved only in the forward (expanding) direction as against the forward-backward movements necessary in both the Wenner and the Schlumberger;
- the proposed method is time-saving due to some of the factors discussed above;
- due to the fact that the method is time-saving plus the fact that only about two people are required for data collection, the method is also cost-saving;
- the method is simple to unambiguously interprete right in the field without resort to the use of a computer. This is so because the appropriate graph(s) can be easily plotted in the field; the plotted graphs are usually linear and they usually show a number of segments which also indicate the number of layers sampled by the data. Furthermore, the thickness of each layer can be easily determined by reading off on the electrode separation axis, the point of intersection of adjacent linear segments and making the necessary subtractions to determine the layer thickness while the resistivity value of each layer can be determined using the simple line analysis method derived in this work.

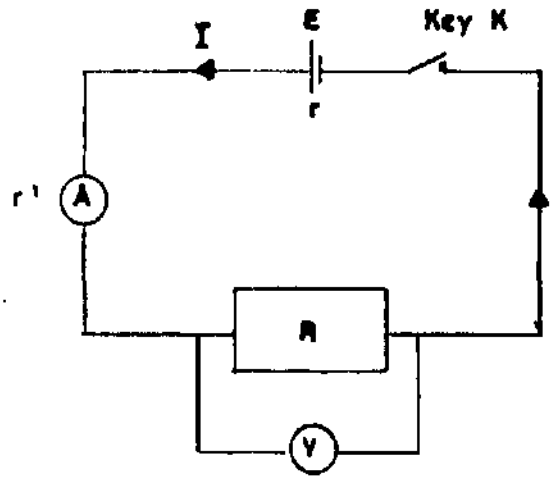
CHAPTER TWO

PRINCIPLE AND THEORY OF THE PROPOSED VARIANT OF THE TWO-ELECTRODE D.C. RESISTIVITY METHOD

2.1 Principle of the Proposed Two-electrode Configuration (Method)

The proposed variant of the two-electrode method discussed in this work is a mode of the unfocused system in which only the two current electrodes are used in the measurement of earth resistivity with the potential electrodes completely eliminated. The present work has as its basis the measurement of the resistance and hence the resistivity of an ohmic conductor of a given length and cross-sectional area in the simplified circuit shown in figure 2.1. In a simple laboratory work, the circuit is usually used to verify Ohm's law. The resistance r' of the current measuring instrument is usually very small; far less than r and R so that it can conveniently be regarded as negligible. The problem of galvanic electrical resistivity surveying as visualized in this work is analogous to the circuit of figure 2.1.

The circuit of figure 2.1 can again be used to verify the term `terminal potential difference' in a circuit. By definition, the `terminal p.d.' refers to the potential difference across the terminals of a driving cell when the circuit is `closed'. The electromotive force (e.m.f.) of the cell, refers to the potential difference across the terminals of the cell when the circuit is `open'. Once the circuit is closed, that is, when the resistor of resistance R ohms is connected up as shown in figure 2.1 and the key K is switched on, it is found that the potential difference across the terminals of the cell become less than the e.m.f.



E — the applied e.m.f.

I — current flowing through the circuit

A — ammeter

V — voltmeter reading voltage developed across the resistor, R

r — internal resistance of the power source

r' — resistance of the current measuring instrument

Figure 2.1: Simple circuit to verify Ohm's Law

of the cell. The difference between the e.m.f. and the observed p.d. is called the `lost volt'. If two voltmeters having the same characteristics are connected, one across the terminals of the cell, and the other across the terminals of the external resistance R, it is observed that both readings are the same. That is, the voltage across the terminals of the cell when on closed circuit is the same as the voltage across the resistor whose resistance R is to be determined. If this voltage is V, and the amount of current flowing in the circuit is I, then R can be calculated from Ohm's law using

$$R = V/I \qquad \ldots.2.1$$

The resistivity, ρ, of the conductor can thus be determined using the equation:

$$\rho = RA/l \qquad \ldots.2.2$$

where l - length of the conductor
A - cross-sectional area of the conductor
and R - resistance of the conductor

The above discussion forms the underlying principle of the proposed variant of the two-electrode array discussed in this work. From the above discussion, it seems possible that the resistance R can be found by measuring the voltage across the terminals of the supply source. The terminal p.d. decreases as current flows from the battery and increases as the external resistance R increases (Nelkon and Parker, 1982).

In the measurement of earth resistance, if R represents the resistance of the earth material between the two current electrodes, then, by measuring the terminal p.d. across the power source when current I is being delivered into the

earth, a calculation of R can be made without necessarily having the potential electrodes involved.

2.2 Assumptions Made In The Proposed Two-electrode Configuration

In the application of the proposed two-electrode arrangement to the model and the true earth, the following basic assumptions were made:

- the earth material in each layer 'sampled' by the current from the current electrodes, is homogeneous and isotropic;

- the earth materials or layers are horizontally stratified;

- the volume of the earth material sampled by the current from the current electrodes at separation L can be approximated by the volume of an equivalent horizontal cylinder whose radius, x, is equal to half the radial distance of current flow from each current electrode, that is, $x = r/2 = L/4$, and the material is of the same volume as the hemisphere whose volume, v is $^{2}/_{3}\pi r^{3}$;

- each current electrode is a current point source or sink;

- the pattern of current flow between the two current electrodes in the assumed homogeneous earth is either hemispherical or near spherical whether or not a new layer is encountered;

- the earth resistance is in series because the current traverses the earth in the vertical direction.

Therefore, the average resistivity of the earth material can be expressed as:

$$\rho = \frac{\sum_{i=1}^{n} \rho_i v_i}{\sum_{i=1}^{n} v_i} \qquad \ldots.2.3$$

where n is the number of layers sampled by the current at the maximum electrode separation L_n and Σv is the volume of earth material sampled;

- for each homogeneous layer, the resistance of the sampled earth is proportional to the volume of the earth material sampled. Therefore, the resistance per unit volume, k, of a given layer sampled is considered a constant;
- each electrode separation, L is assumed to sound a new layer although some of these layers, by the closeness or linearity of their k values, are expected to, in reality, indicate their belonging to the same layer;
- the mode of electrical conduction in the earth material is assumed to be ohmic.

The assumption that the earth material between the two current electrodes is homogeneous and isotropic is well known not to be generally valid. For an isotropic medium, it is expected that the outward current flow from the positive current electrode must be the same in all directions into the earth (Van Nostrand and Cook, 1966), no current flows upward because the air has infinite resistivity. Hence, the current lines are uniformly spaced radial lines and the equipotential surfaces are concentric hemispheres with their centres at the current electrodes (Van Nostrand and Cook, 1966). For the two current electrodes involved, a top view imagination of the pattern formed by both the current lines

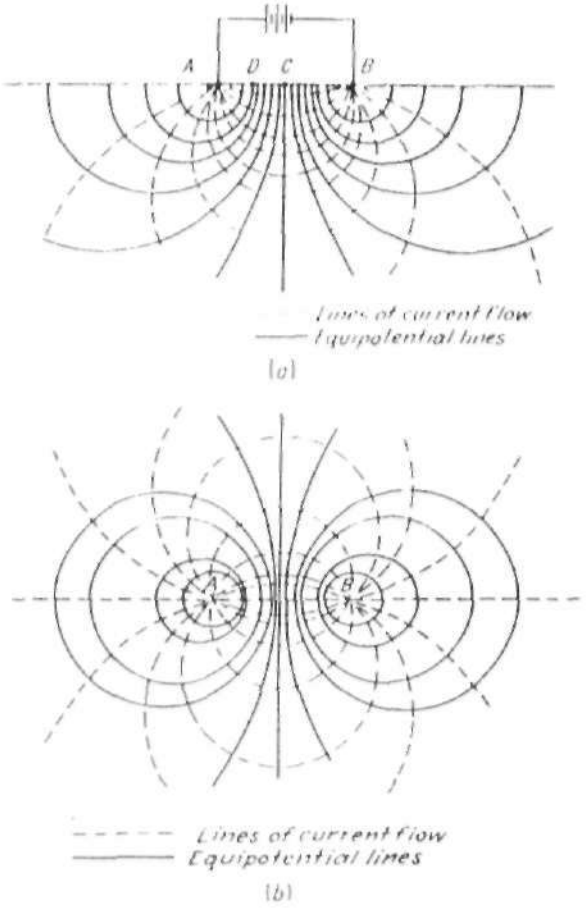
and the equipotentials show co-axal concentric circles (fig.2.2). Although it is known that the earth is heterogeneous in nature, but the homogeneity assumption is not only a fair representation of the possibility of such existence to a finite depth extent within the earth, but it also lends a lead to the analysis of the problem in a situation where there is a sharp departure from the (homogeneous) nature of the top surface or of an underlying bed from the (homogeneous) nature of the overlying bed. In which case, it is expected that the slope of a supposed straight line graph will change when the underlying bed is of a different material or composition from that of the overlying bed.

The assumption that the pattern of current flow between the two current electrodes form a hemispherical bowl of volume $v = {}^{2}/_{3}\pi r^{3}$ implies that the volume increases with increasing electrode separation. The pattern is now imagined to be confined to a cylinder of radius x ($=\frac{1}{2}r$) and length l.

2.3 Theory Of The Proposed Two-electrode Configuration (Method)

In deriving a suitable formula for the proposed two-electrode arrangement based on the previously stated assumptions, figures 2.3 to 2.5 are necessary in understanding the volume of the earth material trapped within each current hemispherical or near-spherical bowl as the current electrode separation is varied.

By considering the electrode spacings L_{i-1} and L_i in figure 2.3, and calling into play the eighth assumption, it is observed that part of the hemisphere described by the separation L_i is of resistivity ρ_1; the remainder (the shaded part) is of resistivity ρ_2. This shaded part is a spherical cap. It therefore implies that the sum of the



Equipotential lines and flow lines: (*a*) below the earth's surface in vertical plane of electrodes; (*b*) on plane of earth's surface; electrodes at *A* and *B*.

Figure 2.2: Equipotential Lines and Flow Lines

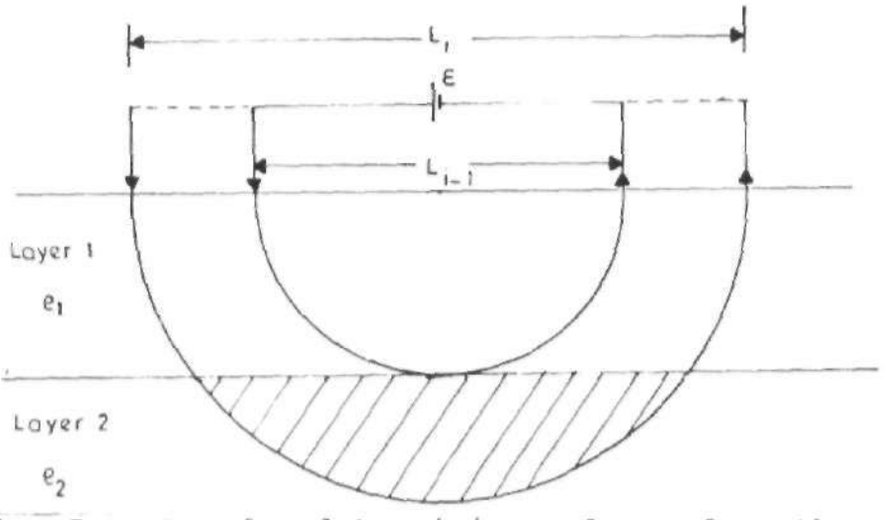


Figure 2.3: Geometry for determining volume of earth trapped within a layer using the hemispherical model

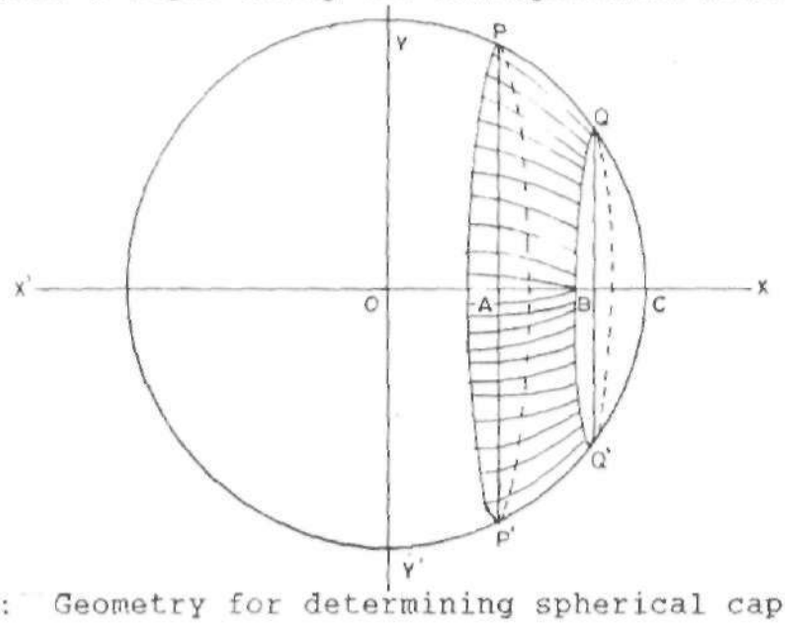


Figure 2.4: Geometry for determining spherical cap volume

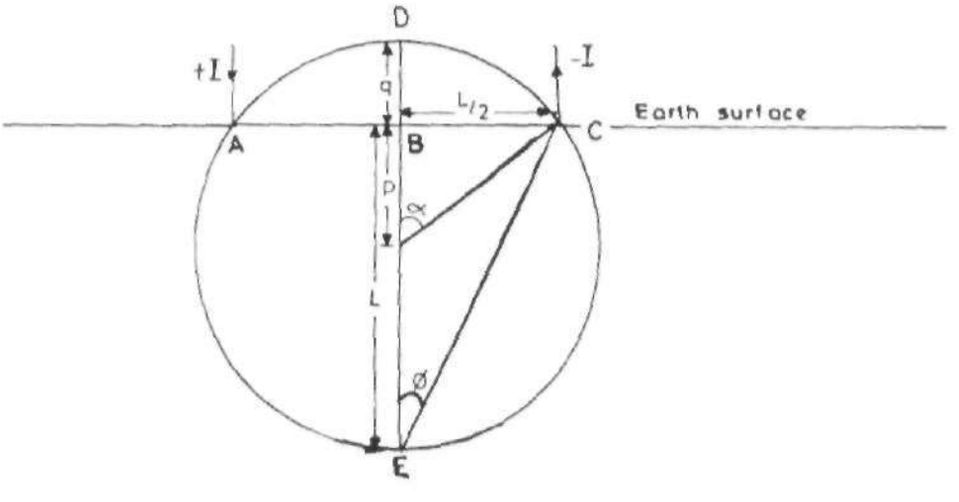


Figure 2.5: Geometry for determining volume of earth trapped within a layer using the near-spherical model

volumes of the spherical cap of resistivity ρ_2, and the unshaded part of the hemisphere, of resistivity ρ_1, makes up the totality of the hemispherical bowl. Considering that part of the hemispherical bowl having resistivity ρ_2, it is necessary to apply the expression for the volume of part of a sphere between two parallel planes to compute the volume of each earth layer traversed by the current flow. This same consideration is applicable to the near-spherical bowl.

The equation of a circle is $x^2 + y^2 = r^2$

The volume of a sphere is $v = {}^4/_3\pi r^3$

This implies that the volume of a hemisphere is ${}^2/_3\pi r^3$, where r is the radius of the sphere of which the hemisphere is a part of.

In figure 2.4, let the quadrant YOC of the circle $x^2 + y^2 = r^2$ rotating about OX describe a hemisphere. Let two parallel planes whose distances from O be given by OA = a and OB = b, mark out the segment whose volume v is required. Using

$$v = \int \pi y^2 dx \qquad \ldots.2.4$$

(rotation about the x-axis, volumes of solids of revolution), then

$$y^2 = r^2 - x^2 \qquad \ldots.2.5$$

Therefore,

$$v = \int_a^b \pi(r^2-x^2)dx = \pi[r^2x - {}^1/_3x^3]_a^b$$

$$= \pi(b-a)[r^2 - {}^1/_3(b^2+ab+a^2)] \qquad \ldots.2.6$$

If b = r, the part of the sphere becomes a spherical cap. Therefore,

$$v = \pi(r-a)[r^2 - {}^1/_3(r^2+ar+a^2)] \qquad \ldots.2.7$$

When a = 0, the spherical cap becomes a hemisphere (Abbott, 1980).

The result of equation (2.7) is applied to the hemispherical and the near-spherical models below.

-- *the Hemispherical Model*

In figure 2.3 , let $L_{i-1} = L_1$ and $L_i = L$ then $a = \frac{1}{2}L_1$ and $r = \frac{1}{2}L$. Hence,

Volume of spherical cap

$$= \pi(r-a)[r^2 - {}^1/_3(r^2+ar+a^2)]$$

$$= {}^1/_{24}\pi(L-L_1)(2L^2-LL_1-L_1^2)$$

$$= {}^1/_{24}\pi(2L^3-3L^2L_1+L_1^3) \qquad ....2.8$$

Volume of remaining part = Volume of hemisphere - Volume of spherical cap 2.9

$$= {}^1/_{12}\pi L^3 - {}^1/_{24}\pi(2L^3-3L^2L_1+L_1^3)$$

$$= {}^1/_{24}\pi L_1(3L^2-L_1^2) \qquad ...2.10$$

Relating the above results to figure 2.3 implies that

$v_1 = {}^1/_{24}\pi L_1(3L^2-L_1^2)$, that is,

$v_1 = {}^1/_{24}\pi L_{i-1}(3L_i^2-L^2_{i-1})$

and $v_2 = {}^1/_{24}\pi(2L_3-3L^2L_1+L_1^3)$, that is,

$v_2 = {}^1/_{24}\pi(2L_i^3-3L_i^2L_{i-1}+L^3_{i-1})$

The volume of the hemisphere is therefore

$$v = {}^1/_{12}\pi L_i^3 = 0.2618L_i^3$$

-- *the Near-Spherical Model*

Figure 2.5 shows the geometry of the near-spherical model used in this work. From figure 2.5, taking the

approximate probing depth at electrode spacing L to be L, then from Pythagoras theorem,

$$r^2 = (\tfrac{1}{2}L)^2 + p^2 = \tfrac{1}{4}(L^2+4p^2) \quad \ldots.2.11$$

but $$r = p + q \quad \ldots.2.12$$

and $$r = L - p \quad \ldots.2.13$$

Substituting equation 2.13 into equation 2.11

reduces to

$$p = {}^{3}/_{8}L \quad \ldots.2.14$$

Hence, from equation 2.13,

$$r = L - {}^{3}/_{8}L = {}^{5}/_{8}L \quad \ldots.2.15$$

From the theorem of product of intersection of chords of a circle, AB.BC = DB.BE ,that is, $(\tfrac{1}{2}L).(\tfrac{1}{2}L) = q.L$. Hence

$$q = \tfrac{1}{4}L \quad \ldots.2.16$$

In determining the volume of part of the sphere in empty space, the geometry of figure 2.5 shows that the part of the sphere whose short axis is of length q ends up in empty space above the earth surface. This region forms a spherical cap whose volume is to be removed from the volume of sphere to give the volume of part of sphere within the homogeneous medium.

Using equations (2.7) and (2.14), the volume of the spherical cap simplifies to

$$v_{cap} = 0.033854\pi L^3 = 0.106356L^3 \quad ..2.17$$

The volume v of part of sphere within the homogeneous earth is found using

$$v = v_{sphere} - v_{cap} \quad \ldots.2.18$$

but $v_{sphere} = {}^{4}/_{3}\pi({}^{5}/_{8}L)^3$ using equation (2.15),

that is $v_{sphere} = 0.325521\pi L^3 = 1.022654L^3 \quad \ldots.2.19$

Thus, $v = (0.325521 - 0.033854)\pi L^3$

that is $v = 0.2916667\pi L^3 = 0.9162978L^3 \quad \ldots.2.20$

Equation 2.20 represents the volume of part of sphere within the homogeneous earth.

Considering the situation whereby part of the current flowing in the near-spherical bowl of volume $v = 0.9162978L^3$ is trapped within a layer of resistivity ρ_1, and the remainder is trapped in a region of resistivity ρ_2 such that it forms a spherical cap within the second layer. Let

L_1 represent the electrode spacing when the current flow pattern was just touching (and therefore tangential to) the interbedded plane,

L the new electrode spacing,

v^* the volume of spherical cap formed in layer 2,

and v^{**} the volume of earth trapped within the current boundary in layer 1 (fig. 2.3).

Using $r = {}^{5}/_{8}L(= 0.625L)$ and $a = 0.625L_1$, equation 2.7 gives

$$v^* = 0.625\pi(L-L_1)[(0.625L)^2 - {}^{1}/_{3}\{(0.625)^2L_1L + (0.625)^2L_1^2\}]$$

$$= 0.2556634(2L^3 - 3L^2L_1 + L_1^3) \quad \ldots.2.21$$

but $v = v^* + v^{**} \quad \ldots.2.22$

thus, $v^{**} = 0.9162978L^3 - v^* \quad \ldots.2.23$

Equation (2.23) represents the volume of the remaining part entrapped in layer of resistivity ρ_1 .

The derivation of the formula for layer bulk resistivity ρ_b using the two-electrode arrangement is approached in two basic ways. These are by considering the equivalent cylinder of the hemisphere formed by the earth material sampled in order to find its resistivity, and by computing the `specific resistance' or `specific resisitivity' of the sampled hemisphere from its measured bulk resistance or bulk resistivity.

2.3.1 The "equivalent cylinder" approach

An equation relating the volume of the assumed hemisphere or of the near-sphere formed by the sampled earth material to that of the approximate equivalent cylinder is arrived at as follows:

-- *The Hemispherical Model*: Volume of a hemisphere of radius, r is $v = {}^{2}/_{3}\pi r^3$

For an electrode spacing L, r = L/2. Therefore,
Volume v, of the hemisphere is

$$v = {}^{2}/_{3}\pi(\tfrac{1}{2}L)^3 = {}^{1}/_{12}\pi L^3 = 0.2618L^3 \qquad .....2.24$$

implying that $\sum_{i=1}^{n} v_i = 0.2618L_i{}^3$

For an equivalent cylinder of radius, $x = \frac{1}{2}r = \frac{1}{4}L$, its volume

$$v = \pi x^2 l = \pi(\tfrac{1}{4}L)^2 l = {}^{1}/_{16}\pi L^2 l \qquad .....2.25$$

As the volume of the equivalent cylinder equals the volume of the hemisphere, then

$${}^{1}/_{16}\pi L^2 l = {}^{1}/_{12}\pi L^3$$

that is $l = {}^{4}/_{3}L$ ...2.26

but the cross-sectional area of the cylinder is $A = \pi x^2$

therefore $A = {}^{1}/_{16}\pi L^2$ 2.27

Equation (2.27) divided by equation (2.26) gives

$$A/l = {}^{3}/_{64}\pi L = 0.14726216L \quad .....2.28$$

By definition, the resistance R of the equivalent cylinder is given by equation (1.18a)

Substituting equation (2.28) into equation (1.18a) implies

$$R = ({}^{64}/_{3\pi})\rho/L$$

$$\rho_b = {}^{3}/_{64}\pi RL \quad ....2.29$$

but again $R = V/I$, then

$$\rho_b = {}^{3}/_{64}\pi LV/I \quad ....2.30$$

that is $\rho_b = aLV/I$ 2.31

Equation (2.31) is consistent with the expression for the resistivity of the earth material in the other common electrode arrays such as the Wenner and the Schlumberger arrangements in which ρ is always expressed in the form of equation (1.19), that is $\rho = KV/I$, where K is a constant, called the geometric factor of the configuration.

In equation (2.31), $K = aL$ and has the dimension of length.

Equation (2.30) gives the expression for obtaining the bulk resistivity of the earth material sampled for a particular value of the electrode spacing L.

-- ***The Near-Spherical Model:*** Volume of the near-spherical model is $v = 0.9162978L^3$ implying that $\sum_{i=1}^{n} v_i = 0.9163L_i^3$

Radius of the equivalent cylinder is $r = \frac{1}{2}L$ .2.32

Cross-sectional area, A of the equivalent cylinder is

$$A = \pi r^2 = \tfrac{1}{4}\pi L^2 = 0.25\pi L^2 \quad ...2.33$$

Volume v_c of the equivalent cylinder is

$$v_c = Al = 0.25\pi L^2 l \qquad \ldots.2.34$$

where l - the effective length of the cylinder

As the volume of the equivalent cylinder equals the volume of the remaining part of sphere within the homogeneous earth structure, then equating equation (2.40) to equation (2.26), gives

$$0.25\pi L^2 l = 0.2916667\pi L^3$$

then
$$l = 1.1667L \qquad \ldots.2.35$$

Dividing equation (2.33) by equation (2.35) gives the dimensional constant

that is
$$\frac{A}{l} = \frac{0.25\pi L^2}{1.16667L} = 0.2142856\pi L \qquad \ldots.2.36$$

Using equation (2.36) in equation (2.2) implies that

$$\rho_b = 0.2142856\pi LV/I \approx 0.6732LV/I \qquad \ldots.2.37$$

where ρ_b is the bulk resistivity and all other parameters are as earlier defined. Therefore $\rho_b = KV/I$ where $K \approx 0.6732L$ Equation (2.37) is consistent with the form of equations (1.19) and (2.31).

The near-spherical and the hemispherical bulk resistivity values are related by:

$$\rho_{near\text{-}spherical} = 4.571428\rho_{hemispherical} \qquad \ldots.2.39$$

In the case of more than one layer, for a given L_i, the bulk resistivity of the j^{th} layer is given by

$$\rho_j = \frac{\sum_{i=1}^{n} \rho_i v_i}{\sum_{i=1}^{n} v_i} \; ; \quad i=j= 1, 2, 3, \ldots, n \qquad \ldots.2.40$$

where n is the number of layers sampled by the current at the maximum electrode separation, L.

Thus, for a two-layer case, if the electrode separation L_{i-1} gives a bulk resistivity ρ_1, and the electrode separation L_i gives a bulk resistivity ρ_{2b}, then

$$\rho_{2b}v = \rho_1 v_1 + \rho_2 v_2 \qquad \ldots.2.41$$

from which $$\rho_2 = \frac{\rho_{2b}v - \rho_1 v_1}{v_2} \qquad \ldots.2.42$$

where ρ_2 is the true resistivity of the second layer. Equation (2.42) can be used to compute the resistivity of the new layer defined by the new sounding separation, L_i for the two-layer case.

2.3.2 The "specific resistance" approach

In this approach, the seventh assumption is called into play. The implication of this assumption is that if R(= V/I) is the measured resistance for a given spread length L and v is the volume of the earth material sampled, then the resistance per unit volume, otherwise termed "specific resistance" for the layer is given as

$$k = R/v \qquad \ldots.2.43$$

Figure 2.7 shows that a new hemispherical volume is sounded for a new L_i. By making suitable subtraction, the volume of the hemisphere trapped within each layer is subsequently calculated. The value of k at various stages is an indication of layer homogeneity or inhomogeneity. For a single homogeneous layer, the k values for the sample spread within the layer are expected to be close but far different from those associated with another (adjacent) layer; k values within a single layer may also bear a linear

relationship of the type $y = mx + c$ with themselves but not with those associated with another adjacent homogeneous layer.

Sample equations for the determination of the "specific resistance" values for various layers are next shown.

2.4 General Equations For Different Number Of Layers Using The Specific Resistance Approach

2.4.1 The n-layer overburden case

Using the two-electrode array, it is assumed that the electrodes are expanded about the centre n times until the basement is just encountered at the (n+1)th expansion.

Figure 2.7 shows the layering in the n-layer overburden case. Skipping intermediate values and working out the equations for the n-layers, it was observed that;

- *for the hemispherical model,*

$$v_n = {}^{1}/_{24}\pi(L_n-L_{n-1})(2L_n^2-L_{n-1}^2- L_{n-1}L_n);$$

$$n = 2, 3..... \qquad ....2.44$$

$$v_r = {}^{1}/_{24}\pi(L_r-L_{r-1})(3L_n^2-L_r^2-L_{r-1}^2-L_{r-1}L_r);$$

$$r = 1, 2, 3,...,n-1 \qquad ....2.45$$

$$L_0 = L_{-1} = L_{-2} = ... = L_{-n} = 0; \quad r = 1, 2, 3,...,n-1$$

$$v_1 = {}^{1}/_{24}\pi L_1(3L_n^2-L_1^2); \; n = 2, 3, 4,..... \qquad .....2.46$$

Equation (2.44) is the expression for the spherical cap formed by the new L value. It is the volume of the nth layer, assumed to be encountered by the current flow pattern from the current electrodes separated by a distance L.

Equation (2.45) is the expression for finding the various volume(s) described between the smallest value of L, that is L_1, and the maximum value of L, which is L_n.

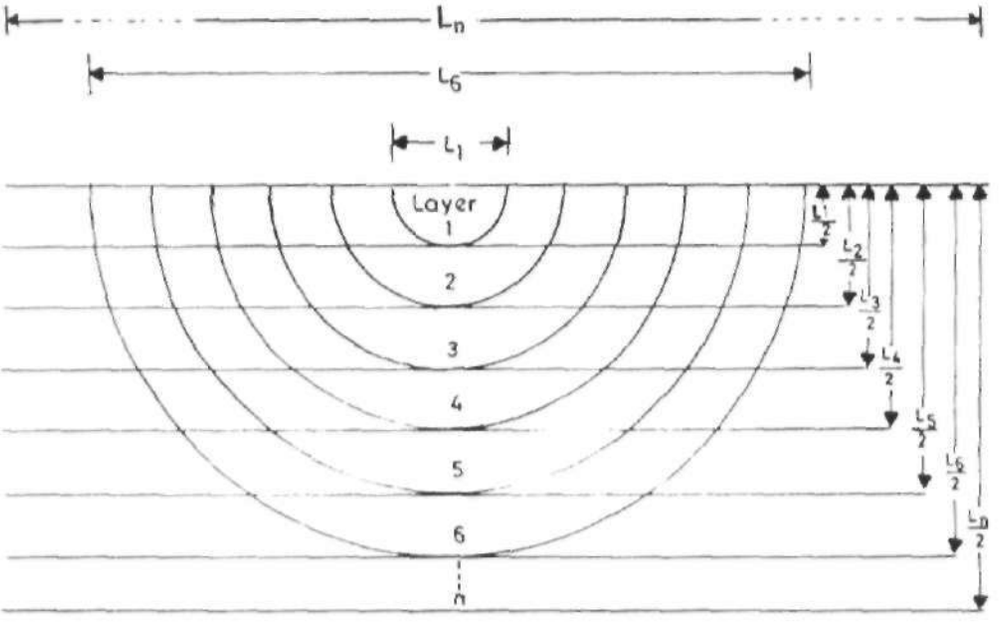


Figure 2.6 Earth layering at electrode spacing L_n [n-Layer Case of Earth Layering]. (hemispherical model)

Equation (2.46) is the expression for finding the volume of the first layer described between the surface and the top boundary of the second layer at electrode spacing L_n.

- For the near-spherical model,

$$v_n = 0.2556634(L_n-L_{n-1})(2L_n^2-L_{n-1}L_n-L_{n-1}^2);$$

$$n = 2, 3, \ldots\ldots \qquad \ldots.2.47$$

$$v_r = 0.2556634(L_r-L_{r-1})(3L_n^2-L_r^2-L_{r-1}^2-L_{r-1}L_r);$$

$$r = 1, 2, 3, \ldots, n-1 \qquad \ldots.2.48$$

$$L_o = L_{-1} = L_{-2} = \ldots = L_{-n} = 0; \quad r = 1, 2, 3, \ldots, n-1$$

$$v_1 = 0.9162978L_1^3-0.2556634(2L_n^3-3L_n^2L_1+L_1^3);$$

$$n = 2, 3, 4, \ldots\ldots\ldots \qquad \ldots.2.49$$

By slotting in the appropriate values of r and n when necessary, equations (2.44) to (2.49) are used to generate values of the volume(s) to be used in expressions such as

$$R_n = \sum_{i=1}^{n} k_i v_i; \quad n = 1, 2, 3, \ldots\ldots \qquad \ldots\ldots.2.50$$

and

$$k_n = \frac{R_n - \sum_{i=1}^{n} k_i v_i}{v_n}; \quad n = 1, 2, 3, \ldots\ldots \qquad \ldots.2.51$$

Similarly, expressions such as

$$\rho_n = \sum_{i=1}^{n} g_i v_i; \quad n = 1, 2, 3, \ldots\ldots \qquad \ldots.2.52$$

and

$$g_n = \frac{\rho_n - \sum_{i=1}^{n} g_i v_i}{v_n}; \quad n = 1, 2, 3, \ldots\ldots \qquad \ldots.2.53$$

be used to calculate the "specific resistivity" of the layer of the earth where g_n is the specific resistivity of the earth layer.

It is to be noted that for each value of L, a new value of k is computed. The values of k so obtained can then be compared and used in composing the layers into the appropriate geoelectric layers.

2.4.2 Typical equations for different number of layers

Applying the earlier derived equations to the homogeneous model, as example

for the two-layer case,

$$v_1 = {}^1/_{12}\pi L_1^3 = {}^1/_{24}\pi(2L_1^3)$$

where L_1 is the separation at the nth electrode separation

using this in equation (2.43) implies

$$\sum_{i=1}^{n} k_i v_i = R_n \qquad \ldots.2.54$$

where for $i = n = 1$, $k_1 = R_1/v_1$

that is, $$k_1 = \frac{R_1}{{}^1/_{24}\pi(2L_1^3)} \qquad \ldots.2.55$$

for the three-layer case,

$$v_2 = {}^1/_{24}\pi(2L_2^3)$$

$$v_1 = {}^1/_{24}\pi(2L_2^3 - 3L_2^2L_1 + L_1^3)$$

$$v_1 - v_2 = {}^1/_{24}\pi(3L_2^2L_1 - L_1^3) = {}^1/_{24}\pi L_1(3L_2^2 - L_1^2)$$

implying that $$k_2 = \frac{R_2 - {}^1/_{24}\pi k_1 L_1(3L_2^2 - L_1^2)}{{}^1/_{24}\pi(2L_2^3 - 3L_2^2L_1 + L_1^3)} \qquad ..2.56$$

for the four-layer case,

$$V_{L_3} = {}^{1}/_{24}\pi(2L_3^3)$$

$$V_{L_2} = {}^{1}/_{24}\pi(2L_3^3 - 3L_3^2L_2 + L_2^3)$$

$$V_{L_1} = {}^{1}/_{24}\pi(2L_3^3 - 3L_3^2L_1 + L_1^3) - {}^{1}/_{24}\pi(2L_3^3 - 3L_3^2L_2 + L_2^3)$$

$$= {}^{1}/_{24}\pi[3L_3^2(L_2 - L_1) + L_1^3 - L_2^3]$$

$$V_{L_1} = {}^{1}/_{24}\pi L_1(3L_3^2 - L_1^2)$$

Applying that:

$$n_3 = \frac{{}^{1}/_{24}\pi k_1 L_1(3L_3^2 - L_1^2) - {}^{1}/_{24}\pi[3L_3^2(L_2 - L_1) + L_1^3 - L_2^3]}{{}^{1}/_{24}\pi(2L_3^3 - 3L_3^2L_2 + L_2^3)} \quad \ldots.2.57$$

Applying the same set of equations to the near-spherical model, as example

for the two-layer case,

$$V_{L_1} = 0.9162978L_1^3 = sL_1^3$$

Applying that $k_1 = R_1 \text{ÇL} L_1^3$ 2.58

where s = 0.9162978

for the three layer case,

$$V_{L_3} = sL_3^3$$

$$V_{L_2} = c(2L_3^3 - 3L_3^2L_1 + L_1^3)$$

$$V_{L_1} = (s - 2c)L_2^3 + c(3L_2^2L_1 - L_1^3) = sL_2^3 - c(2L_2^3 - 3L_2^2L_1 + L_1^3)$$

$$n_2 = k_2$$

$$n_2 = \frac{k_2[(s - 2c)L_2^3 + c(3L_2^2L_1 - L_1^3)]}{c(2L_2^3 - 3L_2^2L_1 + L_1^3)} \quad \ldots.2.59$$

where c = 0.2556634

for the four-layer case,

$$V_{L_3} = sL_3^3$$

$$V_{L_2} = c(L_3 - L_2)(2L_3^2 + L_3L_2 - L_2^2) = c(2L_2^3 - 3L_2^2L_1 + L_1^3)$$

$$V_{L_1} = c(3L_3^2L_2 - 3L_3^2L_1 + L_1^3 - L_2^3)$$

$$R_1 = sL_3^3 - c(L_3 - L_1)(2L_3^3 - L_3L_1 - L_1^2)$$

Applying that

$$R_2 = k_1[sL_3^3 - c(L_3 - L_1)(2L_3^3 - L_3L_1 - L_1^2) + k_2c(3L_3^2L_2 - 3L_3^2L_1 + L_1^3 - L_2^3)$$

$$c(2L_3^3 - 3L_3^2L_2 + L_2^3)$$

...2.60

The procedure for the determination of the number of layers, layer parameters such as thickness and resisitivity value, is quite different in this method from the one adopted in determining similar parameters using the equivalent cylinder approach. While the equivalent cylinder approach is expected to involve mostly graphical determination of the layer parameters, the specific resistance approach will be analytical in nature. Though it may not be able to specifically give the resistivity value for each layer, nevertheless, it will serve the same purpose in that the "specific resistance" will be almost a constant for a single homogeneous layer and thereby be a good yardstick for determining the number of layers. It is noted that for a unit cube of volume, the specific resistance is equivalent to the resistivity of the material.

CHAPTER 3

LABORATORY SCALE MODEL STUDIES

3.1 Introduction

In laboratory model studies, geologic structures are simulated by small-scale models of a size readily handled in the laboratory. It therefore makes it mandatory that, in laboratory scale modelling, similitude should be achieved between the model and the full-scale system. In modelling resistivity methods, suitable conducting media which allow the flow of current are used. This is usually an electrolyte, in which the scaled model body or target structure(s) is(are) placed. The above statement is known to be strictly valid when a body whose characteristics are to be studied is placed inside a medium of electrolyte or earth material which forms the environment for the body. A situation of this sort exists in a case such as when a metallic lamina to be studied is placed in a body of water which forms the environment. However, in a situation as exists in this modelling experiment, in which the environment itself is being studied, the above statement and subsequent statements as regards the scaling factor, though not out of place, or irrelevant, may not be fully applicable.

Due to the nature of the investigations carried out in this modelling experiment, in which the medium was investigated, suitably scaled homogeneous, isotropic electrolytes and earth materials were used to simulate and configure the real earth condition. In experimenting over the electrolyte and earth materials, each of the materials used was in turn placed in a tank made of transparent perspex. Perspex is a highly resistive non-conducting

material. It is most desirable not only because the use of a conductor would greatly affect the pattern of current flow hence the measured response, but also for its great strength and transparency. Because it only dissolves readily in solvents such as chloroform, and bonds together very well when adhesives such as glue are used in putting sheets and pieces of it together, it therefore provides a strong support for the electrolyte and earth materials put into it. The electrolyte and earth materials used in this experimentation are water, lateritic clay, river sand and, a combination of lateritic clay and river sand called `mixed-soil'. The perspex base of the tank represents the basement in the real earth situation. In the experimentation, a situation whereby a single homogeneous layer of earth material is in direct contact with the base of the tank is referred to as either a single overburden case or a two-layer case for it to be in conformity with similar address in the real earth situation. In the laboratory work, the two-layer case, the three-layer case and the four-layer case in different combinations were considered.

3.2 Scaling Factor of the Model System

The characteristic parameter of a conducting medium is the conductivity, σ (or resistivity, ρ) while the current density J and electric field strength E form the field parameters.

The potential field distribution within a source-free medium is described by

-- the equation of continuity,
   $\nabla \cdot J_c = 0$, and
-- Ohm's law

$$J_c = -\sigma \nabla \phi$$

where J_c is the conduction current density and ϕ is a scalar potential.

In order to have an accurate simulation of the full-scale system, both the model and full-scale systems must satisfy the above equations.

Applying the principle of similitude through dimensional analysis,

-- the basic dimensions (and units) in the potential field problem are length L (metre), mass M (kilogramme), time T (second) and electric current I (ampere).

-- by letting α, β, τ and ϵ to be the scale factors for the length, mass, time and electric current respectively, the SI base units as related in the model and full-scale systems are as follows:

$$L = \alpha L', \quad \text{that is} \quad L/L' = \alpha \qquad \ldots\ldots 3.1(a)$$
$$M = \beta M', \quad \text{that is} \quad M/M' = \beta \qquad \ldots\ldots 3.1(b)$$
$$T = \tau T', \quad \text{that is} \quad T/T' = \tau \qquad \ldots\ldots 3.1(c)$$
$$I = \epsilon I', \quad \text{that is} \quad I/I' = \epsilon \qquad \ldots\ldots 3.1(d)$$

where the primed quantities represent the full-scale system and the unprimed quantities represent the model scale system.

In a conductive medium, the observed potentials due to a current flowing through it are determined by the resistivity (or conductivity) of the medium, the strength of the current flowing through it, and the distance from the current source (Mwenifumbo, 1980). This simply implies that four variables, namely the potential ϕ, the resistivity ρ (or conductivity, σ), the current strength I, and the distance L from the current source are involved in the solution to the resistivity problem.

The dimensions of the variables are worked out and summarized as seen from table 3.1 below

Table 3.1 Dimensions of scaling variables

	ρ	ϕ	L	I	σ
L	3	2	1	0	-3
M	1	1	0	0	-1
T	-3	-3	0	0	3
I	-2	-1	0	1	2

Using the scale factors of equation (3.1) and the dimension matrix in table 3.1, we can relate the parameters of the model and the full-scale system as follows:

$$\rho = a^3\beta\tau^{-3}\epsilon^{-2}\rho' \quad \ldots.3.2(a)$$

$$\sigma = a^{-3}\beta^{-1}\tau^3\epsilon^2\sigma' \quad \ldots.3.2(b)$$

$$\phi = a^2\beta\tau^{-3}\epsilon^{-1}\phi' \quad \ldots.3.3$$

Combining equations (3.2) and (3.3), we have

$$\sigma\phi = a^{-1}\epsilon\sigma'\phi' \quad \ldots.3.4$$

implying that

$$\sigma\phi L/I = \sigma'\phi'L'/I' \quad \ldots.3.5$$

$\phi L/I$ has the dimensions of resisitivity and hence each side of equation (3.5) is a dimensionless quantity.

By making $\phi/I = R$, equation (3.5) may be written as

$$\sigma RL = \sigma'R'L' \quad \ldots\ldots3.6$$

thereby reducing the number of independent variables to three.

If for instance we want to model a conductor on a linear dimensional scale structure of 1:100 and resistance of 1:10, that is $L = 10^{-2}L'$ and $R = 10^{-1}R'$, then the scale factor for the resistivity will be obtained from

$$\frac{R'}{R}\cdot\frac{L'}{L} = \frac{\rho'}{\rho} \qquad \ldots\ldots 3.7$$

$$\frac{10}{1}\cdot\frac{100}{1} = \frac{\rho'}{\rho}$$

..

implying that $\rho' = 10^3 \rho$

that is, the resistivity scale factor will be 10^3. The implication of this is that a measurement of the resistivity made in the model will need to be multiplied by the scale factor for a rough estimate of the expected order of the real earth resistivity to be obtained.

In the present study, a model length of 1.0m was used to simulate a field length of the order of 10^2m, implying that L:L' = 1:100. The resistance was modelled on a thousand to one ratio, that is R:R' = 10^3:1. Hence, from equation (3.9), we arrive at

$$\rho' = 10^{-1}\rho$$

that is, if during the model study a resistivity value of say 2010.0 Ωm is measured, representing in this system, a sort of tank field representation, then the expected true resistivity will be 201.0 Ωm.

3.3 The Experimental Set-up

3.3.1 The apparatus

The laboratory scale model apparatus used in the laboratory experimentation is schematically shown in figure 3.1. It consists of

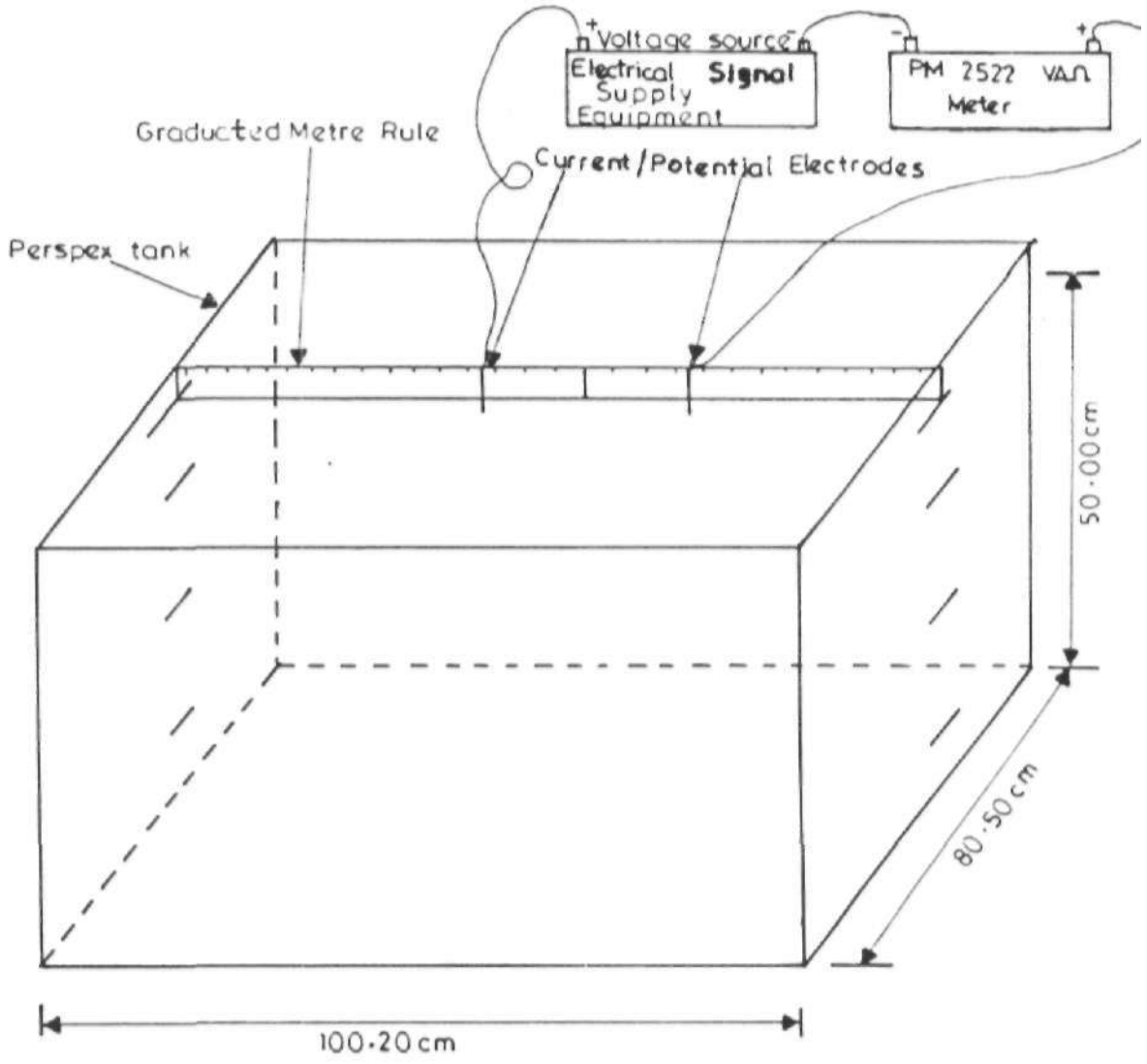


Figure 3.1 Scale Model Tank Apparatus

- a tank which holds the simulating electrolyte/earth material.
- a framework for carrying the electrodes across the tank, and
- the measuring equipment.

The model tank was wholly constructed of transparent perspex. This was to enable the easy visibility of the content of the tank so as to be able to correct for uneveness of surface or make cross-measurement of the thickness of layers. The tank itself was encased in an iron frame which provided adequate support and protection against breakage of the tank. The top of the tank was open to the air.

The tank had an internal length of 100.2cm, an internal width of 80.5cm and an effective depth (depth from the bottom level of the electrode carriage to the inner bottom part of the tank) of 50.0cm.

In the model set-up, copper electrodes of 1.20mm diameter were used as current electrodes. This was because platinum electrodes - a better option, known to have low polarization impedance and high resistance to corrosion, were unavailable. Albeit, the low-resistivity value of refined copper made it a good substitute. The copper electrodes, projecting 0.3 cm from the tubing (the covering insulator) were each mounted in a slide and clip-on form so that their positions/separations along the carrying framework was easily adjusted by sliding them along the metre-rule carriage. The electrodes could therefore be moved to any desired position across the tank with a minimum lateral positioning accuracy of 0.6 mm.

In supplying electrical energy to the electrolyte/earth material and the measurement of the desired response of such a material, the following equipment was used:

-- Universal LABPACK H.T. and L.T. Power Supply Type LAB59R: This equipment was used to supply mainly the d.c. (OHz) signal to the simulating electrolyte/earth material in the model tank. When necessary, it was found suitable to supply higher voltage and current to the earth material at line frequency (50Hz). The range of d.c. voltage that could be supplied by this equipment was from zero to about 300V at a current range of zero to 8A. It could also supply a.c. voltage at 50Hz from zero to about 25V with the current range from zero to 8A.

-- PHILIPS PM 5106 LF Generator 10Hz - 100KHz: This equipment, which has a frequency range from zero to about 100 kHz, was used primarily to feed a.c. at different frequencies of interest to the simulating electrolyte/earth material in the model tank. The equipment was capable of delivering a maximum voltage of about 10.3 volts thereby making it very suitable and easy to handle in a laboratory work of this nature.

-- PHILIPS PM 2522 Digital VAΩ Meter: This equipment was used to measure both the input signal (current and voltage) from the power supply unit (as they are being fed into the earth material) and the output signal from the simulating electrolyte/earth material.

-- TRIO, 10MHZ Double - Beam Oscilloscope CS - 1562A.: This equipment was used to monitor both the input and output signals in checking the amplitude level and phase shift between them.

3.3.2 Determination of the tank characteristics

In most of the resistivity field systems, use is made of either very low frequency a.c. (<50Hz) or commutated d.c. sources. According to Mwenifumbo (1980), because of difficulties due to polarization at the electrode-electrolyte interface, these very low operating frequencies are sometimes found to be unsuitable in model systems. Although frequencies up to 1500Hz have been used in electrolytic tank model studies, it is equally necessary that the advantages of reduced polarization effects obtained at higher frequencies be balanced against the problems of greater stray capacitative currents in the measuring circuit and cable induction when selecting an optimum value for the operating frequency. Experiments were conducted to determine the operating frequency to be used in the studies using both the Wenner array and the proposed two-electrode method. Figure 3.2 shows the plot of current, I against frequency, f for determining the operating frequency.

The first medium of experimentation in the tank was water.

In the determination of the apparent resistivity of the tank water as a function of frequency, the Wenner array at electrode spacings of 2cm, 5cm, 10cm and 30cm was used, with the observation point situated at the centre of the tank. Figure 3.3 shows the apparent resistivity of water as a function of frequency for the electrode spacings mentioned while the resistivity of water as a function of frequency for the two-electrode method with the electrode spacings of 2cm, 5cm, 6cm, 10cm, 15cm, 30cm and 90cm is

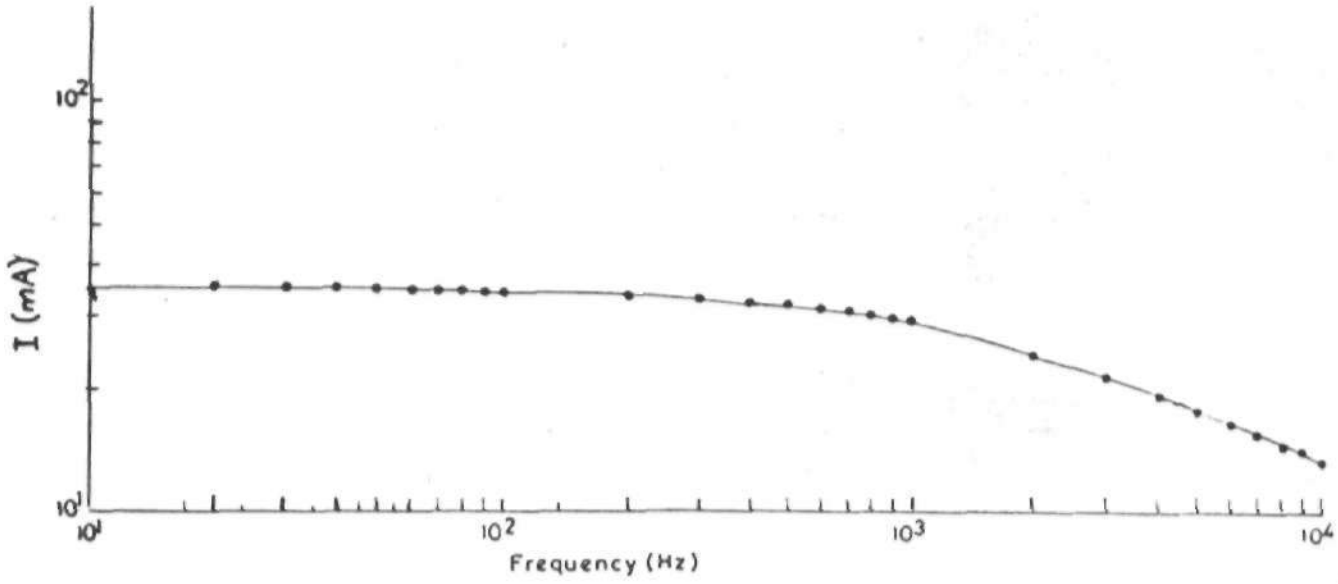


Figure 3.2 Graph of current I against frequency f used in determining the operating frequency

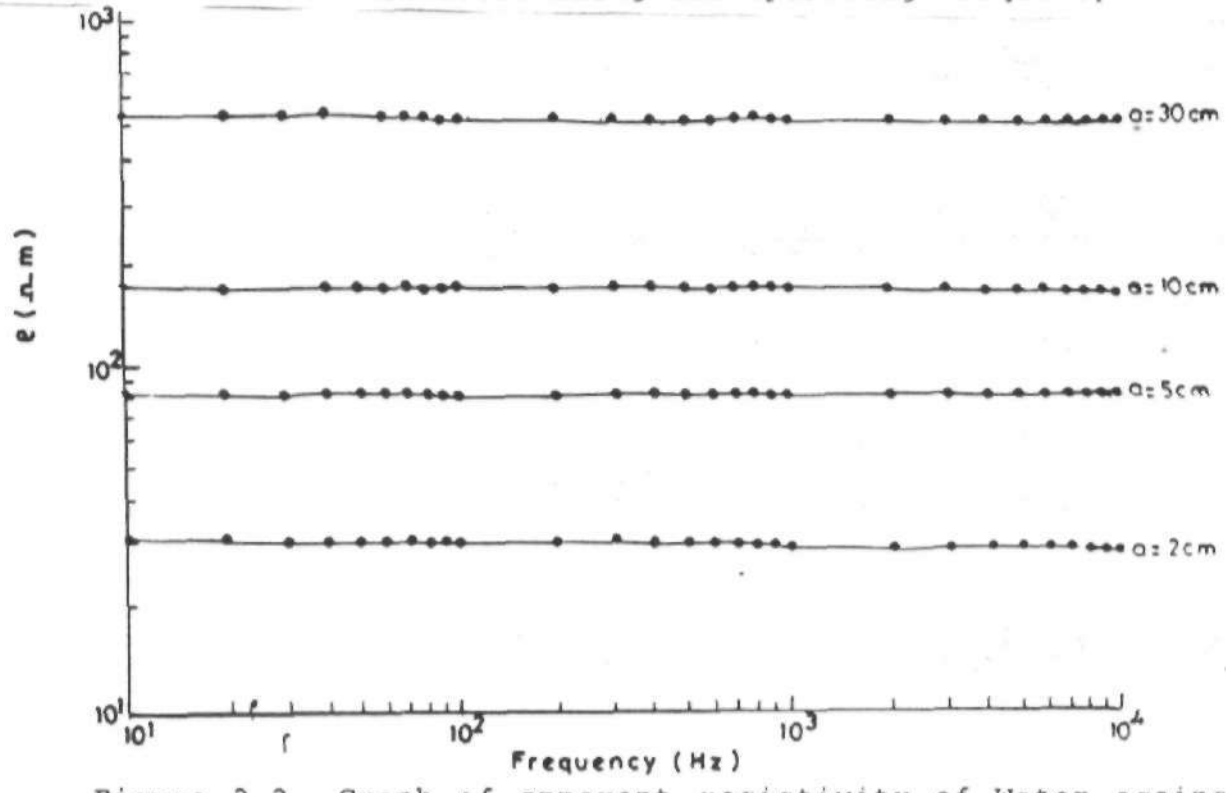


Figure 3.3 Graph of apparent resistivity of Water against frequency for Wenner array using different electrode spacings.

shown in figure 3.7 . Similar results for the lateritic clay, mixed-soil and river sand used in the experiment are shown in figures 3.4 to 3.6, and 3.8 to 3.10.

From figures 3.2 to 3.10 it can be seen that any frequency between 10Hz and 200Hz could be conveniently used in this experimental set-up except for the 0Hz and, the line source (50Hz) and its harmonics.

The capacitative coupling effect was also studied by observing the frequency response of the potential field distribution when a point source was placed in the tank water. From figure 3.11, iÇL can be seen that this capacitative coupling effect comes into play slightly within the range of 100Hz to 600Hz and becomes more pronounced at frequencies greater than 1000Hz. In the present set of experiments, a set of frequencies 0, 10, 20, 30, 40, 50, 60, 90 and 125Hz were tried in order to find out which one(s) gave the best result in terms of stability of readings and good alignment of computed resistivity values. Low-frequency values of 20, 30, 40 and 60Hz were found to give more stable readings than the other tried frequencies. However, in the end, all of the frequencies gave good alignment of the computed resistivity value. The best result was nevertheless given by the 40Hz frequency.

3.3.3 Experimental procedure

The set-up for conducting the model tank experiment is as shown in figure 3.1.

In the course of the experimentation, water - an electrolyte, was alongside with two major earth materials, namely lateritic clay and river sand, used as the major medium of experimentation. A subsidiary make-up earth material, here called mixed-soil, which was a mixture of

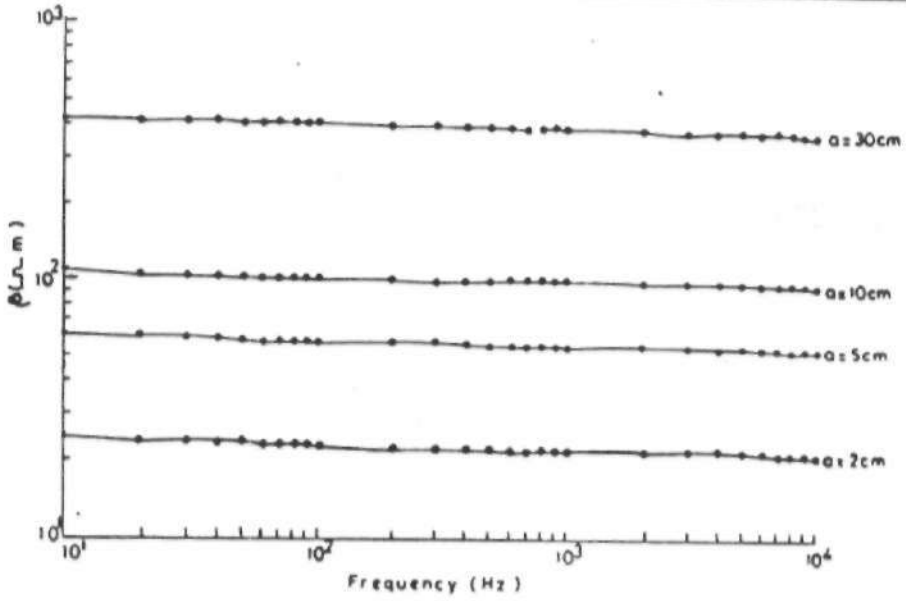


Figure 3.4 Graph of apparent resistivity of Lateritic Clay against frequency for Wenner array using different electrode spacings.

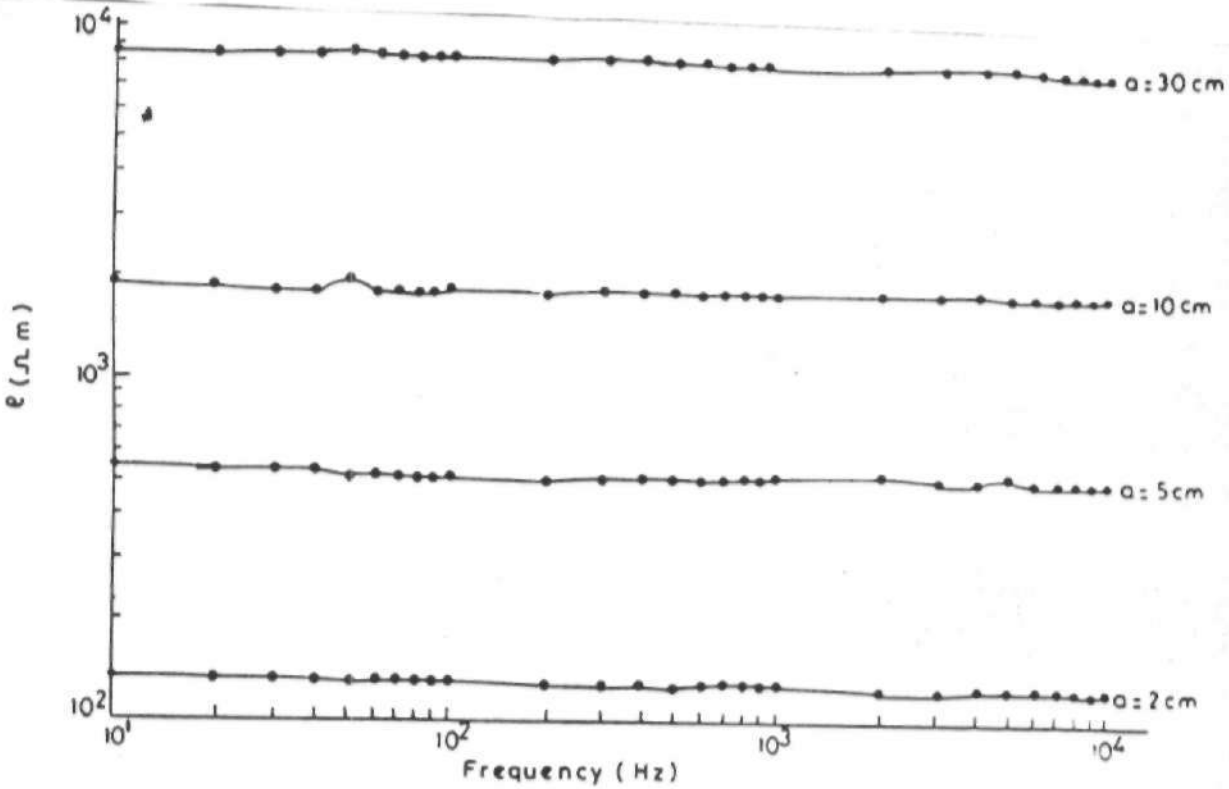


Figure 3.5 Graph of apparent resistivity of Mixed-soil against frequency for Wenner array using different electrode spacings.

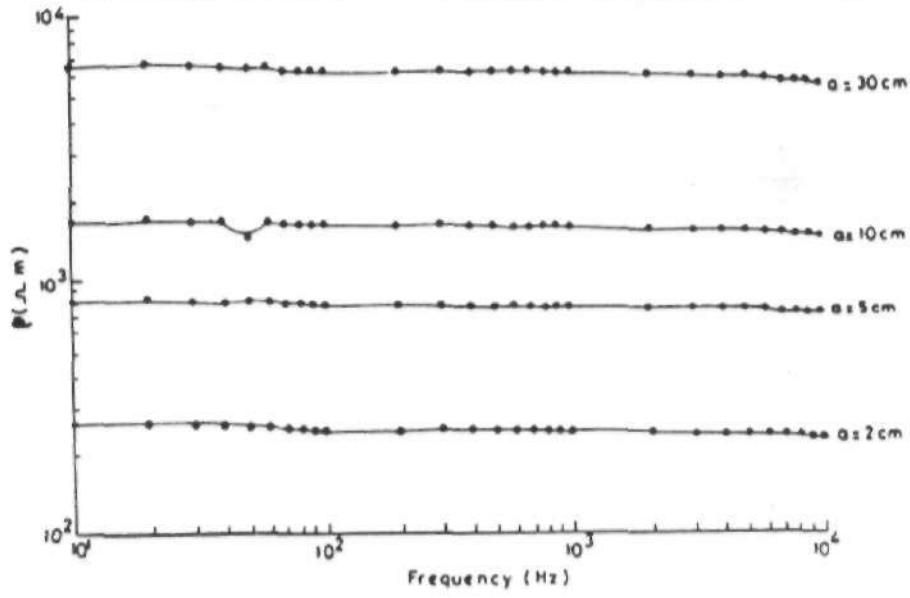


Figure 3.6 Graph of apparent resistivity of River Sand against frequency for Wenner array using different electrode spacings.

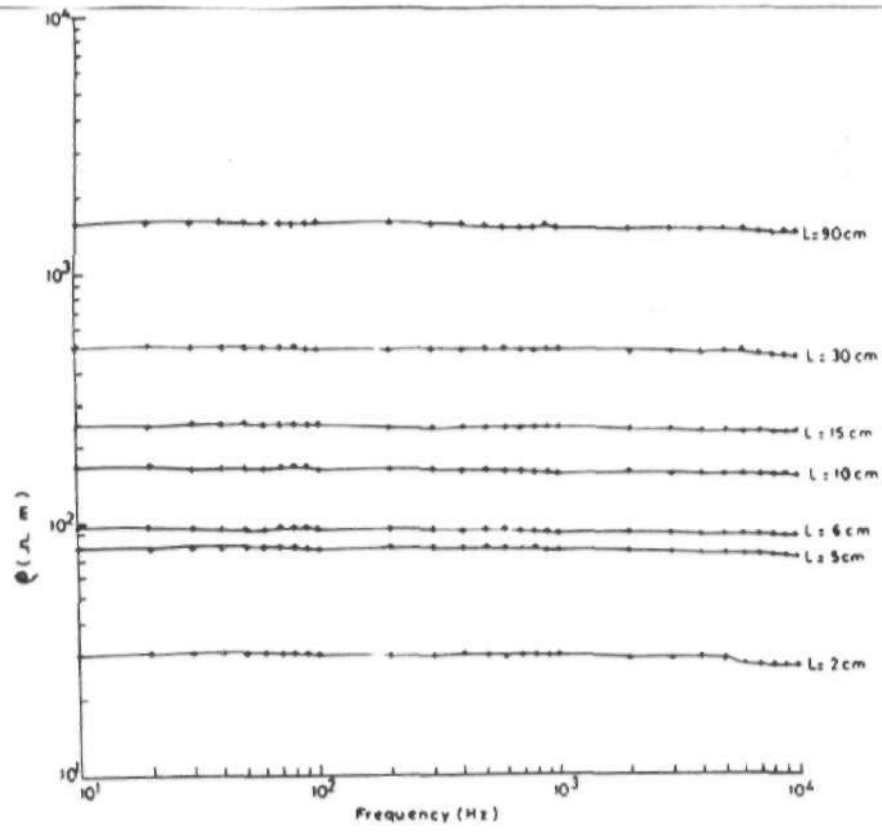


Figure 3.7 Variation of bulk resistivity with frequency for Water. (Two-electrode method)

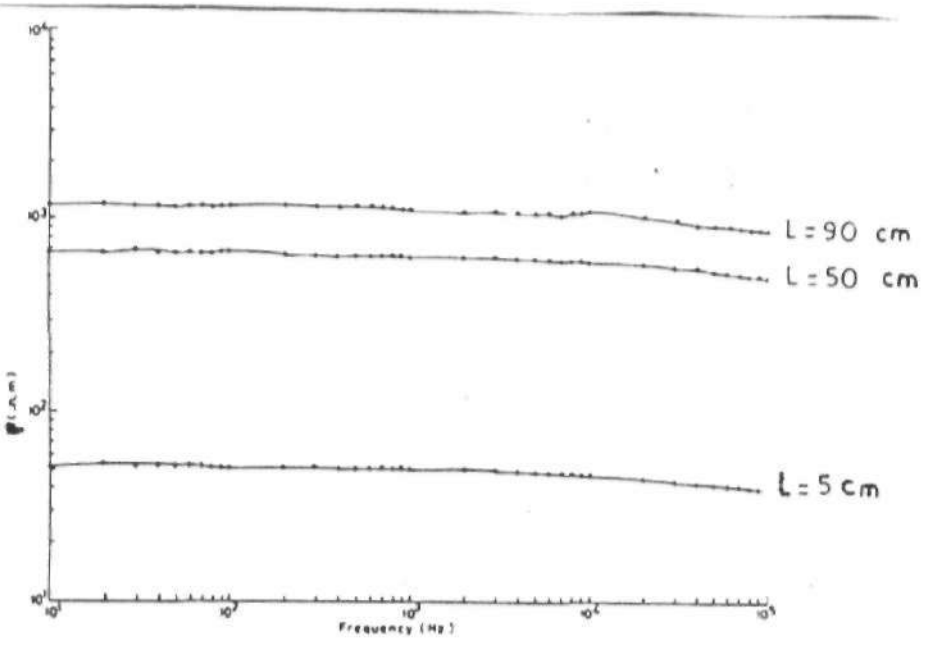


Figure 3.8 Variation of bulk resistivity with frequency for Lateritic Clay. (Two-electrode method)

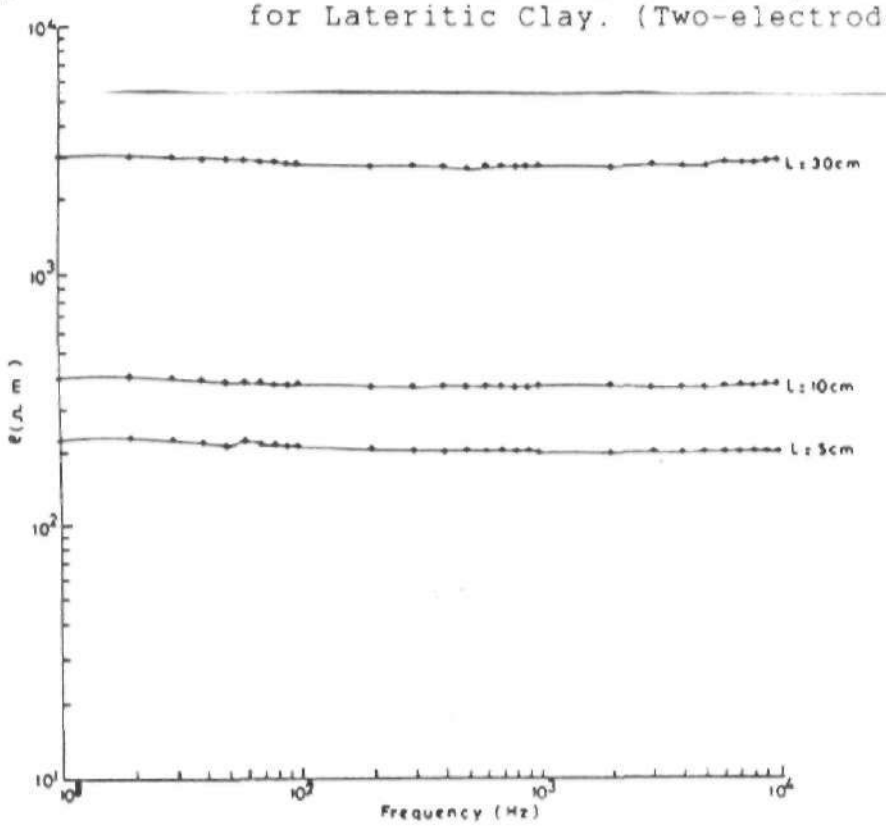


Figure 3.9: Variation of bulk resistivity with frequency for Mixed-soil. (Two-electrode method)

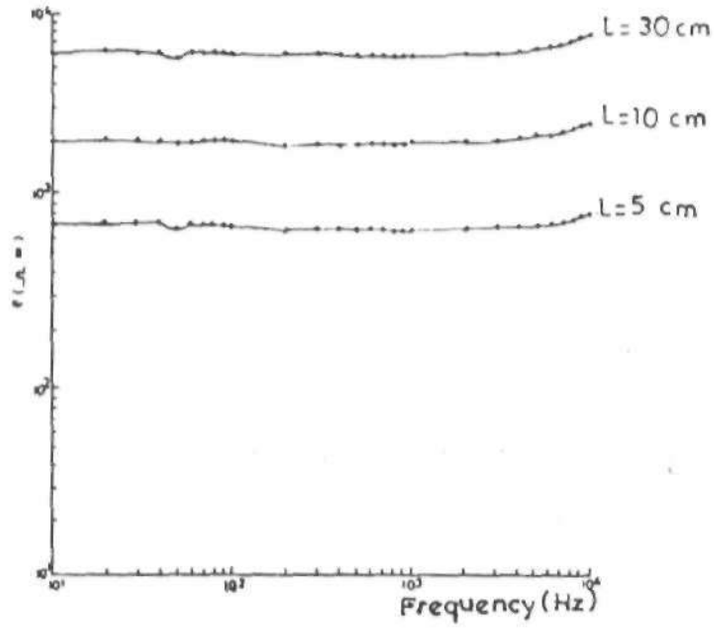


Figure 3.10 Variation of bulk resistivity with frequency for River Sand. (Two-electrode method)

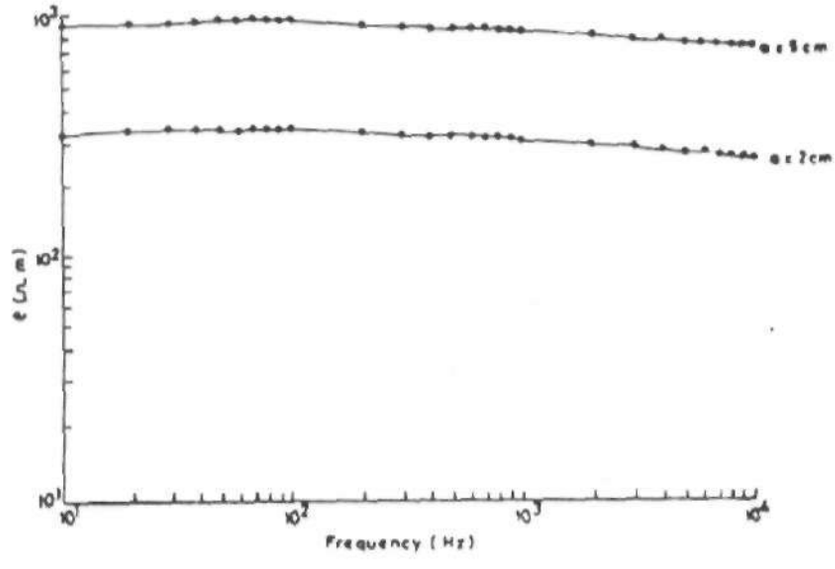


Figure 3.11 Graph of Apparent Resistivity against Frequency (using Wenner Array) to show capacitative coupling effect

lateritic clay and river sand in the ratio of 1 to 3 was also used to represent the material whose conductivity and resistivity lie between that of lateritic clay and river sand.

The lateritic clay was sourced from the Kubanni river basin. It was composed of fine, well-grounded particles of soil which were also clayey in nature. The lateritic clay formed the topsoil of the Kubanni river valley. It is part of the older remnants which are recognized by their reddish-brown cellular aspects and relative freedom from impurity (Wright and McCurry, 1970).

The river sand was equally sourced from the Kubanni river basin, directly from the river bed. It was composed of coarse grains with the grain size being between 0.25mm and 0.35mm in diameter. It formed part of the wash-off and sediment deposition along the bed of the main channel of the Kubanni river. Because of the grain size, it was very porous and therefore hardly retained water over a long period of time; most of the pore spaces were filled with air. This condition, coupled with the quartz content and composition of river sand made its resistivity to electrical flow of current to be very high.

In carrying out resistivity survey over the electrolyte/earth materials, the central part of the tank along the long axis of the tank was chosen as the profile length. Two methods were available for use. These were by:

-- Keeping an electrode fixed close to one end of the 100cm long axis and moving the other electrode(s), or

-- Starting at the 50cm mark as the central position, and expanding all the electrodes about this centre.

The first method was not used

-- because of the tank wall effect on current distribution from the fixed electrode placed close to the wall, much error might then accrue;

-- because the sounding point was always fixed, this method might not be the best for this work as each time the array was expanded, the sounding point was shifted.

In order to present a visible, easily interpretable analysis, a set of graphical output were proposed for the two-electrode method. These are

-- A plot of bulk resistivity against the electrode spacing, L.

This is easily observable from the expression

$\rho = aLV/I$

that is,

$$\rho = (aR)L \qquad \ldots\ldots 3.10$$

A change in the underlying layer resistivity from the resistivity of the overlying layer was expected to show up as a change in the slope of the graph.

-- A term called `normalized resistivity' (which was derived by dividing the bulk resistivity at the first electrode spacing by the bulk resistivity at each of the subsequent electrode spacings) was plotted against the reciprocal of electrode spacing, L.

This is easily seen using $\rho = aRL$ and $\rho_1 = aR_1L_1$

then,

$$\frac{\rho_1}{\rho} = \frac{R_1}{R}.\frac{L_1}{L} \qquad \ldots\ldots 3.11$$

which becomes

$$\left[\frac{\rho_1}{\rho}\right] \propto \frac{1}{L}, \quad \text{if } L_1 = 1.0 \qquad \ldots\ldots \quad 3.12$$

The same result as for equation (3.10) was expected.

-- The 'specific resistance' or 'specific resistivity' could be plotted against the electrode spacing, L.

The specific resistance, k, was derived using the expression of equations (2.52) and (2.53) where all the parameters are as defined in section 2.3.2 and 2.4. At each value of L, a new value of k was calculated. The values of k for a single homogeneous layer were expected to either be very close or equal at a set of values of L; it was equally expected that they might progressively vary at a low but constant rate in some cases particularly at the transition zones where a progressive ascent or descent was expected.

In all the processes mentioned above, the depth to interface and hence the thickness of a layer of interest could easily be found by estimating the value of L at which point a change in the slope of the graph was observed.

The procedure of interpretation was expected to be more favourable when the bulk resistivity was plotted against L on a log-linear graph scale.

3.3.4 Sources of error

Sources of error in electrolytic tank model studies may be classed into two major categories; these according to Mwenifumbo(1980) are

-- those due to inaccuracies in experimental techniques. and

-- those due to the inexactness of the analogy between the actual problem and that represented by the model.

The first group includes electrical circuit errors as well as mechanical and surface tension errors. In the second group are the polarization effects and boundary errors. This can as in this experiment, include errors due to the actual current flow pattern geometry as against the assumed geometry and also, the depth of investigation alongside the depth of current penetration.

In minimizing the electrical circuit errors, the following steps were taken

-- All cables were properly shielded and earthed so that no ground loops were introduced into the system.
-- The source and the measuring circuits were made to have a common ground in order to minimize the stray voltages induced from the mains.
-- Both the input and output voltage signals were monitored on the oscilloscope to ensure that they were relatively noise-free and to detect any phase shift.
-- The operating frequency of the source signal was chosen not to lie close to the 50Hz line frequency or to be a harmonic of the line frequency although for comparison of results, the 50Hz line frequency was also made use of.

Inaccurate positioning of the electrodes, inhomogeneity and misalignment of the electrodes normally constitute the bulk of mechanical errors encountered during an experiment of this nature. In the construction of the mechanical parts of the model tank, efforts were made to ensure that these errors were reduced to the barest minimum. To achieve this, it was ensured that all distances

could be measured to within 0.5mm at any given point within the tank and all distance measurements were referenced to the centre of the tank.

3.3.5 Precautions taken

Tank Wall Effect: In electrolytic tank model studies of `open' potential fields (fields in a half space), errors are introduced because the halfspace is terminated by the tank walls. The effects of the tank walls were assessed experimentally by observing the change in the potential field when the electrode system was moved towards the walls. A number of profiles were run along the central longitudinal line of the tank with both the Wenner array and the proposed two-electrode method. Figure 3.12 shows the electrode configuration and the relative positions of the electrodes with respect to the tank walls. Figure 3.13 shows the experimental apparent resistivity profile for the central longitudinal line using the Wenner array and the experimental resistivity profile for the same line using the two-electrode method. In assessing the side wall effects, it was assumed that the bottom of the tank was of sufficient depth so that its effects on the surface potentials were negligible. The long side walls of the tank were treated as perfectly insulating planes of infinite extent.

The experimental results for electrode spacings of 2cm and 10cm are also shown in figure 3.13. From the graphs, there is almost not much evidence to show that the short side walls have much effect on the resistivity value at considerable distances from the walls. For the 2cm electrode spacing, the closest distance of investigation from the wall was about 6cm while it was about 25cm for the 10cm spacing in the case of the Wenner array. For the two-

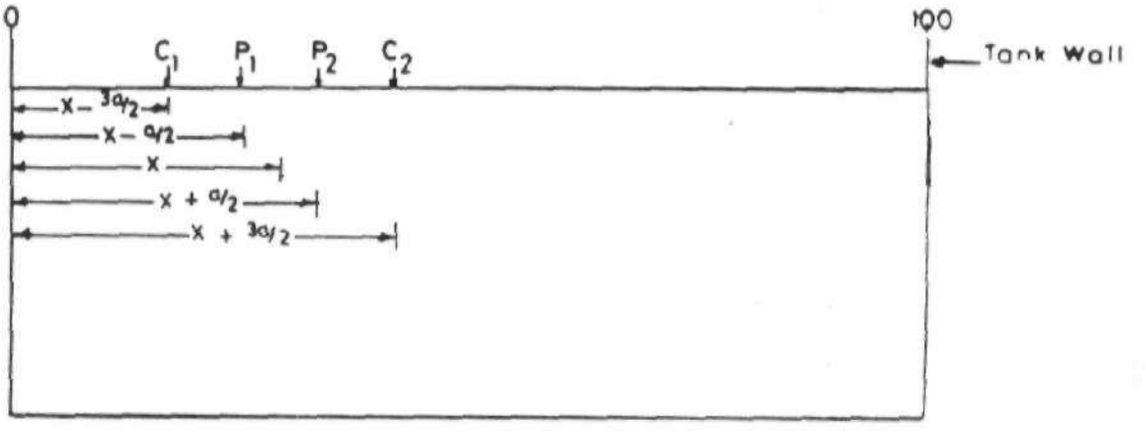


Figure 3.12 Relative Positions of Electrodes with respect to the Tank Walls for Wenner Configuration

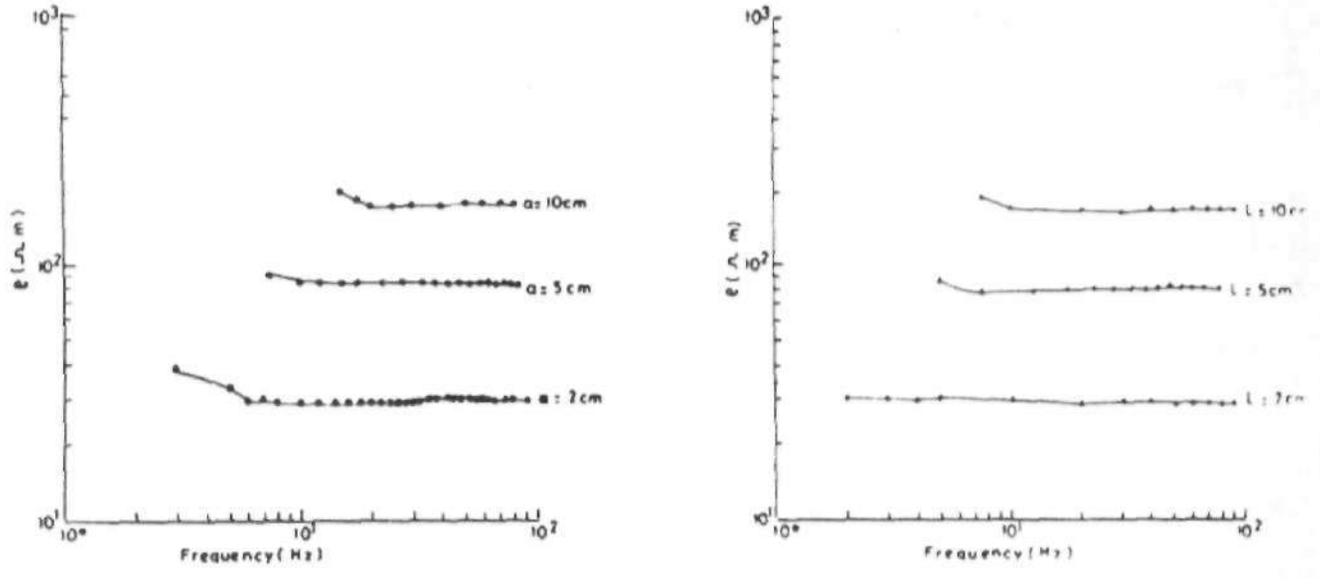


Figure 3.13 Graph of resistivity against frequency for investigating the side tank wall effect

electrode method , the closest distance of investigation from the short side walls was about 2cm for the 2cm electrode spacing while it was about 10cm for the 10cm electrode spacing.

The effects of the bottom of the tank were equally investigated experimentally. This was done by running a number of profiles along the central longitudinal line of the tank using the Wenner array. The electrode spacing, A, was chosen in relation to the depth, Z, of the water in the tank. Each time the water depth was reduced, the choice of A to Z was accordingly adjusted so that relatively large number of readings could be taken. For each profile, Wenner depth sounding was made. Figure 3.14 shows the graphical results of this investigation for the Wenner array depth sounding, with the centre of the sounding situated at the centre of the tank. It could be seen from figure 3.14 that the influence of the bottom of the tank came into effect when the ratio of the electrode spacing to the depth of the bottom of the tank from the water surface (that is, A/Z) was greater than 0.14. The effects of the bottom floor of the tank were investigated under the assumption that the side walls were of negligible effect.

In the subsequent discussion of the results, all the experiments were conducted well within the region that was relatively free of tank wall effects.

Control Experiments: In order to check and control the reliability of the present modelling experiment, a number of control experiments were conducted. These control experiments were actually conducted in order to access guide resistivity values of the electrolyte/earth materials and therefore ensure the reliability of observed data.

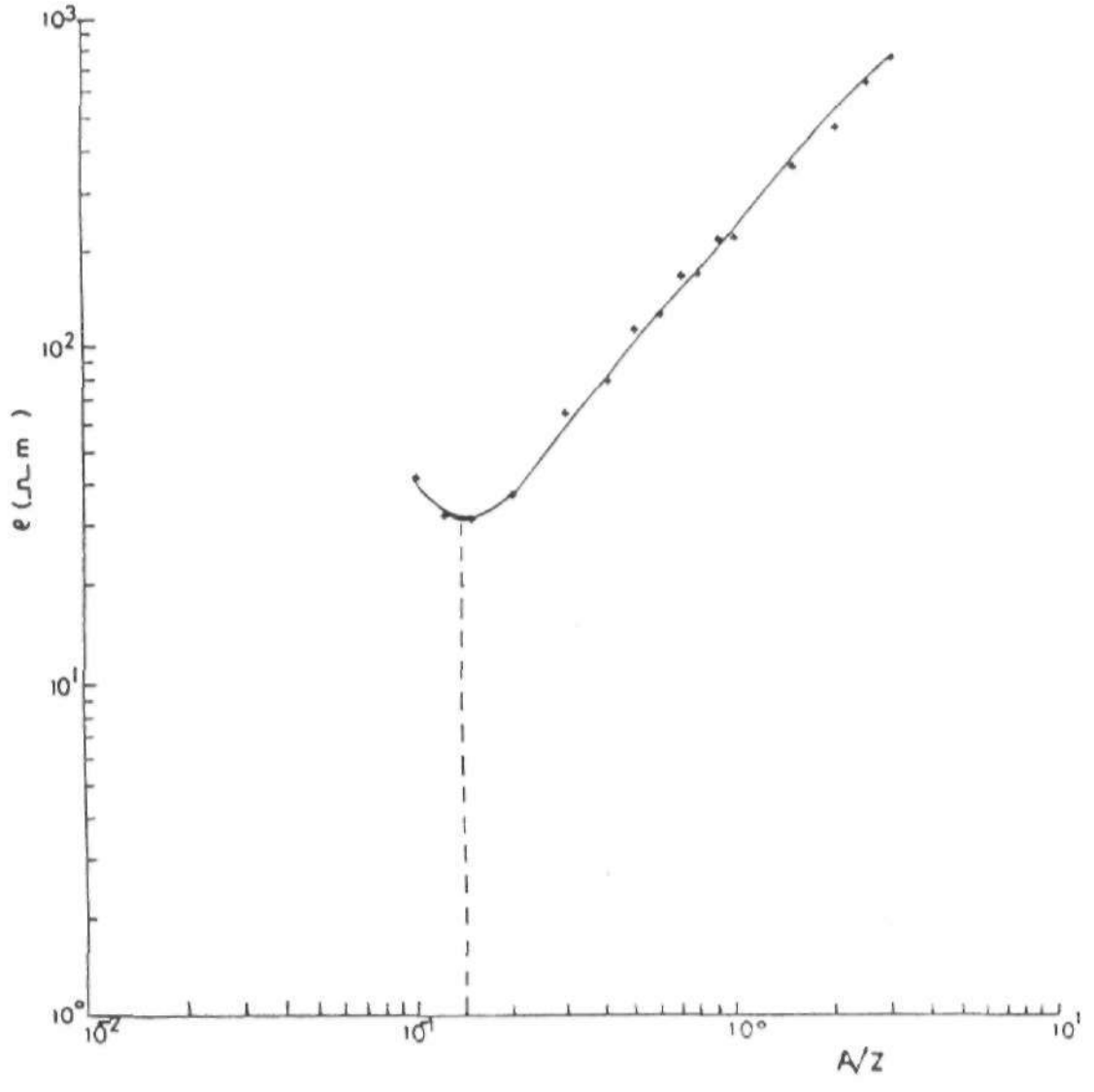


Figure 3.14 Graph of resistivity against A/Z for investigating the effect of the bottom of the tank.

The following describes and explains the control experiments:

Determination of Water / Earth Material Resistivity:

-- The resistivity of the water in the tank was determined by running a profile along the central longitudinal traverse of the tank. The experiment was performed using both the Wenner array and the proposed two-electrode configuration with electrode spacings a = L = 2cm, 5cm, and 10cm. The results of these are shown in figure 3.15.

Under normal and ideal circumstances, a conductivity bridge should have been used alongside this method for comparison purposes. Due to the non-availability of the conductivity bridge, these values were however compared with results obtained using a laboratory type metre bridge and the tube method. The results of these are shown in Table 3.2. Similar procedure was done for the other earth materials.

-- The electrolyte/earth material was first tightly packed in an open-ended cylindrical glass tube to whose ends were affixed two metal plates of the same diameter as the internal diameter of the cylindrical glass tube as shown in figure 3.16. For this geometry, it was quite easy to calculate the dimensional parameters and hence determine the resistivity of the enclosed material. The result of the resistivity value so determined was expected to give the true rather than the apparent resistivity of the earth material

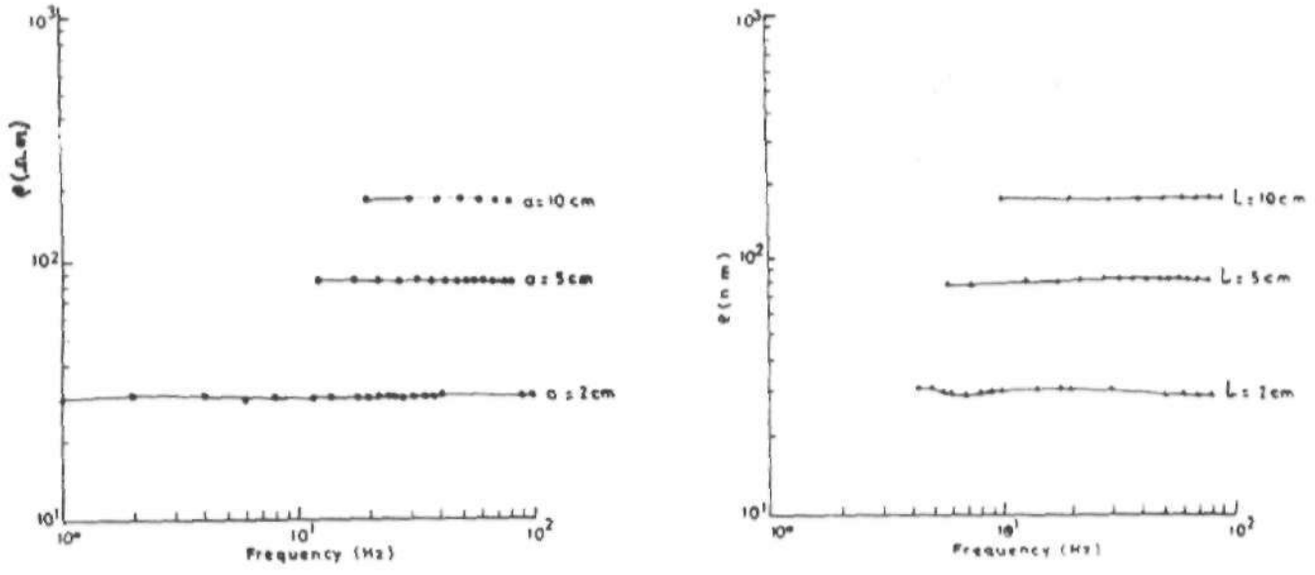


Figure 3.15: Graph of resistivity against electrode spacing showing the value of water resistivity (for Wenner and Two-electrode Arrays).

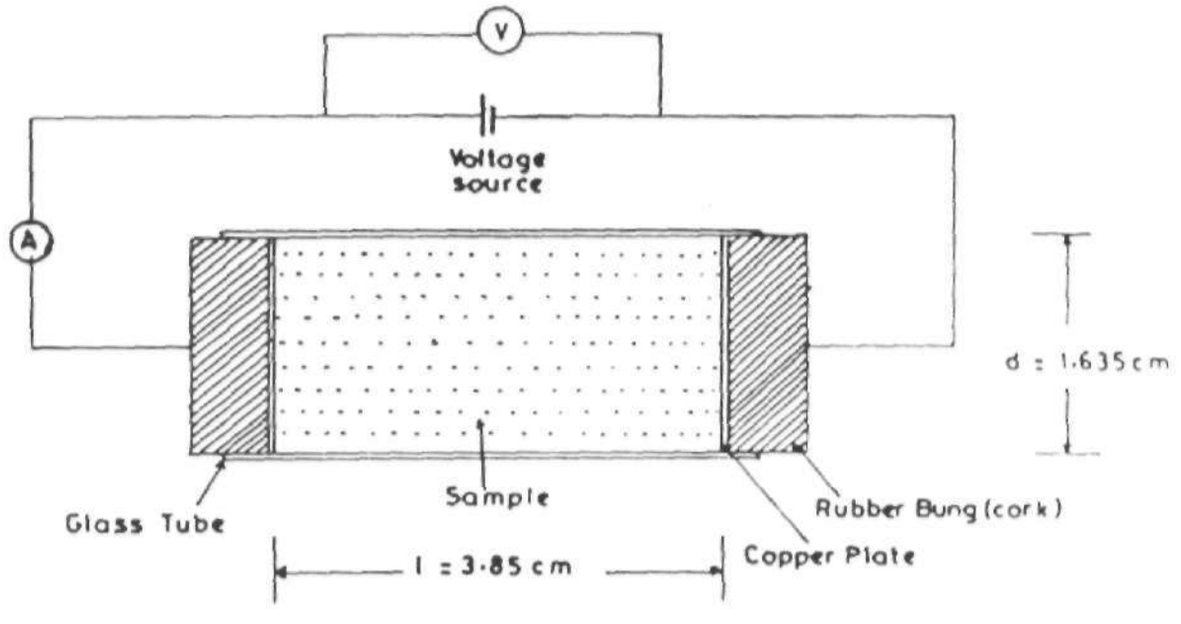


Figure 3.16 Experimental setup for determining the actual resistivity values of samples used

enclosed. It was therefore aimed at serving as the true guide value for this parameter. Connecting leads were passed to the metal plates through rubber bungs which served as corks. The average internal diameter, d, of the tube was 1.635 cm while its effective length, l, after being filled with the electrolyte/earth material and closed up was about 3.85cm. Low frequency a.c. or pure d.c. was then passed into the tube arrangement. The voltage drop V, across the terminals and the amount of current I, flowing through were then taken. This method is hereafter called the Tube Method.

The expression of equations (1.27b) and (2.1), that is, $R = V/I$ was used to compute the average resistance, R of the electrolyte/earth material enclosed in the tube. Similarly, noting that the cross-sectional area

$$A = \pi d^2/4 \qquad \ldots\ldots \quad 3.11$$

and, substituting this in the expression of equation (2.2) that is, $\rho = RA/l$, the equation

$$\rho = \pi Rd^2/4l \qquad \ldots\ldots \quad 3.12$$

that is,

$$\rho = 0.5453366 \times 10^{-2} R \qquad \ldots\ldots\ldots \quad 3.13$$

obtained after the substitution of the numerical values of R, d and l was used to compute the average true resistivity, ρ, of the electrolyte/earth material enclosed in the tube. This method was applied on the electrolyte and all the earth materials namely, water, lateritic clay, river sand and mixed-soil, used in this experimentation.[IXAI] The numerical results of

resistivity values obtained are shown in Table 3.2.

Typical calculation, for water, is given below:

V = 9.97 volts; I = 143.7 mA

therefore $R = V/I = 6938.8\ \Omega$

from which

$\rho = 0.5453366 \times 10^{-2} \times 6938.8 = 38\ \Omega\text{-m}$

-- Instead of passing pure d.c. or low-frequency a.c. directly into the tube arrangement used above, the terminals of the tube were connected to a metre bridge with the contents of the tube as the unknown resistance, X. This was balanced by a choice of known resistance, R on the metre bridge. A d.c. source was used.

-- The corresponding values of L (the distance of the balance point from the end of the bridge wire where the unknown resistance was connected) were obtained. A graph of R against (100-L)/L was plotted and the mean line through the points was drawn. The slope of the graph was then calculated to give the value of the unknown resistance X.

The resistivity of the electrolyte/earth material was calculated using the expression.

$$\rho = aX/l \qquad \ldots\ldots \quad 3.14$$

where ρ - the resistivity of the earth material

a - cross-sectional area of the tube

l - effective length of the tube

TABLE 3.2 Computed Resistivity Values using Wenner, Two-Electrode, Tube and Metre Bridge Methods.

	Resistivity Values (Ωm)			
	Wenner	Two-Electrode	Tube	Metre Bridge
Water	31	34	38	40
Lateritic Clay	33	32	34	33
River Sand	844	1000	1721	4788
Mixed-soil	524	217	245	55

3.4 Data Processing

In the use of electrical method of geophysical prospecting, two distinct bedding cases can be considered; these are the horizontal bedding and the dipping bedding. Horizontal bedding has been given by far, the greatest attention in electrical prospecting for two reasons: firstly, the mathematics for the horizontal-bed problem is relatively simple. Secondly, the problem of determining the depth to horizontal or nearly horizontal beds is of great economic importance in petroleum exploration, groundwater and engineering problems. The electrical theory for horizontal bedding has had more success in groundwater and engineering problems, which usually involve finding the thickness of overburden or finding the depth to a shallow key horizon, than in petroleum exploration problems which usually involve key horizons at relatively great depths (Van Nostrand and Cook, 1966).

The general problem of resistivity prospecting in plane parallel boundaries is developed by assuming that all of space is divided into a large but finite number of regions each of which is bounded by parallel planes; each of all the finite regions has different values for the resistivity and thickness.

There are basically three schools of thought on electrical prospecting for horizontal beds; these are, the

curve-matching, the empirical, and the direct-interpretation schools. The curve-matchers assume a geological situation and construct a theoretical resistivity curve based upon that assumption. Although these assumed conditions and theoretical curves can be organized into charts to cover a wide range of conditions even before the fieldwork is done, this method is essentially one of trial and error (Van Nostrand and Cook, 1966).

In the empirical school approach (Van Nostrand and Cook, 1966), field curves are first obtained. If there is a good geological control, the salient features of the curves are then related to known geological contacts. Such features consist of maxima, minima, inflection points, and incongruous breaks in the curves. They then try to follow the geological contacts away from the region of control by observing the behaviour of the resistivity curves in the new regions. Otherwise, they examine the series of field curves for `breaks' which seem to persist in all the curves. These breaks are then attributed to some horizontal discontinuity in resistivity at a depth corresponding to the electrode separation at which the break occurs.

The direct-interpretation school, which was started by the work of Slichter in 1933, involved the use of the measured resistivity data in a mathematical operation to determine directly the horizontal layering which gave rise to the data (Van Nostrand and Cook, 1966). By `direct interpretation' is meant a method in which the measured potentials or measured resistivities are used in some mathematical process to determine directly the actual resistivity of the earth as a function of depth. Noted is

the fact that direct interpretation techniques require a tremendous amount of computation time.

The processing and analysis of electrical geophysical data collected using common electrode configurations such as the Wenner and the Schlumberger arrays among others become relatively easy because of the availability of adequate interpretation techniques for such systems. The non-availability of such interpretation technique for either the arrangement developed by Roy and Apparao (1971) or for the arrangement worked on in this treatise make the full interpretation of the results of this work much more tedious.

It must be stressed again at this point that, as earlier stated, the scope of this work does not extend to the realm of either developing a suitable field instrument for the arrangement, or developing an interpretation technique for the arrangement. The exact aim of conducting this experiment was to find out if this arrangement was capable or incapable of delineating horizontal layerings within the earth structure between the top surface and the basement.

The solution of electrical resistivity problem using the direct interpretation technique assumes a single current electrode on the surface of an earth in which the resistivity varies with depth. The applicability of Laplace's equation is also assumed. The conductivity is assumed to vary with depth only. According to Keller and Frischknecht (1966), the resistivity of the earth may vary in the vertical direction according to the law

$$\rho_z = \rho_1 e^{\pm \alpha z} \qquad \ldots\ldots 3.15$$

where ρ_1 - the resistivity of the surface layer

z - the layer thickness

and α- a parameter defining the rate of increase (or decrease) of resistivity with depth

In solving electrical resistivity problem across an interface, two conditions, according to Van Nostrand and Cook (1966), become very important

-- there must be a continuity of the potential or the appropriate function at all points in space except at the current source;

-- the normal component of current density or the appropriate function at the boundaries must also be continuous across the boundaries.

Within the earth structure, there is no sharply defined boundary between adjacent layers but rather there is a gradual gradation of one layer into another. There is therefore a gradual continuation of conductivity and its derivative to a certain extent across the interface. Hence, the interpretation of the two-electrode array hinges much on the manipulation of equation (3.15) and its derivative.

Pekeris (1940), gave the procedure for determining the variation of conductivity with depth for the case of a horizontally layered earth. Pekeris gave the function to be used in locating the m^{th} boundary as

$$f_m(\lambda) = \frac{k_{m-1}[e^{-2\lambda t_{m-1}} f_{m-1}(\lambda) - k_{m-1}k_{m-2}]}{k_{m-2} - k_{m-1}e^{-2\lambda t_{m-1}} f_{m-1}(\lambda)} \quad \ldots.3.16$$

$$\text{where } k_m = \frac{\rho_m - \rho_{m-1}}{\rho_m + \rho_{m-1}} \quad \ldots.3.17$$

$$\text{and } t_{m-1} = z_m - z_{m-1} \quad \ldots.3.18$$

t_{m-1} - is the thickness of the (m-1)th bed.

λ - is a constant parameter of Slichter's "kernel" $k(\lambda)$ having the dimension of L^{-1}, and varying between 0 and ∞

In addition to the large amount of computations involved, one of the possible objections to the direct method of interpretation is the difficulty of measuring the potentials sufficiently accurately in the neighbourhood of an isolated current electrode. This difficulty is especially serious for points at some distance from the electrode if the effects of greater depths are sought (Van Nostrand and Cook, 1966).

The type of analysis as given by Pekeris (1940) would have been the easiest and most suitable for this mode of the two-electrode array if it were possible to express the potential distribution in terms of the Wenner-type potentials.

Sanker Narayan and Ramanujachary (1967), proposed a simple direct method using graphical approach. The method used the general expression for apparent resistivity as measured by any electrode configuration, that is,

$$\rho_a = KR \qquad \ldots.3.19$$

where K is the geometric factor having the dimension of length.

$$\frac{1}{\rho_a} = \frac{1}{KR} \qquad \ldots.3.20$$

Using K = cL, where c is a constant, the expression

$$\frac{L}{\rho_a} = \frac{1}{cR} \qquad \ldots.3.21$$

was arrived at for the Wenner array. When a plot of 1/cR against L was made, a straight line graph was obtained. The graph had a slope of $1/\rho$ and passed through the origin. The point of intersection of adjacent segments of the graph projected on the L axis gave the depth to interface. The intercept on the 1/cR axis gave $h_i[\rho_{i+1}-\rho_i]/\rho_i\rho_{i+1}$.

As a result of the failure of computational methods to correctly estimate the layer resistivity values, due to the fact that the exact nature of signal transfer and the interdependency between these layers are not well known, effort was made to estimate these values directly from the graph. A simple graphical analysis was employed to determine the layer resistivities and thicknesses in this work. The following sets of graphical approaches were attempted:

-- plotting the linear-linear graph with the normalized resistivity on the vertical axis and the reciprocal of the electrode separation on the horizontal axis;
-- plotting the log-log graph with the bulk resistivity on the vertical axis and the electrode separation on the horizontal axis;
-- linearizing the positive aspect of equation (3.15) logarithmically to obtain

$$\log\rho_z = \alpha z + \log\rho_1 \qquad .....3.22$$

if $z = L$, then

$$\log\rho_L = \alpha L + \log\rho_1 \qquad .....3.23$$

A graph of the bulk resistivity ρ_b at electrode separation L was therefore plotted against L. Plotting this on a semi-log graph, implies that the intercept of the first segment on the vertical axis is the resistivity ρ_1 of the top layer. The nature of the graph is as shown in figure 3.17. In the graph of figure 3.17, the following representations are made

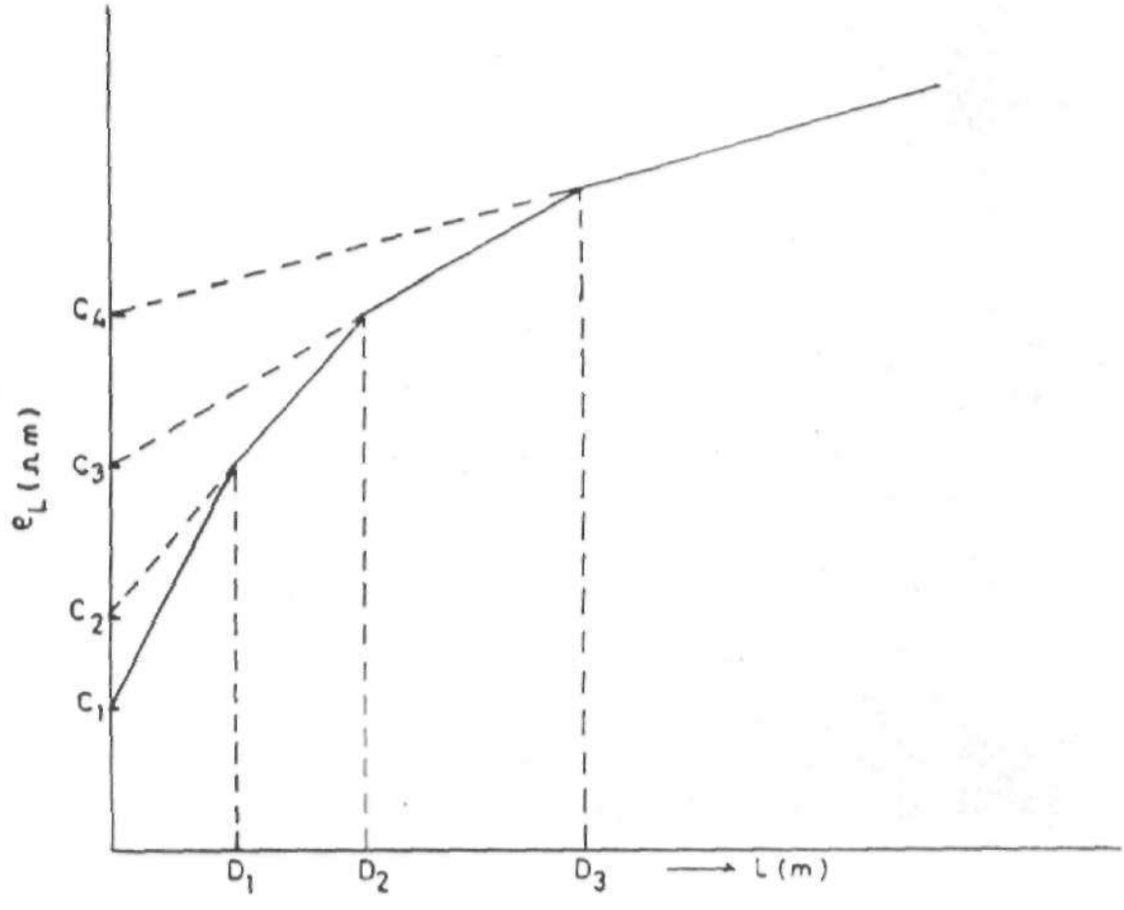


Figure 3.17 Graph of bulk resistivity against electrode spacing on log-linear scale for a four layered earth model

$D_2 = d_1 + d_2$
$D_3 = D_2 + d_3$
$D_n = D_{n-1} + d_n$
d_1 - thickness of the first layer;
d_2 - thickness of the second layer;
d_3 - thickness of the third layer;
d_n - thickness of the nth layer;

The layer thickness was estimated on the L axis as the value of L at which two layers/graph segments intersect or, where there was a change of slope value. From the sketch, c_1 is correctly estimated as the resistivity of the first layer. In all the models, this estimate of the top layer resistivity was in close agreement with the values obtained using any of the earlier mentioned methods such as the tube and the metre-bridge methods. It is viewed that the observed response over the second layer does not represent only the response of that layer to the input signal but represents the total response of the layer and of the overlying layer(s). The exact nature of signal response, partition and contribution by each layer was not known but it is assumed here that the intercept c_2 represents the average resistivity of the first and second layers. The same holds for c_3, c_4, and so on.

In estimating the layer resistivity, a simple graphical method of analysis was adopted thus:

Considering say, the equations of the first and second layers, that is,

$y_1 = s_1x + c_1$, for the first layer,
and $y_2 = s_2x + c_2$, for the second layer.

For the two equations to represent the same layer, albeit with a little shift of origin or intercept, then, they must

have the same inclination. The second equation need then to be steered and linearized along the first equation. This results in a situation whereby

$$s_1x + [c_1] = s_2[s_1/s_2]x + [c_2] \quad \ldots 3.24$$

that is, $s_1x = s_2[s_1/s_2]x + [c_2 - c_1]$

with c_1 and c_2 ignored.

It is here adduced that where graphically two adjacent layers lie parallel to one another, although segmented, they both represent the same layer in which there could likely have been a vertical faulting of the layer. Both sides of equation (3.24) have the same slope. The ratio s_1/s_2 is here called the straightening factor or slope index of the adjoining layers. This deduction was used in estimating the layer resistivity values from the top layer to the basement. In which case, the departure of the underlying layer from the direction of linearization of the overlying layer was sought after. The straightening factor is therefore the measure of this departure. For both the model study and the field study, the layer resistivity values were estimated from the log-linear graph plot of bulk resistivity against electrode spacing.

In estimating the layer resistivity values graphically, the following steps were taken:

The expected resistivity values were classed as

-- low, if resistivity value lies between 1 Ω-m and about 100 Ω-m;

-- medium, if resistivity value lies between 100 Ω-m and about 400 Ω-m;

-- high, if resistivity value was greater than 400 Ω-m;

-- moderately high, if resistivity value lies between 400 Ω-m and about 800 Ω-m;
-- very high, if resistivity value was greater than 800 Ω-m;

The intercepts of the layers on the vertical axis were read off from the graph

-- the intercept of the first layer on the vertical axis was taken as the resistivity of the first layer;
-- the intercepts of the underlying layers down to the basement were compared with the computed layer resistivity values.

The slope index relationship of the basement to the immediate overlying layer was observed with the understanding that

-- if the index is low, then the immediate overlying layer is of either medium or high resistivity depending on the index value;

-- if the index is high, then the immediate overlying layer is of either low or medium resistivity depending on the index value.

Two possible conditions for discrimination namely the closeness and negativity of slope values, which equally appeared to be naturally imposed were applied in fixing the position of the basement.

-- The basement is positioned where the slope value of the underlying layer become either very close to that of the overlying layer or positioned immediately above the layer having a negative slope value.

Using the basis of the knowledge of the top layer resistivity and the slope index relationship of the basement to the immediate overlying layer, a construct for the intermediate layer(s) was then made to take into account the observations mentioned and therefore compose the best possible combination that could give shape to the observations.

Similar expressions as in equation (3.24) were expected for the third and fourth layers and beyond for layers that are more than two in composition.

The layer resistivity computation procedure is shown in Appendix A3.

According to Mwenifumbo (1980), the interpretation of the results of the model structure may be a little different from the interpretation of the actual field results. Moreover, the accuracies may be greatly varied. This is necessitated by the fact that more constraints are introduced into the model studies than is usually obtainable in the real earth situation. The implication of the above statement is therefore that a wide variation in accuracies of the results between the model study and the real earth situation is not impossible.

3.5 Typical Model Data and Results

Data collected in the model study are presented. The data show the variation of voltage V, and current I, with changes in the electrode separation L, using the proposed two-electrode method. Also presented is the interpreted result over each composition. The results were mainly derived from the graphical plot of the bulk resistivity against electrode separation.

3.5.1 Two-layer cases (single overburden)

Water over Perspex:

TABLE 3.3 Typical Model Data for Water over Perspex

L(m)	V(v)	I(mA)
0.05	7.02	1.247
0.10	7.02	1.172
0.15	7.02	1.186
0.20	7.02	1.143
0.25	7.02	1.162
0.30	7.02	1.124
0.35	7.02	1.138
0.40	7.02	1.112
0.45	7.02	1.103
0.50	7.02	1.141
0.55	7.02	1.134
0.60	7.02	1.290
0.65	7.02	1.248
0.70	7.02	1.220
0.75	7.02	1.171
0.80	7.02	1.193
0.85	7.02	1.153
0.90	7.02	1.162

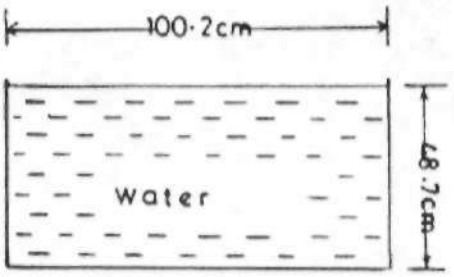


Figure 3.18 Water in model tank

Figure 3.19 shows the plot of the bulk resistivity against electrode spacing for the single overburden case of table 3.3 with water as the electrolyte/material medium.

From the plot, it could be seen that there was no segmentation of the first part, the first part is an exponential curve, only the points in the second part approximated to a straight line. The first part connected the second part at a point which is about the thickness of the first layer. Since the first layer is perfectly homogeneous, the exponential curve observed was not unexpected; it is in consonance with equation (3.15). The resistivity of the first layer was estimated to be 34.ohm-metres at the point where the curve intercepted the vertical axis. In the original experiment of figure 3.18, the thickness of water in the tank was 48.7cm. From figure (3.19), the thickness of water was estimated to be 49.0cm

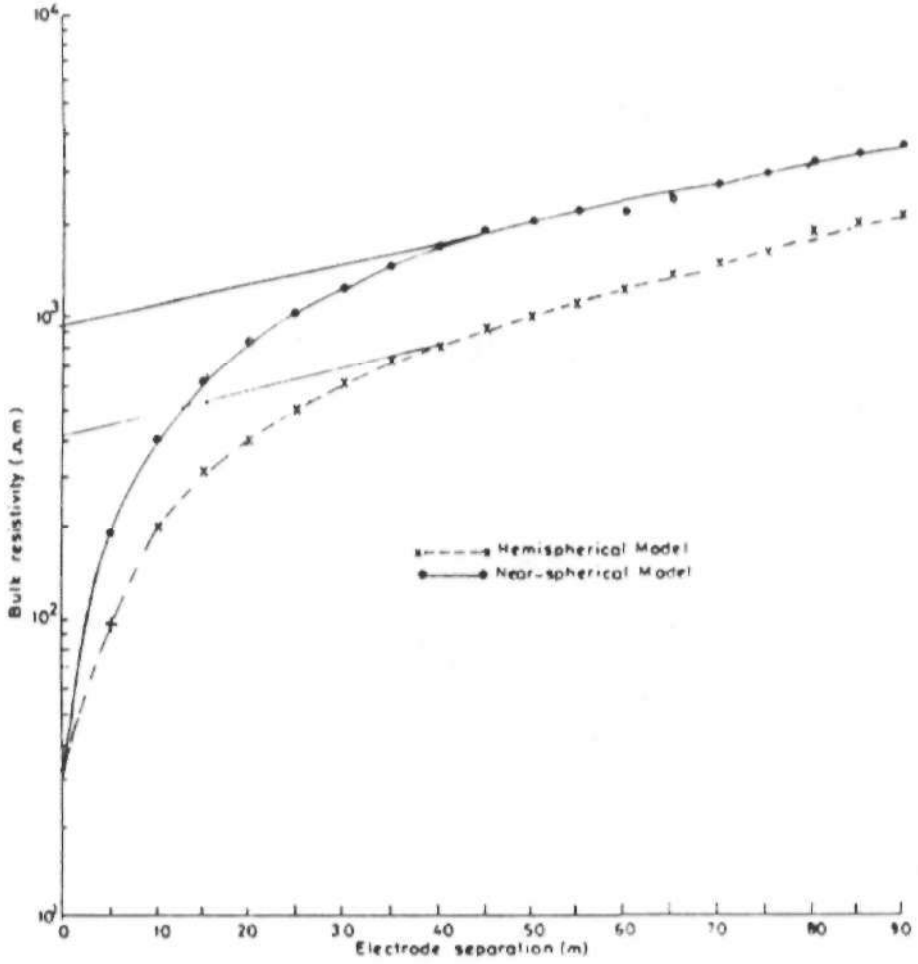


Figure 3.19 Graph of bulk resistivity against electrode spacing for water on perspex

at the point of intersection between the first part and the second part. This is only an error of about 0.62%.

The water resistivity value of 34. ohm metres obtained from the graph of figure (3.17) compared favourably well with the 30.8 Ω-m obtained using Wenner profiling (a = 2cm), and the 37.8 Ω-m obtained using the tube. It is equally not too far from the 40.4 Ω-m obtained using the metre bridge method.

Lateritic Clay over Perspex:

TABLE 3.4 Model Data for Lateritic Clay over Perspex

L(m)	V(v)	I(mA)
0.05	9.87	1.838
0.10	9.85	1.810
0.15	9.86	1.624
0.20	9.86	1.596
0.25	9.86	1.547
0.30	9.86	1.563
0.35	9.87	1.520
0.40	9.89	1.490
0.45	9.89	1.478
0.50	9.88	1.445
0.55	9.88	1.593
0.60	9.89	1.493
0.65	9.89	1.803
0.70	9.90	1.763
0.75	9.88	1.554
0.80	9.88	1.735
0.85	9.88	1.692
0.90	9.88	1.593

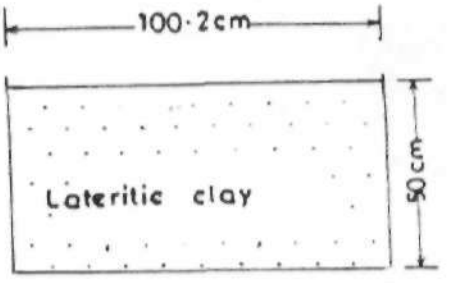


Fig. 3.20 Lateritic Clay in model tank

Figure 3.21 shows the plot of bulk resistivity against electrode separation for the single overburden case of table 3.4 with lateritic clay as the material medium.

Like in figure 3.19, there is no segmentation of the first part of the graph in figure 3.21 while the points in the second part approximated to a straight line. This is the basement. The first part is an exponential curve; its resistivity was estimated to be about 32.0 Ω-m. This value is in close agreement with 32.5 Ω-m obtained with Wenner

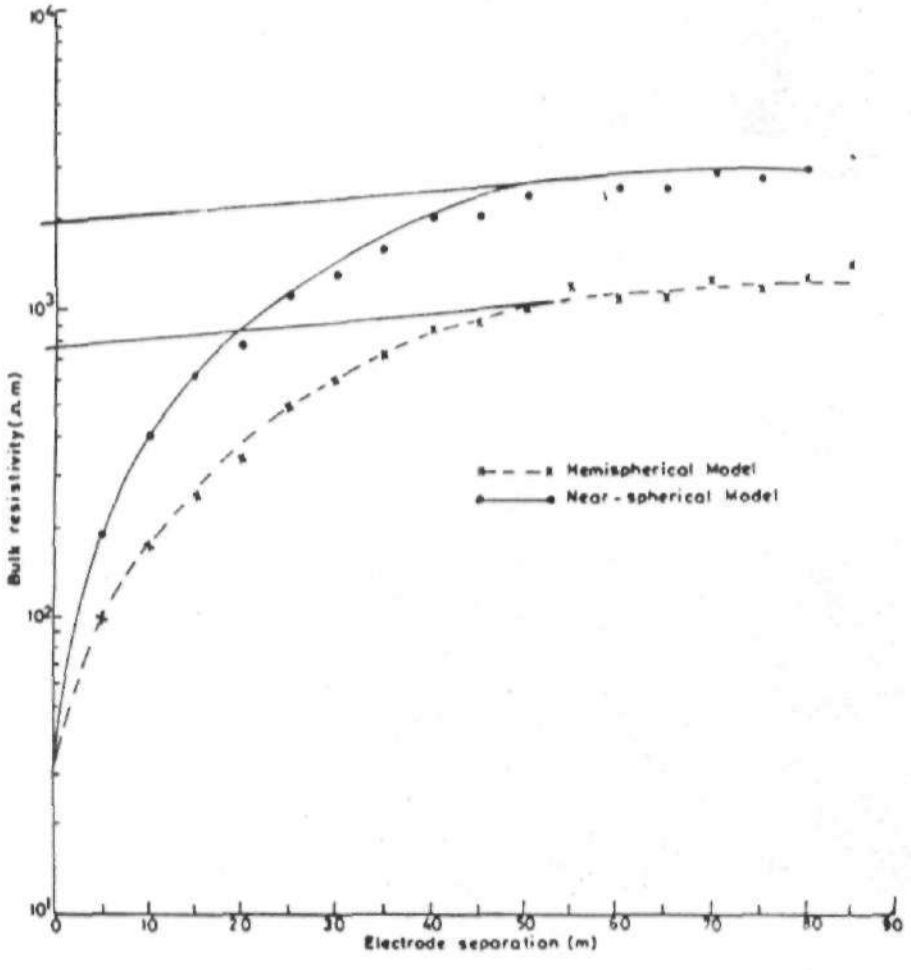


Figure 3.21 Graph of bulk resistivity against electrode spacing for lateritic clay on perspex

profiling (a = 2cm), 33.9 Ω-m obtained using the tube, and 33.0 Ω-m obtained using the metre bridge.

In the original experiment of figure 3.20, the lateritic clay emplaced was 50cm thick. From the graph, the first part intersects the second part at the 51.0 cm point. This means that the layer thickness as read from the graph was only about 2.0% in error.

River Sand over Perspex:

TABLE 3.5 Model Data for River Sand over Perspex

L(m)	V(v)	I(mA)
0.05	9.94	0.042
0.10	9.94	0.038
0.15	9.94	0.042
0.20	9.93	0.038
0.25	9.94	0.040
0.30	9.93	0.042
0.35	9.93	0.048
0.40	9.93	0.042
0.45	9.94	0.045
0.50	9.93	0.043
0.55	9.94	0.042
0.60	9.94	0.040
0.65	9.94	0.042
0.70	9.94	0.043
0.75	9.94	0.036
0.80	9.94	0.038
0.85	9.94	0.046
0.90	9.94	0.040

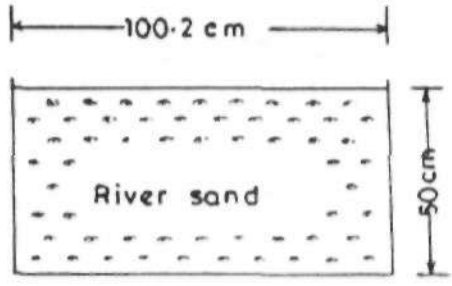


Fig. 3.22 River Sand in model tank

Figure 3.23 shows the plot of bulk resistivity against electrode separation for the single overburden case of table 3.5 with river sand as the material medium.

As was experienced in both figures 3.19 and 3.21, there is no segmentation of the first part of the graph in figure 3.23 while the points in the second part approximated to a straight line. The first part is an exponential curve; its resistivity was estimated to be about 1000 Ω-m. This value is far from the 844 Ω-m obtained with Wenner profiling (a = 2cm). The value obtained using

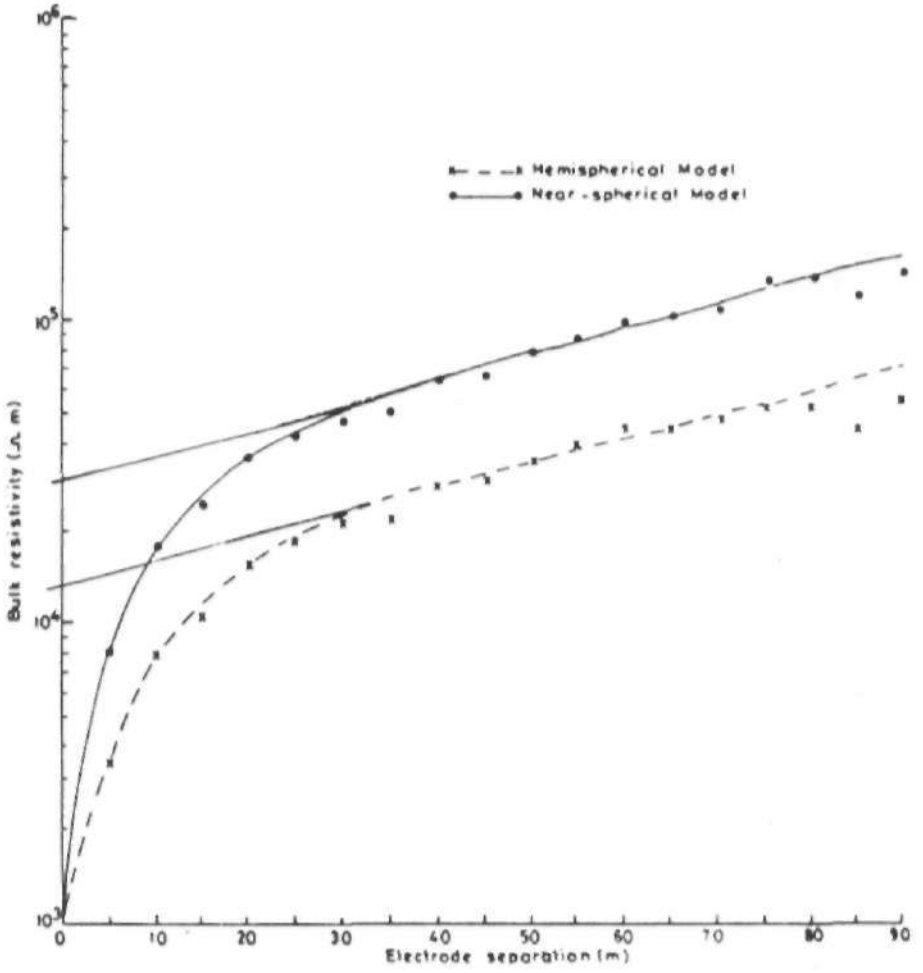


Figure 3.23 Graph of bulk resistivity against electrode spacing for river sand on perspex

the tube was 1721 Ω-m while no good result was obtained for the metre bridge for reasons earlier explained.

The thickness of river sand emplaced in the original experiment of figure 3.22 was 50.0 cm. From the graph, the first part intersected the second part at the 47.5 cm point. This thickness was just about 5.0% in error.

3.5.2 Three-layer cases

Lateritic Clay on River Sand on Perspex:

TABLE 3.6 Model Data for Lateritic Clay on River Sand on Perspex

L(m)	V(v)	I(mA)
0.01	10.03	4.17
0.02	10.04	3.53
0.03	10.04	3.37
0.04	10.04	3.23
0.05	10.04	3.22
0.06	10.04	3.10
0.07	10.04	3.04
0.08	10.04	3.08
0.09	10.04	3.02
0.10	10.04	2.96
0.15	10.03	2.96
0.20	10.03	2.82
0.25	10.03	2.77
0.30	10.03	2.76
0.35	10.03	2.75
0.40	10.03	2.61
0.45	10.04	2.58
0.50	10.04	2.60
0.55	10.04	2.60
0.60	10.03	2.55
0.65	10.03	2.42
0.70	10.03	2.43
0.75	10.03	2.40
0.80	10.03	2.36
0.85	10.03	2.24
0.90	10.03	2.16
0.95	10.03	2.17

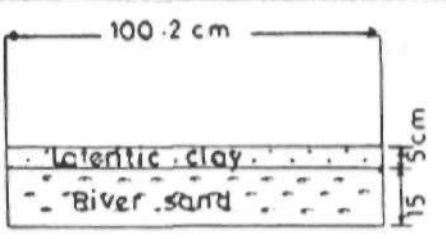


Fig 3.24: Lateritic Clay on River sand in model tank (3-layer model)

The composition of table 3.6 was made with Lateritic clay of thickness 5cm emplaced on river sand of thickness 15cm thickness. These values are only approximate but valid within a variation very much less than 1.0%.

Below are the results as obtained from figures 3.25(a) and (b). From figure 3.25(a), only the layer thickness could be fairly estimated.

Model Thickness	Calculated Thickness	Percentage Error
$d_1 = 0.050m$	$D_1 = d_1 = {}^1/_{21.0} = 0.048m$	- 4.8%
$d_2 = 0.150m$	$D_2 = {}^1/_{4.75} = 0.211m$	+ 5.3%
$D = 0.200m$	$d_2 = D_2 - D_1$	
	$\Rightarrow d_2 = 0.163m$	+ 8.6%

Slope of the first layer, $s_1 = 9.196 \times 10^{-3}m$

Slope of the second layer, $s_2 = 7.762 \times 10^{-3}m$

From figure 3.25(b), the layer thickness(es) is(are) obtained/read-off directly from the graph.

Model Thickness	Graphical Thickness	Percentage Error
$d_1 = 0.050$ m	$d_1 = 0.048$ m	- 5.0%
$d_2 = 0.150$ m	$D_2 = 0.155$ m	- 22.5%
$D = 0.200m$	$d_2 = 0.108$ m	+ 28.3%

$s_1 = {}^1/_5(\ln 50 - \ln 7.6) = 0.376775m^{-1}$
$s_2 = {}^1/_{10}(\ln 98 - \ln 26) = 0.132709m^{-1}$
$s_3 = {}^1/_{10}(\ln 155 - \ln 112) = 0.0325m^{-1}$

Using the expressions of equations (3.15), (3.22) and (3.24), the layer resistivity could be estimated thus:

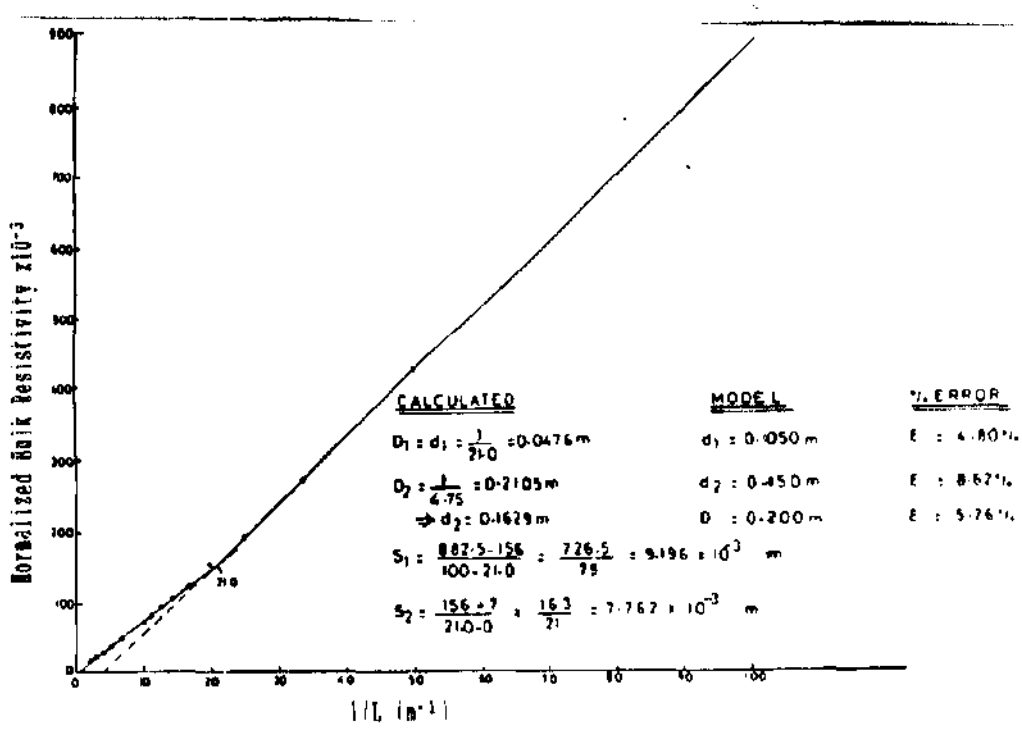


Figure 3.25(a) Typical Graph of Normalised Bulk Resistivity Against 1/L for Clay on River Sand on Basement (3-layer model)

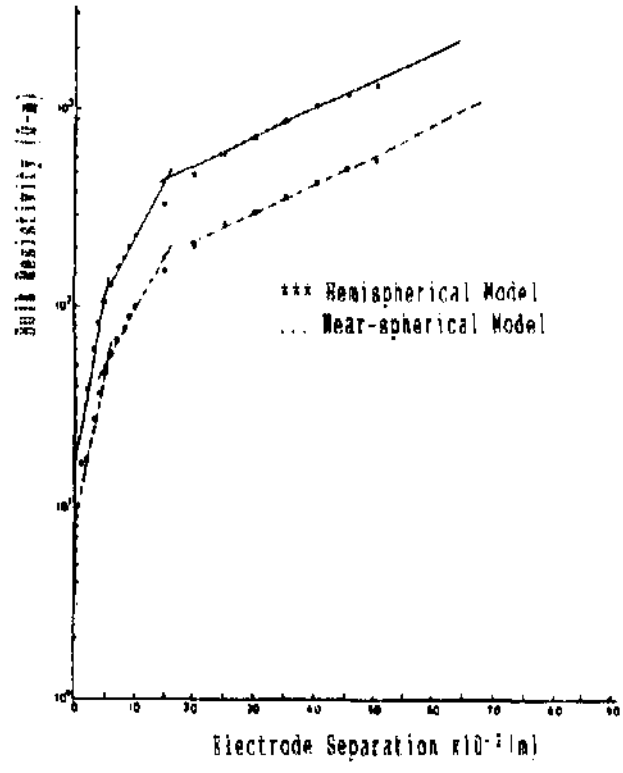


Figure 3.25(b) Typical Graph of Bulk Resistivity Against Electrode Spacing for Clay on River Sand on Basement (3-layer model)

For the first layer,

ρ_1 = 7.6 x 10 ohm metres

It is noted that 7.6 is in the first decade and it is the intercept of the first segment on the ordinate. The factor of 10 came in as a result of the resistivity modelling factor of 10^{-1} obtained in the experiment.

Hence, ρ_1 = 76. ohm metre.

For the second layer s_1/s_2 = 2.83911

Therefore ρ_2 = 76 x 2.83911 = 216. Ω-m

This value of resistivity is far lower than expected for river sand.

For the third layer, s_2/s_3 = 4.083354

Therefore ρ_3 = 216. x 4.083354 = 881. Ω-m

Although this is also much lower than expected but the values of ρ_1, ρ_2, and ρ_3 still follow the expected trend of $\rho_1 < \rho_2 < \rho_3$. The low value of ρ_2 and its subsequent effect on ρ_3 could be adduced to the presence of water within the intergranular spaces of the river sand at this initial stage of the experiment.

There is a close agreement between the depths arrived at in figures 3.25(a) and 3.25(b) in which the top layer thickness was evaluated as 4.76 cm and 4.75 cm respectively. The thickness of the second layer was evaluated to be 16.29 cm and 10.75 cm respectively. The resistivity of the first layer is believed to be accurately estimated because of its closeness in order to the expected value.

The general procedure for computing the layer resistivities for the laboratory scale modelling is shown in Appendix A3.

River Sand on Lateritic Clay on Perspex:

TABLE 3.7 Model Data for River Sand on Lateritic Clay on Perspex

L(m)	V(v)	I(mA)
0.01	9.73	0.315
0.02	9.73	0.246
0.03	9.72	0.227
0.04	9.72	0.220
0.05	9.72	0.216
0.06	9.71	0.204
0.07	9.71	0.205
0.08	9.70	0.212
0.09	9.70	0.231
0.10	9.69	0.191
0.15	9.69	0.178
0.20	9.69	0.176
0.25	9.69	0.165
0.30	9.69	0.178
0.35	9.69	0.155
0.40	9.69	0.155
0.45	9.69	0.212
0.50	9.68	0.414
0.55	9.68	0.154
0.60	9.68	0.147
0.65	9.68	0.160
0.70	9.68	0.199
0.75	9.67	0.169
0.80	9.67	0.223
0.85	9.67	0.162
0.90	9.67	0.144
0.95	9.67	0.150

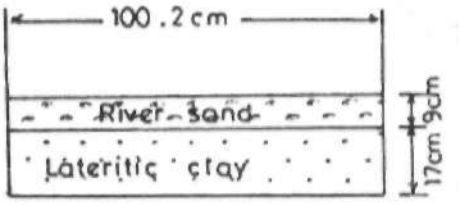


Fig. 3.26: River Sand on Clay in model tank (3-layer model)

The composition of table 3.7 was made with river sand of 9cm thickness as in figure 3.26 emplaced on lateritic clay of 17cm thickness, thereby making the total thickness of earth material in the model tank to be 26cm.

Below are the results as obtained from figures 3.27(a) and 3.27(b). Only the layer thickness could be fairly

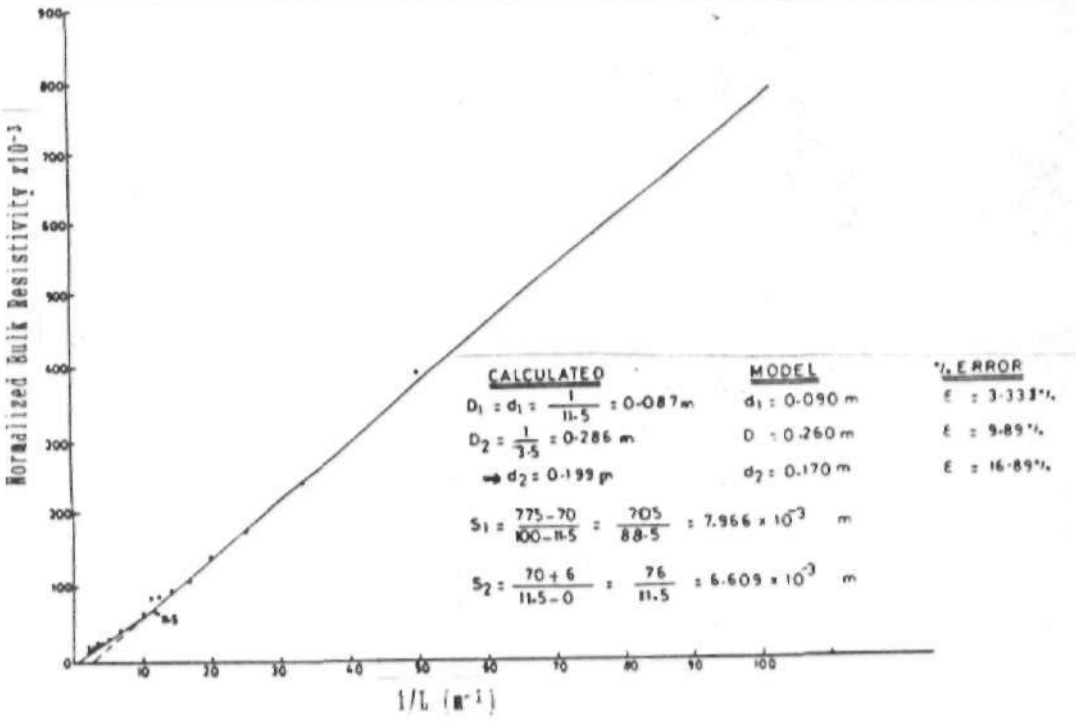


Figure 3.27(a) Graph of normalised bulk resistivity against 1/L for river sand on clay on basement

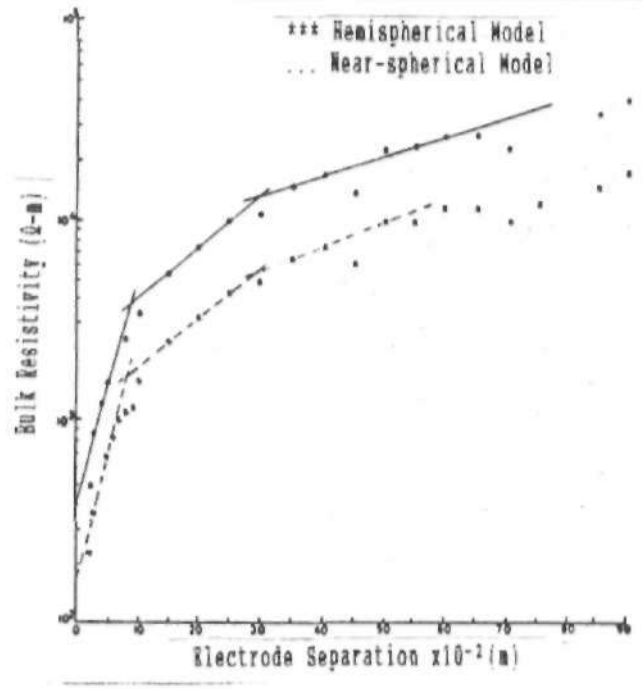


Figure 3.27(b) Graph of bulk resistivity against electrode spacing for river sand on clay on basement

estimated from the normalized bulk resistivity against the reciprocal of electrode separation graph shown in figure 3.27(a).

Model Thickness	Calculated Thickness	Percentage Error
d_1 = 0.090 m	$D_1 = d_1$ = 0.087 m	- 3.3%
d_2 = 0.170 m	$D_2 = {}^1/_{3.5}$ = 0.286 m	+ 9.9%
D = 0.260 m	=> d_2 = 0.199 m	+16.9%

$s_1 = 7.966 \times 10^{-3}$m
$s_2 = 6.609 \times 10^{-3}$m

From figure 3.27(b),

Model Thickness	Graphical Thickness	Percentage Error
d_1 = 0.090 m	d_1 = 0.080 m	+ 11.1%
d_2 = 0.170 m	D_2 = 0.300 m	+ 15.4%
D = 0.260 m	=> d_2 = 0.220 m	+ 29.4%

$s_1 = {}^1/_{10}$ (ln 2700 - ln 170) = 0.276521m^{-1}
$s_2 = {}^1/_{10}$ (ln 3100 - ln 990) = 0.0470726m^{-1}
$s_3 = {}^1/_{10}$ (ln 4200 - ln 3500) = 0.018232m^{-1}

Similar interpretation as was performed for the case of lateritic clay on river sand was done to yield

ρ_1 = 1700 Ω-m; h_1 = 8.0 cm = 0.080 m
ρ_2 = 351. Ω-m; h_2 = 22.0 cm = 0.220 m
ρ_3 = 1098. Ω-m; h_3 = ∞

3.5.3 Four-layer cases

Lateritic Clay on Mixed-soil on River Sand on Perspex:

Lateritic Clay of thickness 3.0 cm was emplaced on Mixed-soil of thickness 5.0 cm which was in turn emplaced on River Sand of thickness 15.0 cm in the model tank. The total thickness of earth material therefore emplaced on the basement was 23.0cm (fig.3.28). It should once again be noted that the quoted values of thicknesses are only fairly approximate as a result of possible non-uniformity in the eveness of bedding plane. The table of values for this composition is shown in Table 3.8.

TABLE 3.8 Model Data for Lateritic Clay on Mixed-soil on River Sand on Perspex

L(m)	V(v)	I(mA)
0.01	10.10	4.16
0.02	10.10	3.47
0.03	10.10	3.22
0.04	10.10	2.82
0.05	10.09	3.04
0.06	10.08	3.14
0.07	10.09	2.97
0.08	10.07	2.97
0.09	10.08	2.90
0.10	10.08	2.83
0.15	10.07	2.85
0.20	10.07	2.73
0.25	10.07	2.64
0.30	10.06	2.65
0.35	10.06	2.67
0.40	10.06	2.54
0.45	10.06	2.60
0.50	10.05	2.58
0.55	10.05	2.47
0.60	10.04	2.52
0.65	10.05	2.46
0.70	10.04	2.40
0.75	10.04	2.45
0.80	10.04	2.42
0.85	10.04	2.37
0.90	10.04	2.27
0.95	10.04	2.12

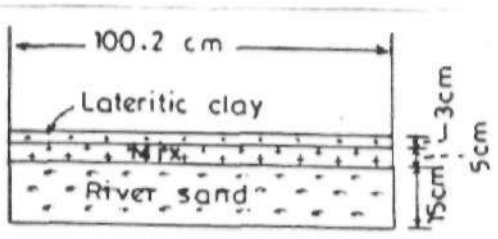


Fig. 3.28 Clay on Mixed-soil on River Sand in model tank (4-layer model)

Figures 3.29(a) and 3.29(b) show the graphical results as obtained for this composition. From figure 3.29(a),

Model Thickness	Calculated Thickness	Percentage Error
$d_1 = 0.030m$	$D_1 = d_1 = 1/L^{0.5} = 0.049$ m	+ 62.7%
$d_2 = 0.050m$	$D_2 = 1/9.5 = 0.105m$	+ 31.6%
$d_3 = 0.150m$	$d_2 = 0.057m$	+ 13.0%
$D = 0.230m$	$D_3 = 1/4.0 = 0.250m$	+ 8.7%
	$\Rightarrow d_3 = 0.153m$	- 3.5%

$s_1 = 8.390 \times 10^{-3}$m
$s_2 = 8.909 \times 10^{-3}$m
$s_3 = 6.316 \times 10^{-3}$m

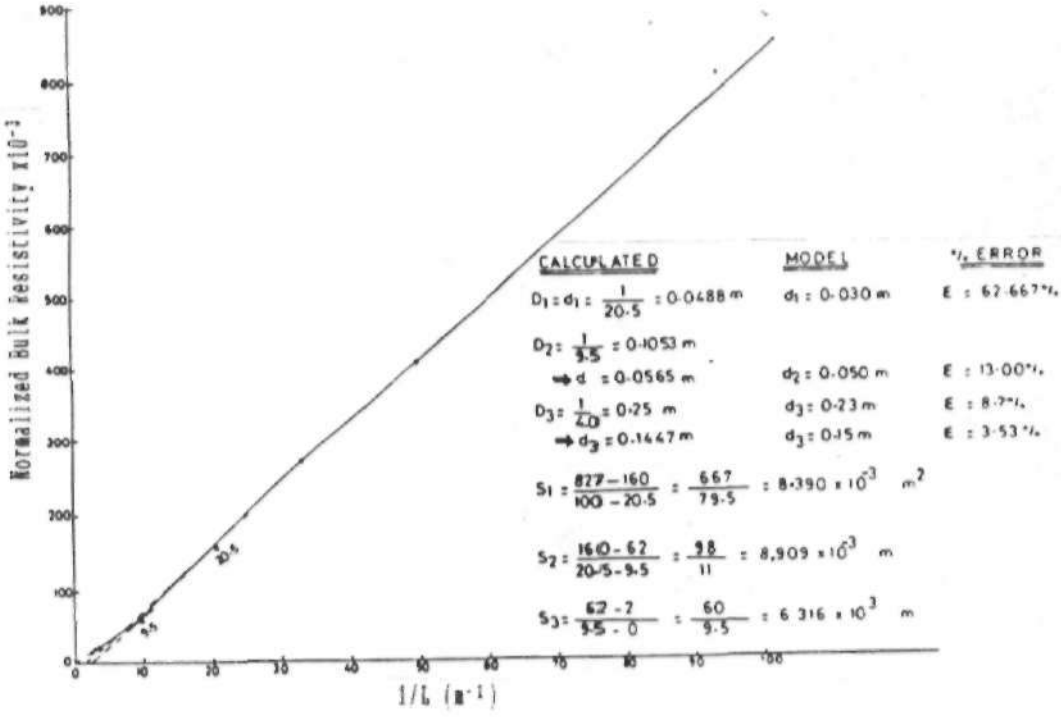


Figure 3.29(a) Graph of normalised bulk resistivity against 1/L for Clay on Mixed-soil on River Sand on Basement (4-layer model)

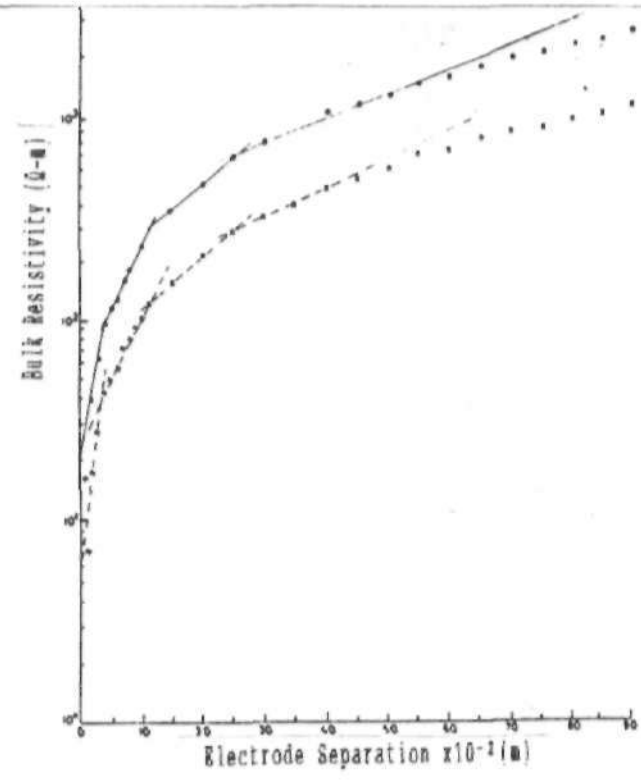


Figure 3.29(b) Graph of bulk resistivity against electrode spacing for Clay on Mixed-soil on River Sand on Basement (4-layer model)

Model Thickness	Graphical Thickness	Percentage Error
d_1 = 0.030m	d_1 = 0.038m	+ 25.0%
d_2 = 0.050m	D_2 = 0.110m	+ 37.5%
d_3 = 0.150m	d_2 = 0.073m	+ 45.0%
D = 0.230m	D_3 = 0.255m	+ 10.9%
	=> d_3 = 0.1450m	- 3.3%

$s_1 = {}^1/_{10}$ (ln 1000 - ln 6.6) = 0.5021m^{-1}
$s_2 = {}^1/_{10}$ (ln 105 - ln 23.5) = 0.1497m^{-1}
$s_3 = {}^1/_{10}$ (ln 115 - ln 62) = 0.06178m^{-1}
$s_4 = {}^1/_{10}$ (ln 173 - ln 123) = 0.03411m^{-1}

The layer resistivities were calculated thus:

s_1 = 0.5021m^{-1} s_2 = 0.1497m^{-1} s_3 = 0.06178m^{-1}
s_4 = 0.0341m^{-1}

s_1/s_2 = 3.354044 s_2/s_1 = 0.2981477
s_2/s_3 = 2.4231142 s_3/s_2 = 0.412692
s_3/s_4 = 1.8112 s_4/s_3 = 0.5521204

c_1 = 66 Ω-m c_2 = 235 Ω-m c_3 = 620 Ω-m c_4 = 1230 Ω-m

$\rho_1 = c_1$ = 66 Ω-m; h_1 = 3.75cm=0.0375m
ρ_2 = 66 x 3.354044 = 221. Ω-m; h_2 = 7.25cm=0.0725m
ρ_3 = 221.x 2.4231142 = 536. Ω-m; h_3 = 14.5cm=0.1450m
ρ_4 = 536.x 1.8112 = 972. Ω-m; h_4 = ∞

Lateritic Clay on River Sand on Lateritic Clay on Perspex:

In this composition of table 3.9, lateritic clay of thickness 5.5cm was emplaced on river sand of thickness 10.0cm which was in turn emplaced on another layer of lateritic clay of thickness 17.0cm.

The graphical results obtained for this composition are shown in figures 3.31(a) and 3.31(b).

From figure 3.31(a),

Model Thickness	Calculated Thickness	Percentage Error
d_1 = 0.055m	$D_1 = d_1 = {}^1/_{23.5}$ = 0.043 m	-22.6%
d_2 = 0.100m	$D_2 = {}^1/_{7.5}$ = 0.133m	-14.0%
d_3 = 0.170m	d_2 = 0.091m	- 9.3%
D = 0.325m	$D_3 = {}^1/_{3.5}$ = 0.286m	-12.0%
	=> d_3 = 0.153m	-10.0%

XCAIII

TABLE 3.9 Model Data for Lateritic Clay on River Sand on Lateritic Clay on Perspex

L(m)	V(v)	I(mA)
0.01	9.89	5.31
0.02	9.90	4.60
0.03	9.90	4.41
0.04	9.90	4.28
0.05	9.90	4.20
0.06	9.90	4.15
0.07	9.89	4.05
0.08	9.90	4.09
0.09	9.90	4.12
0.10	9.90	4.15
0.15	9.90	3.92
0.20	9.90	3.89
0.25	9.90	3.90
0.30	9.90	3.84
0.35	9.90	3.65
0.40	9.90	3.67
0.45	9.90	3.61
0.50	9.90	3.11
0.55	9.90	3.70
0.60	9.90	3.64
0.65	9.90	3.49
0.70	9.90	3.15
0.75	9.90	3.43
0.80	9.90	3.28
0.85	9.90	3.26
0.90	9.90	3.08
0.95	9.90	2.64

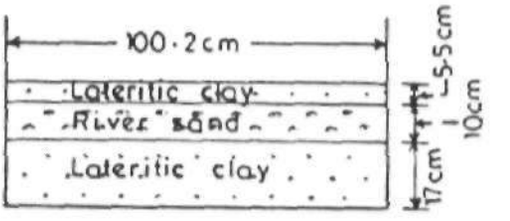


Fig. 3.30 Clay on River Sand on Clay in Model Tank (4-layer model)

$s_1 = 9.281 \times 10^{-3}m$
$s_2 = 8.25 \times 10^{-3}m$
$s_3 = 7.2 \times 10^{-3}m$

From figure 3.31(b),

Model Thickness	Graphical Thickness	Percentage Error
$d_1 = 0.055m$	$d_1 = 0.050m$	- 9.1%
$d_2 = 0.100m$	$D_2 = 0.148m$	- 6.5%
$d_3 = 0.170m$	$d_2 = 0.098m$	- 2.5%
$D = 0.325m$	$D_3 = 0.365m$	+12.3%
	$\Rightarrow d_3 = 0.218m$	+27.9%

$s_1 = {}^1/_{10}$ (ln 190 - ln 7.4) $= 0.3246m^{-1}$
$s_2 = {}^1/_{10}$ (ln 72 - ln 21) $= 0.1232m^{-1}$
$s_3 = {}^1/_{10}$ (ln 106 - ln 73) $= 0.0373m^{-1}$
$s_4 = {}^1/_{10}$ (ln 152 - ln 119) $= 0.0245m^{-1}$

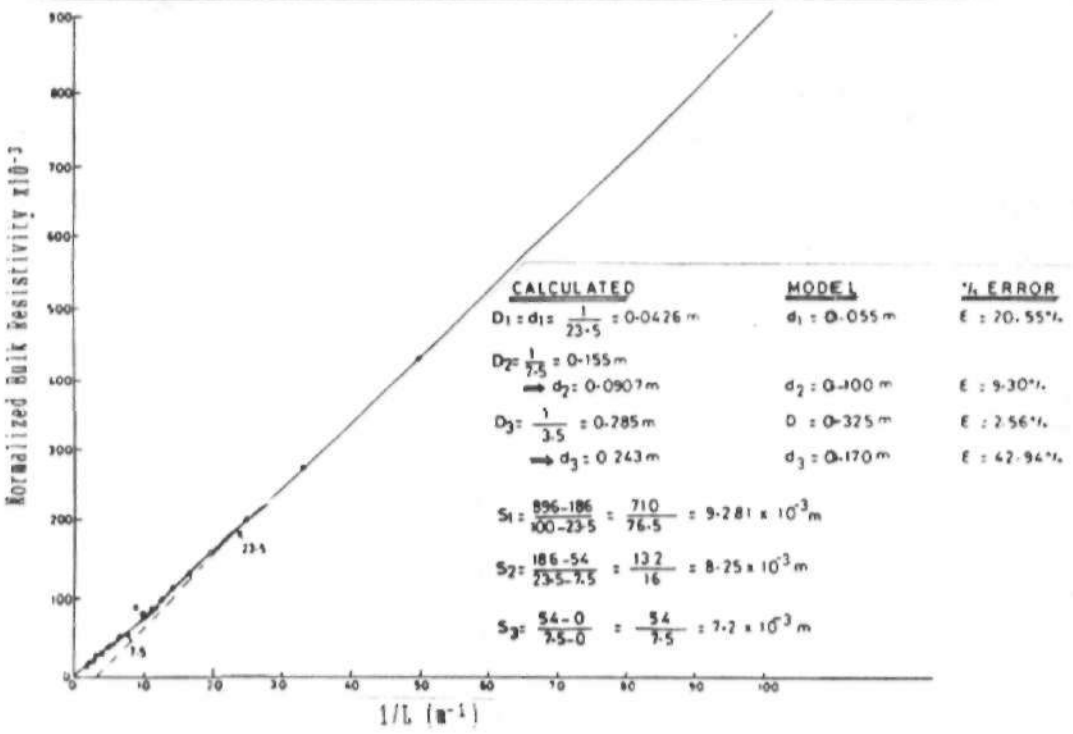


Figure 3.31(a) Graph of normalised bulk resistivity against 1/L for Clay on River Sand on Clay on Basement

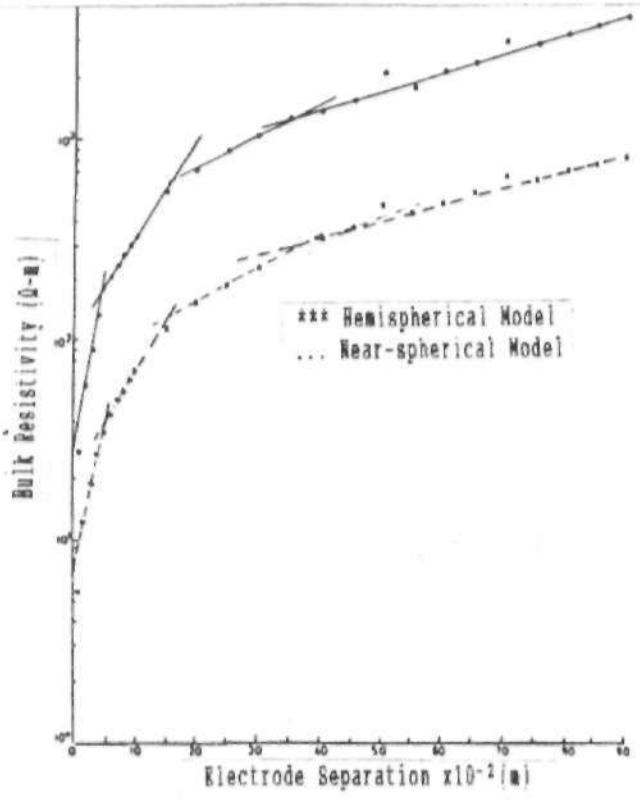


Figure 3.31(b) Graph of bulk resistivity against electrode spacing for Clay on River Sand on Clay on Basement

ρ_1 = 74. Ω-m
ρ_2 = 195. Ω-m
ρ_3 = 644. Ω-m
ρ_4 = 980. Ω-m

h_1 = 5.0 cm = 0.050m
h_2 = 9.8 cm = 0.098m
h_3 = 21.8 cm = 0.218m
h_4 = ∞

Mixed-soil on Lateritic Clay on River Sand on Perspex:

TABLE 3.10 Model Data for Mixed-soil on Lateritic Clay on River Sand on Perspex

L(m)	V(v)	I(mA)
0.01	10.06	0.825
0.02	10.06	0.840
0.03	10.06	0.940
0.04	10.05	1.123
0.05	10.05	1.046
0.06	10.05	0.943
0.07	10.05	0.856
0.08	10.03	0.914
0.09	10.03	0.791
0.10	10.03	0.709
0.15	10.03	0.750
0.20	10.02	0.957
0.25	10.02	0.850
0.30	10.02	0.750
0.35	10.01	0.797
0.40	10.01	0.779
0.45	10.00	0.786
0.50	10.00	0.768
0.55	10.00	0.836
0.60	10.00	0.956
0.65	10.00	0.831
0.70	10.00	0.785
0.75	9.98	0.734
0.80	9.98	0.698
0.85	9.98	0.627
0.90	9.98	0.718
0.95	9.98	0.597

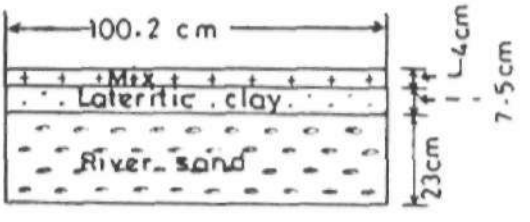


Fig. 3.32 Mixed-soil on Clay on River Sand in Model Tank (4-layer case)

In this composition, of table 3.10 and figure 3.32, 4.0cm thick of Mixed-soil was emplaced on 7.5cm thick lateritic clay which was also emplaced on about 23.0 cm thick river sand. The total emplaced thickness was 34.5 cm.

Figures 3.33(a) and 3.33(b) shows the graphical results obtained for this composition.

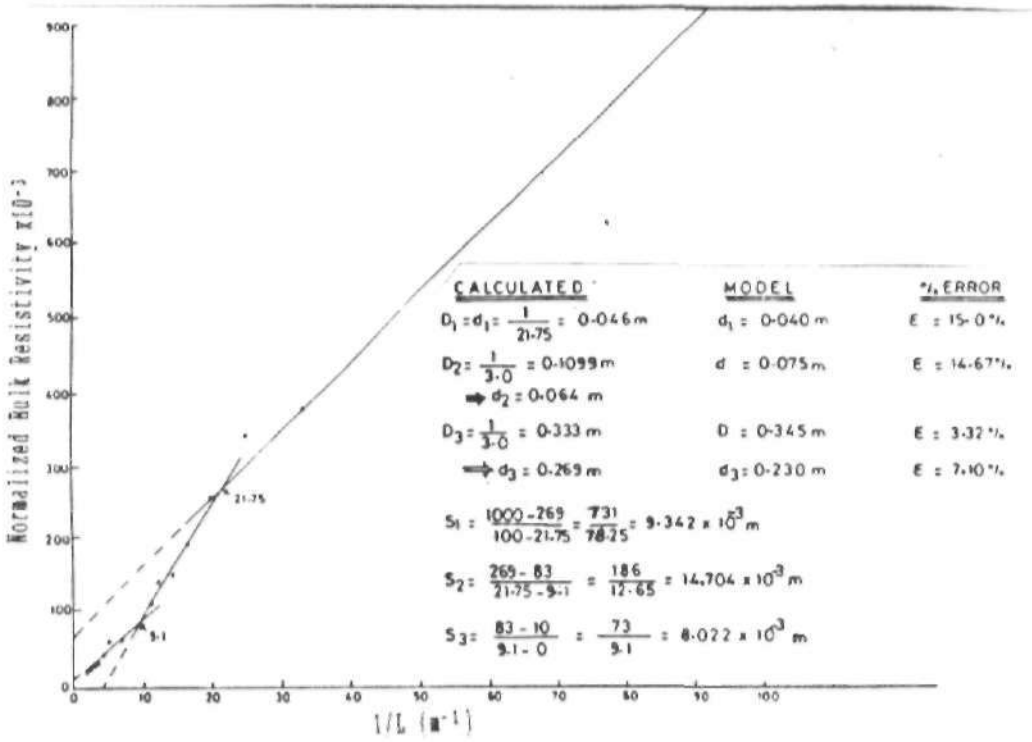


Figure 3.33(a) Graph of normalised bulk resistivity against 1/L for Mixed-soil on Clay on River Sand on Basement

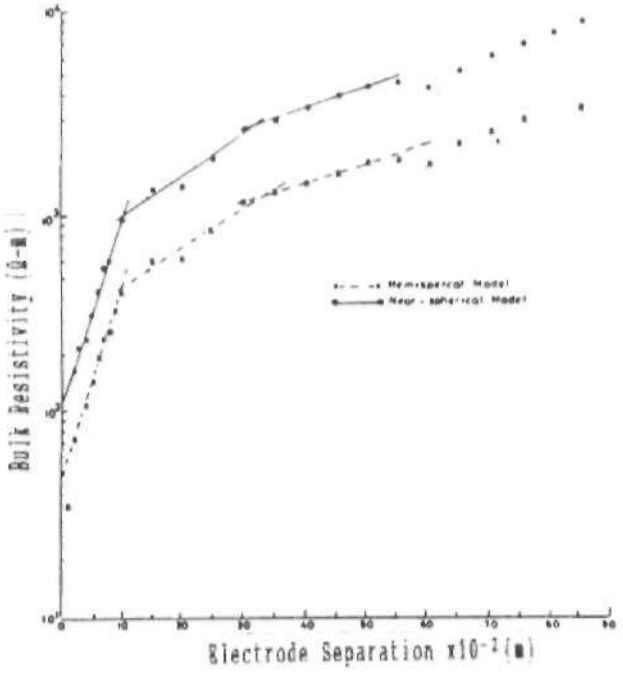


Figure 3.33(b) Graph of bulk resistivity against electrode spacing for Mixed-soil on Clay on River Sand on Basement

From figure 3.33(a),

Model Thickness	Calculated Thickness	Percentage Error
d_1 = 0.040m	$D_1 = d_1 = {}^1/_{21.75} = 0.046$ m	+15.0%
d_2 = 0.075m	$D_2 = {}^1/_{9.1} = 0.110$m	+46.533%
d_3 = 0.230m	d_2 = 0.064m	-14.67%
D = 0.345m	D_3 = 0.345m	0.00%
	=> d_3 = 0.230m	0.00%

$s_1 = 9.342 \times 10^{-3}$m
$s_2 = 14.704 \times 10^{-3}$m
$s_3 = 8.022 \times 10^{-3}$m

From figure 3.33(b)

Model Thickness	Graphical Thickness	Percentage Error
d_1 = 0.040m	d_1 = 0.025m	-37.5%
d_2 = 0.075m	D_2 = 0.103m	-10.9%
d_3 = 0.230m	d_2 = 0.078m	+ 3.3%
D = 0.345m	D_3 = 0.333m	- 3.6%
	=> d_3 = 0.230m	0.0%

$s_1 = {}^1/_{10}$ (ln 5600 - ln 22) = $0.554m^{-1}$
$s_2 = {}^1/_{10}$ (ln 430 - ln 54) = $0.2075m^{-1}$
$s_3 = {}^1/_{10}$ (ln 435 - ln 275) = $0.04586m^{-1}$
$s_4 = {}^1/_{10}$ (ln 745 - ln 590) = $0.02333m^{-1}$

Applying similar interpretation procedure as before, we obtain

ρ_1 = 220 Ω-m	h_1 = 2.5 cm = 0.025m
ρ_2 = 82. Ω-m	h_2 = 7.8 cm = 0.078m
ρ_3 = 373. Ω-m	h_3 = 23.0 cm = 0.230m
ρ_4 = 733. Ω-m	$h_4 = \infty$

River Sand on Mixed-soil on Lateritic Clay on Perspex:

The composition of table 3.11 and figure 3.34, was made with 3.0 cm thickness of river sand overlying a 7.0 cm thick Mixed-soil, which in turn was emplaced on a 17.0 cm thick lateritic clay.

Figures 3.35(a) and 3.35(b) show the graphical results for this composition.

TABLE 3.11 Model Data for River Sand on Mixed-soil on Lateritic Clay on Perspex

L(m)	V(v)	I(mA)
0.01	9.90	0.205
0.02	9.90	1.77
0.03	9.90	0.150
0.04	9.89	0.170
0.05	9.89	0.157
0.06	9.88	0.203
0.07	9.88	0.233
0.08	9.88	0.178
0.09	9.88	0.181
0.10	9.88	0.163
0.15	9.88	0.193
0.20	9.88	0.173
0.25	9.88	0.151
0.30	9.88	0.138
0.35	9.88	0.137
0.40	9.88	0.148
0.45	9.88	0.162
0.50	9.88	0.189
0.55	9.88	0.136
0.60	9.88	0.147
0.65	9.88	0.136
0.70	9.88	0.152
0.75	9.88	0.145
0.80	9.88	0.151
0.85	9.88	0.149
0.90	9.88	0.162
0.95	9.88	0.151

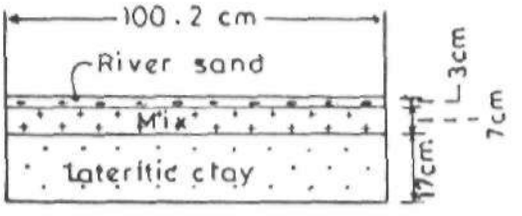


Fig. 3.34: River Sand on Mixed-soil on Clay in Model Tank (4-layer model)

From figure 3.35(a),

Model Thickness	Calculated Thickness	Percentage Error
$d_1 = 0.030m$	$D_1 = d_1 = {}^1/_{33.2} = 0.030m$	0.0%
$d_2 = 0.070m$	$D_2 = {}^1/_{4.75} = 0.211m$	-13.0%
$d_3 = 0.170m$	$d_2 = 0.057m$	-18.7%
$D = 0.270m$	$D_3 = {}^1/_{3.5} = 0.286m$	+ 5.8%
	$\Rightarrow d_3 = 0.199m$	+16.9%

$s_1 = 11.272 \times 10^{-3}m$
$s_2 = 5.392 \times 10^{-3}m$
$s_3 = 13.043 \times 10^{-3}m$

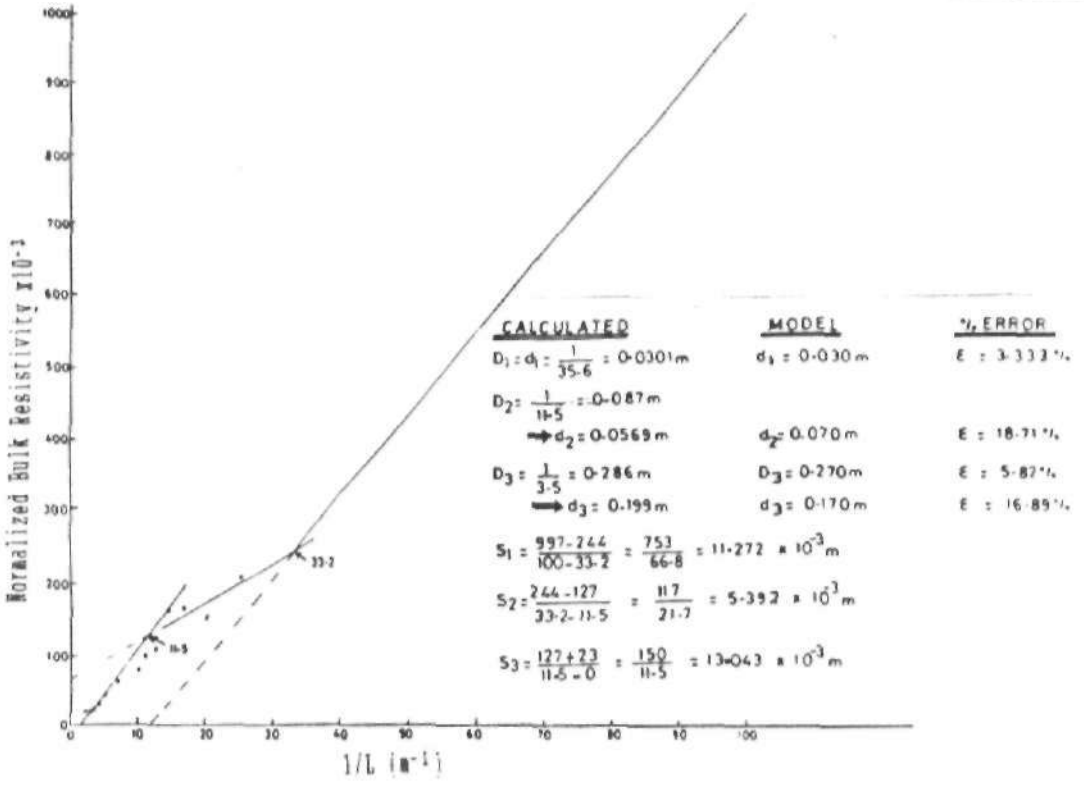


Figure 3.35(a) Graph of normalised bulk resistivity against 1/L for River Sand on Mixed-

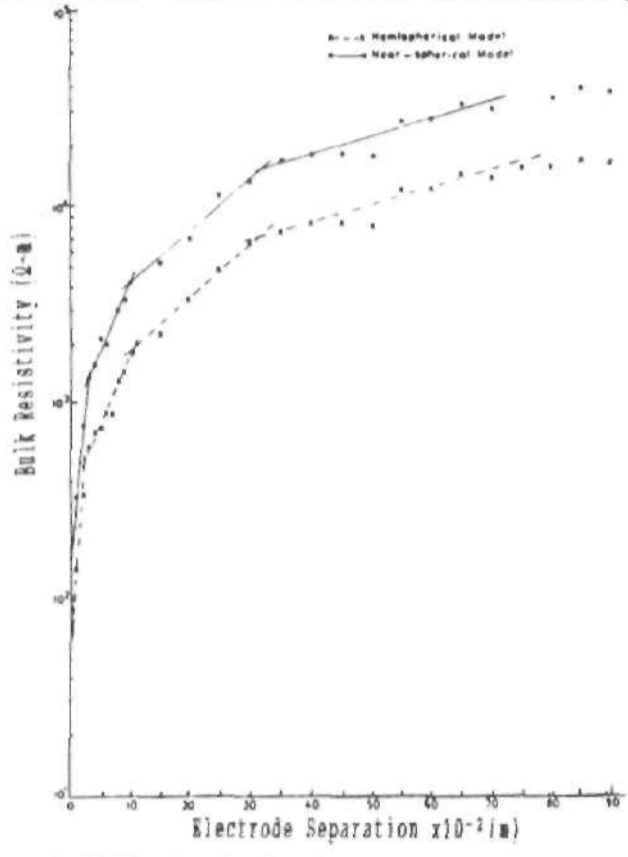


Figure 3.35(b) Graph of bulk resistivity against electrode spacing for River Sand on Mixed-soil on Clay on Basement

From figure 3.35(b),

Model Thickness		Graphical Thickness	Percentage Error
d_1 =	0.030m	d_1 = 0.026m	-13.3%
d_2 =	0.070m	D_2 = 0.103m	+ 2.5%
d_3 =	0.170m	d_2 = 0.008m	+ 9.3%
D =	0.270m	D_3 = 0.318m	+17.6%
	=>	d_3 = 0.213m	+25.0%

$s_1 = {}^1/_{10}$ (ln 120000 - ln 68) = $0.7476m^{-1}$
$s_2 = {}^1/_{10}$ (ln 1800 - ln 320) = $0.1727m^{-1}$
$s_3 = {}^1/_{10}$ (ln 1800 - ln 970) = $0.0618m^{-1}$
$s_4 = {}^1/_{10}$ (ln 4400 - ln 3600) = $0.0201m^{-1}$

Adopting similar procedure as before, we obtain

ρ_1 = 680. Ω-m h_1 = 5.0 cm = 0.050m
ρ_2 = 157. Ω-m h_2 = 7.7 cm = 0.077m
ρ_3 = 56. Ω-m h_3 = 21.3 cm = 0.213m
ρ_4 = 173. Ω-m h_4 = ∞

The basement value is far lower than expected. This may likely be due to its effect being effectively masked by the highly conductive layers overlying it.

3.5.4 Model horizontal profiling with the two-electrode array

An attempt was made to investigate the ability of the two-electrode array to delineate vertical contacts. An arrangement whereby a block of lateritic clay 35cm in length, 50 cm wide and 50 cm thick was sandwitched between two blocks of river sand was made. The arrangement is as shown in figure 3.36. Horizontal profilings using the Wenner array with a = 2cm and a = 5cm were then run across the tank along the middle of the tank parallel to the long axis of the tank. Similar profiles were run using the two-electrode array with L = 2cm and L = 5cm.

The results of the horizontal profiling using the two arrays are shown in figures 3.37 and 3.38. The results show

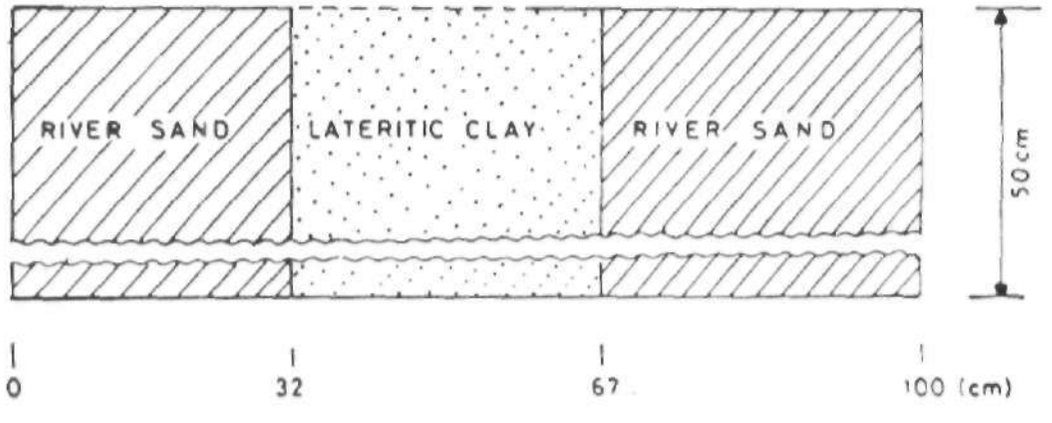


Figure 3.36 Earth Material Composition/Arrangement for Horizontal Profiling

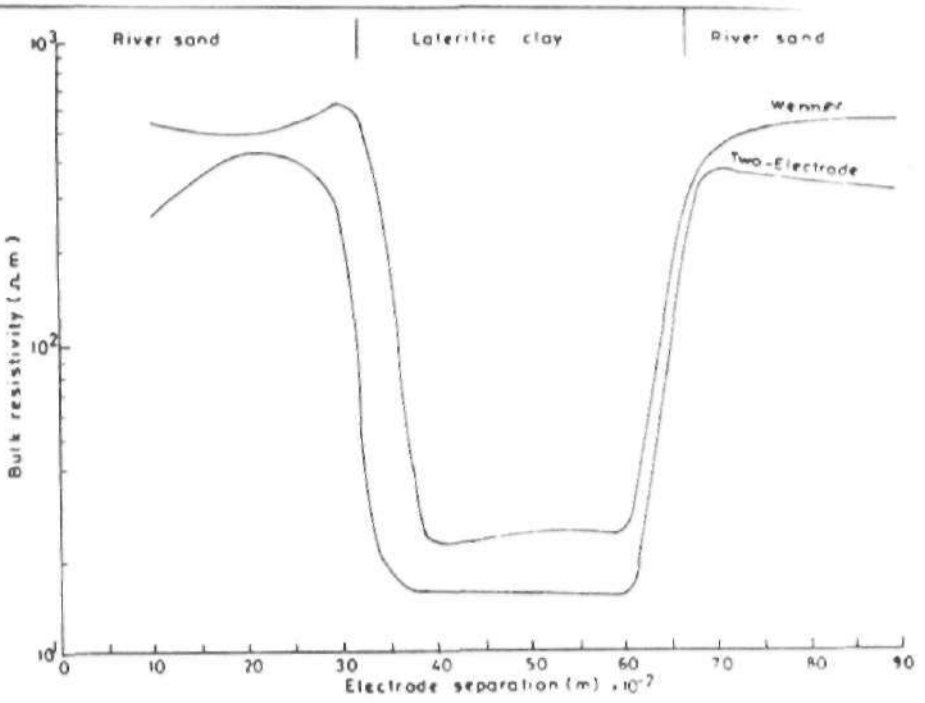


Figure 3.37 Horizontal profiling with Two-electrode (L = 2 cm) and Wenner (a = 2cm).

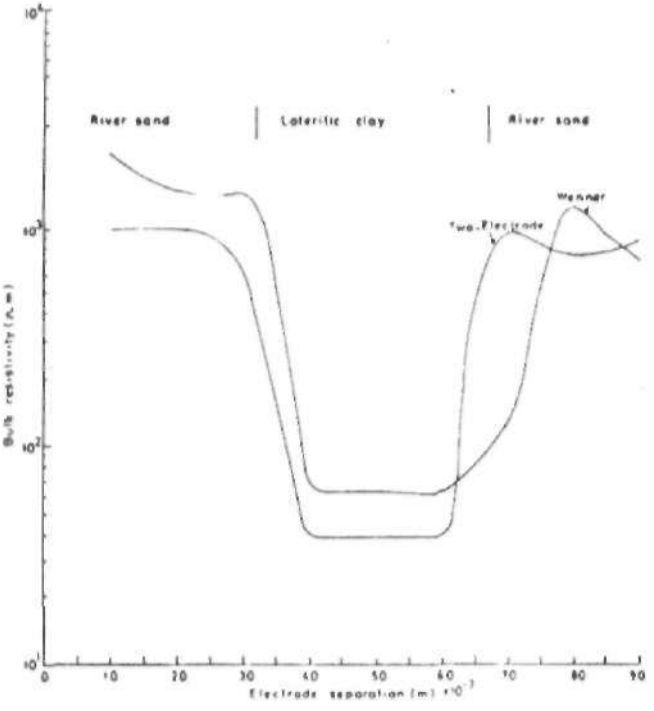


Figure 3.38 Horizontal profiling with Two-electrode (L = 5 cm) and Wenner (a = 5cm).

that the proposed two-electrode array delineates the different portions as good as the Wenner array does. The two-electrode array promises to be a good substitute for the Wenner array judging from a comparison of figures 3.37 and 3.38. The contacts between the blocks of River Sand and the block of Lateritic Clay were well defined, and accurately too, by the two-electrode array. Moreover, the measured resistivity curves and the resistivity values of both the two- electrode array and the Wenner array are very much comparable. The values are shown in Table 3.12 to Table 3.15.

TABLE 3.12 Horizontal Profiling with Wenner (a = 2cm)

Position (cm)	V(v)	I(mA)	R(kΩ)	ρ (Ω-m)
10	3.81	0.091	41.868	526.130
20	4.99	0.131	38.092	478.673
30	8.79	0.182	42.297	606.914
40	3.66	2.100	1.743	21.901
50	4.05	2.140	1.893	23.782
60	3.76	1.980	1.899	23.863
70	2.89	0.089	32.472	408.054
80	4.22	0.099	42.626	535.657
90	4.82	0.115	41.913	526.695

TABLE 3.13 Horizontal Profiling with Wenner (a = 5cm)

Position (cm)	V(v)	I(mA)	R(Ω)	ρ (Ω-m)
10	3.77	0.054	69.815	2193.297
20	3.30	0.069	47.826	1502.501
30	9.10	0.199	45.729	1436.608
40	3.49	1.603	1.177	68.398
50	3.82	1.843	2.073	65.116
60	0.14	60.070	32.000	62.832
70	0.80	0.190	74.061	127.577
80	3.26	0.078	41.795	1313.025
90	2.70	0.114	23.684	744.061

TABLE 3.14 Horizontal Profiling with Two-Electrode Method (L = 2cm).

Position (cm)	V(v)	I(mA)	R(Ω)	ρ (Ω-m)
10	9.72	0.221	43.982	259.0757
20	9.72	0.138	70.435	414.8951
30	9.72	0.219	44.384	261.441
32	9.71	1.181	8.222	48.431
40	9.68	3.750	2.581	15.205
50	9.68	3.810	2.541	14.966
60	9.69	63.790	2.557	15.060
67	9.71	0.280	34.679	204.274
70	9.71	0.150	961.069	359.727
80	9.71	0.171	56.784	334.483
90	9.72	0.183	53.115	312.872

TABLE 3.15 Horizontal Profiling with Two-Electrode Method (L = 5cm).

Position (cm)	V(v)	I(mA)	R(Ω)	ρ (Ω-m)
10	9.71	0.144	67.431	992.9977
20	9.71	0.139	69.856	1028.716
30	9.71	0.234	41.496	611.075
40	9.68	3.380	2.864	42.174
50	9.67	3.610	2.679	39.447
60	9.67	3.440	2.811	41.396
65	9.70	0.307	31.596	465.291
70	9.70	0.144	67.361	991.974
80	9.71	0.187	51.925	764.660
90	9.70	0.157	61.783	909.836

In order to ensure the homogeneity of the top layer in each of the compositions attempted during experimentation, a fair run of horizontal profiling was made using both the Wenner array and the two-electrode array. Whenever the surface resistivity was found to be averagely non-uniform, that is, a large variation in surface resistivity was observed, a re-mixing of the surface/top layer material was then usually undertaken.

3.6 Deductions

From the result of the horizontal profiling undertaken in the model study, it is evident that the proposed variant of the two-electrode array can be another good method for horizontal profiling alongside the Wenner array if it works this fine under field condition.

It was observed from the processed data of the model studies that the depth to interface is approximately equal to the electrode spacing, implying that, the actual depth of investigation for this variant of the two- electrode array is about equal to the electrode spacing. This is not in agreement with the theory that the pattern of current flow within a homogeneous and isotropic earth is hemispherical.

Also observed during the experimental studies was the fact that a certain set of input signal frequencies, namely 30Hz, 40Hz and 60Hz, gave very stable readings of voltage and output current. The produced graphical results of figure 3.39 showed that in a situation whereby we could not have, for field use, equipment which can operate at these frequencies, any other commonly available frequencies such as d.c. (0Hz) and line frequency (50 Hz), (where there are no overhead electric power lines to cause interference and distortions) could be used. The graph of figure 3.39 compares the laboratory model study data collected for water using the variant of the two-electrode array at frequencies of 0Hz, 40Hz and 50Hz. The points and curves are very close; the intercepts on the vertical axis (that gave the resistivity of the medium) and the depth estimates are about the same for the three frequencies compared.

In drawing the lines joining points that represented each layer in the graphical output, only visual estimate of the best line of fit was made without resort to the use of linear regression analysis procedure. This visual method of line fitting was definitely bound and expected to introduce errors into the estimates of layer thickness(es) and layer resistivity thereof made. To minimize the error, as best as possible, the best line of fit under the prevailing conditions was drawn.

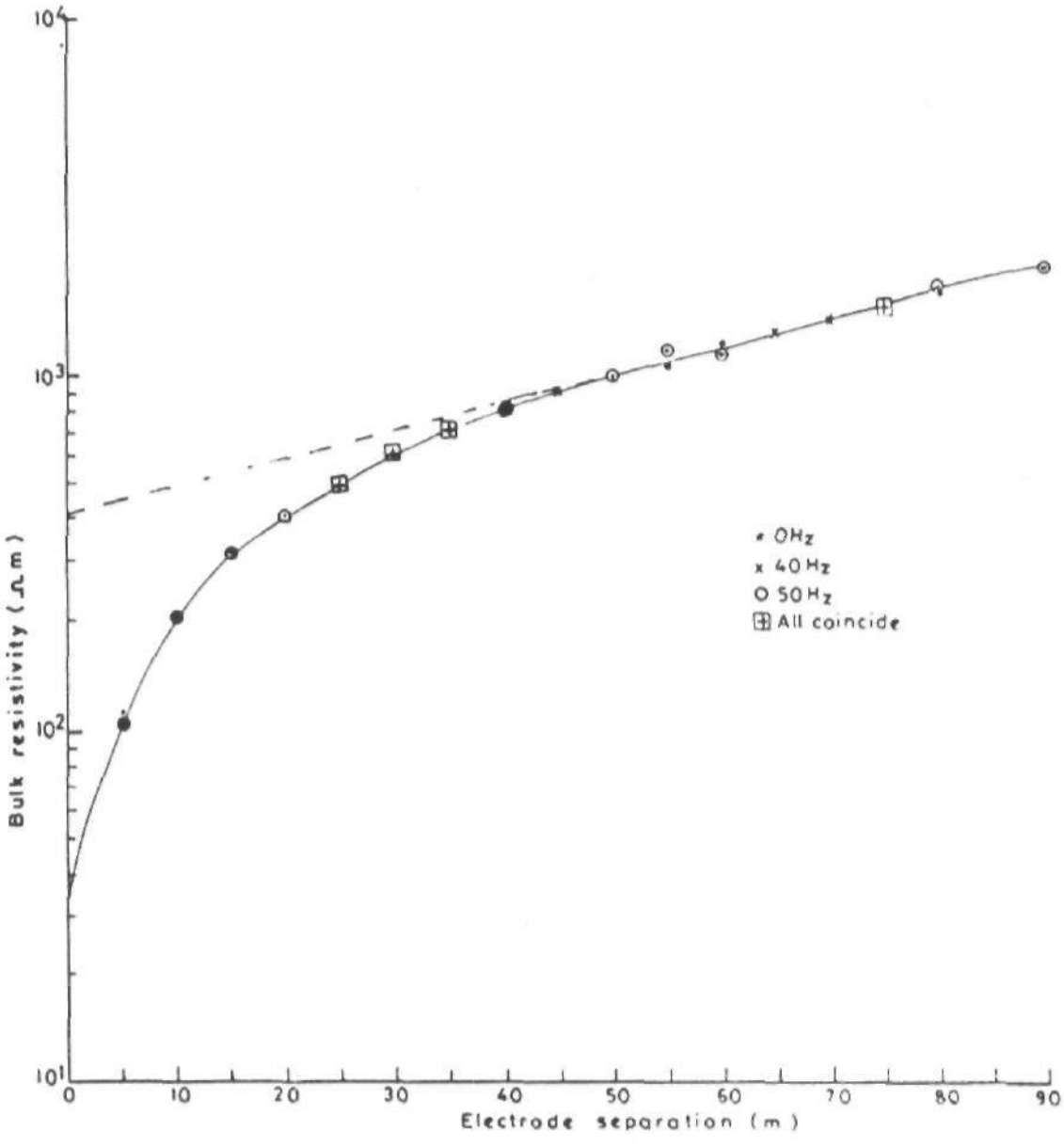


Figure 3.39: Graph of bulk resistivity against electrode spacing showing results at 0 Hz, 40 Hz, and 50 Hz for water using the two-electrode method

CHAPTER FOUR

THE FIELD SURVEY

4.1 Instrumentation

4.1.1 Designing a suitable instrument

As mentioned earlier on, this research work does not have as one of its main goals, the design and development of a field instrument for the proposed method. However, it was observed during the experimental studies that certain set of input frequencies, namely 30Hz, 40Hz and 60Hz, gave very stable readings of voltage and output current. This prompted the attempt to design an equipment that could be used for the field survey such that the equipment could be operated at any one of the stable frequencies in order to achieve stable and more reliable data than when operating at frequencies of either 0Hz or 50Hz.

The designed instrument is made up of four circuits namely the multivibrator circuit, the buffer circuit, the current amplification circuit, and the transformer circuit. The instrument uses a 12 volt d.c. source as its input, and generates a high voltage a.c. signal of desired frequency as its output.

The Multivibrator Circuit: The heart of the designed equipment is the multivibrator circuit. Multivibrators are two-stage amplifiers/transistor switching circuits with strong positive voltage feedback in which the output of each stage is fed to the input of the other by coupling resistors or capacitors (Shea, 1953). As a result, the transistors are driven alternately into saturation and cut-off thereby giving rise to complementary outputs (Duncan, 1982).

In the design of the instrument, the free-running or astable multivibrator was used to oscillate the incoming

d.c. signal. The free-running multivibrator has no stable states; it switches automatically from one state to the other at a rate determined by the two CR interstage couplings within the circuit (Havill and Walton, 1975). It consequently generates a continuous stream of square pulses.

It is possible to generate a continuous train of square-wave pulses of equal mark-to-space ratio by applying shaping techniques to a sinusoidal oscillation. This method is used where the highest frequency stability is essential and calls for a regenerative type of switching circuit where pulse duration and repetition frequency are controlled by one circuit (Cowles, 1976). This exactly is the requirement of this work, and the free-running multivibrator simply fits in.

In controlling the frequency and hence the pulse duration of the instrument, a double potentiometer was used in conjuction with the two CR couplings. The circuit is symmetrical and the mark-to-space ratio is one. The frequency f is therefore

$$f = \frac{0.693}{CR} \qquad \text{(Maddock, 1969)} \qquad \ldots.4.1$$

The Buffer Circuit: The buffer circuit has as its input, the output signal from the multivibrator circuit. The two circuits were coupled using the direct coupling method.

The circuit is basically an emitter-follower or common-collector amplifier with 100% series negative voltage feedback. It is a broad-band amplifier used to couple high impedance circuits into low-impedance loads.

The amplifier transfers the input voltage to the output load without requiring voltage step-down, as in a transformer (Cowles, 1976). Thus the common-collector stage provides an impedance step-down and current-gain that makes the a.c. emitter voltage to follow the base signal with a loss of only one or two percent (Cowles, 1976). They are therefore described as buffer amplifiers since they impose very little electrical load on the input signal source and yet have a sufficiently low value of input impedance load (Morris, 1978). This circuit is therefore essentially one having the following characteristics:

- the gain is approximately unity
- the amplifier is non-phase inverting
- the input impedance is high
- the output impedance is low

(Morris, 1978)

This circuit was used to couple the multivibrator circuit to the current amplification circuit.

The Current Amplification Circuit: This circuit was used to raise the level of output current from the buffer circuit. The circuit is mainly composed of a Darlington connection which allows us to obtain the maximum input impedance possible from a transistor (McGray and Cahill, 1973). It enhances the buffer action of the emitter-follower. The large β possible with the Darlington connection allows the emitter-follower circuit to be designed to have a very large input resistance; the high effective β value increases the current gain but does not increase the voltage gain (Uffenbeck, 1982). The Darlington configuration therefore is also an excellent buffer stage

since it gives a voltage gain of approximately one, a current gain of approximately β^2, a high input impedance and a low output impedance.

The Transformer Circuit: Two transformer stages were incorporated into the equipment

- a 9V - 0 - 9V centre-tapped transformer which was used to amplify the output voltage from the current amplification circuit, to a transformer output of approximately 240V.

- a transformer which receives as its input, the output from the first stage transformer, to give a set of switched output of 240V, 480V, 720V and 960V respectively.

Because of the voltage step-up achieved by the transformer circuit, current was stepped down and hence a lower output current than achieved at the current amplification stage was recorded. The output current was 21mA at 240 V, this was found to be too low judging from the field work requirement.

The leads from the second transformer were connected to the measuring instruments and the current electrodes in a similar fashion to that shown in figure 4.1 in which the instrument is represented by the power source.The instrument could not however be used for the field work mainly because its output current level was found to be too low, especially at very high voltages.

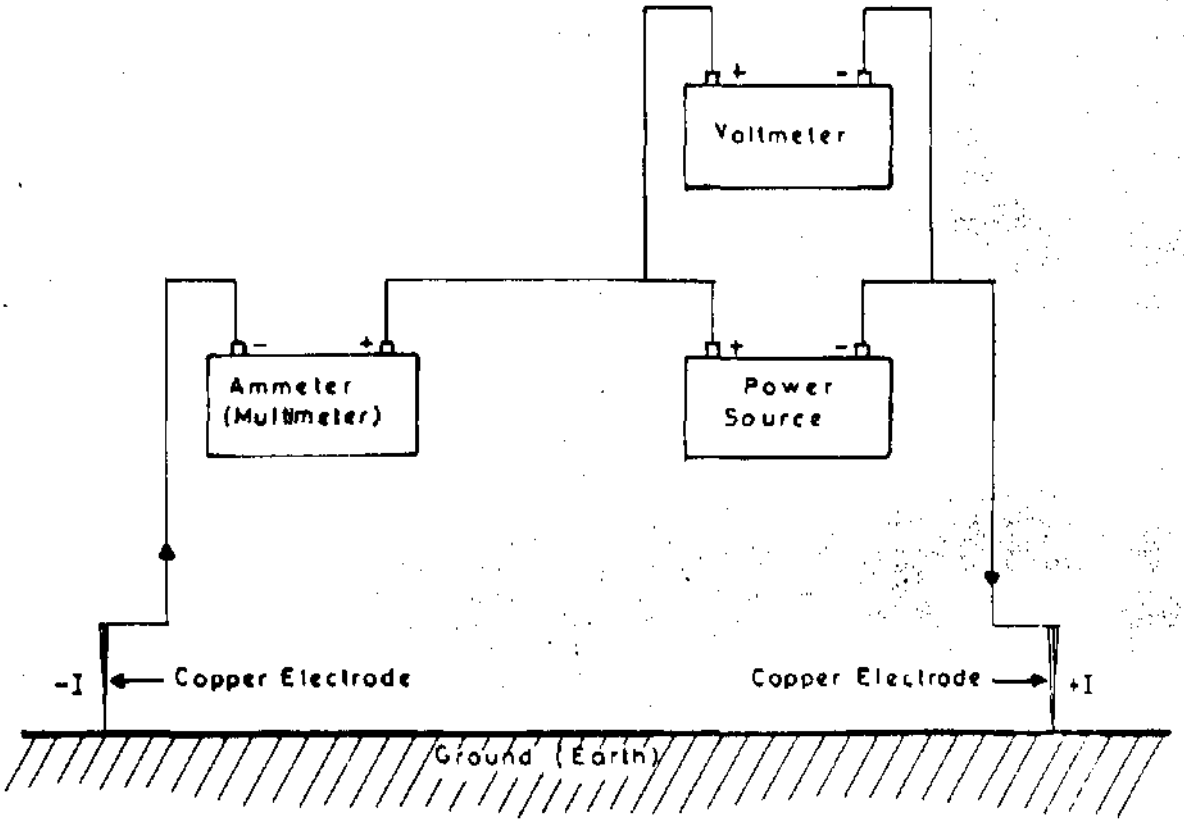


Figure 4.1:Arrangement of the Field Equipment used for the Field Survey

4.1.2 Instrument used for the field work

As a result of the unresolved problems of the constructed field equipment, it was adjudged more reasonable to use a well tested equipment. The results of the model studies show that although the voltage and current measurements were not very stable at 0Hz and 50Hz respectively, yet the graphical results at these frequencies were as good as those obtained when operating at such frequencies whose voltage and current measurements were very stable. Choice was therefore made of using suitable power units which could deliver current into the earth at either 0Hz or 50Hz frequencies and also pick up response signals from the earth at these frequencies.

Figure 4.1 shows the arrangement of the field equipment used for the two-electrode array aspect of the field survey. The field equipment consists of the signal source - an Ealing high voltage power supply unit, 0- 500V, capable of delivering a maximum current of 250mA; an analogue voltmeter of a range 0-300 volts; a digital ammeter set from the digital multimeter PM2522; connecting wires and, two copper electrodes. An electricity generator was used to power the power supply unit and the digital multimeter. An SAS 300 terrameter was used to carry out both the horizontal and vertical profiling surveys using the Wenner and the Schlumberger arrays Because of its light weight and digital output, the terrameter combines portability with ease of reading to make the measuring procedure less cumbersome.

4.2 The Field Work

4.2.1 The choice of the project (field test) area

The area used to test the proposed method under field conditions is the Kubanni River Basin.

The basin was chosen on the ground that a lot of work had been undertaken within the basin by various researchers. There is therefore an abundance of information about the basin, most especially geologic and geoelectric information. This implies that its geologic, hydrogeologic and geophysical parameters are well known hence making the basin a good ground for testing a new method such as the variant of the two-electrode method investigated in this work.

The river basin occupies the centre of the South-Eastern sector of the Zaria sheet (No 102 S.W.) of the 1:50,000 sheet ordinances series of the Nigeria ordinances survey maps. It is approximately bounded by latitudes 11°4'25"N and 11°10'45''N and longitudes 7°36'56"E and 7°44'22"E (Shemang, 1990). The basin has an average area of about 150 km² (Egbeifo, 1978). It lies on a plateau with a height of about 570 metres above mean sea level, and has a dendritic drainage pattern. The basin is elongated in the NW-SE direction (Figure 4.2); being the direction of dominant faulting and jointing in the basement complex of Nigeria (McCurry, 1970).

Between 1962 and now, a sizeable number of researchers have carried out intensive and extensive work on different aspects of the Kubanni River Basin. These works, as diverse in nature as they are, ranges from geographical, geological, and hydrogeological to geophysical characteristics of the basin.

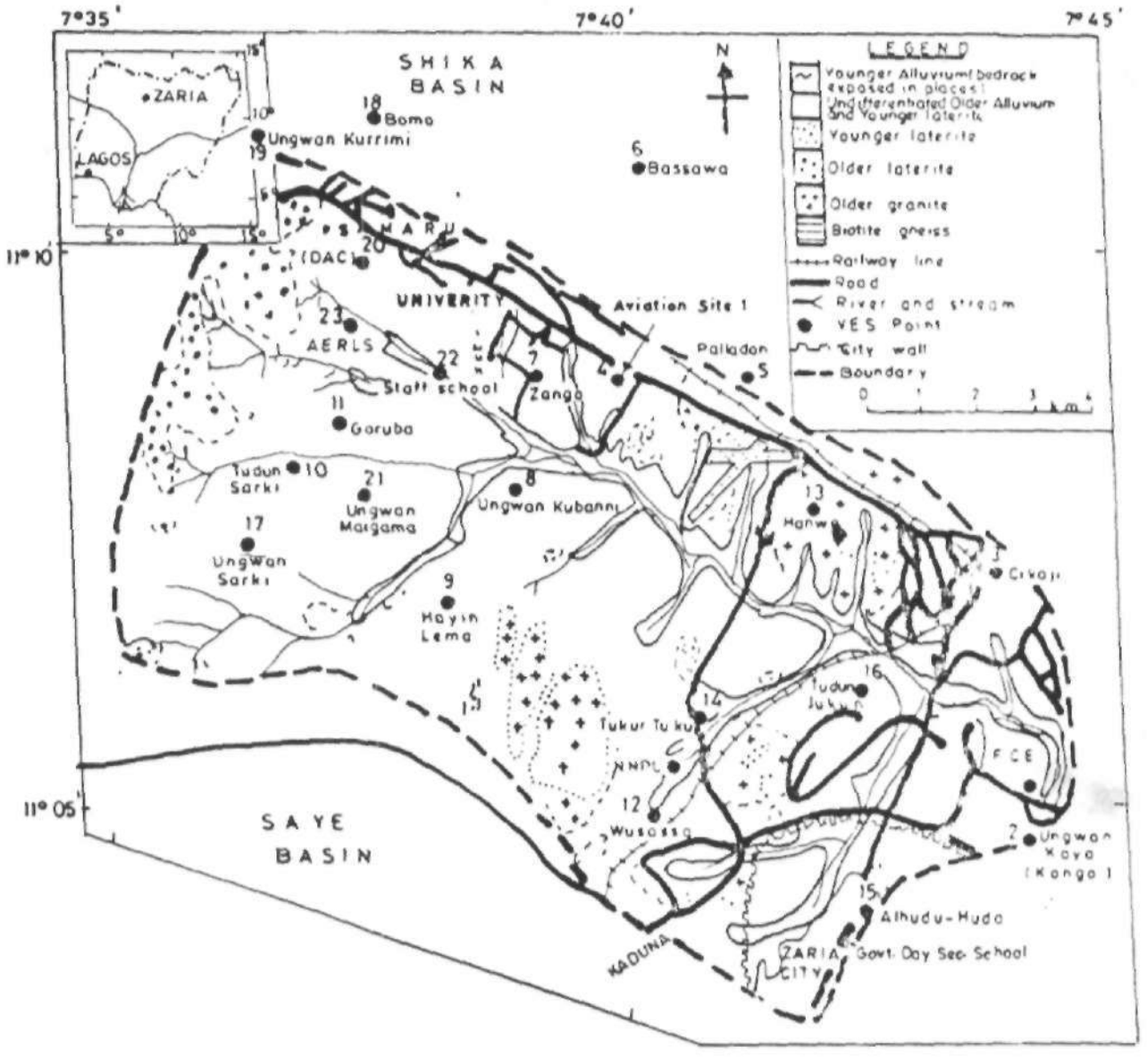


Figure 4.2: Location Map of the Area under Study (After Shemang, 1990) showing the Sounding Points.

Wright and McCurry (1970) in their study of the basement geology of Zaria sheet 102 S.W. within which the Kubanni basin lies, have reported that part of the basement complex which covers the entire Zaria area is made up mostly of older granites and biotite granite-gneiss (Figure 4.3a,b).

Egbeifo (1978) has established that the depth to the water table at various locations within the Kubanni basin ranges between 3 and 10 metres. He also concluded that the thickness of the weathered basement aquifer within the basin ranges from about 1 to 30m. Akpoborie (1972), suggested that the presence of joints and fractures predominantly controls the flow of underground water in the Samaru creek. Ososami (1968) has assessed the depth to bedrock in the basin to vary in thickness from less than 1m to about 30m. Olugbemiro (1985) has estimated the depth to bedrock around the Jama'a Kubanni village in the basin to be about 36m. This has been corroborated by the borehole drilling work done by Messrs Preussag Nigeria Limited in 1985.

Hassan (1987) in his geoelectrical investigations of the Western half of the Kubanni basin reported the undulation of the bedrock in his study area. He concluded that the depth to the basement in the area is generally increasing towards the Southern part. He also suggested the existence of a great depression in the Southern part of his study area which trends SE-NW and occupies about 40% of his study area.

The most recent electrical survey in the area is that of Shemang (1990) who has conducted electrical depth soundings at selected well sites within the Kubanni River

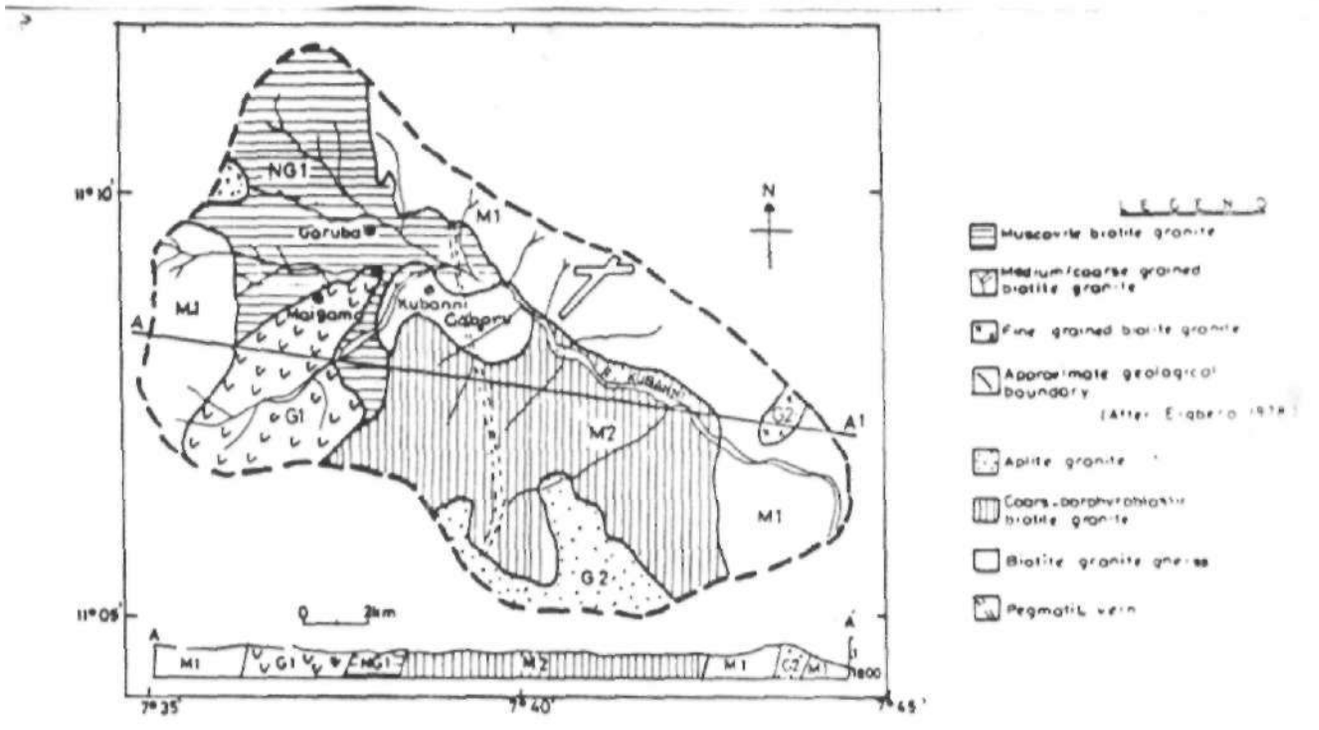


Figure 4.3 (a) Basement Geology of Kubanni Basin (After Egbeifo, 1978).

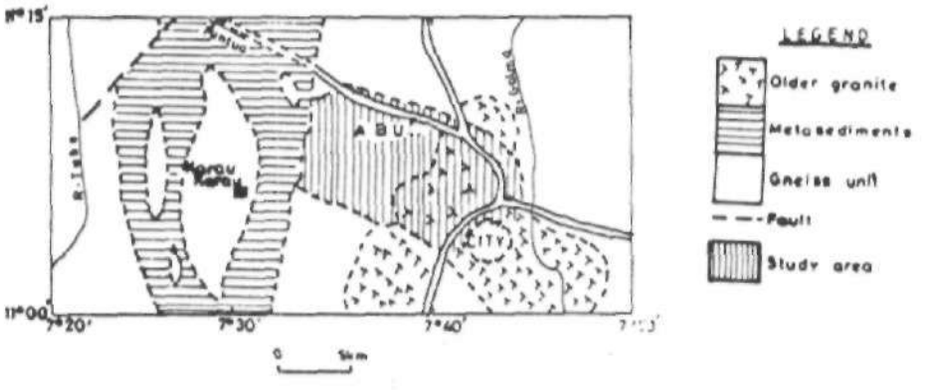


Figure 4.3 (b) The Geology of Parts of the Quarter Degree Sheets 101 and 102 (After McCurry 1970).

Basin. He reported that the resistivity values of the topmost layer in the basin ranged from 50 Ω-m at Cikaji to 781 Ω-m at the Government Day Secondary School, Zaria City. He estimated the depth to basement range to be from about 3 m, just west of the university dam to about 44 m around Ungwan Kubanni, with the average depth-to-basement in the basin being about 12 m. He concluded that the depth to basement is generally decreasing towards the Southern part of the basin. He also confirmed and completely delineated (mapped) the existence of a depression earlier reported by Hassan (1987) in the Southern part of his study area. Shemang's interpreted VES data suggested that the overburden, in most parts of the basin, is made up of two different rock types, except in some few places where only one rock type has been interpreted, which overlie the fresh basement. Shemang's VES data show that the overburden is mostly made up of clays, silts and sands (topsoil), weathered basement, fresh laterite and weathered laterite.

The most recent geophysical work in the basement is credited to Bajeh (1992) who conducted a ground magnetic survey of the basin. His results, in most cases, have corroborated the findings of Shemang (1990). He established the depth to basement within the basin to be between 0 m and about 50 m. This range is only about six metres deeper than that of Shemang which is between 3 m and 44 m.

4.2.2 Geology of the project area (Kubanni Basin)

The Basement Complex: The Nigerian Basement Complex, shown in figure 4.4, covers more than half the surface area of Nigeria, mostly the Western part, the North Central part and the Eastern flank bordering the Cameroons. The Kubanni basin, situated in the North Central part of Nigeria is

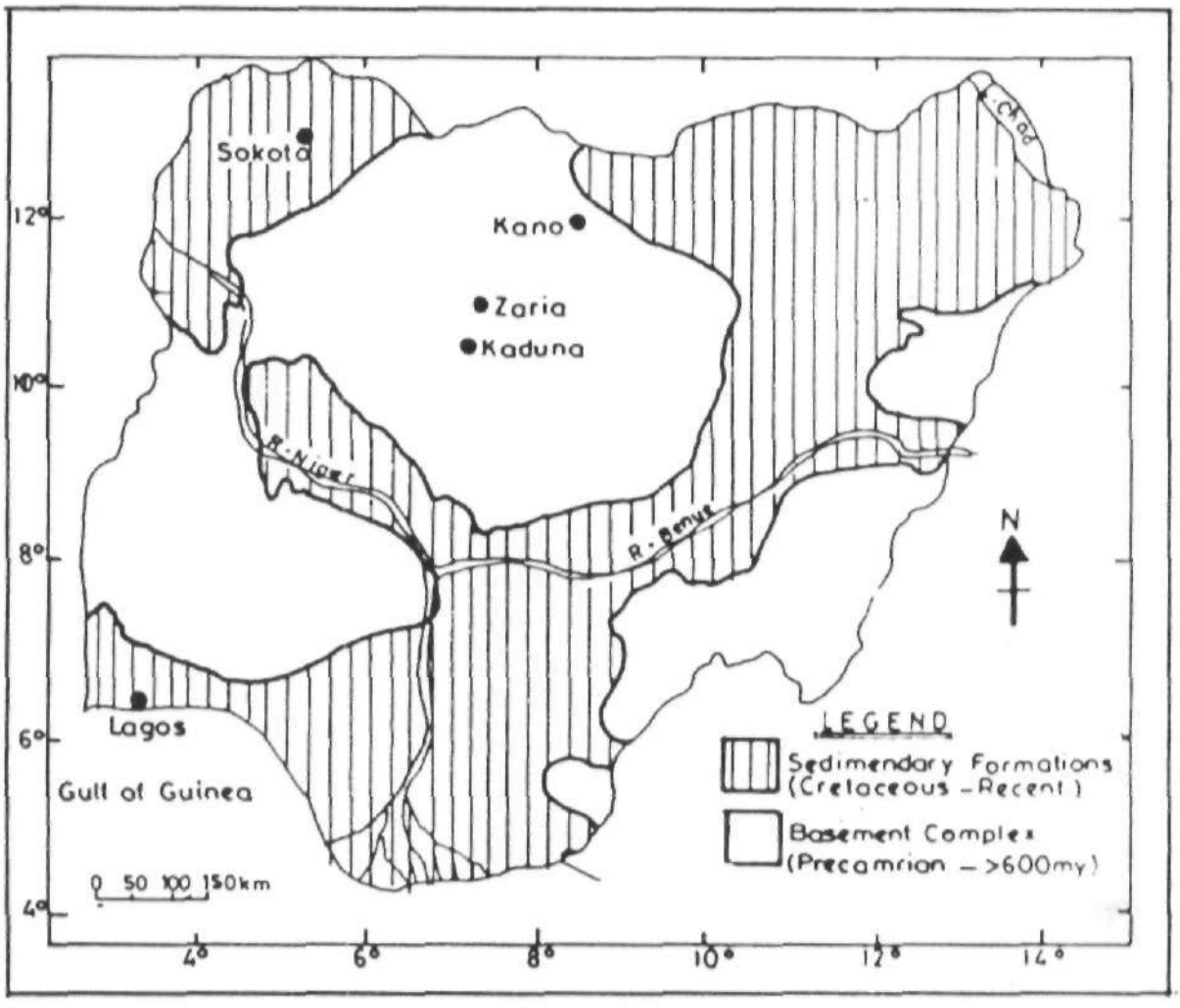


Figure 4.4: Simplified Geological Map of Nigeria (Courtesy of G.S.N.).

therefore underlain by Precambrian rocks of the Nigerian Basement Complex (Figure 4.3a).

The older granites which predominate in the area are non-porphyritic and variably foliated. They form groups of inselbergs and low whalebacks. Cross-cutting sheets and irregular masses of pegmatites, applite and vein quartz are widespread. The gneiss complex which are primarily composed of quartz, oligoclase, biotite and occassionally porphyroblastic microline is another basement rock present in the basin; it is medium to coarse grained and moderately to weakly foliated (McCurry, 1970).

The different basement rocks found in the basin and which are covered by Quarternary to Recent deposits can be summarised as follows:

- coarse prophyrritic-biotite granite;
- medium-coarse grained biotite granite gneiss;
- applite granite with pegmatites and quartz veins cutting across most of the bodies;
- weathered basement which is part of the basement complex that has been weathered and disintegrated beyond recognition (Shemang, 1990).

The Superficial Deposits: According to Egbeifo (1978), the superficial deposits that cover most of the basement rocks in the basin act as recharge areas to the aquifer where they are underlain by weathered basement. These deposits are the Older laterites and Quarternary deposits which constitute the sporadically distributed Older and Younger alluviums. The Older laterite remnants are recognized partly by their topographical relationships and thickness up to 7 m and partly by their reddish-brown cellular aspects and relative freedom from impurity (Wright

and McCurry, 1970). The Younger alluvium which consists of grey-brown sands, silts and clays is the product of the most recent cycle of erosion. It is over 10 m thick in some places (Olowu, 1967). The superficial deposits rest almost everywhere on the weathered basement. The thickness of the weathered zone is not certain but there is evidence that it can attain 16 m or more especially in places where the older laterite is still preserved (McCurry, 1970).

Tables 4.3 (a and b) respectively show the resistivity values of rock types in the basement areas and the resistivity values of earth materials in the Kubanni Basin as used in previous works in the basin (Shemang, 1990).

4.2.3 The data collection

The field work was undertaken in June 1993. The area covered by the study is the entire Kubanni Basin. As much as possible, stations in the present work were sited in some of the villages covered by Shemang in 1990 although his stations were not exactly reoccupied as their exact location were not known. In all, twenty-four stations were occupied. Vertical electrical sounding was performed in twenty-three of these stations while horizontal profiling was performed in one of these twenty-three, and the twenty-fourth station. A total of thirty-one vertical electrical soundings were made; a sounding each in twenty-two of the twenty-three stations mentioned and nine sounding stations established in NAERLS alone. Two depth horizontal profiling was undertaken in NAERLS and one depth horizontal profiling was made across the lower channel of the ABU Dam.

In order to establish the correctness of the interpreted results of the two-electrode method, use was

made of the Schlumberger array and the two-electrode method on one hand for vertical electrical sounding, and the use of the Wenner array and the two-electrode method on the other hand for horizontal profiling in the field survey. This was aimed at enabling a comparison to be made between the results of the two-electrode method and the results obtained using other standard and established methods for vertical electrical sounding and horizontal profiling. The interpreted results obtained using the two-electrode method were compared with the results obtained using the standard interpretation techniques for both of the Schlumberger array and the Wenner array.

TABLE 4.1 Typical Resistivity Values of Earth Materials in Basement

(a) Resistivity Values of Rock Types in Basement Areas (After Shemang, 1990)

Rock Type	Resistivity (Ohm-m)
Fadama loam	30 - 90
Clay, silt and sand	100 - 200
Sand and gravel	100 - 180
Weathered laterite	200 - 500
Fresh laterite	501 - 800
Weathered basement	20 - 100
Fresh basement	> 1000

(b) Resistivity Values of Materials in the Kubanni Basin (After Shemang, 1990)

Rock Type	Resistivity (Ohm-m)
Fadama loam	30 - 70
Clay, silt and sand	71 - 200
Sand and gravel	100 - 180
Weathered laterite	181 - 500
Fresh laterite	501 - 800
Weathered basement	20 - 150
Fractured basement	600 - 1000
Fresh basement (Crystalline)	>1000

Figure 4.2 also shows the distribution of the twenty-four stations at which the field surveys were carried out within the Kubanni River Basin.

The main aims of carrying out this field test are

- to find out if the result of the model study in reality represents the real earth situation, in which case the inferences and deductions drawn from the laboratory work were corroborated by, and transferable to the real earth situation;

- to find out if the two-electrode array could, in the real earth situation, delineate the different layerings within the earth structure between the earth surface and the basement.

During the field survey, adequate care was taken to ensure the reliability of the collected data as follows:

- Apart from ensuring that all electrical components were well grounded, it was equally ensured that there were no open joints. This was aimed at eliminating current leakage into the ground; current leakage introduces a pseudo-source into the earth and thereby induces errors in the measured response.

- Because of the dependence of measured response on the electrode spacing, L, adequate care was taken to ensure that accurate measurement of L was made at each electrode separation.

- Of utmost importance to the measurement of layer resistivity using the two-electrode array is the condition that the resistivity of the surface layer be uniform (Rust, 1938; Van Nostrand and Cook, 1966). To ensure this, at every station and sites investigated during the field survey, a horizontal profiling of the surface layer was always carried out. In order to be certain that only the surface layer was being profiled, a small electrode spacing of a = 1 m was always applied using the Wenner configuration and L = 1 m applied using the two-electrode array. This value of electrode spacing was chosen since the depth of investigation for either of the two arrays was not expected to be greater than this value at this electrode spacing. Moreover, doing so ensured that the measurements were made at the same electrode spacing so that the readings could easily be compared if need be.

As earlier stated, during the field survey both vertical and horizontal profiling was carried out. The major horizontal profiling work was carried out along

-- two profiles, each 600 m long in NAERLS, with Wenner array a = 30 m and two-electrode method L = 30 m spread, and

-- one profile 600 m long across the Kubanni river channel near the ABU Dam, with Wenner array a = 60 m and two-electrode method L = 60 m spread.

4.3 Data Analysis and Interpretation

4.3.1 Treatment of field data obtained using the proposed method

Using the field equipment arrangement of figure 4.1, the driving voltage, V, and the current, I, flowing through the earth were read off from the analogue voltmeter and the digital multimeter respectively. The resistance R, of the earth material between the current electrodes was calculated using the usual expression of equation (1.17b). The resistivity of the earth material was then calculated using equation (2.30).

A set of the computed apparent resistivity values for a particular profile form the field resistivity data collected for that sounding station. The computed apparent resistivity values were, in both cases of vertical electric sounding and horizontal profiling, plotted on a log-linear graph based on the theory of equation (3.15).

This interpretation technique took into consideration the fact that when a particular layer is sounded, the response as picked up on the surface by the measuring instrument represents the contribution of that layer itself and the overlying layer(s). The layer resistivity was then calculated as a function of the resistivity of the overlying layer. The procedure for calculating the layer resistivity is given as follows:

- the slope values were calculated;
- the slope indices/straightening factors and their reciprocals were calculated;
- the closeness of the slope values were checked to determine the location of the basement; the

basement is then identified as the layer with the first of the two of such very close slope values;

- the intercept of each layer on the vertical axis were read off; the most important being the intercept of the first layer on this axis;
- the intercept of the first layer on the vertical axis was fixed as the resistivity of the top layer ;.
- the resistivity value(s) of the underlying layer(s) were composed by multiplying the computed resistivity value of the overlying layer with either the straightening factor or its reciprocal for the layer; these were used in such a way that the basement value will not be too low or too high. A decision therefore had to be taken for each layer so that the product of the multiplying quantities would match the composition;.
- the point of intersection of adjacent segments of the graph projected on the L axis was read off. This is the depth to interface between the layers; the thickness of the overlying layer was then calculated by working out the neccessary subtractions.

The geoelectric two-electrode VES interpretation for all the stations covered are shown in Appendix C1.

In interpreting the field data obtained using the proposed method, the interpretation applied to the model data in section 3.4 was also applied. Moreover, the interpretation was strictly tied to the geology of the field test area.

4.3.2 Treatment of field data obtained using the Schlumberger array

The SAS 300 terrameter gave a direct output reading of the earth resistance R. For each current electrode spacing in relation to the potential electrode spacing, a new value of R was measured by the terrameter. A set of apparent resistivity values for a particular profile form the field resistivity data collected for that sounding station. The apparent resistivity values, ρ_a was computed using the equation

$$\rho_a = KR \qquad \ldots\ldots 4.1$$

where K is the geometric factor of the configuration. K was calculated using the expression

$$K = \pi\left[\frac{a^2}{b} - \frac{b}{4}\right] \qquad \ldots\ldots 4.2$$

where a is half of the current electrode spacing

and b is the potential electrode spacing.

For the Wenner configuration, a = 1.5b, hence

$$K_{Wenner} = 2\pi b \qquad \ldots\ldots 4.3$$

The computed apparent resistivity was plotted against L (half the current electrode spacing) on a bi- logarithmic scale for the vertical electric sounding. For the horizonal profiling, either of a log-log or a log-linear graph would do.

The interpretation of data from electrical sounding survey involves expressing in geological terms the information given by the measured apparent resistivity

data. For the interpretation to be reliable, a considerable practical experience with the method in use as well as a versed knowledge of the geology of the area under study is necessary. For the purpose of this work, all available geological information on the field test area was taken into consideration to guide in the interpretation. As usual, each layer of rock type in the area was assumed to be homogeneous and isotropic, implying that the lateral variation in conductance was ignored.

In interpreting the VES data collected in this work using the Schlumberger configuration, a computer program written and developed by Mooney (1980) was used. The use of the computer programs involves the following steps:

- the assumption and supply of a trial model; this involves the supply of a realistic earth model as a first model to be used by the program; the parameters of the assumed model fed into the computer at this stage include the number of data points, the number of layers, the field resistivity data, the resistivity value of each layer and the thickness of each layer; the parameters of the initial model were determined using the partial curve-matching procedure (Keller and Frischknecht, 1966);

-- computation of the theoretical field curve were expected from the trial model;

-- comparison of the computed resistivity curve with the observed field resistivity curve; and

-- modification of the model, where necessary, to improve the agreement between the computed and

the observed data until the best possible agreement is achieved.

Stages two and three were automatically executed by the computer program by making use of the parameters supplied in the first stage. Step four is achieved by the interpreter who modifies the trial model for the program to re-execute stages two and three. The program make use of the supplied initial parameters to compute a theoretical apparent resistivity curve which it then compares with the observed field curve and then iteratively modifies the initial parameters until the best fit between the observed field curve and the computed curve was obtained. The iterative process was terminated only when the error falls below a specified cut-off value or the process had gone through a specified number of iterations. The process, at this point, falls back to the interpreter who, if not satisfied with the match, or found out that the computer interpretation did not fit the geologic parameters of the study area, goes back to modify the initial parameters and the whole process is repeated all over again until a geologically acceptable interpretation is achieved.

Figure 4.5 shows the geoelectric interpretation of the depth sounding data at Station 1 (FCE Zaria) following the earlier discussed four stages of interpretation. The observed field data are represented by dots while the computed resistivity values are represented by crosses. The r.m.s error, which is a measure of fit between the computed and observed curves was 15.318 for the input model (zero iteration) and 8.060 after twenty iterations.

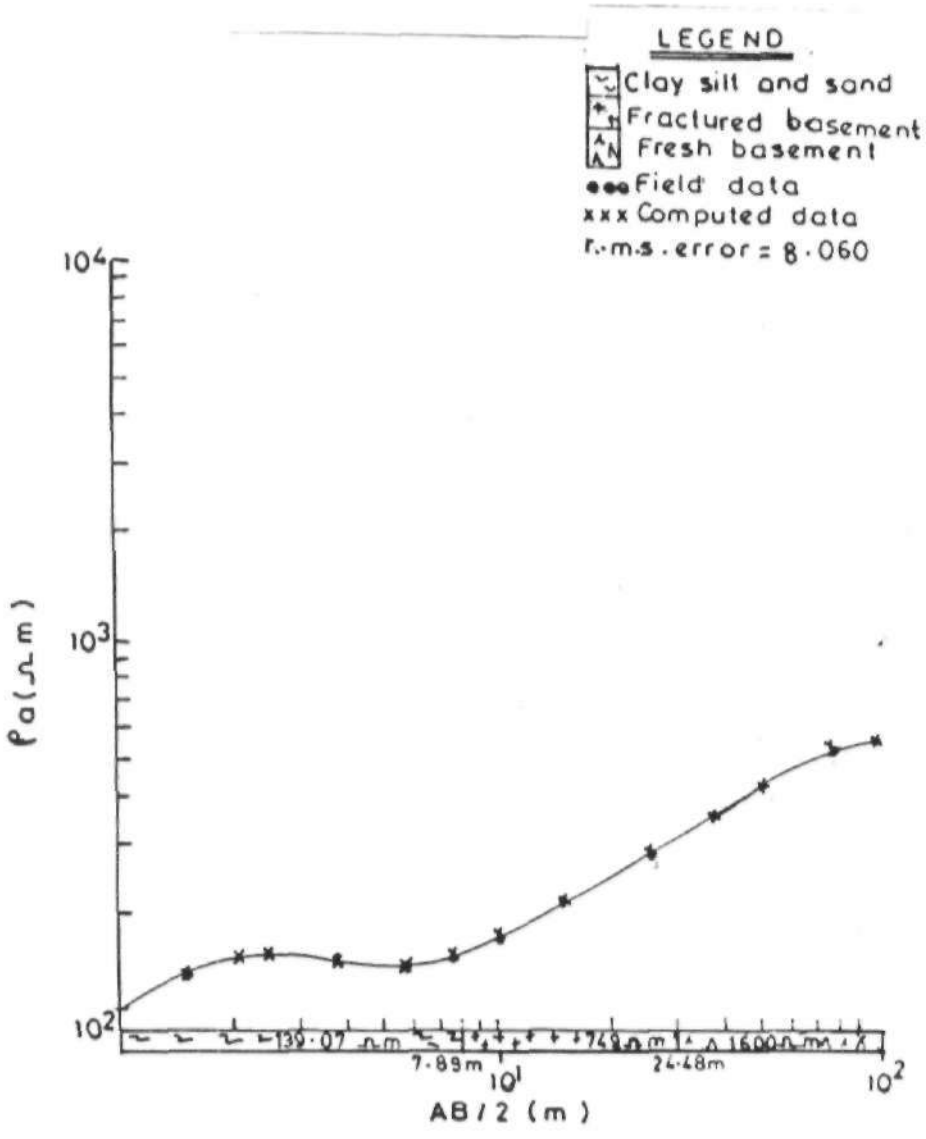


Figure 4.5: Interpreted Schlumberger Values for FCE, Zaria

In order to improve the accuracy of the interpreted data and hence minimize the number of iterations, a number of steps had been taken at the data collection stage. These include ensuring that the electrode spacing was increased at a constant logarithmic interval and, making six data points to lie within each decade of AB/2 as required by the computer program used for the interpretation of the data.

The geoelectric Schlumberger VES interpretation for all the stations covered are shown in Appendix C2.

The interpretation of the data collected in the process of horizontal profiling using the Wenner configuration and the two-electrode array involve

- plotting the field resistivity data on a log-linear scale, and
- reading off the resistivity value at any point of interest along the apparent resistivity against electrode separation profile so constructed. The resistivity profile shows the lateral variation of the top layer resistivity along the profile length.

In this case a computer interpretation is unnecessary.

4.4 Horizontal Profiling Results

4.4.1 Field data obtained using the proposed method

As earlier stated in section 4.1.3, the major horizontal profiling was carried out in NAERLS and at the ABU Dam site.The graphical result of this profile is shown in figure 4.8. The entire field data obtained using the two-electrode array are shown in Tables 4.2 to 4.7. while the graphical results are shown in figs. 4.6 to 4.8 .

TABLE 4.2 NAERLS Profile 1

P	V(v)	I(mA)
1	30.0	60.1
2	34.0	60.2
3	42.0	59.8
4	46.0	59.6
5	44.0	59.5
6	37.0	60.2
7	32.1	60.3
8	29.9	60.2
9	28.4	60.2
10	28.1	59.9
11	29.2	60.1
12	30.2	60.3
13	30.7	59.9
14	31.3	59.9
15	31.9	60.0
16	32.1	60.2
17	33.9	60.0
18	32.5	60.0
19	33.0	60.1
20	33.4	60.0

TABLE 4.3 NAERLS Profile 2

P	V(v)	I(mA)
1	37.0	60.3
2	39.5	60.1
3	38.4	60.2
4	40.3	60.1
5	41.3	59.9
6	42.2	59.8
7	44.6	59.6
8	44.4	59.7
9	40.8	59.9
10	40.8	59.9
11	40.7	60.0
12	39.1	60.1
13	40.8	59.9
14	42.3	59.8
15	40.9	59.9
16	41.0	59.9
17	40.7	59.9
18	40.7	59.9
19	40.8	59.8
20	40.9	59.7

TABLE 4.4 A.B.U. Dam Site

P	V(v)	I(mA)
1	70.0	58.4
2	32.0	59.1
3	42.0	58.9
4	44.1	58.6
5	43.0	58.8
6	40.6	58.5
7	41.5	59.0
8	40.5	58.8
9	40.1	58.9
10	40.0	58.7
11	40.3	58.9
12	40.5	58.9

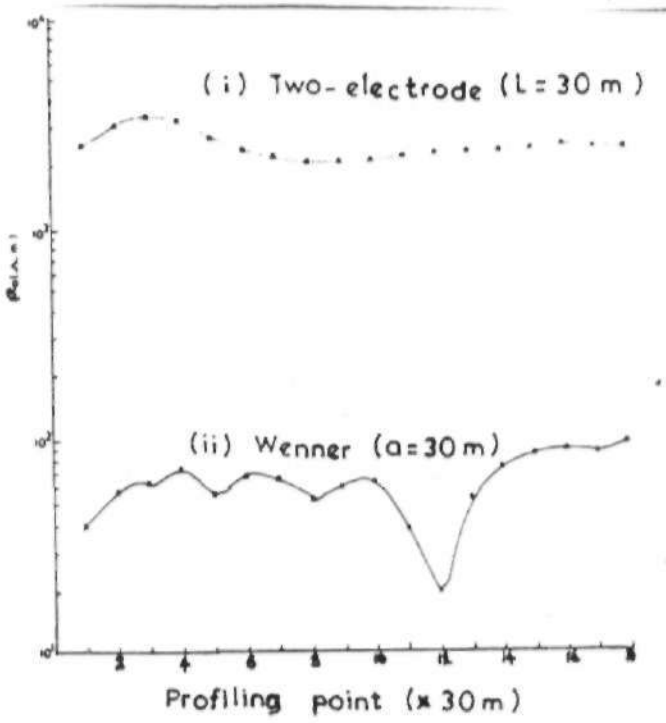


Figure 4.6 Horizontal Profiling. NAERLS Profile 1

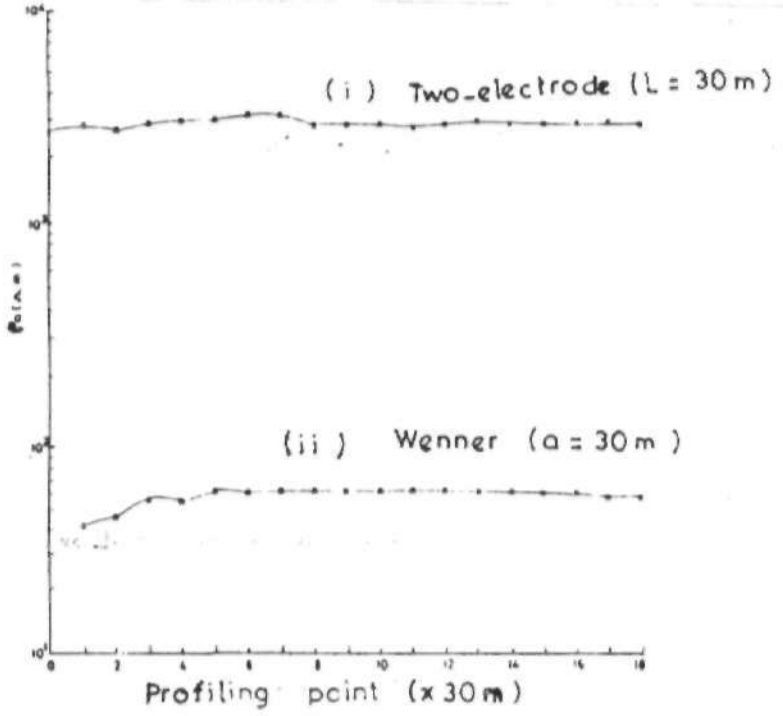


Figure 4.7 Horizontal Profiling. NAERLS Profile 2

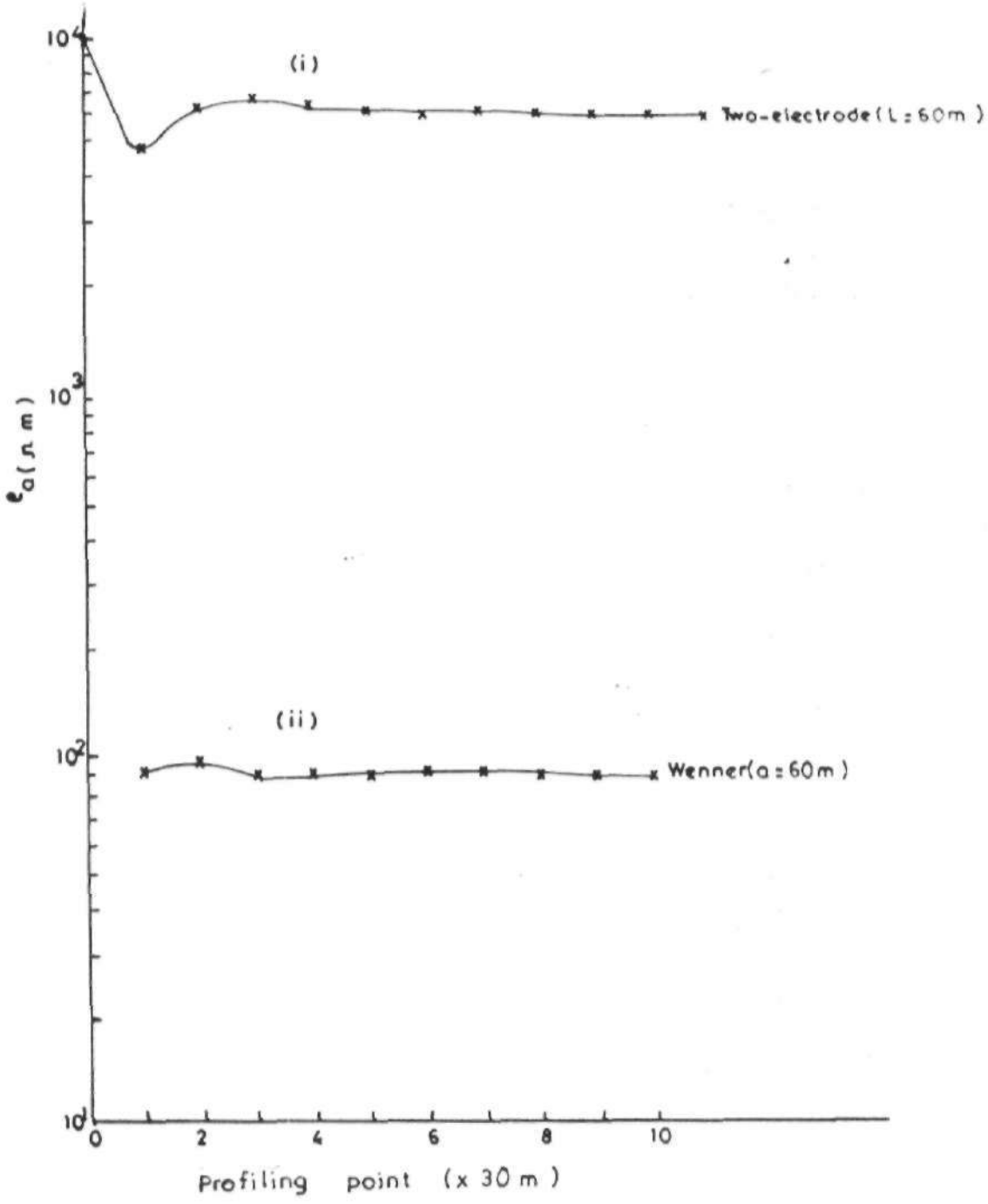


Figure 4.8 Horizontal Profiling for ABU Dam

Horizontal profiling was carried out along two profile lengths in NAERLS. Each profile length of 600m ran from the IAR end towards the Gymnasium end. Profile 1 was laid along the frontage of NAERLS parallel to the wall and tarred road, while profile 2 ran behind the NAERLS building and parallel to profile 1. The resistivity values of profile 1 ranged from about 2,070 Ω-m at the 270 m mark to about 3,400 Ω-m at the 90 m mark. It was found that the subsurface resistivity steadily rose from the 0m mark to its peak at the 90 m mark from where it again steadily decreased to its lowest value at the 270 m mark point. Beyond the 270 m mark point it gently rose uniformly until the end of the profile was reached. The resistivity value of profile 2 appeared to be generally uniform at the depth sampled, the average resistivity being about 3,000 Ω-m.

The result of the horizontal profiling for profile 1 at the NAERLS is shown in figure 4.6 while that for profile 2 is shown in figure 4.7. The kind of horizontal profiling undertaken in this work was not the common surface horizontal profiling usually undertaken in most geophysical surveys. The electrode separations used in this survey were very large, thereby reaching greater sounding depths below the surface. For the NAERLS site, electrode separation a = 30 m was used for the Wenner array and L = 30 m was used for the two-electrode array. The Wenner array therefore investigated a depth of about 10 m (one-third of the current electrode spacing while the two-electrode method investigated a depth of about 30 m (the current electrode spacing spread). This difference in the depth of investigation accounted for the difference in the shapes of the two profiles as shown in figure 4.6 .

Horizontal profiling was also carried out close to the A.B.U.Dam running from the Water Works end to the Ungwan Maigamo end. An electrode spread length of L = 60 m and a = 60 m was used for the two-electrode and the Wenner arrays respectively. The profile length was 600 m. The greatest depth resistivity value of about 10,000 Ω-m was recorded at the 0 m mark and the lowest, of about 4,800 Ω-m, at the 60 m mark. Beyond the 240 m mark, the depth had an average resistivity of about 6,000 Ω-m.

4.4.2 Field data obtained using the Wenner array

Figure 4.6 shows the depth resistivity graph for NAERLS profile 1 taken with a Wenner electrode separation, a = 30 m, along with that taken with the two-electrode array with L=30 m. The graphical result shows that the resistivity at depth is not uniform. The lowest value of about 19.5 Ω-m occurs at the 360 m mark and the highest value of about 98 Ω-m occurs beyond the 540 m mark.

For NAERLS profile 2, there is a depth resistivity low of 41 Ω-m at the 30 m mark. The resistivity at depth generally rose to about 60 Ω-m at the 150 m mark beyond which the resistivity at depth appeared to be uniform at an average value of about 61 Ω-m (Fig. 4.7). The profiling was also taken with a Wenner electrode spacing a = 30 m.

The depth horizontal resistivity profiling with electrode spacing, a = 60 m undertaken at a site close to A.B.U. Dam shows that at the depth of investigation, the resistivity is uniform in this area (Fig. 4.8). The average value being about 90 Ω-m.

The field data obtained using the Wenner array are shown in Tables 4.5 to 4.7.

TABLE 4.5 NAERLS Profile 1

P	R(Ω)	ρ (Ωm)
1	0.204	38.45
2	0.297	55.98
3	0.326	61.45
4	0.375	70.69
5	0.282	53.16
6	0.348	65.60
7	0.336	63.33
8	0.267	50.33
9	0.306	57.68
10	0.325	61.26
11	0.197	37.13
12	0.103	19.42
13	0.271	51.08
14	0.386	72.76
15	0.446	84.01
16	0.467	87.95
17	0.456	85.99
18	0.510	96.11

TABLE 4.6 NAERLS Profile 2

P	R(Ω)	ρ (Ωm)
1	0.215	40.55
2	0.239	45.06
3	0.293	55.17
4	0.287	54.09
5	0.319	60.10
6	0.311	58.66
7	0.325	61.25
8	0.330	62.13
9	0.330	62.13
10	0.322	60.74
11	0.325	61.33
12	0.328	61.86
13	0.318	59.96
14	0.324	61.03
15	0.312	58.88
16	0.311	58.67
17	0.303	57.19
18	0.305	57.44

TABLE 4.7 A.B.U. Dam Site

P	R(Ω)	ρ (Ωm)
1	0.242	91.23
2	0.249	93.87
3	0.231	87.08
4	0.237	89.35
5	0.235	88.59
6	0.241	90.85
7	0.242	91.23
8	0.239	90.10
9	0.235	88.59
10	0.233	87.84

4.5 Depth Sounding Results

4.5.1 Field data obtained using the proposed method

Tables in Appendix B1 show typical depth sounding field data obtained using the proposed method. Typical graphical display of the resistivity data for the stations are shown in Appendix C1. Two approaches have been used for the interpretation of the depth sounding data. These are

the "equivalent cylinder" approach whose theory of interpretation has been given earlier on, and the "specific resistance" approach. In the "specific resistance" approach, following the derived expressions of equations (2.44) to (2.53), the specific resistance of the volume of earth trapped within the hemispherical and near-spherical bowl assumed bounded by the pattern of current flow between the two current electrodes was calculated. Figures in Appendix C3 show typical plot of the specific resistance against electrode spacing for the laboratory model while figures in Appendix C4 show the same plot for the field survey sites. It is evident from these graphs that other than the depth to interface that can be determined from the "specific resistance" against electrode spacing plot, no other meaningful deduction(s) can be made. This therefore rules out the usefulness of the specific resistance approach in providing an adequate interpretation to the problem of the two-electrode method.

In using the "equivalent cylinder" approach, equations (3.15) and (3.23) came in handy. The adopted interpretation approach was able to provide means of estimating the layer resistivity from the intercept of each segment on the vertical axis, and the layer thickness from the point of change of slope of the graph as read off on the horizontal (electrode spacing) axis. Thus, with the equivalent cylinder approach, it was found possible to obtain a rough estimate of the layer resistivity and the layer thickness. Typical layer resistivity values graphically deduced for FCE (Fig.4.9) are shown below

$s_1 = 0.266883 m^{-1}$ $\quad$ $s_2 = 0.03562 m^{-1}$

$s_1/s_2 = 7.4925$ $\quad$ $s_2/s_1 = 0.1334667$

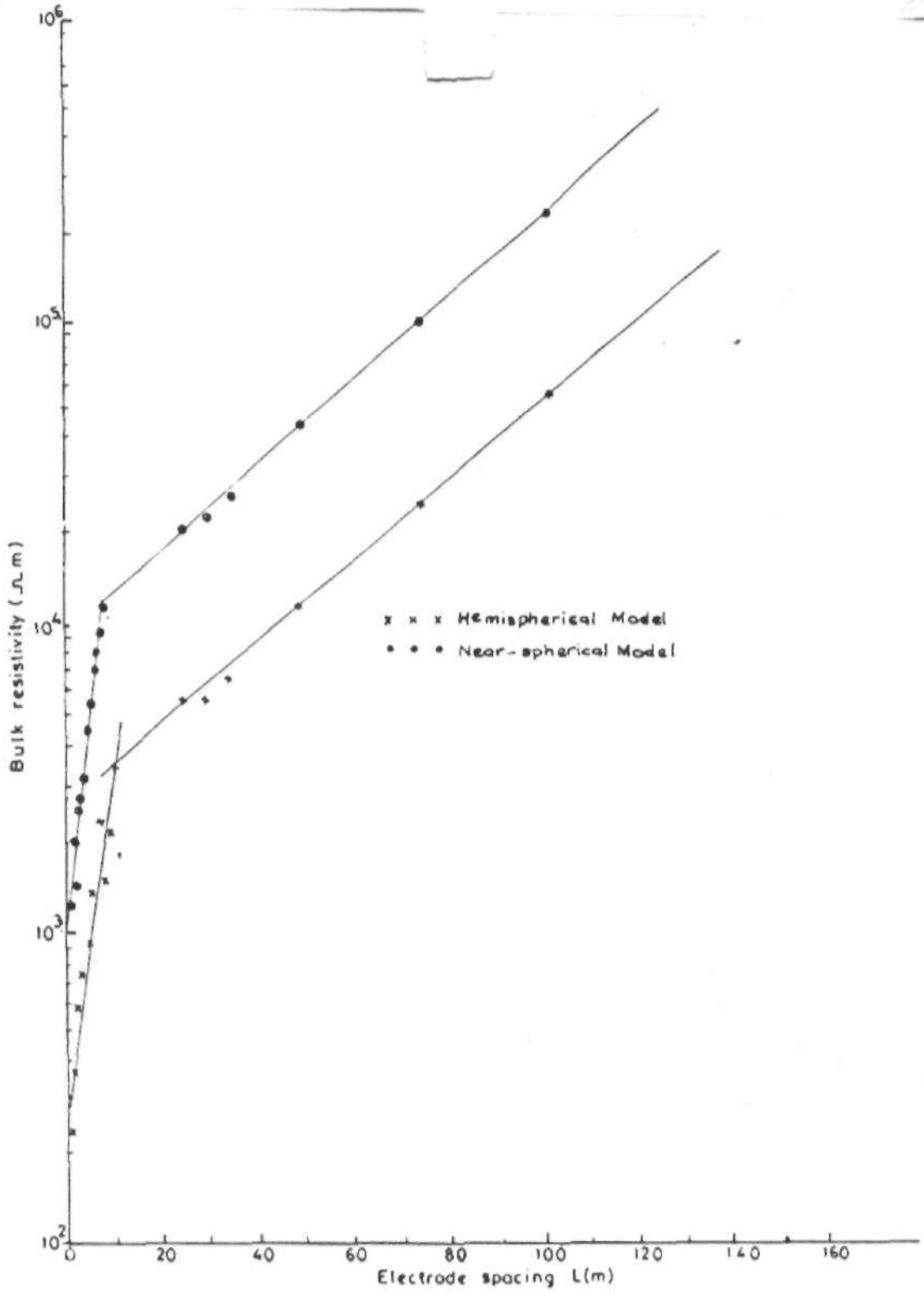


Figure 4.9: Graph of Bulk Resistivity Against Electrode Spacing for FCE Zaria, Using the Two-Electrode Method.

c_1 = 260Ωm c_2 = 2750Ωm

$\rho_1 = c_1$ = 260Ωm; h_1 = 10.0m

ρ_2 = 260 x 7.4925 = 1948.051Ωm; $h_2 = \infty$

Similar procedure was adopted in calculating the layer resistivity for other stations investigated. The result of the two-electrode depth sounding resistivity interpretation as obtained using both the "equivalent cylinder" approach and the specific resistance" approach are shown as part of Table 5.2.

4.5.2 Field data obtained using the Schlumberger array

Tables in Appendix B2 show the typical depth sounding data obtained using the Schlumberger array. Figures in Appendix C2 also show the typical graphical results of the Schlumberger array resistivity data.

The depth sounding data were interpreted using the procedure highlighted by Mooney (1980). The results of the interpreted data using the Schlumberger array are shown as part of Table 5.2.

4.6 Comparison Of Depth To Basement Values Obtained In The Kubanni Basin From This And Previous Works

A comparison is made here between the depth to basement values obtained in the survey area using the two-electrode method with the depth to basement values obtained with the Schlumberger array used in this work on one hand, and on the other hand, with the depth to basement values obtained in the survey area by some of the other previous workers in the study area. Because the proposed two-electrode method is a new method under development, there is the need to standardize the method against other well-known methods for which is available standard

interpretation techniques. This standardization will be in the form of being able to ascertain whether or not the method is able to delineate the earth layers effectively as, or more effectively than, the other methods of investigation used by other workers. Moreover, it is necessary to find out if this method locates the basement the way other methods locate it or not. The comparison will enable us to evaluate the competency and effectiveness of the new method in giving true and reliable information about shallow subsurface conditions and hence determine whether or not it is a method that is good enough for use in electrical geophysical prospecting.

In this work, a depth to basement map of the basin as obtained from the interpreted results of the proposed two-electrode method was produced. This map is shown in figure 4.10(a). Also produced is a depth to basement map of the basin as obtained from the interpreted results of the Schlumberger array used in this work. This map is shown in figure 4.10(b). The nature of the contours of figures 4.10(a) and (b) were compared with the depth to basement map produced by Shemang (1990), shown in figure 4.10(c), and that produced by Bajeh (1992), shown in figure 4.10(d).

The depth to basement map of figure 4.10(a) is well comparable with figures 4.10(c) and (d) in terms of the depth estimate at the various locations they have in common and the direction of trending of the resulting depression. Hassan (1987), Shemang (1990) and Bajeh (1992) reported a depression trending NW-SE and E-W at about the middle of the Western half of the basin. This same depression shows up in figures 4.10(a) and (b). Using the values of Shemang (1990) as the authentic data for previous geoelectric survey in the basin, it was observed that the values of depth to basement used by Shemang (1990) in producing his

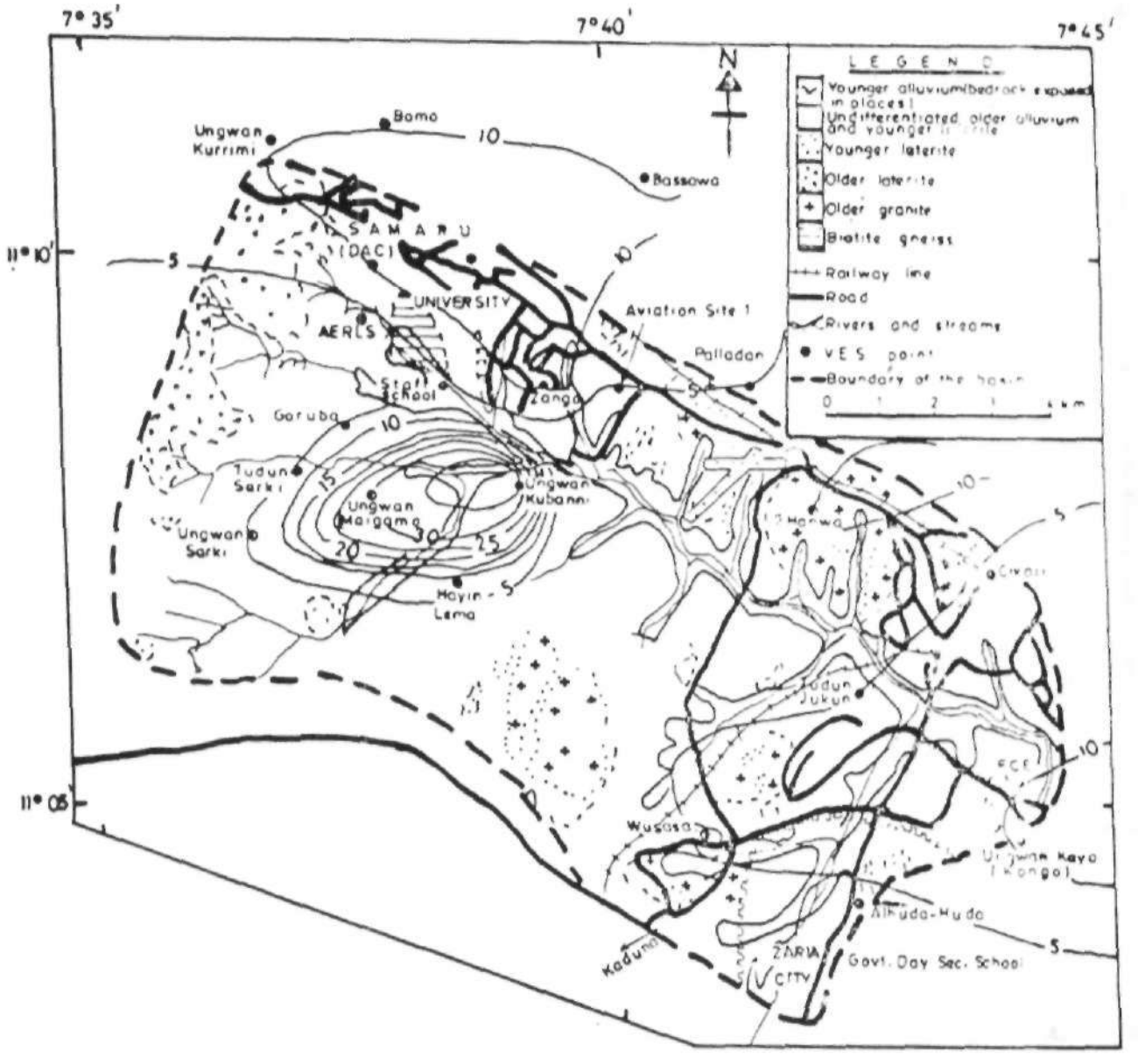


Fig 4.10(a) Depth To Basement (Overburden Thickness) Map Deduced from Electrical Resistivity Data using the Two-Electrode Method Superimposed on the Outcrop Map of the Kubanni Basin.

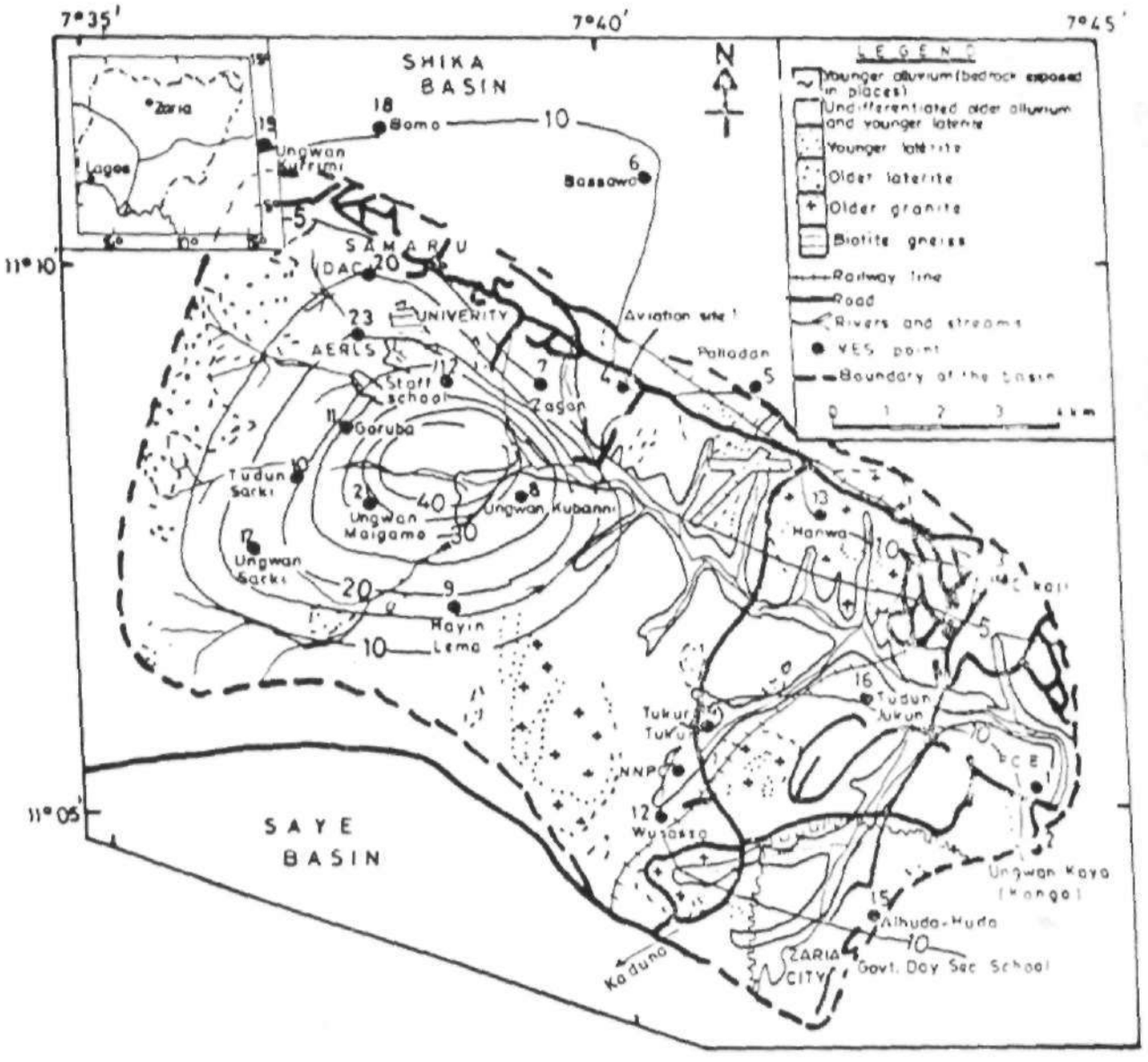


Fig 4.10(b) Depth To Basement (Overburden Thickness) Derived from Schlumberger Sounding Data (used in this work) Superimposed on the Outcrop Map of the Kubanni Basin.

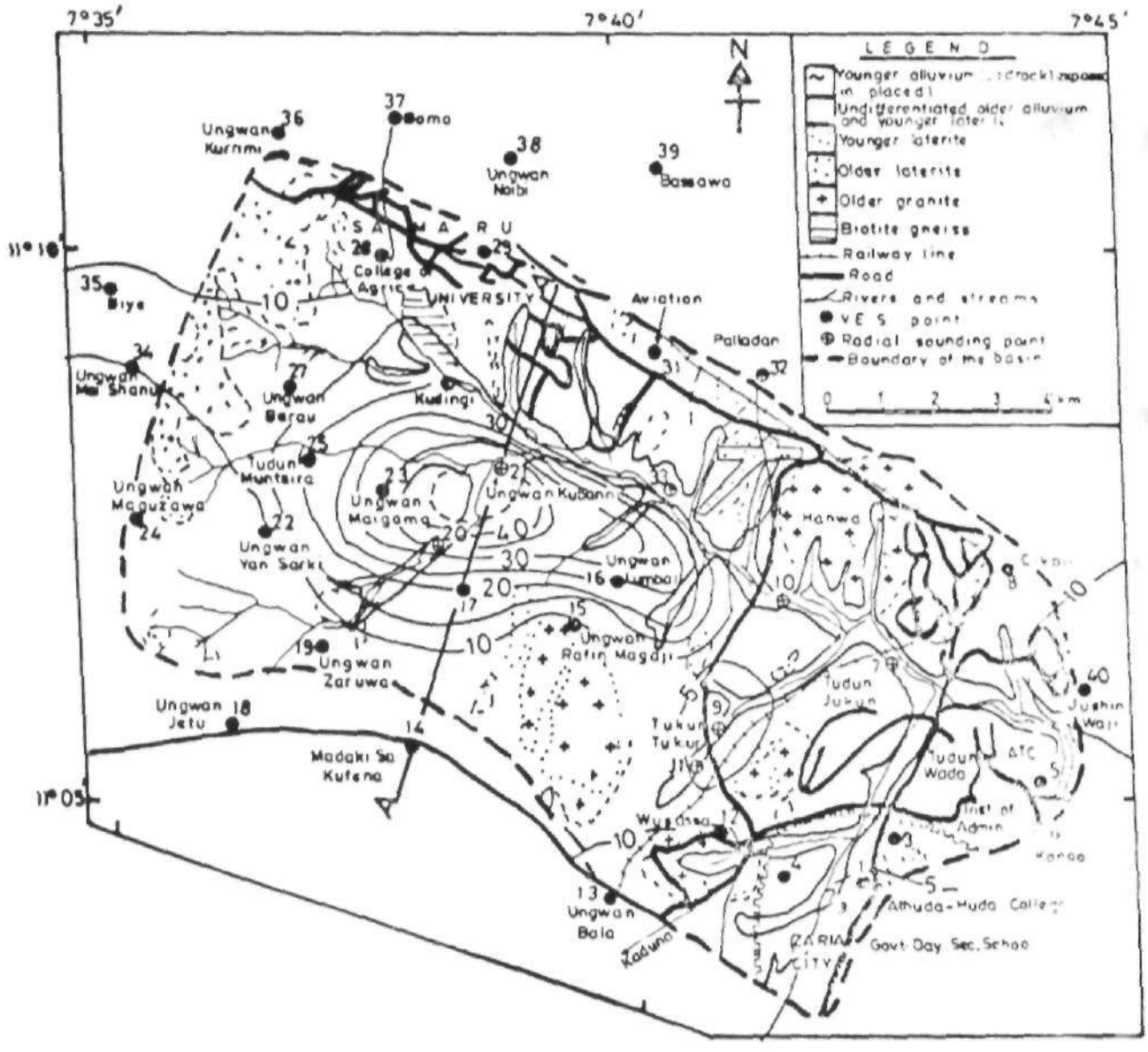


Fig 4.10(c) Depth to Basement (Overburden Thickness) Map Superimposed on the Outcrop Map of the Basin (As obtained by Shemang, 1990)

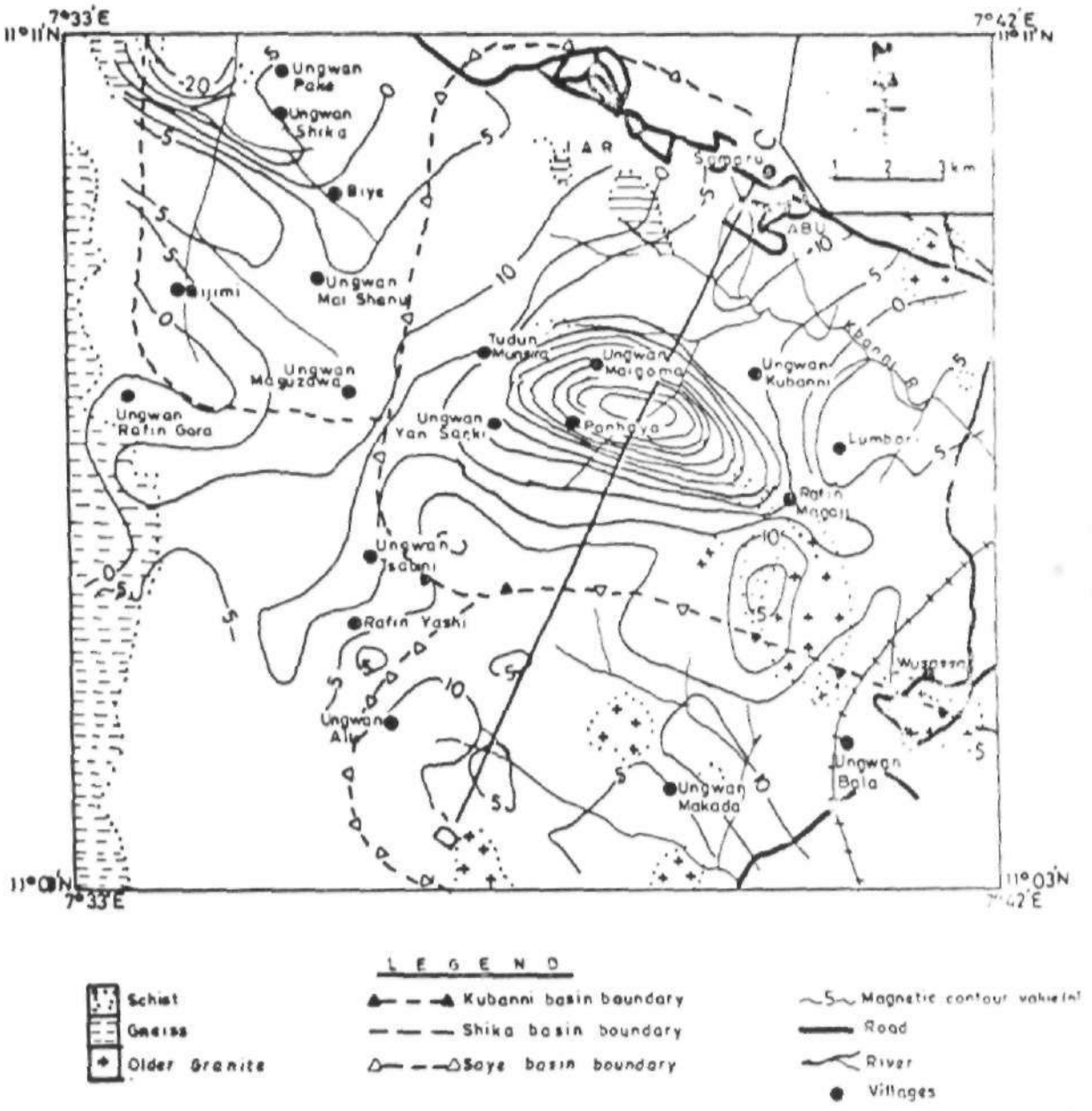


Fig 4.10(d) Depth to Basement (Overburden Thickness) Map Superimposed on the Outcrop Map of the Basin (As obtained by Bajeh, 1990)

map actually correspond with the overburden thicknesses obtained using the two-electrode method except for a very few sites. In most cases, both the Schlumberger and the two-electrode method delineated the same number of layers and recorded about the same depth to basement. Because at least three sounding points must fall in line approximately for it to be possible to pick up a layer convincingly on the graph, it was observed that whenever the top layer became as thin as less than 2 m, it became difficult to pick the layer up on the graph of bulk resistivity against electrode spacing plotted for the two-electrode method. The result of this was usually that the otherwise first layer became merged with the otherwise second layer to form a thicker top layer. The implication of the above is that the method may not be useful in locating thin layers even at the surface except if a smaller electrode spacing is used.

Figure 4.10(a) clearly shows that the depth to basement as defined by the variant of the two-electrode method used here is not much different from the basement as defined by the Schlumberger array. The identification of the basement became even much easier when the discriminators are applied to the two-electrode method. For the variant of the two-electrode method considered here, the depth to basement was found to vary from between 0m and about 45 m in the basin. The basement relief was found to correlate with that shown in figures 4.10(c) and (d). Table 5.2 shows a comprehensive summary of results for this and previous geoelectric works.

CHAPTER FIVE

DEDUCTIONS AND CONCLUSIONS

5.1 Goals And Achievements Of The Present Work

The mode of the two-electrode array as presented in this work has as its goal that, at the completion of its full development, it should be equally useful and versatile in carrying out electrical geophysical surveys to which the common electrode arrays are found applicable. As a first step towards making this mode of the two-electrode array available for use as a major electrical method in prospecting for minerals, groundwater, and buried structures, effort was made in this work to apply the method in prospecting for horizontal layers. The result of the laboratory scale model shows that the mode can easily be used to delineate boundaries of horizontally laid homogeneous layers. The field test results also corroborated the laboratory model results in that when the computed resistivity values were plotted against electrode spacings, soundings which fall in a particular layer all line up and have a common linear relationship between them on the plotted graph. From the results of the resistivity soundings, it could be concluded that each sounding station was distinctly sampled and the layers well delineated by this mode of the two-electrode array. This initial success of the mode in the situations already mentioned, gave a lead to the fact that for a complete success and application of this method to other prospecting activities, a reliable and efficient interpretation technique would have to be developed so that the array would not only show the layerings, detect the buried structures, but also determine the layer/overburden thickness(es) and resistivity correctly and convincingly.

Found most easily adaptable to the present work among the interpretation methods of vertical electrical soundings is the direct method of interpretation. For the common four-electrode Schlumberger arrangement, various direct methods of interpretation have been given by Bernabini and Cardarelli (1978), Mohammed and Habberjam (1977), Rösler and Schallar (1978), and Roy (1978). In an attempt to derive an interpretation regime for the mode of the two-electrode array used in this work, it was observed that all of the above mentioned possible ways out are only well applicable to the four-electrode array. Effort therefore need to be made to modify them suitably to be applicable to the two-electrode array under consideration.

In this work, a simple graphical procedure for computing the layer resistivity was proposed. The procedure was strictly tied to the geology of the area under investigation. Moreover, some possible conditions for discrimination were observed and introduced to help in fixing the position of the basement. The interpretation procedure worked well over the entire stations investigated. Nevertheless, it is not being stated here that it has become a standard rule of interpretation for this method. Noted however is that the theory underlying the adopted procedure compares well with that of Watson and Johnson (1938), Pekeris (1940) and, Sanker Narayan and Ramanujachary (1967).

5.2 Comparison of Model Results (Between the Two-Electrode Array and the Model Values)

The interpreted resistivity and layer thickness values for the VES data collected using the two-electrode method over the model earth material was compared with the originally emplaced model values. From the results,

discussed in section 3.5 and summarized in Table 5.1, it was found out that there was much agreement in layer thickness values between the values obtained using the two-electrode method and the emplaced model values.

Table 5.1 shows the comparison between the results obtained using the two-electrode method and the model values. It was found that both the "equivalent cylinder" approach and the "specific resistance" approach yielded excellent results in terms of the layer thicknesses when compared with the model values. As earlier stated, the result of the "equivalent cylinder" approach is favoured over the "specific resistance" approach. The percentage error ϵ , given in the table was calculated from the comparison between the "equivalent cylinder" approach and the model values in terms of the layer thickness(es).

5.3 Comparison of Field Results

(Of the Two-Electrode Array, the Wenner Array and the Schlumberger Array).

5.3.1 Horizontal profiling

The horizontal profiling as carried out during the laboratory model studies and the field test differ much in nature and intent. The horizontal profiling as executed in the laboratory model was the conventional one in which a small electrode spacing was used to profile the surface layer with the sole aim of either ensuring that the surface resistivity of the host medium was uniform or that a lateral inhomogeneity be detected. The horizontal profiling carried out during the field survey used a large electrode spacing, large enough for the current to get to or close to the basement. In which case, the intention was not to profile the surface layer but to do a sort of depth profiling.

Table 5.1: Comparison of Results Between the Two-Electrode Array and the Model Values

A: Resistivity Values of Major Earth Materials/Electrolyte Used Using Various Methods/Arrays

Method/Array	Resistivity Values in ohm-metre Water	Lateritic Clay	River Sand
Two-electrode (Graphical)	34.	32.	1000.
Wenner (a=2cm)	31.	33.	844.
Tube Method	38.	34.	1720.
Metre Bridge Method	40.	33.	4720.

B: Comparison of Layer Resistivity and Thickness Values Obtained from Direct Measurement

Material	Model Values			Equivalent Cylinder Approach			Thickness Error Estimate (%)	Specific Resistance Approach ρ		Thickness Error Estimate (%)
	ρ	h	H	ρ	h	H		h	H	
Water	38.	48.7	34.	49.0				52.0		
		∞	48.7		∞	49.0	0.6	∞	52.0	6.8
Lateritic Clay	34.	50.0	32.	51.0				41.5		
		∞	50.0		∞	51.0	2.0	∞	41.5	17.0
River Sand	1721.	50.0		1000.	47.5			57.0		
		∞	50.0		∞	47.5	5.0	∞	57.0	14.0
Clay/	34.	5.0		76.	4.8		5.0	6.5		30.0
River Sand	1721.	15.0		216.	10.5		30.0	13.5		10.0
		∞	20.0	851.	∞	15.3	22.5	∞	20.0	0.0
River Sand/	1721.	9.0		1700.	8.0		11.1	10.0		11.1
Clay	34.	17.0		351.	22.0		29.4	11.0		35.3
		∞	26.0	1098.	∞	30.0	15.4	∞	21.0	19.2
Clay/Mix/	34.	3.0		66.	3.8		25.0	3.5		16.7
River Sand		5.0		221.	7.3		45.0	4.5		10.0
	1721.	15.0		536.	14.5		3.3	13.5		10.0
		∞	23.0	972.	∞	25.6	10.9	∞	36.5	58.7
Clay/	34.	5.5		74.	5.0		9.1	6.5		18.2
River Sand/	1721.	10.0		195.	9.8		2.5	10.5		5.0
Clay	34.	17.0		644.	21.8		27.9	13.0		23.5
		∞	32.5	980.	∞	36.5	12.3	∞	30.0	7.7
Mix/Clay/		4.0		220.	2.5		37.5	5.0		25.0
River Sand	34.	7.5		82.	7.8		3.3	10.0		33.3
	1721.	23.0		373.	23.0		0.0	21.5		6.5
		∞	34.5	733.	∞	33.3	3.6	∞	36.5	5.8
River Sand/	1721.	3.0		680.	2.6		13.3	5.0		66.7
Mix/Clay		7.0		157.	7.7		9.3	10.0		42.9
	34.	17.0		56.	21.3		25.0	24.0		41.2
		∞	27.0	173.	∞	31.6	17.6	∞	39.0	44.4

ρ* - could not be accurately determined.

The result of horizontal profiling as executed in the laboratory model studies, discussed in section 3.5.4 and shown in the graphs of figures 3.30 and 3.31, showed a good agreement in the nature and trend of the graphs obtained using both the Wenner and the two-electrode method. There was no match found, as in the laboratory model studies, in the result of the field test between the Wenner and the two-electrode method. The nature and trend of the graphs and resistivity values were found not to match or agree for the two methods as shown in the graphs of figures 4.6 to 4.8. This is principally due to the fact that the depth of current penetration and hence the depth of investigation for the two arrays are very different. According to Roy and Apparao (1971), the depth of investigation for the Wenner array is only 0.12L while the depth of investigation for the mode of the two-electrode array they used is 0.35L. This therefore would account for the difference in measured resistivity as both of the Wenner array and the mode of the two-electrode array used in this work, which has a depth of investigation of about equal to the electrode spacing, were not sounding the same depth. Because of this difference, the field horizontal profiling results of the two arrays could not be adequately compared.

5.3.2 Vertical profiling

Table 5.2 shows the comparison of field results between the two-electrode method and the Schlumberger array used in this work. The results of the work of Shemang (1990) is also shown as part of the table. This is to enable us make good comparison of values, most especially in the situation where investigations were carried out in the same station(s).

Table 5.2: Table Showing Summary of Results Between the Two-electrode and the Four-electrode Methods

ρ - layer resistivity in ohm-metres
h - layer thickness in metres
H - depth to basement in metres

Station	Two-Electrode Method						Four-Electrode Method					
	Equivalent Cylinder Approach			Specific Resistance Approach			Schlumberger			Shemang's Result		
	ρ	h	H	ρ	h	H	ρ	h	H	ρ	h	H
FCE	260.	10.0		-	7.25		139.	7.89		88.	7.0	
	1948.	∞	10.0	-	9.50		749.	16.59		989.	∞	7.0
				-	∞	16.75	1600.	∞	24.48			
UNGWAN KAYA (KONGO)	210.	11.5		-	8.0		46.	7.72		88.	6.0	
	1711.	∞	11.5	-	∞	8.0	105.	∞	7.72	445.	∞	6.0
CIKAJI	84.	6.5		-	4.5		59.	6.0		50.	7.0	
	488.	16.0		-	12.0		80.	4.5		674.	∞	7.0
	1277.	∞	22.5	-	∞	16.5	588.	∞	10.5			
AVIATION SITE I	250.	4.0		-	4.5		258.	5.0		176.	7.0	
	108.	8.0		-	4.5		204.	5.0		1914.	∞	7.0
	734.	∞	12.0	-	∞	9.0	1001.	∞	10.0			
PALLADAN	95.	4.75		-	7.5		164.	5.0		209.	3.0	
	418.	16.00		-	7.5		298.	7.5		74.	7.0	
	826.	∞	20.75	-	∞	15.0	205.	∞	12.5	1914.	∞	10.0
BASSAWA	115.	8.0		-	4.0		84.	8.83		254.	8.0	
	768.	∞	8.0	-	3.0		629.	∞	8.83	693.	∞	8.0
				-	8.0							
				-	∞	15.0						
ZANGO	140.	11.0		-	3.0		210.	3.24		159.	4.0	
	1009.	∞	11.0	-	3.5		201.	2.27		914.	∞	4.0
				-	∞	6.5	270.	∞	5.51			
JAMAA' KUBANNI	45.	6.0		-	9.0		72.	8.04		217.	8.0	
	432.	29.0		-	18.0		26.	21.52		66.	36.0	
	1159.	∞	35.0	-	∞	27.0	191.	∞	29.56	991.	∞	44.0
HAYIN LEMA	165.	8.5		-	7.5		177.	7.65				
	415.	12.0		-	12.5		44.	9.33				
	2041.	∞	20.5	-	∞	20.0	340.	∞	16.98			
TUDUN SARKI	150.	5.5		-	4.5		119.	5.13				
	1347.	∞	5.5	-	3.5		41.	12.22				
				-	7.0		414.	∞	17.35			
				-	∞	15.0						

GORUBA	40.	7.0		-	3.5		93.	6.0				
	1198.	*	7.0	-	4.0		438.	37.5				
				-	7.5		621.	*	42.5			
				-	*	15.0						
WUSASA	60.	6.0		-	4.5		131.	4.35		79.	2.0	
	441.	*	6.0	-	2.75		190.	2.60		106.	8.0	
				-	2.75		120.	3.37		1364.	*	10.0
				-	*	10.0	518.	*	10.32			
HANWA	170.	6.0		-	4.5		132.	4.90		102.	2.0	
	51.	3.8		-	5.5		60.	6.11		67.	7.0	
	1290.	*	9.8	-	*	10.0	440.	*	11.01	1907.	*	9.0
TUKUR-TUKUR	42.	4.75		-	6.0		103.	11.58		459.	3.0	
	277.	9.25		-	3.25		489.	*	11.58	1696.	*	3.0
	1752.	*	14.0	-	*	9.25						
ALHUDAHUDA	140.	3.5		-	3.0		298.	2.74		773.	2.0	
	66.	16.5		-	11.5		90.	9.33		280.	9.0	
	233.	*	20.0	-	*	14.5	1103.	*	12.07	1507.	*	11.0
TUKUR-JUKUN	62.	5.0		-	6.0		290.	1.95				
	305.	11.0		-	12.0		597.	5.60				
	974.	*	16.0	-	*	18.0	295.	*	7.55			
UNGWAN-SARKI	280.	6.5		-	4.25		284.	3.53				
	45.	19.0		-	13.0		82.	14.44				
	920.	*	25.5	-	*	17.25	1766.	*	17.97			
BOMO	125.	8.5		-	5.5		122.	3.31		129.	3.0	
	810.	*		-	5.5		263.	8.91		28.	7.0	
				-	*	11.0	980.	*	12.22	1596.	*	10.0
KURRIKI-BOMO	60.	3.25		-	6.75		42.	7.90		95.	11.0	
	438.	5.75		-	3.25		293.	4.01		1242.	*	11.0
	940.	*	9.0	-	10.0		537.	*	11.11			
				-	*	20.0						
DAC	230.	2.75		-	6.0		294.	5.0				
	822.	7.25		-	4.5		259.	7.2				
	1369.	*	10.0	-	*	10.5	462.	*	12.22			
HAIGAMO	220.	5.0		-	4.5		175.	3.79		162.	5.0	
	68.	24.0		-	8.0		97.	29.71		74.	30.0	
	588.	*	29.0	-	*	12.5	578.	*	33.50	601.	*	35.0
ABU STAFF-SCHOOL	260.	5.0		-	4.5		276.	5.0				
	47.	23.0		-	23.0		87.	20.0				
	734.	*	28.0	-	*	27.5	139.	*	25.00			
MAERLS	30.	3.00		-	7.0		69.	3.20				
	126.	4.10		-	6.5		131.	4.41				
	1226.	7.15		-	*	13.5	181.	7.32				
	2176.	*	14.3				595.	*	14.93			

As in the model study, there was found to be reasonably good match between the values of layer thickness(es) obtained using the two-electrode method and the Schlumberger array. However, in some cases they neither delineated the same number of layers nor estimated the same depth to basement.

5.4 Recommendations For Future Work

The present work on the current-current mode of the two-electrode array still form the beginning of investigations into the applicability of this mode to various electrical geophysical problems. Since this work forms the beginning of such investigations, other interested investigators may need to look at the problem of the use of this mode from other important angles.

For the realisation of a complete success of this mode of the two-electrode array, it is hereby suggested that:

- An equipment should be developed for use in the field survey. The field equipment should be able to deliver a current of about 250 mA at a voltage of about 700 volts operating at a frequency less than 50 Hz; preferably between 2 Hz and 10 Hz. During the course of this investigation, an attempt was made to develop a suitable field equipment. The equipment developed was able to deliver a voltage of up to 720 volts operating at 40 Hz using a 12 volts d.c. input source. The equipment was only able to deliver a current of about 21 mA at 240 volts and a current of less than 5 mA was delivered at 720 volts. Because of its low current output at high voltages, the equipment was found very much unfit for the field work for which it was initially designed.

- The method should be tested on a site where it is known that a substantial deposit of a known ore or mineral is available. The thickness of the mineral/ore deposit should be reasonably large so that its effect would not be masked by the signal responses from the overlying and the underlying earth materials.

- Wherever this mode of the two-electrode array is tested, effort should be made to make a seismic refraction survey alongside the method even if other electrical prospecting methods are applied. From the field survey undertaken in this work, it was evident that if a seismic refraction survey had been undertaken alongside the two-electrode method, a better comparison of results could have been possible. Moreover, those stations that showed regions of faulting could have easily been verified, and corroborated or otherwise, by the result of the seismic refraction survey.

- The proposed interpretation technique should be adequately tested to ensure its reliability and suitability to every field situation. If however it is found not sufficiently appropriate, a suitable and effective interpretation should be developed for the method. From the experience gathered from both the laboratory model studies and the field investigation, it might be worth it to try out the use of the variation of the driving potential, V, and current, I, with electrode spacing, L, to derive an interpretation technique. Equally possible is a line analysis of the segmentation of the graph. Another envisaged possibility in the course of finding a suitable interpretation technique for this array may be to find

out the form of U(r) that will fit this mode of the two-electrode array so that necessary equations can be used in developing a direct interpretation technique.

- This mode of the two-electrode array should be applied in the field for greater depth investigation. In this wise, the lateral extent of electrode spacing should be made larger than the 200m used in this work depending on the depth of interest. The result should be compared with the result of deep sounding survey conducted using deep sounding array such as the Lee configuration. If the experimentation is successful, it may lead to the application of this method in the search for more valuable minerals at depth.

- An attempt should be made to make this mode of the two-electrode array to be insensitive to lateral inhomogeneities so that the condition that the entire ground/host earth surface should be homogeneous can be rendered unnecessary. The advantage of this will be that the electrodes can be placed at any point on the surface, and take measurements without the readings being affected by the nature of the locality in which the electrode(s) is(are) placed. A basic solution to this problem may likely be found in the design of the field equipment developed for this method.

5.5 Conclusions

Another mode of the two-electrode system has been investigated in this work. In this mode, here called the current-current (C-C) mode, measurements were taken using only the two current electrodes with the potential electrodes completely eliminated. Use was made of the values of the driving potential, V and the corresponding

current, I flowing between the two current electrodes at an electrode spacing, L in determining the resistance and hence the resistivity of the earth material between the two current electrodes.

The mode of the two-electrode array discussed in this work has a series of advantages over the conventional four-electrode array. Among these envisaged advantages are:

- ease of handling: in terms of the number of electrodes that would need to be moved during the field survey, the manpower need, and the non-logarithmic electrode spacing intervals;

- cost effectiveness: as a result of reduction in overhead cost due to fewer manpower need; as only two electrodes would need to be moved at the same time, and the ground measurements would be more direct without the need for overlapping measurements;

- ease of interpretation: as the interpretation was envisaged not to involve rigorous computer use and to involve more of graphical estimation of layer parameters; and

- greater depth of investigation: both the model studies and the field survey showed that the depth of investigation is approximately equal to the electrode spacing.

From the model studies, it was evident that the amount of current capable of flowing into the earth media was mainly controlled by the nature and therefore the conductivity of the surface layer. Where the surface layer is highly conductive, more current flows, such as in the case where clay overlaid other earth materials. Less

current will therefore flow when the surface layer is highly resistive such as in the case where river sand overlaid other earth materials. It was also evident from the model studies that the effect of a layer may be masked by the signal responses of the adjacent layers. In a situation where the earth material's resistivity sharply contrasted the resistivities of earth materials overlying and underlying it; in which case it is sandwitched between two earth materials of about the same resistivity, if its thickness becomes too small, it may never be detected. It will therefore have to be of an appreciable thickness for its presence to be detected. This condition is evident in such a situation as when clay was sandwitched between two layers of river sand or when river sand was sandwitched between two layers of clay. For such a layer to be detectable will require that the electrode intervals be such that three or more samplings could be effected within the layer. This is quite possible because this mode of the two-electrode array does not require that a logarithmic electrode spacing interval be used as in the case of an array such as the Schlumberger array on which the interpretation program imposes the requirement of six soundings per decade in a certain ratio for the data to be interpretable. Hence, any number of soundings can be made within a certain length depending on how detailed the study is supposed to be.

Although the laboratory study suggested that a low-frequency alternating current would be most adequate for the field experimentation, but because an effective and efficient field equipment could not be put in place in good time, direct current source was therefore used during the field survey. The use of a d.c. source was equally investigated and supported by the model studies where it

was found that the overall result using a d.c. or a line source is as good as that obtained using any other frequency below 50 Hz. The field data, though in few cases failed to properly align, also showed that the d.c. source might not be as bad as we had thought it to be. In the majority of stations sampled, the data points aligned perfectly well along a particular line and, in some other cases where they were not perfectly aligned, they showed a particular trend and direction of alignment which enabled a best line of fit to be drawn through the points. All the results presented in the graphs of bulk resistivity against electrode spacing for the model studies and field test are as actually obtained. They have not been subjected to any statistical adjustment or alignment neither have they been manually manipulated. The same goes for other results presented in this work.

The laboratory model study and field investigations of this mode of the two-electrode array have elucidated the viability of conducting electrical geophysical prospecting survey for horizontal layers using the method. The field investigation has also helped in answering some basic questions as regards the layering of the earth structure from the top layer to the basement within the Kubanni Basin.

Among the major contributions of the study are:

- the ability of this mode, the C-C mode, of the two-electrode array to compete fairly with the Wenner array in the process of horizontal profiling;
- the capability of the C-C mode to detect and effectively delineate horizontal layers;

- the capability of the C-C mode to correctly estimate layer thickness and the depth to basement;

There was found to be no detailed previous work done in the Kubanni Basin in the fields of seismic and gravity investigations. Results of these investigations would have been of much assistance in the comparison of the results of the C-C mode with other methods rather than with just the results of previous electrical measurements taken within the basin. It is of note that for now, only an abundance of information on electrical studies of the Kubanni Basin is available. The work of Hassan (1987) and Shemang (1990) among others, form the bulk of the resistivity data for the Kubanni Basin. Magnetic survey of the basin is very recent. The magnetic survey conducted by Bajeh (1992) showed that the depth to basement within the basin varies between 0m and about 50m. Ogah (1990) conducted seismic surveys along fourteen profiles in three villages namely Ungwan Kubanni, Maigamo and Hayin Lema, within the basin. From his study, he concluded that the depth to seismic basement was between 15m and 40m in the areas he worked on in the basin. By using more of other geophysical methods such as gravity and seismic within the basin, the basement could be better defined. Umego (1990) suggested a comparison and correlation of depth to basement values using integrated methods of investigation. From the result of the two-electrode method used in this work, the depth to basement for Ungwan Kubanni was found to be about 35 m, for Maigamo it was about 29 m and, for Hayin Lema it was found to be about 20.5 m. These values are well within the range got by Ogah (1990) using seismic refraction method.

From the summary of results outlined in Tables 5.1 and 5.2, it is quite obvious that of all the approaches outlined, the "specific resistance" approach is the most unsuccessful. This is mainly as a result of its dependence on the volume of earth trapped within the current bowl defined. This volume is outrightly unmeasurable. Moreover, because of inaccuracies in the predicted current flow pattern and tracks due to unknown subsurface conditions, the said volume can never be accurately estimated to make an interpretation technique such as the "specific resistance" approach workable. The interpretation technique adopted for the "equivalent resistance" approach though may not be too perfect, is in most cases comparable with the computer analysis result for the Schlumberger configuration. It is believed that using a commutated voltage source, a source equipment capable of eliminating local inhomogeneity effect and a suitable interpretation technique, the reliability of the C-C mode results would be enhanced and the mode would compare favourably well, even with the Schlumberger array, in vertical electric sounding survey.

The results of the depth to interface deduced from the graphs for the field study supported such results from the model studies that suggested that the probing depth for the C-C mode of the two-electrode array may be about equal to the electrode separation. This therefore implies that the assumption that the pattern of current flow within a homogeneous isotropic earth is hemispherical may not be true afterall as far as the depth of investigation is concerned. However, from the result of the layer

resistivity computed from the graphs, it was found that the layer resistivity values computed using the near-spherical model was in most cases between four and five times the values computed using the hemispherical model for the same parameter. The resistivity values obtained for this parameter using the hemispherical model compared well with that obtained for the Schlumberger array. It can therefore be deduced that the hemispherical model is a better model as far as the determination of layer resistivity is concerned. In conclusion, a balance is struck in that the hemispherical model is seen as a better choice to use in determining the layer resistivity while both the hemispherical model and the near-spherical model give the same estimate of layer thickness. The hemispherical model is therefore adequate for use in estimating layer resistivity and layer thickness but the near-spherical model still remain the actual representation of the pattern and depth of current flow within the earth between two current electrodes. A comparison of the top layer resistivity and thickness obtained using the hemispherical model and the near-spherical model with the Schlumberger array result for the field study.is shown in Table 5.3 .

TABLE 5.3 Comparison of Top Layer Resistivity and Thickness Values Obtained Using the Hemispherical and the Near-Spherical Models, of the Two-Electrode Method, with the Schlumberger Array Result for the Field Study.

Station	Graphical Estimate				Schlumberger	
	Hemispherical		Near-spherical			
	ρ_1(Ωm)	h_1(m)	ρ_1(Ωm)	h_1(m)	ρ_1(Ωm)	h_1(m)
FCE	260	10.0	800	10.0	139.	7.9
UNGWAN KAYA (KONGO)	210	11.5	1000	11.5	46.	7.7
CIKAJI	84	6.5	420	6.5	59.	6.0
AVIATION -SITE I	250	4.0	1500	4.0	258.	5.0
PALLADAN	95	4.8	500	4.8	164.	5.0
BASSAWA	115	8.0	520	8.0	84.	8.9
ZANGO	140	11.0	640	11.0	210.	3.2
JAMAA'- KUBANNI	45	6.0	200	6.0	72.	8.2
HAYIN LEMA	165	8.5	860	8.5	177.	7.7
TUDUN SARKI	150	5.5	700	5.5	119.	5.1
GORUBA	40	7.0	145	7.0	93.	6.0
WUSASA	60	6.0	240	6.0	131.	4.4
HANWA	170	6.0	800	6.0	132.	4.9
TUKUR-TUKUR	42	4.8	260	4.8	103.	11.6
ALHUDAHUDA	140	3.5	500	3.5	298.	2.7
TUKUR-JUKUN	62	5.0	440	5.0	290.	2.0
UNGWAN-SARKI	280	6.5	270	6.5	284.	3.5
BOMO	125	8.5	630	8.5	42.	3.3
KURRIMI BOMO	60	3.3	360	3.3	122.	7.1
DAC	230	2.8	1100	2.8	294.	5.0
MAIGAMO	220	5.0	840	5.0	175.	3.8
STAFF- SCHOOL	260	5.0	1300	5.0	276.	5.0
NAERLS	30	3.0	190	3.0	69.	3.2

REFERENCES

Abbott, P. (1980). Calculus. Hodder and Stoughton, London.

Akpoborie, I.A. (1972). Hydrogeological Control of Structures along Samaru Creek. Unpublished B.Sc. Thesis. Ahmadu Bello University, Zaria.

Apparao, A. and Roy, A. (1971). Resistivity Model Experiments 2 Geoexploration, 9(4): 195-205.

Apparao, A. and Roy, A. (1973). Field Results for Direct Current Resistivity Profiling with Two-Electrode Array. Geoexploration, 11(1): 21-44.

Apparao, A., Roy, A. and Mallick, K. (1969). Resistivity Model Experiments. Geoexploration, 7(1): 45-54.

Bajeh, I. (1992). Ground Magnetic Investigation of the Kubanni River Basin, Zaria. Unpublished M.Sc. Thesis. Ahmadu Bello University, Zaria.

Bernabini, M. and Cardarelli, E. (1978). The Use of Filtered Bessel Functions in Direct Interpretation of Geoelectrical Soundings. Geophysical Prospecting, 26(4): 841-852.

Brizolari, E. and Bernabini, M. (1979). Comparison between Schlumberger Electrode Arrangements and Some Focused Electrode Arrangements in Resistivity Profiles. Geophysical Prospecting, 27(1): 233-244.

Collett, L.S. and Katsube, T.J. (1973). Electrical Parameters of Rocks in Developing Geophysical Techniques. Geophysics, 38(1): 76-91.

Cowles, L.G. (1976). A Sourcebook of Modern Transistor Circuits. Prentice-Hall Inc., New Jersey.

Das, U.C. and Ghosh, D.P. (1973). Interpretation of Dipole Sounding Curves. Geophysical Prospecting, 21(2): 379-400.

Dobrin, M.B. (1976). Introduction to Geophysical Prospecting. McGraw-Hill Book Co. Inc., New York.

Duncan, T. (1982). Physics. John Murray (Publishers) Ltd., London.

Egbeifo, C. (1978). Hydrogeology of the Kubanni Drainage Basin, Zaria. Unpublished M.Sc. Thesis. Ahmadu Bello University, Zaria.

Gupta, R.N. and Bhattacharya, P.K. (1963). Unipole Method of Electrical Profiling. Geophysics, 28(4): 608-616.

Hassan, M. (1987). Geoelectrical Investigations of the Western Half of the Kubanni River Basin, Zaria. Unpublished M.Sc. Thesis, Ahmadu Bello University, Zaria.

Havill, R.L. and Walton, A.K. (1975). Elements of Electronics for Physical Scientists. Macmillan Press Ltd., London.

Katsube, T.J. and Collett, L.S. (1973). Measuring Techniques for Rocks with High Permittivity and High Loss. Geophysics, 38(1): 92-105.

Keller, G.V. and Frischknecht, F.C. (1966). Electrical Methods in Geophysical Prospecting. Pergamon Press, New York.

Kumar, R. (1974). Direct Interpretation of Two-Electrode Resistivity Soundings. Geophysical Prospecting, 22(2): 224-237.

Maddock, R.J. (1969). Intermediate Electronics. Book 2. Butterworth and Co. (Publishers) Ltd., London.

Mares, S. (1984). Introduction to Applied Geophysics. D. Reidel Publishing Co., Boston.

McCurry, P. (1970). The Geology of Degree Sheet 21, Zaria. Unpublished M.Sc. Thesis. Ahmadu Bello University, Zaria.

McGray, J.A. and Cahill, T.A. (1973). Electronic Circuit Analysis for Scientists. John Wiley and Sons, New York.

Mohammed, S.A.G. and Habberjam, G.M. (1977). An Example of the Application of the Rules of Composition in Resistivity Interpretation. Geophysical Prospecting, 25(1): 52-60.

Mooney, H.M. (1980). Handbook of Engineering Geophysics Vol.2: Electrical Resistivity. BISON Instruments Inc., Minnesota.

Morris, N. (1979). Industrial Electronics. Tata McGraw-Hill Publishing Co. Ltd., New Delhi.

Mwenifumbo, C.J. (1980). Interpretation of Mise-a-la-Masse Data for Vein Type Bodies. Unpublished Ph.D. Thesis. The University of Western Ontario, London, Canada.

Nelkon, M. and Parker, P. (1982). Advanced Level Physics. Fifth Edition. Heinenmann Educational Books, London.

Ogah, A.J. (1990). The Application of Beam-Forming Technique to Enhance Low Quality Seismic Refraction Data. Unpublished M.Sc. Thesis. Ahmadu Bello University, Zaria.

Olowu, J. (1967). Preliminary Investigations of the Groundwater Conditions in Zaria Sheet 102 S.W.. GSN Report No. 1462.

Olugbemiro, R.O. (1985). Hydrogeology of Jama'a Kubanni Area (Zaria Sheet 102 S.W.). Unpublished B.Sc. Thesis. Ahmadu Bello University, Zaria.

Ososami, I.A. (1968). Assessment of the Groundwater in the Kubanni Valley. Unpublished M.Sc. Thesis. Ahmadu Bello University, Zaria.

Pekeris, C.L. (1940). Direct Method of Interpretation in Resistivity Prospecting. Geophysics, 5(1): 31-42.

Rösler, R. and Schallar, M. (1978). Geoelectric Measurements in Gradient Media and Equivalent Sequences of Layers. Geophysical Prospecting, 26(2): 122-129.

Roy, A. (1978). A Theorem for Direct Current Regimes and Some of its Consequences. Geophysical Prospecting, 26(2): 442-463.

Roy, A. and Apparao, A. (1971). Depth of Investigation in Direct Current Methods. Geophysics, 36(5): 943-959.

Roy, A. and Jain, S.C. (1973). Comparison of Electrode Arrays in Time Domain Induced Polarization. Geophysical Prospecting, 21(4): 626-634.

Rust, W.M. (1938). A Historical Review of Electrical Prospecting Methods. Geophysics, 3(1): 1-6.

Sanker Narayan, P.V. and Ramanujachary, K.R. (1967). An Inverse Slope Method of Determining Absolute Resistivity. Geophysics, 32(6): 1036-1040.

Shear, R.F. (1953). Principles of Transistor Circuits. John Wiley and Sons Inc., New York.

Shemang, E.M. (1990). Electrical Depth Soundings at Selected Well-Sites Within the Kubanni River Basin, Zaria. Unpublished M.Sc. Thesis. Ahmadu Bello University, Zaria.

Smith, D.T. (1955). Geophysical Methods of Oil Prospecting. Leonard Hill Ltd., London NW1.

Symthe, W.R. (1950). Static and Dynamic Electricity. McGraw-Hill Book Co. Inc., New York.

Telford, W.M., Geldart, L.P., Sheriff, R.E. and Keys, D.A. (1976). Applied Geophysics. Cambridge University Press, Cambridge.

Uffenbeck, J.E. (1982). Introduction to Electronics. Prentice-Hall Inc., New Jersey.

Umego, M.N. (1990). Structural Interpretation of Gravity and Aeromagnetic Anomalies Over Sokoto Basin, NW Nigeria. Unpublished Ph.D. Thesis. Ahmadu Bello University, Zaria.

Van Nostrand, R.G. and Cook, K.L. (1966). Interpretation of Resistivity Data. United States Geological Survey Professional Paper 499. U.S. Government Printing Office, Washington, D.C.

Watson, R.J. and Johnson, J.F. (1938). On the Extension of Two-Layer Methods of Interpretation of Earth Resistivity Data to Three or More Layers. Geophysics, 3(1): 7-21.

Wright, J.B. and McCurry, P. (1970). The Geology of the Zaria Sheet 102 S.W. Zaria and its Region. In: Mortimore, M.J. (Ed.) Department of Geography Occasional Paper No 4. Ahmadu Bello University, Zaria.

Zohdy, A.A.R. (1969). A New Method for Differential Resistivity Sounding. Geophysics, 34(6): 924-943.

APPENDIX A1: COMPUTED MODEL SLOPE VALUES USING THE TWO-ELECTRODE METHOD

A1.1 Clay / River Sand / Basement

$s_1 = {}^1/_5 (\ln 50 - \ln 7.6) = 0.376775 m^{-1}$
$s_2 = {}^1/_{10} (\ln 98 - \ln 26) = 0.132709 m^{-1}$
$s_3 = {}^1/_{10} (\ln 155 - \ln 112) = 0.0325 m^{-1}$

A1.2 River Sand / Clay / Basement

$s_1 = {}^1/_{10} (\ln 2700 - \ln 170) = 0.276521 m^{-1}$
$s_2 = {}^1/_{20} (\ln 3100 - \ln 990) = 0.132709 m^{-1}$
$s_3 = {}^1/_{10} (\ln 4200 - \ln 3500) = 0.0325 m^{-1}$

A1.3 Clay / Mixed-Soil / River Sand / Basement

$s_1 = {}^1/_{10} (\ln 1000 - \ln 6.6) = 0.5021 m^{-1}$
$s_2 = {}^1/_{10} (\ln 105 - \ln 23.5) = 0.1497 m^{-1}$
$s_3 = {}^1/_{10} (\ln 115 - \ln 62) = 0.06178 m^{-1}$
$s_4 = {}^1/_{10} (\ln 173 - \ln 123) = 0.03411 m^{-1}$

A1.4 Clay / River Sand / Clay / Basement

$s_1 = {}^1/_{10} (\ln 190 - \ln 7.4) = 0.3246 m^{-1}$
$s_2 = {}^1/_{10} (\ln 72 - \ln 21) = 0.1232 m^{-1}$
$s_3 = {}^1/_{10}$ ÇLn 106 - ln 73) $= 0.0373 m^{-1}$
$s_4 = {}^1/_{10} (\ln 152 - \ln 119) = 0.0245 m^{-1}$

A1.5 Mixed-Soil / Clay / River Sand / Basement

$s_1 = {}^1/_{10} (\ln 5600 - \ln 22) = 0.554 m^{-1}$
$s_2 = {}^1/_{10} (\ln 430 - \ln 54) = 0.2075 m^{-1}$
$s_3 = {}^1/_{10} (\ln 435 - \ln 275) = 0.04586 m^{-1}$
$s_4 = {}^1/_{10} (\ln 745 - \ln 590) = 0.02333 m^{-1}$

A1.6 River Sand / Mixed-Soil /Clay / Basement

$s_1 = {}^1/_{10} (\ln 120000 - \ln 68) = 0.7476 m^{-1}$
$s_2 = {}^1/_{10} (\ln 1800 - \ln 320) = 0.1727 m^{-1}$
$s_3 = {}^1/_{10} (\ln 1800 - \ln 970) = 0.0618 m^{-1}$
$s_4 = {}^1/_{10} (\ln 4400 - \ln 3600) = 0.0201 m^{-1}$

APPENDIX A2: COMPUTED FIELD SLOPE VALUES USING THE TWO-ELECTRODE METHOD

A2.1 ECE

$S_1 = {}^1/_{10}$ (ln 3750 − ln 260) = 0.26688m^{-1}
$S_2 = {}^1/_{10}$ (ln 6700 − ln 2750) = 0.03562m^{-1}

A2.2 UNGWAN KAYA (KONGO)

$S_1 = {}^1/_{10}$ (ln 1550 − ln 210) = 0.20000m^{-1}
$S_2 = {}^1/_{10}$ (ln 2500 − ln 1530) = 0.02455m^{-1}

A2.3 CIKAJI

$S_1 = {}^1/_{10}$ (ln 5200 − ln 84) = 0.41256m^{-1}
$S_2 = {}^1/_{20}$ (ln 3350 − ln 810) = 0.07098m^{-1}
$S_3 = {}^1/_{20}$ (ln 3700 − ln 2150) = 0.02714m^{-1}

A2.4 AVIATION SITE 1

$S_1 = {}^1/_{10}$ (ln 14000 − ln 250) = 0.402535m^{-1}
$S_2 = {}^1/_{20}$ (ln 26000 − ln 800) = 0.174062m^{-1}
$S_3 = {}^1/_{40}$ (ln 14000 − ln 5020) = 0.025641m^{-1}

A2.5 PALLADAN

$S_1 = {}^1/_{10}$ (ln 25000 − ln 95) = 0.55728m^{-1}
$S_2 = {}^1/_{20}$ (ln 3900 − ln 1100) = 0.12657m^{-1}
$S_3 = {}^1/_{20}$ (ln 3950 − ln 2080) = 0.06414m^{-1}

A2.6 BASSAWA

$S_1 = {}^1/_{10}$ (ln 2000 − ln 115) = 0.285597m^{-1}
$S_2 = {}^1/_{20}$ (ln 2000 − ln 850) = 0.042783m^{-1}

A2.7 ZANGO

$S_1 = {}^1/_{10}$ (ln 1500 − ln 140) = 0.237158m^{-1}
$S_2 = {}^1/_{20}$ (ln 2550 − ln 1320) = 0.032923m^{-1}

A2.8 JAMA'A KUBANNI

$S_1 = {}^1/_{10}$ (ln 3000 − ln 45) = 0.41997m^{-1}
$S_2 = {}^1/_{20}$ (ln 900 − ln 375) = 0.04377m^{-1}
$S_3 = {}^1/_{40}$ (ln 1900 − ln 990) = 0.01630m^{-1}

12.9 HAYIN LEMA

$S_1 = 1/10 (\ln 1600 - \ln 165) = 0.22718m^{-1}$
$S_2 = 1/20 (\ln 3350 - \ln 550) = 0.09034m^{-1}$
$S_3 = 1/20 (\ln 3350 - \ln 2320) = 0.01837m^{-1}$

12.10 TUNDUN SARKI

$S_1 = 1/10 (\ln 16000 - \ln 150) = 0.46697m^{-1}$
$S_2 = 1/10 (\ln 900 - \ln 535) = 0.05201m^{-1}$

12.11 GORUBA

$S_1 = 1/10 (\ln 76000 - \ln 40) = 0.75496m^{-1}$
$S_2 = 1/20 (\ln 2400 - \ln 1450) = 0.02520m^{-1}$

12.12 WUSAGA

$S_1 = 1/10 (\ln 6400 - \ln 60) = 0.46697m^{-1}$
$S_2 = 1/10 (\ln 2100 - \ln 590) = 0.06348m^{-1}$

12.13 HANWA

$S_1 = 1/10 (\ln 2700 - \ln 170) = 0.27652m^{-1}$
$S_2 = 1/33 (\ln 3000 - \ln 2250) = 0.00822m^{-1}$
$S_3 = 1/40 (\ln 2500 - \ln 1080) = 0.02098m^{-1}$

12.14 TUKUR TUKUR

$S_1 = 1/8 (\ln 1900 - \ln 42) = 0.76239m^{-1}$
$S_2 = 1/10 (\ln 2800 - \ln 880) = 0.11575m^{-1}$
$S_3 = 1/20 (\ln 4900 - \ln 3400) = 0.01827m^{-1}$

12.15 ALHUDAHUDA

$S_1 = 1/8 (\ln 10000 - \ln 140) = 0.85374m^{-1}$
$S_2 = 1/20 (\ln 5700 - \ln 2560) = 0.04002m^{-1}$
$S_3 = 1/20 (\ln 5700 - \ln 4550) = 0.01127m^{-1}$

12.16 TUKUR JUKUN

$S_1 = 1/10 (\ln 11000 - \ln 62) = 0.51795m^{-1}$
$S_2 = 1/20 (\ln 3900 - \ln 475) = 0.10527m^{-1}$
$S_3 = 1/20 (\ln 2900 - \ln 1500) = 0.03296m^{-1}$

A2.17 UNGWAN GARKI

$S_1 = {}^1/_{10}$ (ln 4300 - ln 280) = 0.27316m^{-1}
$S_2 = {}^1/_{20}$ (ln 3000 - ln 1240) = 0.04418m^{-1}
$S_3 = {}^1/_{30}$ (ln 4300 - ln 2240) = 0.02174m^{-1}

A2.18 BOMO

$S_1 = {}^1/_{5}$ (ln 420 - ln 125) = 0.24239m^{-1}
$S_2 = {}^1/_{20}$ (ln 1500 - ln 710) = 0.03740m^{-1}

A2.19 KURRIMI BOMO

$S_1 = {}^1/_{5}$ (ln 5400 - ln 60) = 0.89996m^{-1}
$S_2 = {}^1/_{10}$ (ln 3000 - ln 680) = 0.12326m^{-1}
$S_3 = {}^1/_{10}$ (ln 3850 - ln 1220) = 0.05746m^{-1}

A2.20 DAC

$S_1 = {}^1/_{5}$ (ln 4500 - ln 230) = 0.59475m^{-1}
$S_2 = {}^1/_{10}$ (ln 5550 - ln 1050) = 0.16650m^{-1}
$S_3 = {}^1/_{20}$ (ln 9100 - ln 3350) = 0.09993m^{-1}

A2.21 MAIGAMO

$S_1 = {}^1/_{10}$ (ln 4000 - ln 220) = 0.29004m^{-1}
$S_2 = {}^1/_{20}$ (ln 3500 - ln 590) = 0.08902m^{-1}
$S_3 = {}^1/_{55}$ (ln 10000 - ln 5700) = 0.01022m^{-1}

A2.22 STAFF SCHOOL

$S_1 = {}^1/_{10}$ (ln 40000 - ln 260) = 0.50360m^{-1}
$S_2 = {}^1/_{20}$ (ln 12700 - ln 2100) = 0.08998m^{-1}
$S_3 = {}^1/_{10}$ (ln 26000 - ln 23200) = 0.00570m^{-1}

A2.23 NABRLS 1

$S_1 = {}^1/_{5}$ (ln 1450 - ln 30) = 0.77562m^{-1}
$S_2 = {}^1/_{10}$ (ln 1200 - ln 190) = 0.18431m^{-1}
$S_3 = {}^1/_{20}$ (ln 2350 - ln 1950) = 0.01897m^{-1}
$S_3 = {}^1/_{50}$ (ln 5000 - ln 2950) = 0.01055m^{-1}

APPENDIX A2 : COMPUTED MODEL RESISTIVITY VALUES USING THE TWO-ELECTRODE METHOD

A2.1 CLAY/ RIVER SAND/ BASEMENT

$s_1 = 0.376775\ m^{-1}$ $s_2 = 0.132709\ m^{-1}$ $s_3 = 0.0325\ m^{-1}$

$s_1/s_2 = 2.83911$ $s_2/s_1 = 0.3522234$
$s_2/s_3 = 4.083354$ $s_3/s_2 = 0.2448967$

$c_1 = 76\ \Omega m$ $c_2 = 260\ \Omega m$ $c_3 = 1120\ \Omega m$

$\rho_1 = c_1 = 76\ \Omega m$ $h_1 = 4.8\ cm$
$\rho_2 = 76 \times 2.83911 \approx 216\ \Omega m$ $h_2 = 10.5\ cm$
$\rho_3 = 216 \times 4.083354 \approx 881\ \Omega m$ $h_3 = \infty$

A2.2 RIVER SAND/ CLAY/ BASEMENT

$s_1 = 0.27652\ m^{-1}$ $s_2 = 0.0570726\ m^{-1}$ $s_3 = 0.018232 m^{-1}$

$s_1/s_2 = 4.8450745$ $s_2/s_1 = 0.2063951$
$s_1/s_3 = 3.130336$ $s_3/s_2 = 0.3194545$

$c_1 = 1700\ \Omega m$ $c_2 = 9900\ \Omega m$ $c_3 = 35000\ \Omega m$

$\rho_1 = c_1 = 1700\ \Omega m$ $h_1 = 8.0\ cm$
$\rho_2 = 1700 \times 0.2063951 \approx 351\ \Omega m$ $h_2 = 22.0\ cm$
$\rho_3 = 351 \times 3.130336 \approx 1098\ \Omega m$ $h_3 = \infty$

A2.3 CLAY/ MIXED-SOIL / RIVER SAND/ BASEMENT

$s_1 = 0.5021 m^{-1}$ $s_2 = 0.1497 m^{-1}$
$s_3 = 0.06178 m^{-1}$ $s_4 = 0.03411 m^{-1}$

$s_1/s_2 = 3.3540414$ $s_2/s_1 = 0.2981477$
$s_1/s_3 = 2.4231142$ $s_3/s_2 = 0.412692$
$s_1/s_4 = 1.8111999$ $s_4/s_3 = 0.5521204$

$c_1 = 66\ \Omega m$ $c_2 = 235\ \Omega m$ $c_3 = 620\ \Omega m$ $c_4 = 1230\ \Omega m$

$\rho_1 = c_1 = 66\ \Omega m$ $h_1 = 3.8\ cm$
$\rho_2 = 66 \times 3.3540414 \approx 221\ \Omega m$ $h_2 = 7.3\ cm$
$\rho_3 = 221 \times 2.4231142 \approx 536\ \Omega m$ $h_3 = 14.5\ cm$
$\rho_4 = 536 \times 1.8112 \approx 972\ \Omega m$ $h_4 = \infty$

A2.4 CLAY/ RIVER SAND / CLAY/ BASEMENT

$S_1 = 0.3246m^{-1}$ $S_2 = 0.1232m^{-1}$
$S_3 = 0.0273m^{-1}$ $S_4 = 0.0245m^{-1}$

$S_1/S_2 = 2.63474$ $S_2/S_1 = 0.379544$
$S_2/S_3 = 3.30295$ $S_3/S_2 = 0.30276$
$S_3/S_4 = 1.52245$ $S_4/S_3 = 0.656836$

$C_1 = 74\ \Omega m$ $C_2 = 210\ \Omega m$ $C_3 = 730\ \Omega m$ $C_4 = 1190\ \Omega m$

$\rho_1 = C_1 = 74\ \Omega m$ $h_1 = 5.0$ cm
$\rho_2 = 74 \times 2.63474 \approx 195\ \Omega m$ $h_2 = 9.8$ cm
$\rho_3 = 195 \times 3.30295 \approx 644\ \Omega m$ $h_3 = 21.8$ cm
$\rho_4 = 644 \times 1.52245 \approx 980\ \Omega m$ $h_4 = \infty$

A2.5 MIXED-SOIL / CLAY/ RIVER SAND/ BASEMENT

$S_1 = 0.554m^{-1}$ $S_2 = 0.2075m^{-1}$
$S_3 = 0.04596m^{-1}$ $S_4 = 0.02333m^{-1}$

$S_1/S_2 = 2.6699$ $S_2/S_1 = 0.3745487$
$S_2/S_3 = 4.52464$ $S_3/S_2 = 0.221012$
$S_3/S_4 = 1.96571$ $S_4/S_3 = 0.5087221$

$C_1 = 220\ \Omega m$ $C_2 = 540\ \Omega m$ $C_3 = 2750\ \Omega m$ $C_4 = 5900\ \Omega m$

$\rho_1 = C_1 = 220\ \Omega m$ $h_1 = 2.5$ cm
$\rho_2 = 220 \times 0.3745487 \approx 82\ \Omega m$ $h_2 = 7.8$ cm
$\rho_3 = 82 \times 4.52464 \approx 373\ \Omega m$ $h_3 = 23.0$ cm
$\rho_4 = 373 \times 1.96571 \approx 733\ \Omega m$ $h_4 = \infty$

A2.6 RIVER SAND/ MIXED-SOIL / CLAY/ BASEMENT

$S_1 = 0.7476m^{-1}$ $S_2 = 0.1727m^{-1}$
$S_3 = 0.0618m^{-1}$ $S_4 = 0.0201m^{-1}$

$S_1/S_2 = 4.328994$ $S_2/S_1 = 0.2310058$
$S_2/S_3 = 2.7944983$ $S_3/S_2 = 0.3578459$
$S_3/S_4 = 3.0746268$ $S_4/S_3 = 0.3252427$

$C_1 = 680\ \Omega m$ $C_2 = 3200\ \Omega m$ $C_3 = 9700\ \Omega m$ $C_4 = 36000\Omega m$

$\rho_1 = C_1 = 680\ \Omega m$ $h_1 = 2.6$ cm
$\rho_2 = 680 \times 0.2310058 \approx 157\ \Omega m$ $h_2 = 7.7$ cm
$\rho_3 = 157 \times 0.3578459 \approx 56\ \Omega m$ $h_3 = 21.3$ cm
$\rho_4 = 56 \times 3.0746268 \approx 173\ \Omega m$ $h_4 = \infty$

APPENDIX A4: COMPUTED FIELD RESISTIVITY VALUES USING THE TWO-ELECTRODE METHOD

A4.1 FCE

$s_1 = 0.266883 m^{-1}$ $s_2 = 0.03562 m^{-1}$

$s_1/s_2 = 7.4925$ $s_2/s_1 = 0.1334667$

$c_1 = 260\ \Omega m$ $c_2 = 2750\ \Omega m$

$\rho_1 = c_1 = 260\ \Omega m$ $h_1 = 10.0$ m
$\rho_2 = 260 \times 7.4925 \approx 1948\ \Omega m$ $h_2 = \infty$

A4.2 UNGWAN KAYA (KONGO)

$s_1 = 0.200 m^{-1}$ $s_2 = 0.02455 m^{-1}$

$s_1/s_2 = 8.14664$ $s_2/s_1 = 0.12275$

$c_1 = 210\ \Omega m$ $c_2 = 1530\ \Omega m$

$\rho_1 = c_1 = 210\ \Omega m$ $h_1 = 11.5$ m
$\rho_2 = 210 \times 8.14664 \approx 1711\ \Omega m$ $h_2 = \infty$

A4.3 CIKAJI

$s_1 = 0.41256 m^{-1}$ $s_2 = 0.070984 m^{-1}$ $s_3 = 0.027143 m^{-1}$

$s_1/s_2 = 5.812$ $s_2/s_1 = 0.17206$
$s_2/s_3 = 2.6152$ $s_3/s_2 = 0.3824$

$c_1 = 84\ \Omega m$ $c_2 = 810\ \Omega m$ $c_3 = 2150\ \Omega m$

$\rho_1 = c_1 = 84\ \Omega m$ $h_1 = 6.5$ cm
$\rho_2 = 84 \times 5.812 \approx 488\ \Omega m$ $h_2 = 16.0$ cm
$\rho_3 = 488 \times 2.6152 \approx 1277\ \Omega m$ $h_3 = \infty$

A4.4 AVIATION SITE 1

$s_1 = 0.40253517 m^{-1}$ $s_2 = 0.174062 m^{-1}$ $s_3 = 0.0256407 m^{-1}$

$s_1/s_2 = 2.3126$ $s_2/s_1 = 0.4324$
$s_2/s_3 = 6.7885$ $s_3/s_2 = 0.14731$

$c_1 = 250\ \Omega m$ $c_2 = 800\ \Omega m$ $c_3 = 5020\ \Omega m$

$\rho_1 = c_1 = 250\ \Omega m$ $h_1 = 4.0$ m
$\rho_2 = 250 \times 0.4324 \approx 108\ \Omega m$ $h_2 = 8.0$ m
$\rho_3 = 108 \times 6.7885 \approx 734\ \Omega m$ $h_3 = \infty$

A4.5 ÇALLADAN

$S_1 = 0.5572754m^{-1}$ $S_2 = 0.12656664m^{-1}$ $S_3 = 0.064135m^{-1}$

$S_1/S_2 = 4.403021$ $S_2/S_1 = 0.2271167$
$S_1/S_3 = 1.9734403$ $S_3/S_2 = 0.5067292$

$C_1 = 95\ \Omega m$ $C_2 = 1100\ \Omega m$ $C_3 = 2080\ \Omega m$

$\rho_1 = C_1 = 95\ \Omega m$ $h_1 = 4.8\ m$
$\rho_2 = 95 \times 4.03021 \approx 418\ \Omega m$ $h_2 = 16.0\ m$
$\rho_3 = 418 \times 1.9734403 \approx 826\ \Omega m$ $h_3 = \infty$

A4.6 BASSAWA

$S_1 = 0.2885597m^{-1}$ $S_2 = 0.0427833m^{-1}$

$S_1/S_2 = 6.6754317$ $S_2/S_1 = 0.149803$

$C_1 = 115\ \Omega m$ $C_2 = 850\ \Omega m$

$\rho_1 = C_1 = 115\ \Omega m$ $h_1 = 8.0\ m$
$\rho_2 = 115 \times 6.6754317 \approx 768\ \Omega m$ $h_2 = \infty$

A4.7 ZANGO

$S_1 = 0.2371578m^{-1}$ $S_2 = 0.0329231m^{-1}$

$S_1/S_2 = 7.203386$ $S_2/S_1 = 0.1388236$

$C_1 = 140\ \Omega m$ $C_2 = 1320\ \Omega m$

$\rho_1 = C_1 = 140\ \Omega m$ $h_1 = 11.0\ m$
$\rho_2 = 140 \times 7.203386 \approx 1009\ \Omega m$ $h_2 = \infty$

A4.8 JAMAA' KUBANNI

$S_1 = 0.4199705m^{-1}$ $S_2 = 0.04377344m^{-1}$ $S_3 = 0.0163m^{-1}$

$S_1/S_2 = 9.5941941$ $S_2/S_1 = 0.10402297$
$S_1/S_3 = 2.6854846$ $S_3/S_2 = 0.3723722$

$C_1 = 45\ \Omega m$ $C_2 = 375\ \Omega m$ $C_3 = 990\ \Omega m$

$\rho_1 = C_1 = 45\ \Omega m$ $h_1 = 6.0\ m$
$\rho_2 = 45 \times 9.5941941 \approx 432\ \Omega m$ $h_2 = 29.0\ m$
$\rho_3 = 432 \times 2.6854846 \approx 1159\ \Omega m$ $h_3 = \infty$

A4.9 HAYIN LEMA

$s_1 = 0.22718134m^{-1}$ $s_2 = 0.09034m^{-1}$ $s_3 = 0.01837m^{-1}$

$s_1/s_2 = 2.5147365$ $s_2/s_1 = 0.3976559$
$s_1/s_3 = 4.9178007$ $s_3/s_2 = 0.2033429$

$c_1 = 165\ \Omega m$ $c_2 = 650\ \Omega m$ $c_3 = 2320\ \Omega m$

$\rho_1 = c_1 = 165\ \Omega m$ $h_1 = 8.5\ m$
$\rho_2 = 165 \times 0.3976559 \approx 415\ \Omega m$ $h_2 = 12.0\ m$
$\rho_3 = 415 \times 4.9178007 \approx 2041\ \Omega m$ $h_3 = \infty$

A4.10 TUDUN SARKI

$s_1 = 0.3660709m^{-1}$ $s_2 = 0.0520128m^{-1}$

$s_1/s_2 = 8.978$ $s_2/s_1 = 0.1113833$

$c_1 = 150\ \Omega m$ $c_2 = 535\ \Omega m$
$\rho_1 = c_1 = 150\ \Omega m$ $h_1 = 5.5\ m$
$\rho_2 = 150 \times 8.978 \approx 1347\ \Omega m$ $h_2 = \infty$

A4.11 GORUBA

$s_1 = 0.754961m^{-1}$ $s_2 = 0.0252m^{-1}$

$s_1/s_2 = 29.958769$ $s_2/s_1 = 0.0333792$

$c_1 = 40\ \Omega m$ $c_2 = 1450\ \Omega m$

$\rho_1 = c_1 = 40\ \Omega m$ $h_1 = 7.0\ m$
$\rho_2 = 40 \times 29.958769 \approx 1198\ \Omega m$ $h_2 = \infty$

A4.12 WUSASA

$s_1 = 0.466971m^{-1}$ $s_2 = 0.0634785m^{-1}$

$s_1/s_2 = 7.3563647$ $s_2/s_1 = 0.1359367$

$c_1 = 60\ \Omega m$ $c_2 = 500\ \Omega m$

$\rho_1 = c_1 = 60\ \Omega m$ $h_1 = 6.0\ m$
$\rho_2 = 60 \times 7.3563647 \approx 441\ \Omega m$ $h_2 = \infty$

A4.12 [illegible]

s_1 = 0.27651m^{-1} s_2 = 0.00822m^{-1} s_3 = 0.0[illegible]09832m^{-1}

s_1/s_2 = 33.64 s_2/s_1 = 0.0297265
s_2/s_3 = 0.301742 s_3/s_2 = 2.5527007

c_1 = 170 Ωm c_2 = 2250 Ωm c_3 = 1080 Ωm

$\rho_1 = c_1$ = 170 Ωm h_1 = 6.0 m
ρ_2 = 170 x 0.0297265 ≈ 51 Ωm h_2 = 3.8 m
ρ_3 = 51 x 25.527 ≈ 1299 Ωm h_3 = ∞

A4.14 TUKUR TUKUR

s_1 = 0.762288m^{-1} s_2 = 0.1157453m^{-1} s_3 = 0.018273m^{-1}

s_1/s_2 = 6.5867776 s_2/s_1 = 0.1518193
s_2/s_3 = 6.3342198 s_3/s_2 = 0.1578726

c_1 = 42 Ωm c_2 = 880 Ωm c_3 = 3400 Ωm

$\rho_1 = c_1$ = 42 Ωm h_1 = 4.8 m
ρ_2 = 42 x 6.5867776 ≈ 277 Ωm h_2 = 9.3 m
ρ_3 = 277 x 6.3342198 ≈ 1752 Ωm h_3 = ∞

A4.15 ALHUDAHUDA

s_1 = 0.85374m^{-1} s_2 = 0.040023m^{-1} s_3 = 0.[illegible]112669m^{-1}

s_1/s_2 = 21.331275 s_2/s_1 = 0.0468795
s_2/s_3 = 3.5522548 s_3/s_2 = 0.2815113

c_1 = 140 Ωm c_2 = 2560 Ωm c_3 = 4550 Ωm

$\rho_1 = c_1$ = 140 Ωm h_1 = 3.5 m
ρ_2 = 140 x 0.468795 ≈ 66 Ωm h_2 = 16.5 m
ρ_3 = 66 x 3.5522548 ≈ 233 Ωm h_3 = ∞

A4.16 TUKUR JUKUN

s_1 = 0.517852m^{-1} s_2 = 0.10527m^{-1} s_3 = 0.0329623m^{-1}

s_1/s_2 = 4.9192424 s_2/s_1 = 0.2032833
s_2/s_3 = 3.1936763 s_3/s_2 = 0.3131187

c_1 = 62 Ωm c_2 = 475 Ωm c_3 = 1500 Ωm

$\rho_1 = c_1$ = 62 Ωm h_1 = 5.0 m
ρ_2 = 62 x 4.9192424 ≈ 305 Ωm h_2 = 11.0 m
ρ_3 = 305 x 3.1936763 ≈ 974 Ωm h_3 = ∞

A4.17 UNGWAN SARKI

$s_1 = 0.273158m^{-1}$ $s_2 = 0.044175m^{-1}$ $s_3 = 0.021738m^{-1}$

$s_1/s_2 = 6.1835427$ $s_2/s_1 = 0.1617185$
$s_2/s_3 = 2.0321556$ $s_3/s_2 = 0.4920882$

$c_1 = 280\ \Omega m$ $c_2 = 1240\ \Omega m$ $c_3 = 2240\ \Omega m$

$\rho_1 = c_1 = 280\ \Omega m$ $h_1 = 6.5\ m$
$\rho_2 = 280 \times 0.1617185 \approx 45\ \Omega m$ $h_2 = 19.0\ m$
$\rho_3 = 45 \times 20.321556 \approx 920\ \Omega m$ $h_3 = \infty$

A4.18 BOMO

$s_1 = 0.2423882m^{-1}$ $s_2 = 0.0379777m^{-1}$

$s_1/s_2 = 6.4813665$ $s_2/s_1 = 0.1542884$

$c_1 = 125\ \Omega m$ $c_2 = 710\ \Omega m$

$\rho_1 = c_1 = 125\ \Omega m$ $h_1 = 6.0\ m$
$\rho_2 = 125 \times 6.4813665 \approx 810\ \Omega m$ $h_2 = \infty$

A4.19 KURRIMI BOMO

$s_1 = 0.899962m^{-1}$ $s_2 = 0.123255m^{-1}$ $s_3 = 0.057461m^{-1}$

$s_1/s_2 = 7.3016148$ $s_2/s_1 = 0.136956$
$s_2/s_3 = 2.14502$ $s_3/s_2 = 0.4661961$

$c_1 = 60\ \Omega m$ $c_2 = 680\ \Omega m$ $c_3 = 1220\ \Omega m$

$\rho_1 = c_1 = 60\ \Omega m$ $h_1 = 3.3\ m$
$\rho_2 = 60 \times 7.3016418 \approx 438\ \Omega m$ $h_2 = 5.8\ m$
$\rho_3 = 438 \times 2.14502 \approx 940\ \Omega m$ $h_3 = \infty$

A4.20 DAC

$s_1 = 0.594751m^{-1}$ $s_2 = 0.166501m^{-1}$ $s_3 = 0.09993m^{-1}$

$s_1/s_2 = 3.5720612$ $s_2/s_1 = 0.2799504$
$s_2/s_3 = 1.6661499$ $s_3/s_2 = 0.600186$

$c_1 = 230\ \Omega m$ $c_2 = 1050\ \Omega m$ $c_3 = 3350\ \Omega m$

$\rho_1 = c_1 = 230\ \Omega m$ $h_1 = 2.8\ m$
$\rho_2 = 230 \times 3.57281612 \approx 822\ \Omega m$ $h_2 = 7.3\ m$
$\rho_3 = 822 \times 1.66615 \approx 1369\ \Omega m$ $h_3 = \infty$

A4.21 MAIGAMO

$S_1 = 0.2900422m^{-1}$ $S_2 = 0.08902m^{-1}$ $S_3 = 0.01022m^{-1}$

$S_1/S_2 = 3.2581689$ $S_2/S_1 = 0.3069208$
$S_2/S_3 = 8.7101161$ $S_3/S_2 = 0.114809$

$C_1 = 220\ \Omega m$ $C_2 = 590\ \Omega m$ $C_3 = 5700\ \Omega m$

$\rho_1 = C_1 = 220\ \Omega m$ $h_1 = 5.0\ m$
$\rho_2 = 220 \times 0.3069208 \approx 68\ \Omega m$ $h_2 = 24.0\ m$
$\rho_3 = 68 \times 8.7101161 \approx 588\ \Omega m$ $h_3 = \infty$

A4.22 STAFF SCHOOL

$S_1 = 0.503595m^{-1}$ $S_2 = 0.0899832m^{-1}$ $S_3 = 0.005697m^{-1}$

$S_1/S_2 = 5.596548$ $S_2/S_1 = 0.1786815$
$S_2/S_3 = 15.794284$ $S_3/S_2 = 0.063314$

$C_1 = 260\ \Omega m$ $C_2 = 2100\ \Omega m$ $C_3 = 23200\ \Omega m$

$\rho_1 = C_1 = 260\ \Omega m$ $h_1 = 5.0\ m$
$\rho_2 = 260 \times 0.1786815 \approx 47\ \Omega m$ $h_2 = 23.0\ m$
$\rho_3 = 47 \times 15.794284 \approx 733\ \Omega m$ $h_3 = \infty$

A4.23 NAERLS 1

$S_1 = 0.7756m^{-1}$ $S_2 = 0.1843m^{-1}$ $S_3 = 0.01897m^{-1}$
$S_4 = 0.010553m^{-1}$

$S_1/S_2 = 4.2083667$ $S_2/S_3 = 9.7133664$ $S_3/S_4 = 1.774899$
$S_2/S_1 = 0.2376218$ $S_3/S_2 = 0.1029509$ $S_4/S_3 = 0.563412$

$C_1 = 30\ \Omega m$ $C_2 = 190\ \Omega m$ $C_3 = 1950\ \Omega m$ $C_4 = 2950\ \Omega m$

$\rho_1 = C_1 = 30\ \Omega m$ $h_1 = 3.0\ m$
$\rho_2 = 30 \times 4.2083667 \approx 126\ \Omega m$ $h_2 = 4.1\ m$
$\rho_3 = 126 \times 9.7133664 \approx 1226\ \Omega m$ $h_3 = 7.15\ m$
$\rho_4 = 1226 \times 1.774899 \approx 2176$ $h_4 = \infty$

APPENDIX B1: FIELD DATA COLLECTED USING THE TWO-ELECTRODE METHOD

B1.1 FCE

L(m)	V(v)	I(mA)
1.0	95.0	57.7
2.0	75.0	58.8
3.0	80.0	58.8
4.0	75.0	58.9
5.0	70.0	58.8
6.0	83.0	58.6
7.5	93.0	57.7
8.0	103.0	58.0
9.0	105.0	58.1
10.0	145.0	57.5
15.0	150.0	20.0
20.0	150.0	20.0
25.0	93.0	58.2
30.0	70.0	58.5
35.0	80.0	58.7
40.0	150.0	18.0
45.0	150.0	19.0
50.0	149.0	20.2
75.0	140.0	57.5
100.0	125.0	57.8
150.0	150.0	22.0
200.0	150.0	23.0

B1.2 USMAN KAYA

L(m)	V(v)	I(mA)
1.0	24.0	59.2
2.0	46.0	59.0
3.0	62.5	59.9
4.0	75.0	59.5
5.0	47.5	59.1
6.0	70.0	59.0
7.5	38.0	59.4
8.0	41.0	59.4
9.0	54.0	59.1
10.0	55.0	59.1
15.0	80.0	59.0
20.0	47.0	59.2
25.0	53.0	59.1
30.0	43.0	59.3
35.0	41.0	59.4
40.0	31.0	59.6
45.0	63.0	59.0
50.0	63.0	59.0
75.0	55.0	59.1
100.0	74.0	59.0
150.0	57.0	59.1
200.0	100.0	59.0

B1.3 CIKAJI

L(m)	V(v)	I(mA)
1.0	49.0	59.2
2.0	40.0	58.4
3.0	40.0	58.4
4.0	35.0	58.5
5.0	59.0	58.1
6.0	69.0	58.2
7.5	55.0	58.5
8.0	51.0	58.4
9.0	36.0	58.8
10.0	63.0	58.3
15.0	64.0	58.4
20.0	65.0	58.3
25.0	35.0	58.9
30.0	65.0	58.4
35.0	87.0	58.0
40.0	62.0	58.4
45.0	63.0	58.5
50.0	66.0	58.4
75.0	86.0	58.0
100.0	95.0	57.9
150.0	102.0	57.8
200.0	120.0	57.5

B1.4 AVIATION

L(m)	V(v)	I(mA
1.0	215.0	56.2
2.0	210.0	55.9
3.0	126.0	57.7
4.0	154.0	57.0
5.0	150.0	57.3
6.0	152.0	57.2
7.5	195.0	56.4
8.0	200.0	56.3
9.0	169.0	56.9
10.0	120.0	57.7
15.0	160.0	57.1
20.0	162.0	57.0
25.0	130.0	57.6
30.0	108.0	57.9
35.0	202.0	56.2
40.0	138.0	57.4
45.0	239.0	55.3
50.0	209.0	56.0
75.0	176.0	56.6
100.0	179.0	56.4
150.0	120.0	57.7
200.0	110.0	57.9

B1.5 DALLADAN

L(m)	V(v)	I(mA)
1.0	72.0	58.2
2.0	193.0	55.0
3.0	107.0	57.6
4.0	99.0	57.8
5.0	72.0	58.4
6.0	54.0	58.9
7.5	57.0	58.8
8.0	67.0	58.6
9.0	53.0	58.9
10.0	60.0	59.2
15.0	74.0	58.5
20.0	80.0	58.6
25.0	85.0	58.4
30.0	84.0	58.4
35.0	74.0	58.7
40.0	76.0	58.7
45.0	48.0	59.2
50.0	55.0	59.0
75.0	172.0	56.9
100.0	196.0	53.5
150.0	40.0	59.4
200.0	41.0	59.4

B1.6 BASSAWA

L(m)	V(v)	I(mA)
1.0	50.0	59.6
2.0	38.0	59.9
3.0	36.0	59.9
4.0	48.5	59.7
5.0	42.5	59.8
6.0	45.0	59.8
7.5	56.0	59.6
8.0	47.0	59.8
9.0	52.5	59.6
10.0	51.5	59.5
15.0	44.0	59.8
20.0	40.0	59.9
25.0	40.0	59.9
30.0	40.0	59.9
35.0	44.5	59.8
40.0	39.5	59.9
45.0	41.5	59.9
50.0	32.0	59.1
75.0	57.0	58.6
100.0	29.0	59.2
150.0	8.0	59.5
200.0	15.0	59.3

B1.7 ZANGO

L(m)	V(v)	I(mA)
1.0	118.0	56.8
2.0	60.0	59.0
3.0	38.8	59.5
4.0	39.0	59.5
5.0	35.0	59.5
6.0	46.0	59.4
7.5	46.0	59.5
8.0	55.0	59.4
9.0	49.0	59.5
10.0	34.0	59.8
15.0	58.0	59.3
20.0	65.0	59.2
25.0	46.0	59.6
30.0	48.0	59.5
35.0	50.0	59.4
40.0	47.5	59.6
45.0	22.5	59.9
50.0	20.0	59.1
75.0	25.0	59.0
100.0	39.0	58.8
150.0	95.0	57.7
200.0	15.0	59.3

B1.8 JAMAA' KUBANNI

L(m)	V(v)	I(mA)
1.0	28.0	58.9
2.0	25.0	59.0
3.0	20.0	59.2
4.0	25.0	59.1
5.0	20.0	59.2
6.0	21.0	59.2
7.5	21.0	59.1
8.0	25.0	59.1
9.0	20.0	59.2
10.0	25.0	59.1
15.0	23.0	59.1
20.0	27.0	59.1
25.0	17.0	59.2
30.0	12.0	59.3
35.0	20.0	59.2
40.0	21.0	59.2
45.0	27.0	58.9
50.0	18.0	59.2
75.0	22.0	59.2
100.0	20.0	59.3
150.0	12.0	59.6
200.0	35.0	59.0

B1.9 BAYAN LEMA

L(m)	V(v)	I(mA)
1.0	30.0	58.4
2.0	60.0	58.5
3.0	90.0	58.7
4.0	120.0	58.8
5.0	150.0	58.9
6.0	180.0	58.9
7.5	225.0	58.8
8.0	240.0	58.4
9.0	270.0	58.4
10.0	300.0	58.3
15.0	450.0	58.3
20.0	600.0	58.5
25.0	750.0	58.6
30.0	900.0	58.6
35.0	1050.0	58.5
40.0	1200.0	58.3
45.0	1350.0	58.1
50.0	1500.0	58.4
75.0	2250.0	58.8
100.0	3000.0	58.4
150.0	4500.0	58.1
200.0	6000.0	58.2

B1.10 BUDUN SARKI

L(m)	V(v)	I(mA)
1.0	45.0	57.8
2.0	66.0	58.6
3.0	66.0	58.7
4.0	66.0	58.8
5.0	45.0	58.2
6.0	56.0	58.9
7.5	42.5	58.2
8.0	30.5	58.2
9.0	27.0	58.1
10.0	60.0	58.2
15.0	60.0	58.3
20.0	30.5	58.5
25.0	29.0	58.6
30.0	24.0	58.6
35.0	60.0	58.5
40.0	59.0	58.3
45.0	37.0	58.1
50.0	35.5	58.1
75.0	41.5	58.5
100.0	64.0	58.4
150.0	52.0	58.1
200.0	60.5	58.4

B1.11 GOMUBA

L(m)	V(v)	I(mA)
1.0	15.0	58.1
2.0	29.0	58.0
3.0	20.0	58.1
4.0	40.0	58.0
5.0	41.0	58.0
6.0	57.0	58.3
7.5	94.0	57.7
8.0	108.0	57.5
9.0	85.0	57.8
10.0	99.5	57.7
15.0	120.0	58.0
20.0	47.5	58.6
25.0	58.5	58.4
30.0	43.0	58.9
35.0	40.0	58.8
40.0	40.0	58.8
45.0	36.0	58.9
50.0	48.5	58.7
75.0	46.0	58.7
100.0	45.0	58.7
150.0	49.0	58.7
200.0	46.0	58.7

B1.12 MUSASA

L(m)	V(v)	I(mA)
1.0	30.0	58.1
2.0	45.0	58.0
3.0	54.0	58.0
4.0	45.0	58.0
5.0	55.5	58.2
6.0	70.5	58.0
7.5	50.0	58.0
8.0	95.0	58.1
9.0	55.0	58.0
10.0	70.5	58.4
15.0	56.0	58.2
20.0	105.0	57.8
25.0	70.0	58.4
30.0	79.0	58.2
35.0	62.5	58.5
40.0	60.0	58.6
45.0	40.0	58.8
50.0	33.0	58.1
75.0	48.0	58.8
100.0	84.0	58.1
150.0	85.0	58.2
200.0	96.0	57.9

B1.13 WAMYA

L(m)	V(v)	I(mA)
1.0	25.0	58.7
2.0	50.0	58.4
3.0	115.0	58.2
4.0	62.5	58.2
5.0	60.0	58.0
6.0	67.5	58.2
7.5	63.5	58.6
8.0	47.0	58.6
9.0	70.0	58.1
10.0	50.0	58.6
15.0	120.0	58.2
20.0	52.0	58.4
25.0	37.0	58.8
30.0	37.0	58.8
35.0	36.0	58.8
40.0	40.5	58.6
45.0	30.5	58.8
50.0	35.0	58.6
75.0	37.0	58.8
100.0	35.0	58.8
150.0	65.0	58.2
200.0	101.5	58.6

B1.14 BUZUZA BUKUR

L(m)	V(v)	I(mA)
1.0	43.0	58.4
2.0	42.0	58.4
3.0	105.0	57.2
4.0	88.5	57.4
5.0	115.0	57.2
6.0	117.0	57.2
7.5	145.0	56.9
8.0	110.0	57.4
9.0	84.0	57.7
10.0	108.0	57.5
15.0	67.0	58.3
20.0	166.0	56.5
25.0	84.5	58.0
30.0	78.0	58.1
35.0	60.0	58.5
40.0	55.0	58.5
45.0	70.0	58.4
50.0	62.5	58.6
75.0	204.5	56.0
100.0	90.0	58.0
150.0	100.5	57.9
200.0	162.0	56.9

B1.15 ALHUDAHUDA

L(m)	V(v)	I(mA)
1.0	146.0	57.1
2.0	204.0	56.0
3.0	250.0	39.8
4.0	174.0	56.4
5.0	250.0	40.6
6.0	209.0	55.8
7.5	178.0	56.3
8.0	144.0	56.9
9.0	100.0	56.7
10.0	156.0	56.7
15.0	115.0	57.5
20.0	112.0	57.6
25.0	250.5	43.9
30.0	232.0	55.3
35.0	197.0	56.2
40.0	194.0	56.2
45.0	165.0	56.5
50.0	61.0	58.4
75.0	55.0	58.6
100.0	70.0	58.4
150.0	71.0	58.5
200.0	102.0	57.9

B1.16 BUKUR JUKUN

L(m)	V(v)	I(mA)
1.0	35.0	58.4
2.0	43.0	58.3
3.0	40.0	58.4
4.0	50.0	58.2
5.0	49.5	58.1
6.0	55.0	58.3
7.5	44.0	58.3
8.0	55.0	58.3
9.0	57.5	57.5
10.0	67.0	57.6
15.0	61.0	58.1
20.0	60.0	58.0
25.0	80.0	57.6
30.0	54.0	58.2
35.0	35.0	58.5
40.0	80.0	57.9
45.0	85.0	57.7
50.0	51.0	58.1
75.0	30.0	58.5
100.0	155.0	56.5
150.0	155.0	56.1
200.0	73.0	58.5

B1.17 UNCHAN CABKI

I(m)	V(v)	I(mA)
1.0	69.0	57.5
2.0	95.0	57.1
3.0	122.0	56.7
4.0	91.0	57.5
5.0	99.0	57.6
6.0	127.0	57.0
7.5	120.0	56.6
8.0	99.0	57.5
9.0	79.0	57.6
10.0	220.0	54.0
15.0	53.0	59.0
20.0	47.5	59.2
25.0	60.0	59.1
30.0	67.0	57.9
35.0	61.0	59.1
40.0	45.0	59.3
45.0	38.0	59.3
50.0	53.0	59.3
75.0	55.0	59.1
100.0	74.0	57.9
150.0	220.0	54.0
200.0	83.0	57.6

B1.18 BOMC

I(m)	V(v)	I(mA)
1.0	64.0	59.2
2.0	45.0	59.4
3.0	97.5	58.0
4.0	58.0	59.1
5.0	34.0	59.6
6.0	36.0	59.6
7.5	36.0	59.6
8.0	35.0	59.6
9.0	27.0	59.8
10.0	29.0	59.8
15.0	34.0	59.7
20.0	30.0	59.8
25.0	30.0	59.8
30.0	30.0	59.8
35.0	40.0	59.5
40.0	48.0	59.5
45.0	60.0	59.3
50.0	50.0	59.4
75.0	87.5	59.0
100.0	55.5	59.4
150.0	35.0	59.8
200.0	56.0	59.4

B1.19 EMBRIMI BOMB

I(m)	V(v)	I(mA)
1.0	53.0	59.1
2.0	50.0	59.0
3.0	94.5	58.4
4.0	70.0	58.7
5.0	98.0	58.2
6.0	95.5	58.3
7.5	90.0	58.6
8.0	115.0	57.9
9.0	90.0	58.3
10.0	99.0	58.1
15.0	61.0	58.9
20.0	79.0	58.6
25.0	80.0	58.5
30.0	81.0	58.3
35.0	55.0	59.0
40.0	52.0	59.0
45.0	42.5	59.2
50.0	44.0	59.2
75.0	26.0	59.5
100.0	110.0	57.8
150.0	110.0	57.9
200.0	60.0	58.8

B1.20 DAC

I(m)	V(v)	I(mA)
1.0	185.0	52.1
2.0	204.0	51.9
3.0	198.0	52.0
4.0	194.0	55.0
5.0	179.0	55.2
6.0	175.0	55.3
7.5	175.0	56.3
8.0	129.0	57.1
9.0	133.0	57.0
10.0	110.0	57.4
15.0	107.0	56.3
20.0	200.0	55.0
25.0	175.0	56.3
30.0	243.0	54.5
35.0	100.0	55.8
40.0	150.0	56.7
45.0	112.5	57.4
50.0	96.0	57.9
75.0	75.0	58.1
100.0	250.0	49.0
150.0	97.0	57.7
200.0	60.0	58.4

B1.21 VAIGAMC

I(m)	V(v)	I(mA)
1.0	80.0	57.5
2.0	76.0	57.8
3.0	72.0	58.1
4.0	84.5	57.7
5.0	72.0	58.0
6.0	84.5	57.8
7.5	116.0	57.2
8.0	85.0	57.8
9.0	81.0	58.5
10.0	85.0	58.4
15.0	82.0	58.5
20.0	69.5	59.0
25.0	100.0	57.7
30.0	71.5	58.9
35.0	84.0	58.7
40.0	85.0	58.2
45.0	100.0	57.7
50.0	76.0	58.8
75.0	60.0	58.9
100.0	70.0	58.2
150.0	55.0	58.7
200.0	62.0	58.9

B1.22 SPARK SCHOOL

I(m)	V(v)	I(mA)
1.0	171.0	56.1
2.0	120.0	56.9
3.0	105.0	55.7
4.0	210.0	55.0
5.0	226.0	50.0
6.0	213.5	55.2
7.5	192.0	55.3
8.0	180.0	55.9
9.0	202.0	56.0
10.0	245.0	55.7
15.0	250.0	53.1
20.0	249.5	53.7
25.0	247.0	54.2
30.0	249.5	51.4
35.0	240.0	45.2
40.0	249.0	50.6
45.0	210.0	48.5
50.0	190.0	55.3
75.0	152.0	55.8
100.0	130.0	56.4
150.0	65.0	57.0
200.0	42.0	59.2

B1.23 MABELS 1

I(m)	V(v)	I(mA)
1.0	25.0	59.7
2.0	27.0	59.6
3.0	30.0	59.3
4.0	40.0	59.3
5.0	39.0	59.3
6.0	37.0	59.3
7.5	40.0	59.3
8.0	40.0	59.1
9.0	45.0	59.0
10.0	65.0	58.6
15.0	70.0	59.6
20.0	87.0	58.3
25.0	101.0	59.0
30.0	45.0	59.0
35.0	44.0	59.1
40.0	50.0	59.2
45.0	48.0	59.0
50.0	39.0	59.2
75.0	30.0	59.4
100.0	35.0	59.3
150.0	38.0	59.2
200.0	23.0	59.5

B1.24 MABELS 2

I(m)	V(v)	I(mA)
1.0	28.0	59.6
2.0	27.0	59.5
3.0	31.0	59.3
4.0	39.0	59.1
5.0	40.0	59.3
6.0	40.0	59.3
7.5	39.0	59.3
8.0	41.0	59.1
9.0	43.0	59.1
10.0	66.0	58.7
15.0	69.0	59.1
20.0	85.0	58.9
25.0	99.0	58.5
30.0	102.0	58.2
35.0	46.0	59.2
40.0	45.0	59.2
45.0	44.0	59.2
50.0	41.0	59.4
75.0	33.0	59.2
100.0	35.0	59.3
150.0	37.5	59.1
200.0	26.0	59.6

B1.25 NAERLS 3

I(m)	V(v)	I(mA)
1.0	30.0	59.7
2.0	28.0	59.7
3.0	32.0	59.6
4.0	30.0	59.7
5.0	40.0	59.7
6.0	41.0	59.7
7.5	39.0	59.6
9.0	42.0	59.7
9.0	43.0	59.7
10.0	66.0	59.6
15.0	67.0	59.6
20.0	96.0	59.6
25.0	100.0	59.6
30.0	102.0	59.6
35.0	45.0	59.6
40.0	45.0	59.6
45.0	44.0	59.6
50.0	41.0	59.6
75.0	39.0	59.6
100.0	35.0	59.6
150.0	36.5	59.6
200.0	34.0	59.6

B1.26 NAERLS 4

I(m)	V(v)	I(mA)
1.0	30.0	59.7
2.0	28.0	59.6
3.0	32.0	59.6
4.0	30.0	59.7
5.0	40.0	59.7
6.0	41.0	59.7
7.5	39.0	59.6
9.0	42.0	59.7
9.0	43.0	59.7
10.0	67.0	59.6
15.0	68.0	59.6
20.0	95.0	59.6
25.0	99.0	59.6
30.0	102.0	59.6
35.0	45.0	59.6
40.0	45.0	59.6
45.0	44.0	59.6
50.0	41.0	59.6
75.0	39.0	59.6
100.0	35.0	59.6
150.0	36.5	59.6
200.0	34.0	59.6

B1.27 NAERLS 5

I(m)	V(v)	I(mA)
1.0	29.0	59.8
2.0	28.0	59.8
3.0	32.0	59.7
4.0	30.0	59.8
5.0	41.0	59.7
6.0	41.0	59.7
7.5	39.0	59.8
9.0	41.0	59.7
9.0	42.0	59.7
10.0	66.0	59.7
15.0	67.0	59.7
20.0	96.0	59.7
25.0	98.0	59.5
30.0	101.0	59.7
35.0	45.0	59.7
40.0	45.0	59.7
45.0	45.0	59.7
50.0	44.0	59.6
75.0	37.0	59.7
100.0	37.0	59.7
150.0	37.5	59.7
200.0	38.0	59.6

B1.28 NAERLS 6

I(m)	V(v)	I(mA)
1.0	29.0	59.8
2.0	28.0	59.8
3.0	32.0	59.8
4.0	30.0	59.8
5.0	39.0	59.8
6.0	39.0	59.8
7.5	39.0	59.8
9.0	42.0	59.8
9.0	43.0	59.8
10.0	69.0	59.8
15.0	68.0	59.8
20.0	95.0	59.8
25.0	99.0	59.8
30.0	102.0	59.8
35.0	45.0	59.8
40.0	45.0	59.8
45.0	44.0	59.8
50.0	41.0	59.7
75.0	40.0	59.7
100.0	37.0	59.8
150.0	37.0	59.8
200.0	36.0	59.8

B1.29 NAERLS 7

I(m)	V(v)	I(mA)
1.0	31.0	59.8
2.0	30.0	59.7
3.0	32.0	59.8
4.0	30.0	59.8
5.0	40.0	59.8
6.0	40.0	59.8
7.5	39.0	59.8
9.0	41.0	59.8
9.0	42.0	59.7
10.0	67.0	59.8
15.0	68.0	59.8
20.0	95.0	57.8
25.0	98.0	57.6
30.0	101.0	57.6
35.0	45.0	59.7
40.0	45.0	59.7
45.0	44.0	59.6
50.0	41.0	59.6
75.0	39.0	59.8
100.0	35.0	59.8
150.0	36.5	59.8
200.0	33.0	59.8

B1.30 NAERLS 8

I(m)	V(v)	I(mA)
1.0	27.0	60.0
2.0	29.0	59.8
3.0	34.0	59.7
4.0	30.0	59.8
5.0	38.0	59.8
6.0	40.0	59.8
7.5	39.0	59.8
9.0	42.0	59.8
9.0	44.0	58.7
10.0	65.0	59.8
15.0	67.0	59.8
20.0	97.0	57.8
25.0	101.0	57.5
30.0	100.0	57.6
35.0	45.0	58.6
40.0	45.0	58.7
45.0	45.0	58.7
50.0	42.0	59.0
75.0	40.0	59.0
100.0	37.0	59.3
150.0	36.0	59.4
200.0	33.0	59.8

B1.31 NAERLS 9

I(m)	V(v)	I(mA
1.0	28.0	59.8
2.0	29.0	59.8
3.0	33.0	59.8
4.0	39.0	59.8
5.0	39.0	59.8
6.0	40.0	59.8
7.5	39.0	59.8
9.0	41.0	59.8
9.0	42.0	58.7
10.0	67.0	59.8
15.0	67.0	59.8
20.0	97.0	57.8
25.0	100.0	57.2
30.0	101.0	57.8
35.0	46.0	58.7
40.0	46.0	58.7
45.0	45.0	58.6
50.0	41.0	58.8
75.0	39.0	59.8
100.0	35.0	59.4
150.0	36.0	59.3
200.0	33.0	59.8

APPENDIX B2: FIELD DATA COLLECTED USING THE SCHLUMBERGER ARRAY

TABLE B2.1 FCE

MN (m)	L = AB/2 (m)	K	R (Ω)	ρ (Ωm)
1.0	1.0	2.3562	47.8	112.6264
	1.5	6.2832	22.0	138.2304
	2.5	18.8500	8.21	154.7585
	3.75	43.3932	3.47	150.5744
	5.0	77.7544	1.914	148.8219
	7.5	175.9292	0.885	155.6973
	10.0	313.3739	0.571	178.9365
6.0	7.5	24.7400	6.42	158.8308
	10.0	47.6475	3.651	73.9134
	15.0	113.0925	1.915	216.5813
	25.0	322.5368	0.925	298.3465
	37.5	731.5984	0.500	365.7992
	50.0	1304.2846	0.345	449.9782
10.0	37.5	433.9325	0.840	364.5033
	50.0	777.5442	0.555	431.5370
	75.0	1759.2919	0.310	545.3805
	100.0	3133.7389	0.180	564.0730

TABLE B2.2 UNGWAN KAYA (KONGO)

MN (m)	L = AB/2 (m)	K	R (Ω)	ρ (Ωm)
1.0	1.0	2.3562	27.40	64.6
	1.5	6.2832	11.66	73.3
	2.5	18.8500	4.70	88.6
	3.75	43.3932	2.14	92.9
	5.0	77.7544	1.310	101.9
	7.5	175.9292	0.580	102.0
	10.0	313.3739	0.320	100.3
3.0	7.5	56.5487	1.927	109.0
	10.0	102.3636	1.060	108.5
	15.0	233.2633	0.497	115.9
	25.0	652.1423	0.247	161.1
	37.5	1470.2654	0.155	227.9
	50.0	2615.6377	0.110	287.7
5.0	37.5	879.6459	0.210	184.7
	50.0	1566.8693	0.293	459.1
	75.0	3530.3647	0.0755	266.5
	100.0	6279.2583	0.00775	48.7

TABLE B2.3 CIKAJI

MN (m)	L = AB/2 (m)	K	R (Ω)	ρ (Ωm)
1.0	1.0	2.3562	24.20	57.02
	1.5	6.2832	8.94	56.17
	2.5	18.8500	3.38	63.71
	3.75	43.3932	1.524	66.13
ÇL	5.0 ÇL	77.7544	0.879	68.35
	7.5	175.9292	0.310	54.54
	10.0	313.3739	0.157	49.20
3.0	7.5	24.7400	1.039	58.75
	10.0	47.6475	0.519	53.13
	15.0	113.0925	0.244	56.92
	25.0	322.5368	0.120	78.26
	37.5	731.5984	0.070	102.92
	50.0	1304.2846	0.047	122.93
10.0	37.5	433.9325	0.239	103.71
	50.0	777.5442	0.157	122.07
	75.0	1759.2919	0.091	160.10
	100.0	3133.7389	0.066	206.83

TABLE B2.4 AVIATION SITE 1

MN (m)	L = AB/2 (m)	K	R (Ω)	ρ (Ωm)
1.0	1.0	2.3562	87.6	206.40
	1.5	6.2832	41.8	262.64
	2.5	18.8500	14.83	279.55
	3.75	43.3932	6.21	269.47
	5.0	77.7544	3.41	265.14
	7.5	175.9292	1.313	231.00
	10.0	313.3739	0.748	234.40
3.0	7.5	24.7400	3.60	203.58
	10.0	47.6475	2.05	209.85
	15.0	113.0925	1.137	265.22
	25.0	322.5368	0.589	384.11
	37.5	731.5984	0.339	498.42
	50.0	1304.2846	0.227	593.75
10.0	37.5	433.9325	1.190	516.38
	50.0	777.5442	0.771	599.49
	75.0	1759.2919	0.397	698.44
	100.0	3133.7389	0.248	777.17

TABLE 92.5 BALADAM

MN (m)	L = AB/2 (m)	K	R (Ω)	ρ (Ωm)
1.0	1.0	2.3562	80.0	188.50
	1.5	6.2832	29.3	184.10
	2.5	18.8500	11.40	214.89
	3.75	43.3932	5.50	242.13
	5.0	77.7544	3.06	237.93
	7.5	175.9292	1.266	222.73
	10.0	313.3739	0.648	203.07
3.0	7.5	24.7400	4.37	247.12
	10.0	47.6475	2.19	224.10
	15.0	113.0925	0.970	226.77
	25.0	322.5368	0.317	226.73
	37.5	731.5984	0.126	185.25
	50.0	1304.2846	0.073	190.94
10.0	37.5	433.9325	0.393	170.54
	50.0	777.5442	0.232	180.39
	75.0	1759.2919	0.115	202.32
	100.0	3133.7389	0.080	250.70

TABLE 92.6 BASSAWA

MN (m)	L = AB/2 (m)	K	R (Ω)	ρ (Ωm)
1.0	1.0	2.3562	45.5	107.21
	1.5	6.2832	15.46	97.14
	2.5	18.8500	4.09	77.10
	3.75	43.3932	1.759	76.29
	5.0	77.7544	1.032	80.24
	7.5	175.9292	0.525	92.36
	10.0	313.3739	0.345	108.11
3.0	7.5	24.7400	1.622	91.72
	10.0	47.6475	1.029	105.33
	15.0	113.0925	0.567	133.26
	25.0	322.5368	0.293	191.08
	37.5	731.5984	0.166	244.06
	50.0	1304.2846	0.101	264.18
10.0	37.5	433.9325	0.585	253.85
	50.0	777.5442	0.374	290.80
	75.0	1759.2919	0.222	390.56
	100.0	3133.7389	0.149	466.93

TABLE 92.7 ZANGO

MN (m)	L = AB/2 (m)	K	R (Ω)	ρ (Ωm)
1.0	1.0	2.3562	87.7	206.64
	1.5	6.2832	31.3	196.66
	2.5	18.8500	11.61	218.85
	3.75	43.3932	5.19	225.21
	5.0	77.7544	2.47	192.05
	7.5	175.9292	1.004	157.39
	10.0	313.3739	0.452	141.65
3.0	7.5	24.7400	3.14	177.55
	10.0	47.6475	1.550	159.69
	15.0	113.0925	0.525	122.46
	25.0	322.5368	0.151	98.47
	37.5	731.5984	0.080	117.62
	50.0	1304.2846	0.057	149.09
10.0	37.5	433.9325	0.271	117.60
	50.0	777.5442	0.185	143.85
	75.0	1759.2919	0.107	188.28
	100.0	3133.7389	0.070	219.36

TABLE 92.8 TAMAA' KUBANNI

MN (m)	L = AB/2 (m)	K	R (Ω)	ρ (Ωm)
1.0	1.0	2.3562	26.6	62.67
	1.5	6.2832	8.79	55.23
	2.5	18.8500	1.553	29.27
	3.75	43.3932	0.584	25.34
	5.0	77.7544	0.356	27.68
	7.5	175.9292	0.170	29.91
	10.0	313.3739	0.097	30.40
3.0	7.5	24.7400	0.548	30.99
	10.0	47.6475	0.330	33.01
	15.0	113.0925	0.157	35.62
	25.0	322.5368	0.066	43.04
	37.5	731.5984	0.039	57.34
	50.0	1304.2846	0.028	73.24
10.0	37.5	433.9325	0.130	56.41
	50.0	777.5442	0.088	68.42
	75.0	1759.2919	0.055	96.76
	100.0	3133.7389	0.035	109.68

TABLE B2.9 TAYIB IDMI

MN (m)	L = AB/2 (m)	V	R (Ω)	ρ (Ωm)
1.0	1.0	2.3562	53.1	125.11
	1.5	6.2832	25.2	158.36
	2.5	19.6500	8.61	169.15
	3.75	43.3932	4.42	191.80
	5.0	77.7544	2.50	194.39
	7.5	175.9292	0.977	171.98
	10.0	313.3728	0.493	154.49
2.0	7.5	24.7400	7.08	174.17
	10.0	47.6475	3.332	158.82
	15.0	113.0925	0.532	124.10
	25.0	322.5360	0.174	112.47
	37.5	721.5084	0.094	138.20
	50.0	1304.2946	0.053	152.17
10.0	37.5	433.9325	0.316	137.12
	50.0	777.5442	0.203	157.84
	75.0	1750.2919	0.112	197.04
	100.0	3133.7399	0.077	241.30

TABLE B2.10 TUDUN SABKI

MN (m)	L = AB/2 (m)	V	R (Ω)	ρ (Ωm)
1.0	1.0	2.3562	47.0	110.75
	1.5	6.2832	17.12	107.57
	2.5	19.6500	6.35	110.78
	3.75	43.3932	2.89	125.41
	5.0	77.7544	1.575	122.45
	7.5	175.9292	0.661	116.33
	10.0	313.3728	0.339	105.93
2.0	7.5	24.7400	2.02	111.70
	10.0	47.6475	1.020	105.03
	15.0	113.0925	0.474	96.57
	25.0	322.5360	0.144	93.01
	37.5	721.5084	0.085	124.07
	50.0	1304.2946	0.059	154.33
10.0	37.5	433.9325	0.275	119.37
	50.0	777.5442	0.211	164.05
	75.0	1750.2919	0.122	214.53
	100.0	3133.7399	0.095	260.50

TABLE B2.11 GOBUBA

MN (m)	L = AB/2 (m)	V	R (Ω)	ρ (Ωm)
1.0	1.0	2.3562	35.0	84.92
	1.5	6.2832	17.00	106.94
	2.5	19.6500	5.533	108.71
	3.75	43.3932	2.234	96.77
	5.0	77.7544	1.115	86.70
	7.5	175.9292	0.397	69.88
	10.0	313.3728	0.188	58.91
2.0	7.5	24.7400	1.464	67.52
	10.0	47.6475	0.676	59.96
	15.0	113.0925	0.246	57.39
	25.0	322.5360	0.448	71.74
	37.5	721.5084	0.068	99.00
	50.0	1304.2946	0.053	136.01
10.0	37.5	433.9325	0.075	110.33
	50.0	777.5442	0.204	159.52
	75.0	1750.2919	0.570	1016.07
	100.0	3133.7399	0.058	3002.12

TABLE B2.12 WUSASA

MN (m)	L = AB/2 (m)	V	R (Ω)	ρ (Ωm)
1.0	1.0	2.3562	60.0	141.37
	1.5	6.2832	22.4	140.74
	2.5	19.6500	6.58	129.33
	3.75	43.3932	2.95	128.11
	5.0	77.7544	1.711	133.04
	7.5	175.9292	0.940	165.36
	10.0	313.3728	0.503	157.67
2.0	7.5	24.7400	2.02	111.70
	10.0	47.6475	1.041	109.45
	15.0	113.0925	0.356	235.33
	25.0	322.5360	0.440	203.01
	37.5	721.5084	0.227	240.45
	50.0	1304.2946	0.156	400.04
10.0	37.5	433.9325	0.717	311.13
	50.0	777.5442	0.402	374.79
	75.0	1750.2919	0.267	466.73
	100.0	3133.7399	0.172	539.00

TABLE B2.13 [illegible]

MN (m)	L = AB/2 (m)	K	R (Ω)	ρ (Ωm)
1.0	1.0	2.3562	48.6	114.51
	1.5	6.2832	20.6	129.41
	2.5	18.8500	6.84	128.93
	3.75	43.3932	2.90	125.84
	5.0	77.7544	1.779	138.33
	7.5	175.9292	0.673	118.40
	10.0	313.3739	0.329	103.10
3.0	7.5	24.7400	2.11	119.32
	10.0	47.6475	0.990	101.34
	15.0	113.0925	0.447	104.27
	25.0	322.5368	0.202	131.73
	37.5	731.5984	0.124	182.31
	50.0	1304.2846	0.088	230.18
10.0	37.5	433.9325	0.375	162.72
	50.0	777.5442	0.297	230.93
	75.0	1759.2919	0.152	267.41
	100.0	3133.7389	0.101	316.51

TABLE B2.14 TUKUP TUKUP

MN (m)	L = AB/2 (m)	K	R (Ω)	ρ (Ωm)
1.0	1.0	2.3562	43.4	102.26
	1.5	6.2832	19.24	120.89
	2.5	18.8500	6.22	117.25
	3.75	43.3932	2.46	106.75
	5.0	77.7544	1.220	94.86
	7.5	175.9292	0.509	89.55
	10.0	313.3739	0.293	91.82
3.0	7.5	24.7400	1.541	87.80
	10.0	47.6475	0.872	88.25
	15.0	113.0925	0.524	122.23
	25.0	322.5368	0.253	171.51
	37.5	731.5984	0.158	232.30
	50.0	1304.2846	0.109	282.49
10.0	37.5	433.9325	0.606	262.96
	50.0	777.5442	0.382	297.02
	75.0	1759.2919	0.172	302.60
	100.0	3133.7389	0.103	322.78

TABLE B2.15 [illegible]

MN (m)	L = AB/2 (m)	K	R (Ω)	ρ (Ωm)
1.0	1.0	2.3562	103.8	244.57
	1.5	6.2832	31.24	196.56
	2.5	18.8500	6.94	130.82
	3.75	43.3932	2.41	104.58
	5.0	77.7544	1.330	103.41
	7.5	175.9292	0.690	118.53
	10.0	313.3739	0.434	136.00
3.0	7.5	24.7400	2.21	124.97
	10.0	47.6475	1.388	142.08
	15.0	113.0925	0.765	179.45
	25.0	322.5368	0.411	268.03
	37.5	731.5984	0.253	371.98
	50.0	1304.2846	0.179	465.20
10.0	37.5	433.9325	0.821	356.26
	50.0	777.5442	0.657	510.95
	75.0	1759.2919	0.318	559.45
	100.0	3133.7389	0.213	667.49

TABLE B2.16 TUKUP JUKUN

MN (m)	L = AB/2 (m)	K	R (Ω)	ρ (Ωm)
1.0	1.0	2.3562	93.5	220.30
	1.5	6.2832	50.64	317.07
	2.5	18.8500	22.82	429.79
	3.75	43.3932	11.11	482.10
	5.0	77.7544	6.11	475.08
	7.5	175.9292	2.10	369.45
	10.0	313.3739	0.936	293.32
3.0	7.5	24.7400	6.54	369.92
	10.0	47.6475	2.89	295.83
	15.0	113.0925	0.953	222.30
	25.0	322.5368	0.606	395.20
	37.5	731.5984	0.162	233.65
	50.0	1304.2846	0.161	421.12
10.0	37.5	433.9325	0.561	243.44
	50.0	777.5442	0.321	249.59
	75.0	1759.2919	0.192	337.79
	100.0	3133.7389	0.125	391.77

TABLE 32.17 [illegible]

MN	L = AB/2	K	h	ρ
	(m)		(m)	(Ωm)
[illegible]	1.0	2.3562	133.0	242.69
	1.5	6.2832	45.44	285.25
	2.5	18.8500	14.44	209.62
	3.75	43.3932	3.74	150.89
	5.0	77.7544	1.607	124.95
	7.5	175.9292	0.521	93.42
	10.0	313.9730	0.287	83.87
[illegible]	7.5	24.7400	1.044	184.89
	10.0	47.6475	1.040	183.99
	15.0	113.0925	0.450	139.40
	25.0	322.5360	0.206	124.24
	37.5	731.5884	0.140	174.95
	50.0	1304.2946	0.083	217.19
[illegible]	37.5	633.0225	0.164	201.34
	50.0	777.5442	0.204	226.27
	75.0	1759.2919	0.224	388.89
	100.0	3133.7388	0.166	520.20

TABLE 32.18 BONO

MN	L = AB/2	K	h	ρ
(m)	(m)		(m)	(Ωm)
1.0	1.0	2.3562	24.1	56.79
	1.5	6.2832	7.05	44.30
	2.5	18.8500	1.952	36.81
	3.75	43.3932	0.910	39.50
GL	5.0	77.7544	0.508	39.50
	7.5	175.9292	0.250	43.98
	10.0	313.9730	0.163	51.18
3.0	7.5	24.7400	0.805	45.50
	10.0	47.6475	0.734	75.13
	15.0	113.0925	0.370	63.88
	25.0	322.5360	0.136	99.68
	37.5	731.5884	0.080	113.10
	50.0	1304.2946	0.052	151.30
10.0	37.5	633.0225	0.075	113.33
	50.0	777.5442	0.105	152.40
	75.0	1759.2919	0.121	213.15
	100.0	3133.7388	0.080	250.74

TABLE 32.19 [illegible]

MN	L = AB/2	K	h	ρ
(m)	(m)		(m)	(Ωm)
1.0	1.0	2.3562	56.1	132.19
	1.5	6.2832	21.6	135.72
	2.5	18.8500	6.33	119.32
	3.75	43.3932	2.68	116.29
	5.0	77.7544	1.592	123.79
	7.5	175.9292	0.754	132.65
	10.0	313.9730	0.384	120.53
3.0	7.5	24.7400	2.55	144.20
	10.0	47.6475	1.398	131.95
	15.0	113.0925	0.532	124.19
	25.0	322.5360	0.170	110.95
	37.5	731.5884	0.074	108.90
	50.0	1304.2946	0.033	93.79
10.0	37.5	633.0225	0.352	108.35
	50.0	777.5442	0.135	105.75
	75.0	1759.2919	0.079	137.22
	100.0	3133.7388	0.052	162.95

TABLE 32.20 DAC

MN	L = AB/2	K	h	ρ
(m)	(m)		(m)	(Ωm)
1.0	1.0	2.3562	122.6	291.23
	1.5	6.2832	43.4	272.69
	2.5	18.8500	13.96	263.15
	3.75	43.3932	5.33	231.29
	5.0	77.7544	3.10	241.04
	7.5	175.9292	1.637	288.00
	10.0	313.9730	1.059	331.55
3.0	7.5	24.7400	6.24	352.96
	10.0	47.6475	3.98	407.41
	15.0	113.0925	2.03	473.53
	25.0	322.5360	0.701	457.15
	37.5	731.5884	0.370	541.00
	50.0	1304.2946	0.240	540.39
10.0	37.5	633.0225	1.010	611.74
	50.0	777.5442	0.526	409.03
	75.0	1759.2919	0.250	439.82
	100.0	3133.7388	0.161	504.53

TABLE B2.21 MAIGAMO

MN (m)	L = AB/2 (m)	K	R (Ω)	ρ (Ωm)
1.0	1.0	2.3562	64.7	152.45
	1.5	6.2832	27.7	174.04
	2.5	18.8500	10.19	192.08
	3.75	43.3932	4.17	180.95
	5.0	77.7544	2.04	158.62
	7.5	175.9292	0.774	136.17
	10.0	313.3739	0.381	119.40
3.0	7.5	24.7400	2.81	158.90
	10.0	47.6475	1.361	139.32
	15.0	113.0925	0.525	122.46
	25.0	322.5368	0.172	112.17
	37.5	731.5984	0.070	102.92
	50.0	1304.2846	0.034	88.93
10.0	37.5	433.9325	0.233	101.11
	50.0	777.5442	0.186	144.62
	75.0	1759.2919	0.072	126.67
	100.0	3133.7389	0.047	147.29

TABLE B2.22 STAFF SCHOOL

MN (m)	L = AB/2 (m)	K	R (Ω)	ρ (Ωm)
1.0	1.0	2.3562	97.0	288.55
	1.5	6.2832	31.8	199.81
	2.5	18.8500	7.69	144.96
	3.75	43.3932	2.58	111.95
	5.0	77.7544	1.409	109.56
	7.5	175.9292	0.565	99.40
	10.0	313.3739	0.315	98.71
3.0	7.5	24.7400	2.06	116.49
	10.0	47.6475	1.040	106.46
	15.0	113.0925	0.533	124.33
	25.0	322.5368	0.214	139.56
	37.5	731.5984	0.097	145.56
	50.0	1304.2846	0.060	130.78
10.0	37.5	433.9325	0.318	138.42
	50.0	777.5442	0.167	129.85
	75.0	1759.2919	0.071	124.93
	100.0	3133.7389	0.044	137.88

TABLE B2.23 NAERLS 1

MN (m)	L = AB/2 (m)	K	R (Ω)	ρ (Ωm)
1.0	1.0	2.3562	31.5	74.220
	1.5	6.2832	13.57	85.263
	2.5	18.8500	5.39	101.602
	3.75	43.3932	2.51	108.917
	5.0	77.7544	1.484	115.388
	7.5	175.9292	0.764	134.410
	10.0	313.3739	0.444	139.138
3.0	7.5	24.7400	2.64	149.289
	10.0	47.6475	1.458	149.246
	15.0	113.0925	0.674	157.220
	25.0	322.5368	0.195	127.168
	37.5	731.5984	0.071	104.389
	50.0	1304.2846	0.041	107.241
10.0	37.5	433.9325	0.245	106.314
	50.0	777.5442	0.083	64.536
	75.0	1759.2919	0.078	137.225
	100.0	3133.7389	0.070	219.362

TABLE B2.24 NAERLS 2

MN (m)	L = AB/2 (m)	K	R (Ω)	ρ (Ωm)
1.0	1.0	2.3562	32.60	76.810
	1.5	6.2832	14.66	92.093
	2.5	18.8500	5.70	107.38
	3.75	43.3932	2.69	116.62
	5.0	77.7544	1.57	121.96
	7.5	175.9292	0.832	146.37
	10.0	313.3739	0.526	164.86
3.0	7.5	24.7400	2.59	146.52
	10.0	47.6475	1.612	165.06
	15.0	113.0925	0.755	176.20
	25.0	322.5368	0.221	144.16
	37.5	731.5984	0.092	120.03
	50.0	1304.2846	0.043	113.26
10.0	37.5	433.9325	0.277	120.07
	50.0	777.5442	0.146	113.40
	75.0	1759.2919	0.077	134.53
	100.0	3133.7389	0.060	189.45

TABLE 02.25 MAPPLS 3

MN (m)	L = AB/2 (m)	K	R (Ω)	ρ (Ωm)
1.0	1.0	2.3562	10.345	95.06
	1.5	5.2032	10.00	114.34
	2.5	18.8500	7.14	134.67
	3.75	43.2832	3.22	139.89
	5.0	77.7544	1.85	143.78
	7.5	175.9292	0.959	170.51
	10.0	313.3728	0.618	193.77
2.0	7.5	24.7400	2.02	164.89
	10.0	47.6475	1.040	198.53
	15.0	113.0925	0.538	216.59
	25.0	322.5360	0.358	140.16
	37.5	731.5884	0.205	140.09
	50.0	1304.2846	0.093	138.02
10.0	37.5	433.9335	0.314	136.23
	50.0	777.5442	0.184	142.71
	75.0	1750.2919	0.100	175.15
	100.0	3133.7200	0.083	260.31

TABLE 02.26 MAPPLS 4

MN (m)	L = AB/2 (m)	K	R (Ω)	ρ (Ωm)
1.0	1.0	2.3562	64.43	151.81
	1.5	5.2032	27.43	142.74
	2.5	18.8500	10.00	188.50
	3.75	43.2832	5.22	221.84
	5.0	77.7544	3.30	256.59
	7.5	175.9292	1.540	270.97
	10.0	313.3728	1.035	324.31
2.0	7.5	24.7400	5.15	201.05
	10.0	47.6475	3.17	324.00
	15.0	113.0925	1.451	339.55
	25.0	322.5360	0.400	255.00
	37.5	731.5884	0.154	207.12
	50.0	1304.2846	0.083	217.01
10.0	37.5	433.9335	0.523	226.95
	50.0	777.5442	0.300	240.01
	75.0	1750.2919	0.140	251.00
	100.0	3133.7200	0.120	407.52

TABLE 02.27 MAPPLS 5

MN (m)	L = AB/2 (m)	K	R (Ω)	ρ (Ωm)
1.0	1.0	2.3562	60.55	142.66
	1.5	5.2032	25.07	163.15
	2.5	18.8500	10.31	194.07
	3.75	43.2832	4.96	215.13
	5.0	77.7544	3.00	240.22
	7.5	175.9292	1.520	269.03
	10.0	313.3728	0.945	296.10
2.0	7.5	24.7400	4.50	250.96
	10.0	47.6475	2.99	297.97
	15.0	113.0925	1.433	334.33
	25.0	322.5360	0.350	233.00
	37.5	731.5884	0.135	200.41
	50.0	1304.2846	0.077	200.62
10.0	37.5	433.9335	0.461	199.95
	50.0	777.5442	0.250	200.63
	75.0	1750.2919	0.139	242.33
	100.0	3133.7200	0.097	304.79

TABLE 02.28 MAPPLS 6

MN (m)	L = AB/2 (m)	K	R (Ω)	ρ (Ωm)
1.0	1.0	2.3562	59.72	140.71
	1.5	5.2032	25.76	151.07
	2.5	18.8500	10.14	191.09
	3.75	43.2832	4.93	214.14
	5.0	77.7544	2.99	232.06
	7.5	175.9292	1.526	270.14
	10.0	313.3728	0.957	300.01
2.0	7.5	24.7400	5.59	315.71
	10.0	47.6475	3.03	300.07
	15.0	113.0925	1.307	304.99
	25.0	322.5360	0.374	244.17
	37.5	731.5884	0.135	199.05
	50.0	1304.2846	0.075	196.14
10.0	37.5	433.9335	0.459	199.17
	50.0	777.5442	0.254	197.52
	75.0	1750.2919	0.143	250.41
	100.0	3133.7200	0.140	438.66

TABLE 20.20 MARRIS 7

AM (m)	L = AB/2 (m)	K	R (Ω)	ρ (Ωm)
1.0	1.0	3.1416	57.49	180.64
	1.5	6.2832	28.07	176.33
	2.5	19.6350	8.02	157.49
	3.75	43.9824	4.10	180.41
	5.0	77.7544	2.39	185.90
	7.5	175.9292	1.260	222.01
	10.0	313.9728	0.760	238.62
2.0	7.5	24.7400	3.00	216.21
	10.0	47.6475	2.47	252.12
	15.0	113.0925	1.102	247.09
	25.0	322.5360	0.314	205.07
	37.5	721.5004	0.115	160.79
	50.0	1304.2840	0.050	151.95
10.0	37.5	433.0925	0.301	150.77
	50.0	777.5440	0.180	155.00
	75.0	1750.2810	0.080	173.50
	100.0	3133.7200	0.065	205.19

TABLE 20.30 MARRIS 8

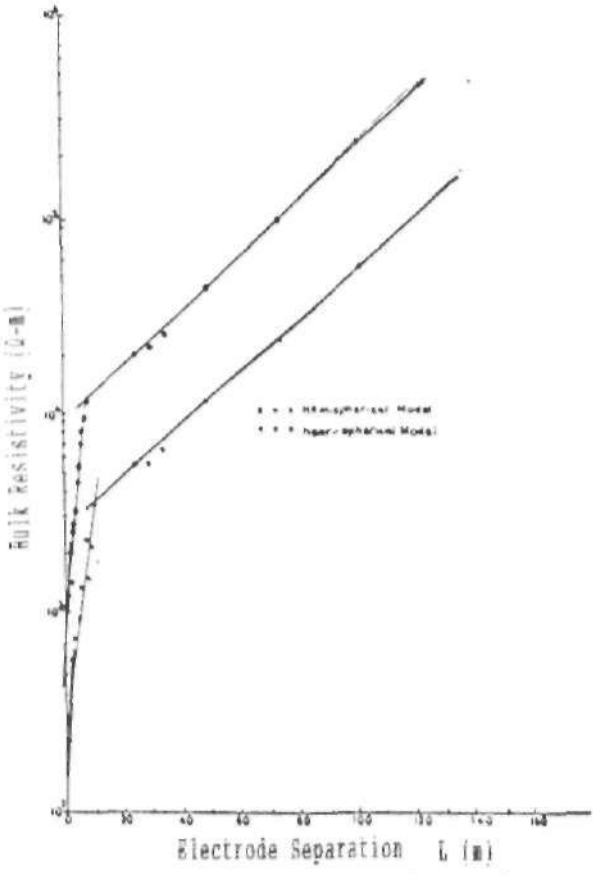
AM (m)	L = AB/2 (m)	K	R (Ω)	ρ (Ωm)
1.0	1.0	3.1416	59.00	185.35
	1.5	6.2832	24.33	152.91
	2.5	19.6350	8.71	171.01
	3.75	43.9824	4.15	182.55
	5.0	77.7544	2.42	188.12
	7.5	175.9292	1.270	223.51
	10.0	313.9728	0.780	244.93
2.0	7.5	24.7400	3.00	224.22
	10.0	47.6475	2.42	247.24
	15.0	113.0925	1.074	240.01
	25.0	322.5360	0.321	205.10
	37.5	721.5004	0.112	172.12
	50.0	1304.2840	0.062	162.05
10.0	37.5	433.0925	0.400	173.54
	50.0	777.5440	0.266	162.21
	75.0	1750.2810	0.112	197.10
	100.0	3133.7200	0.088	278.73

TABLE 20.31 MARRIS 9

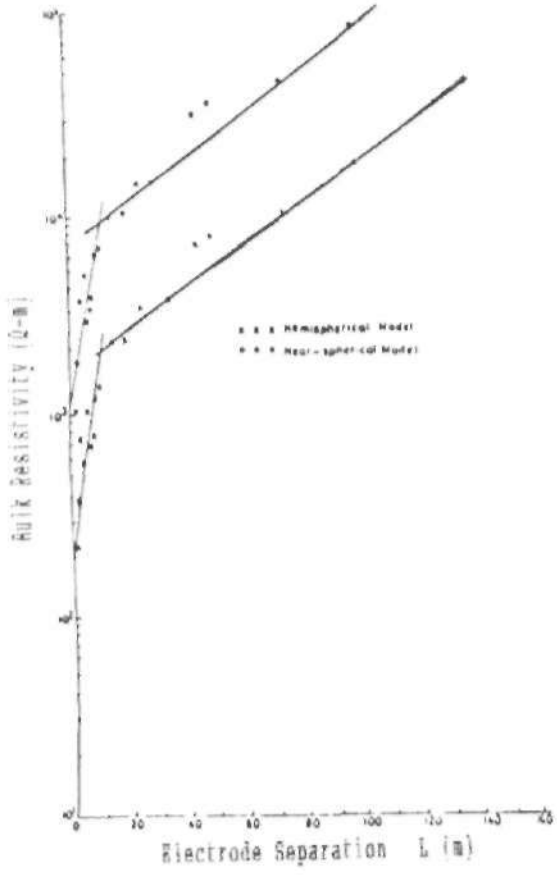
AM (m)	L = AB/2 (m)	K	R (Ω)	ρ (Ωm)
1.0	1.0	3.1416	57.49	158.82
	1.5	6.2832	24.24	152.31
	2.5	19.6350	8.02	170.11
	3.75	43.9824	4.20	182.20
	5.0	77.7544	2.35	180.17
	7.5	175.9292	1.264	222.33
	10.0	313.9728	0.830	260.07
2.0	7.5	24.7400	4.07	230.07
	10.0	47.6475	2.41	250.14
	15.0	113.0925	1.03	236.85
	25.0	322.5360	0.322	210.02
	37.5	721.5004	0.115	160.99
	50.0	1304.2840	0.060	157.17
10.0	37.5	433.0925	0.392	170.21
	50.0	777.5440	0.202	157.11
	75.0	1750.2810	0.115	203.23
	100.0	3133.7200	0.090	283.16

APPENDIX C1: INTERPRETED VERTICAL ELECTRICAL SOUNDING FIELD DATA USING TWO-ELECTRODE METHOD: (GRAPH OF BULK RESISTIVITY AGAINST ELECTRODE SPACING)

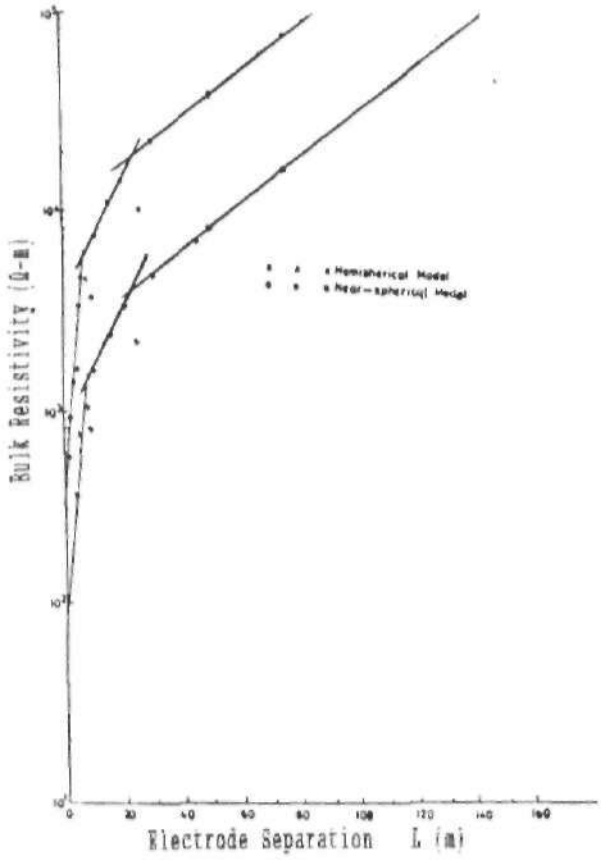
C1.1: FCE, Zaria



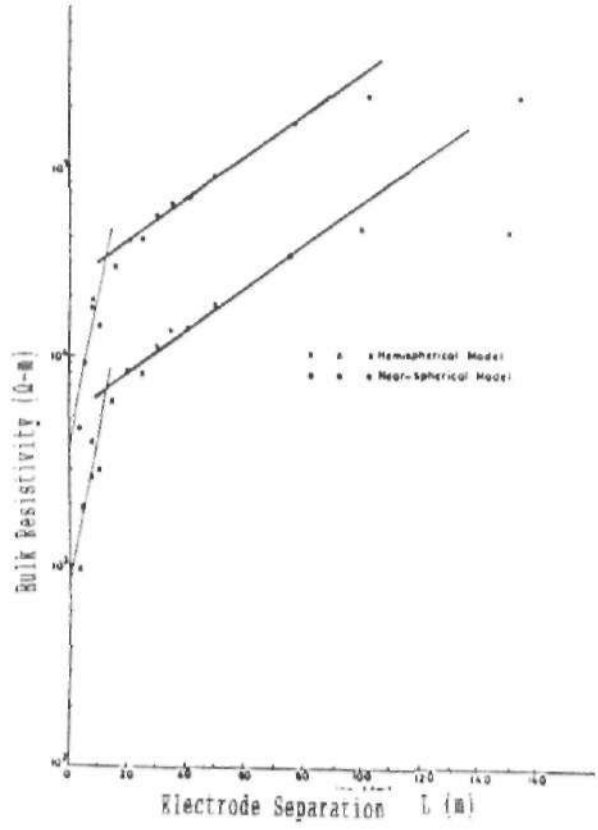
C1.2: UNGWAN KAYA (KONGO)



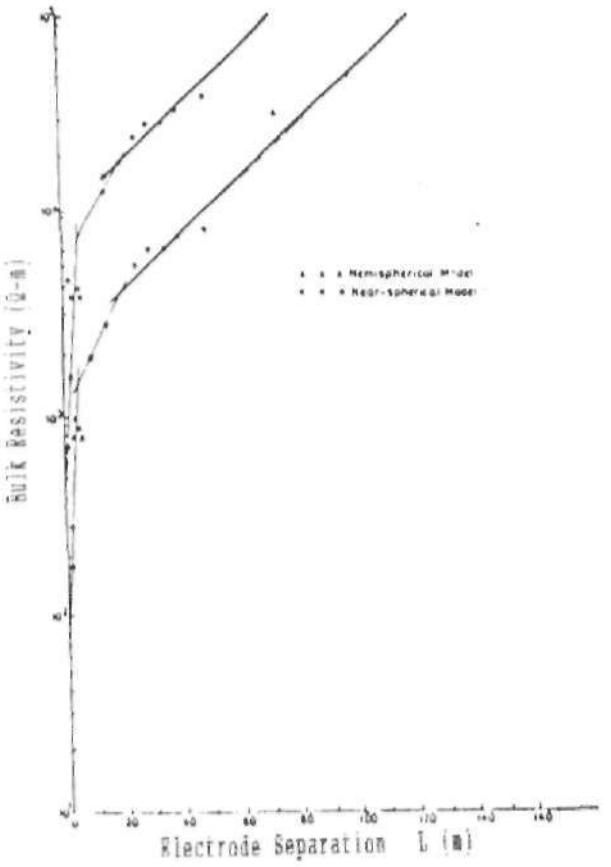
C1.3: CIKAJI



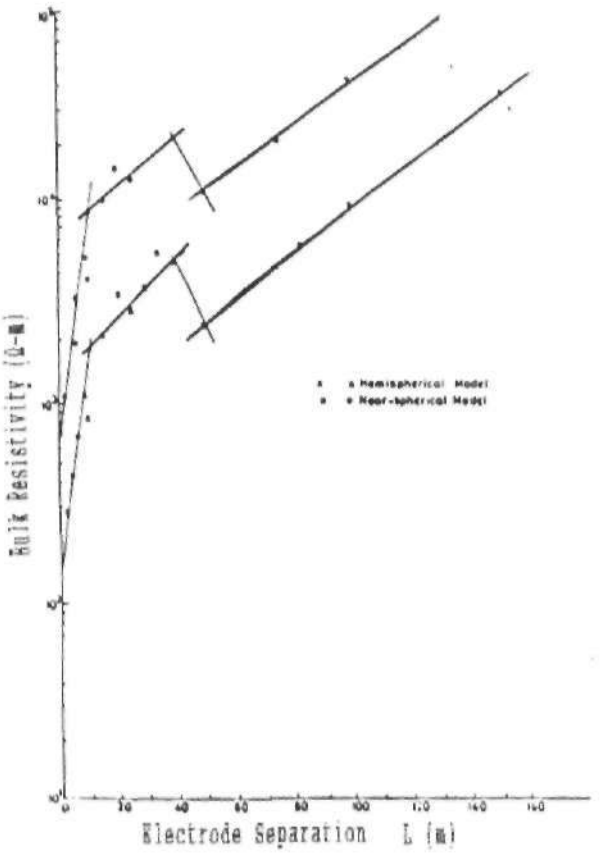
C1.4: AVIATION SITE 1



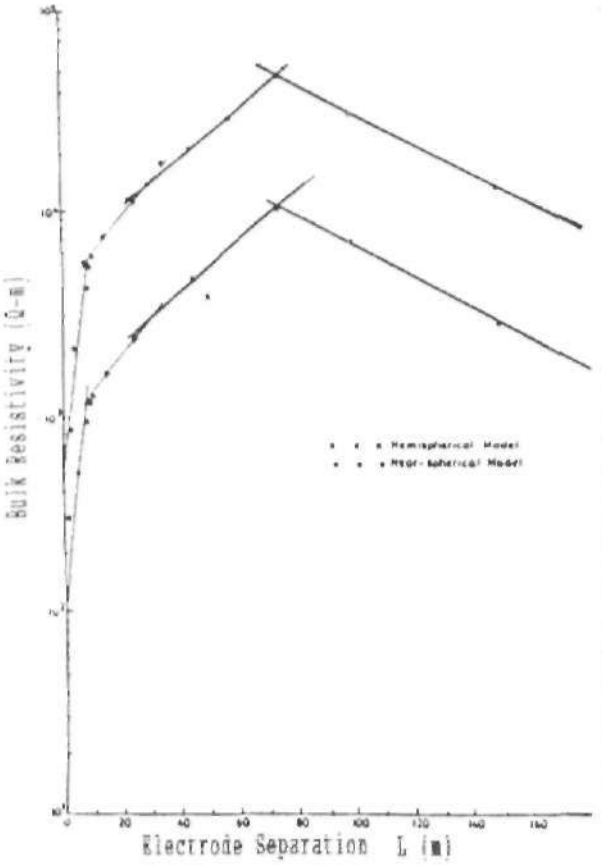
C1.5: PALLADAN



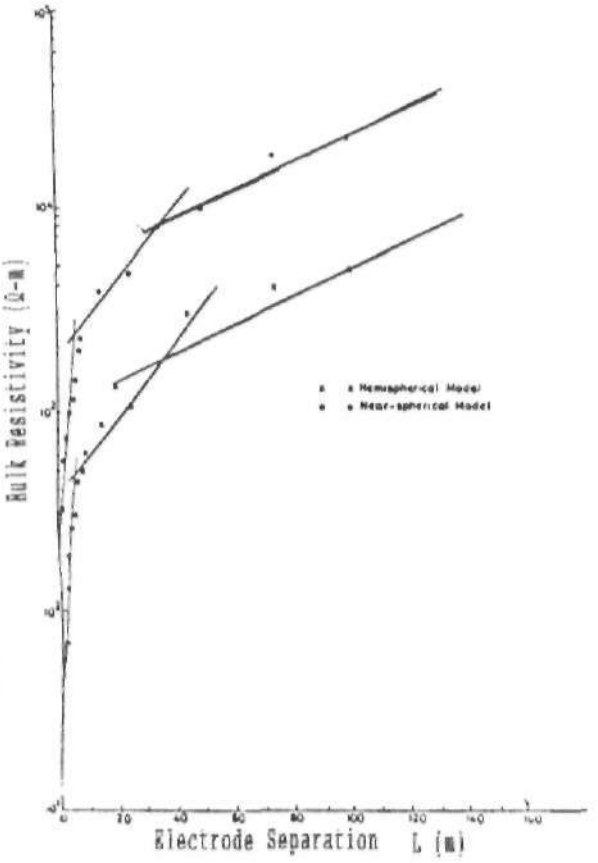
C1.7: ZANGO



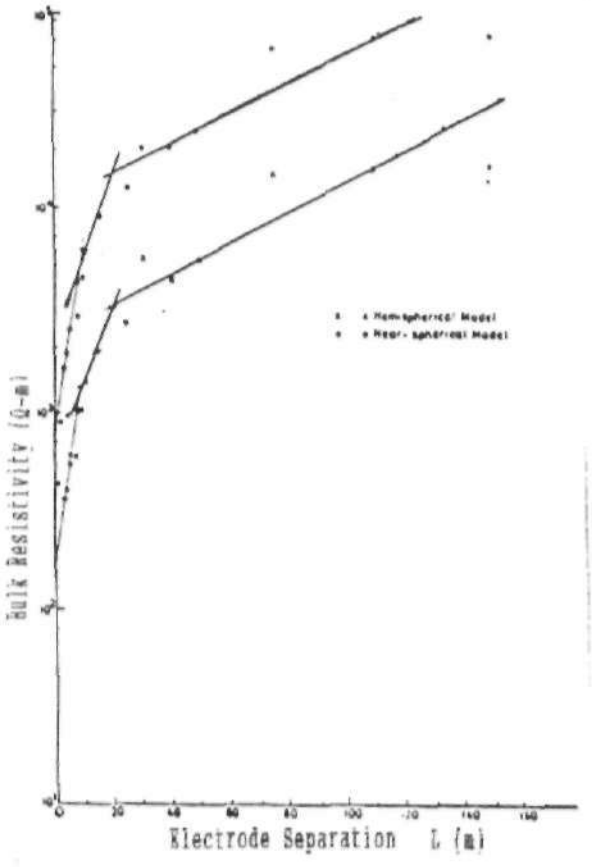
C1.6: BASSAWA



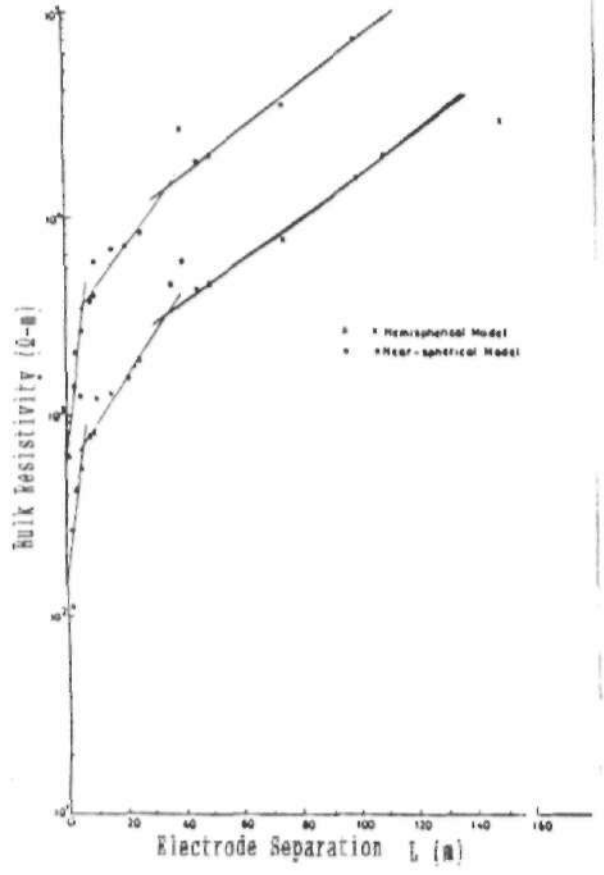
C1.8: JAMAA' KUBANNI



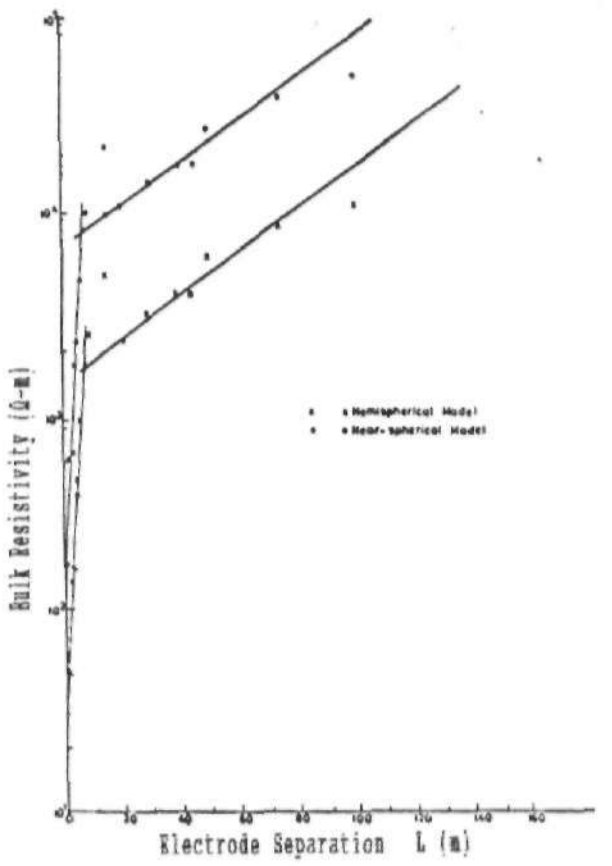
C1.9: HAYIN LEMA



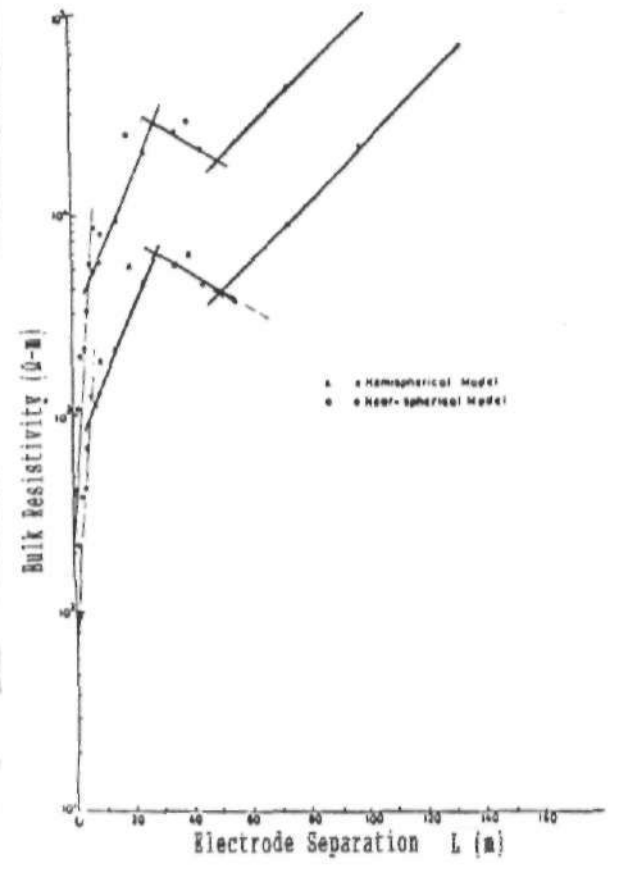
C1.10: TUDUN SARKI



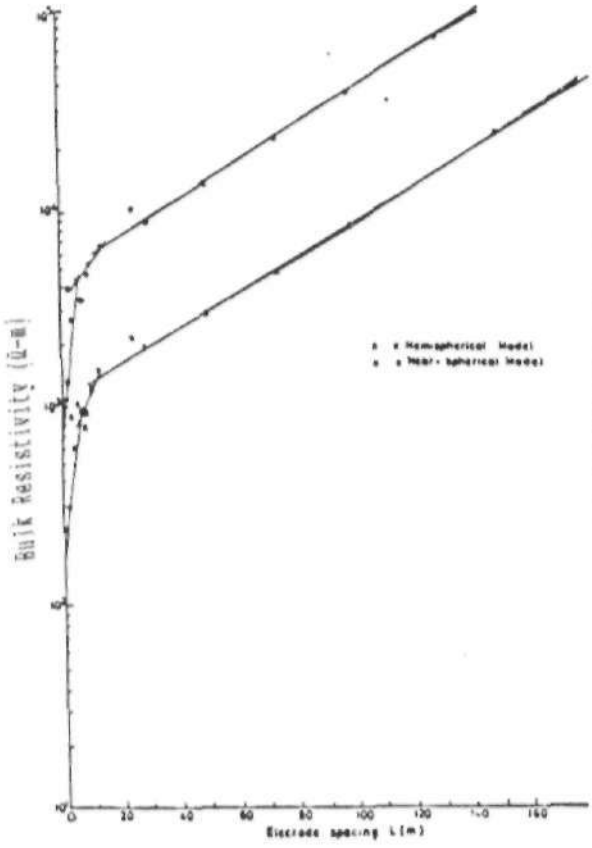
C1.11: GORUBA



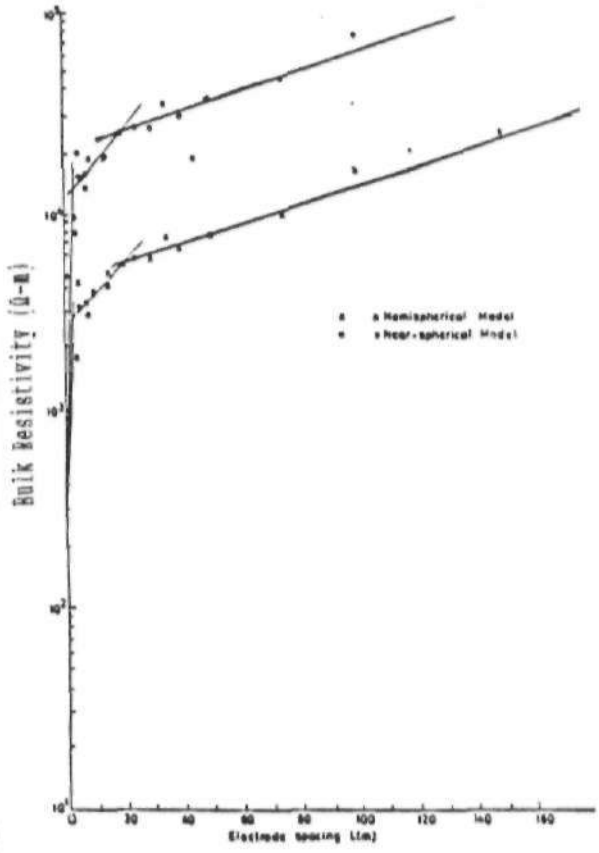
C1.12: WUSASA



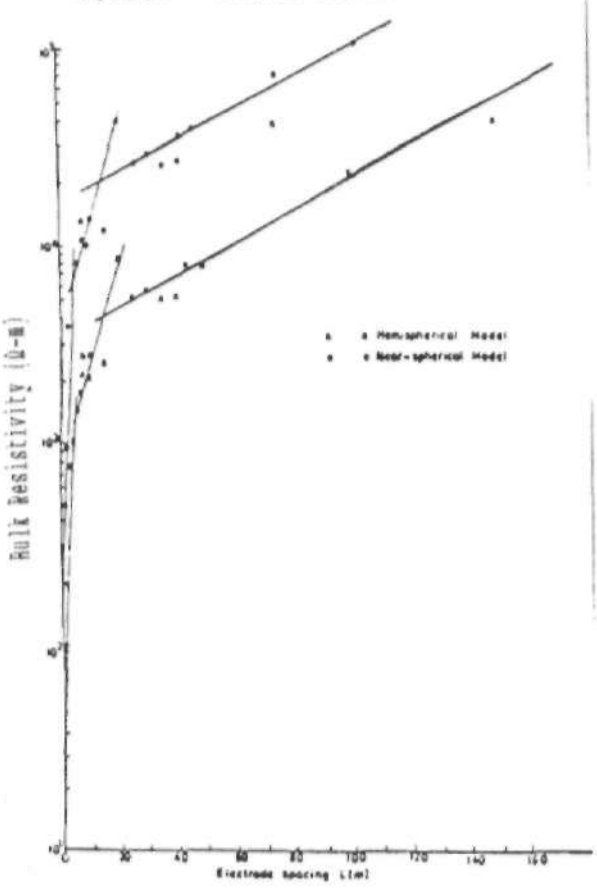
C1.13: HANWA



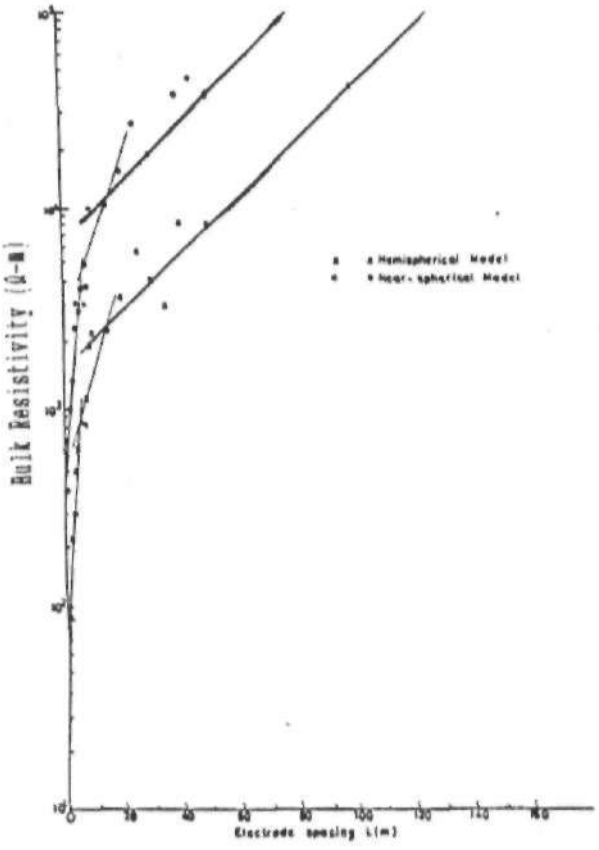
C1.15: ALHUDAHUDA



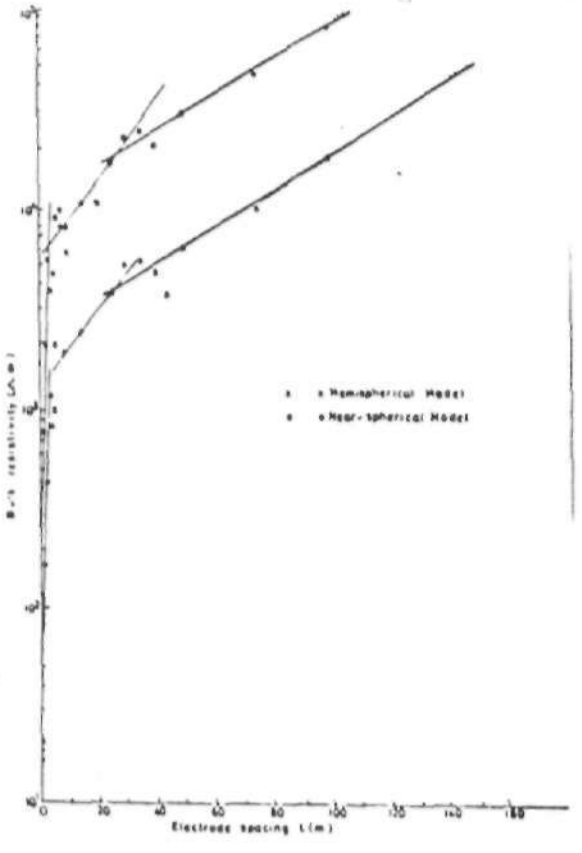
C1.14: TUKUR TUKUR



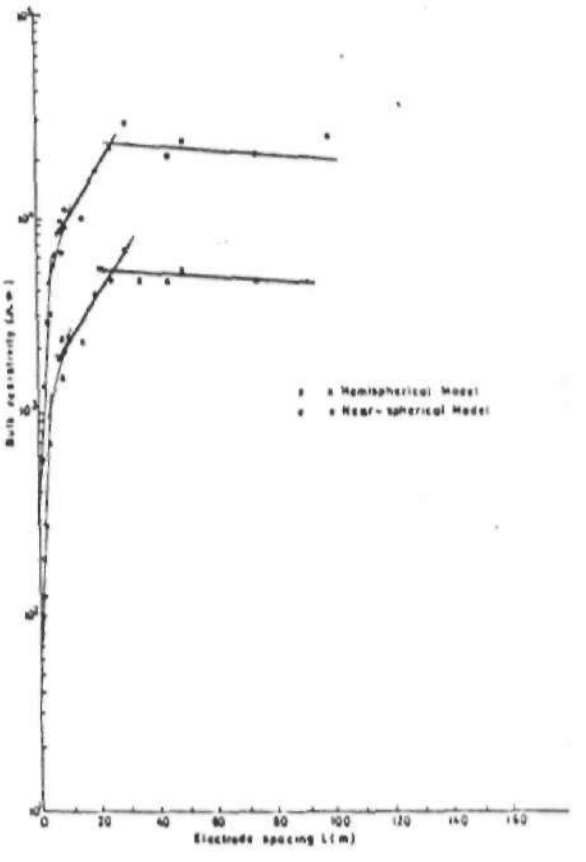
C1.16: TUKUR JUKUN



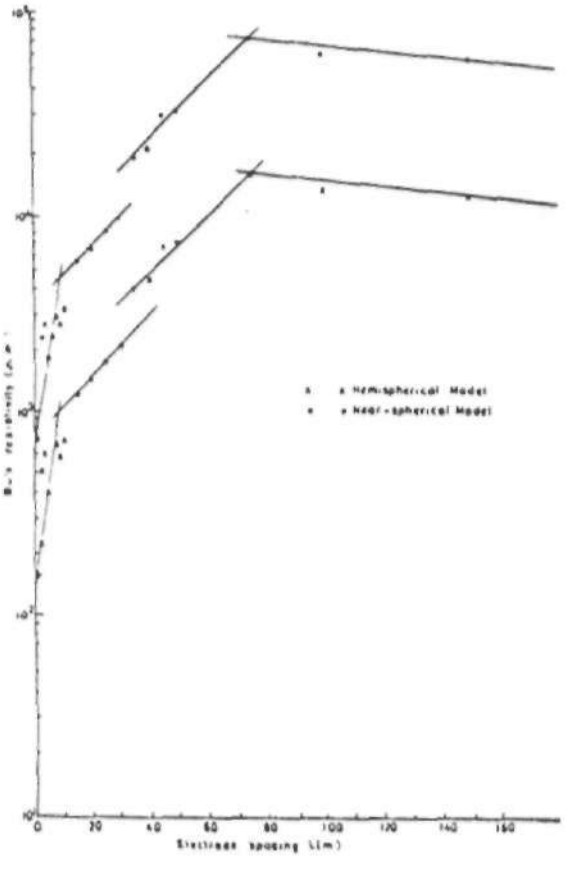
C1.17: UNGWAN SARKI



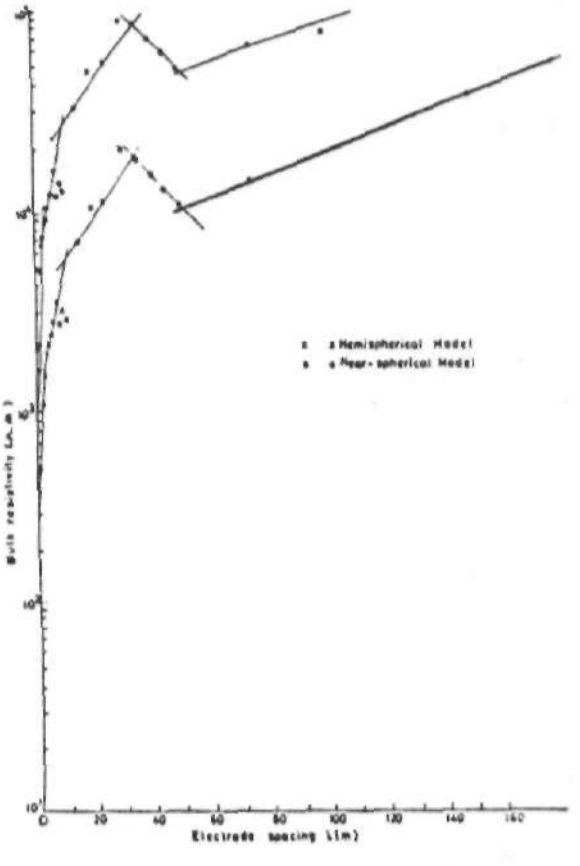
1.1): KURRIMI BOMO



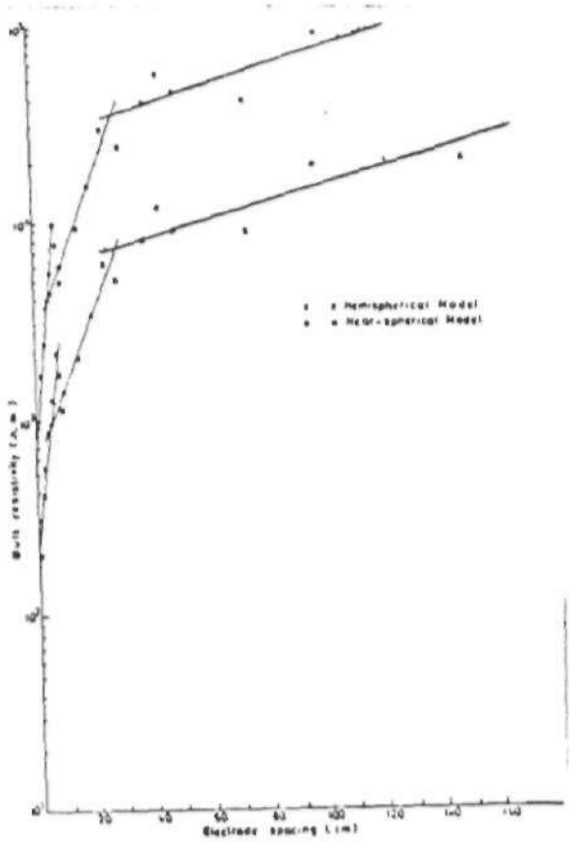
C1.18: BOMO



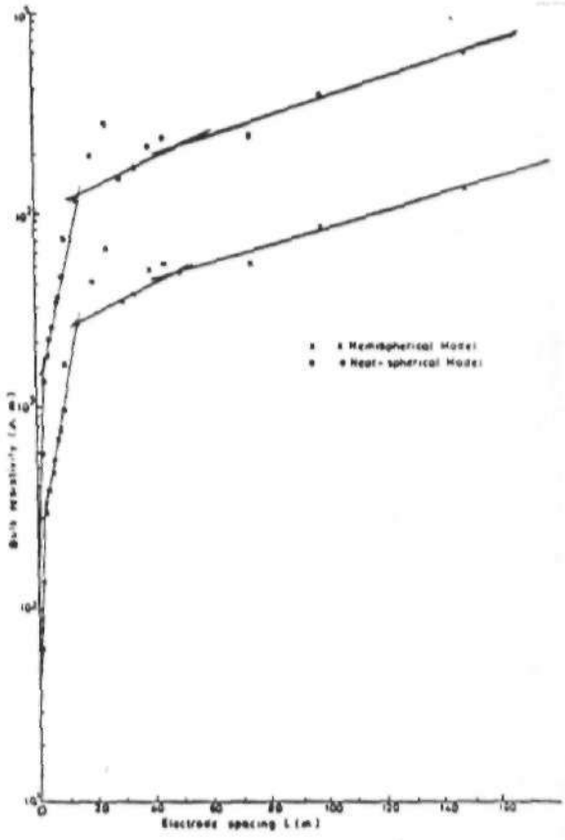
C1.20: DAC



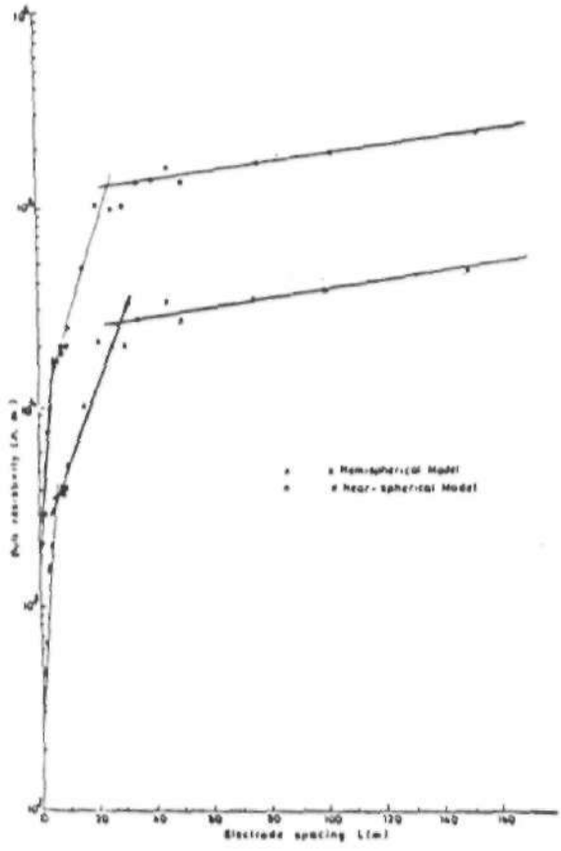
C1.21: MAIGAMO



C1.23: NAERLS 1

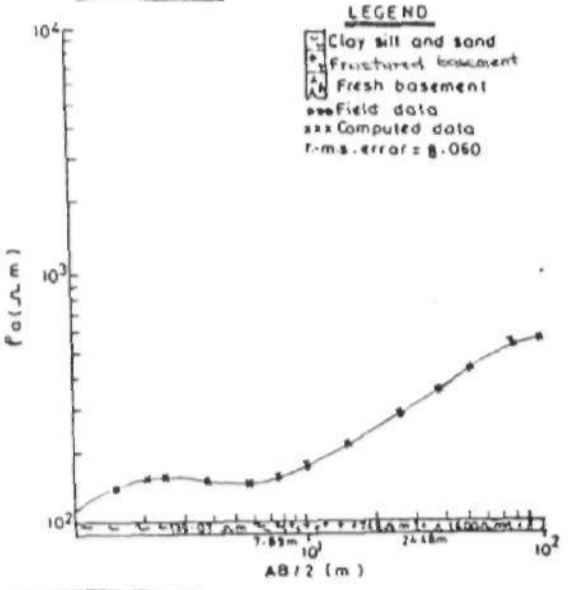


C1.22: STAFF SCHOOL

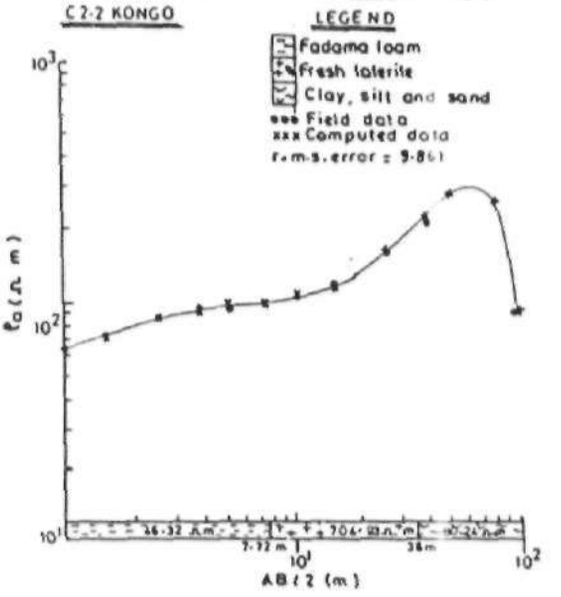


APPENDIX C2: INTERPRETED VERTICAL ELECTRICAL SOUNDING FIELD DATA USING THE SCHLUMBERGER ARRAY: (GRAPH OF APPARENT RESISTIVITY AGAINST AB/2)

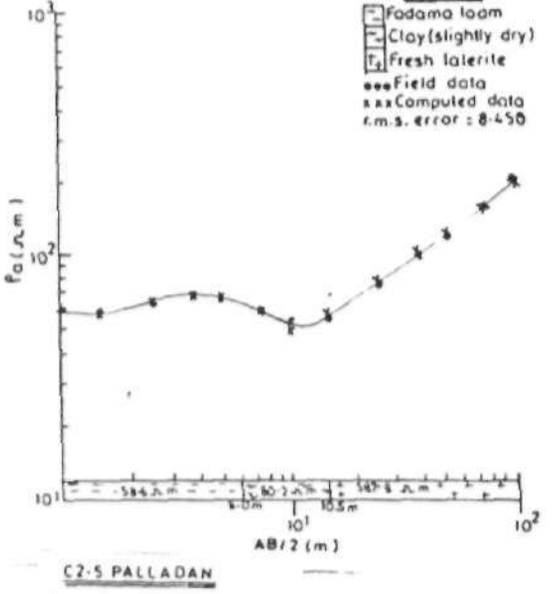
C2-1 FCE ZARIA



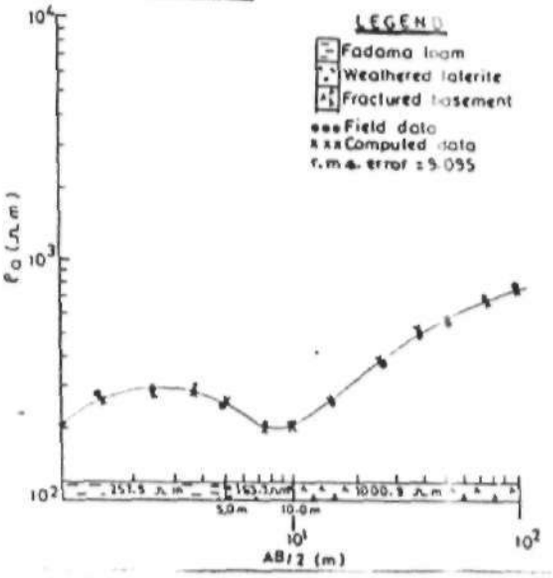
C2-2 KONGO



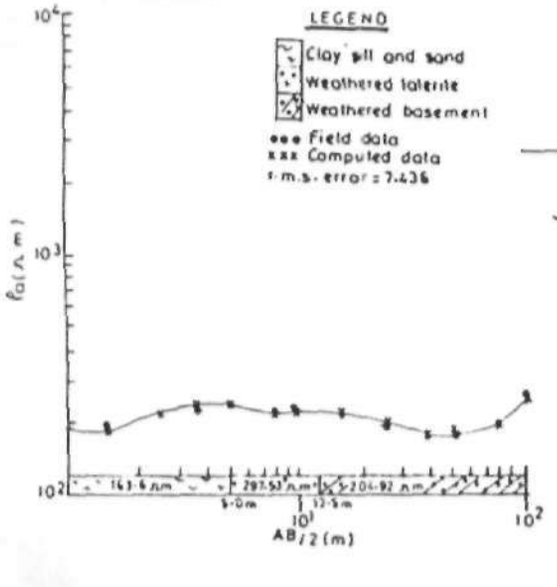
C2-3 CIKAJI



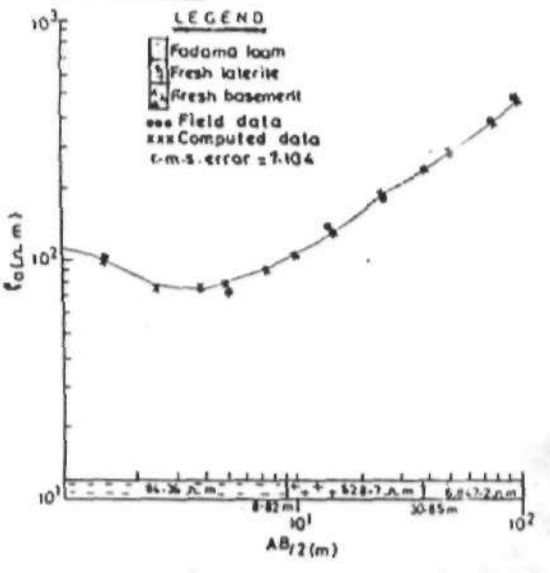
C2-4 AVIATION SITE 1



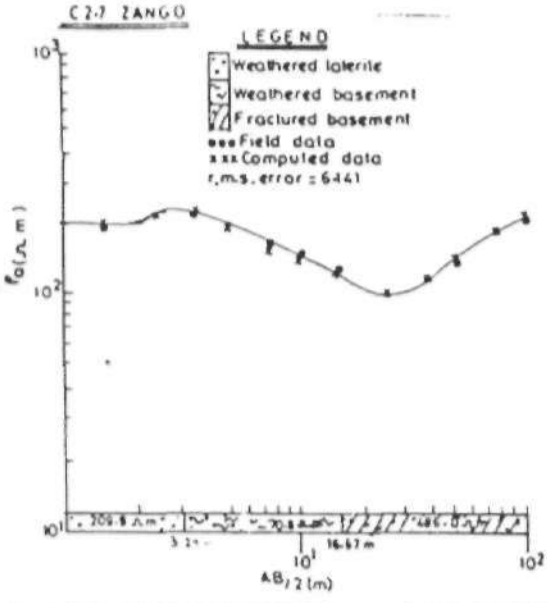
C2-5 PALLADAN



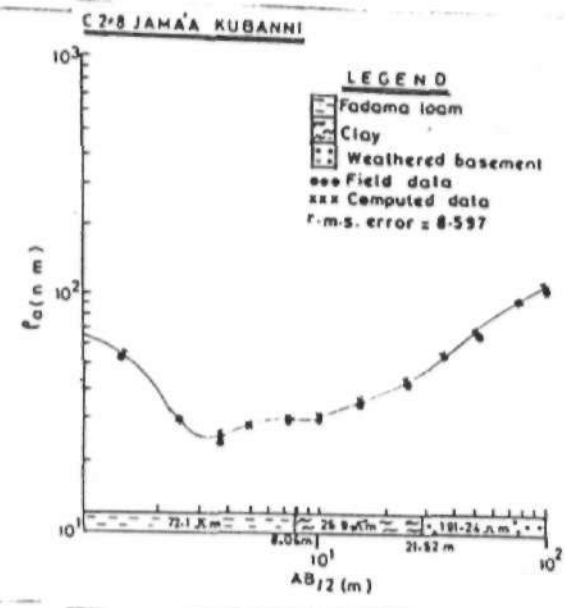
C2-6 BASSAWA



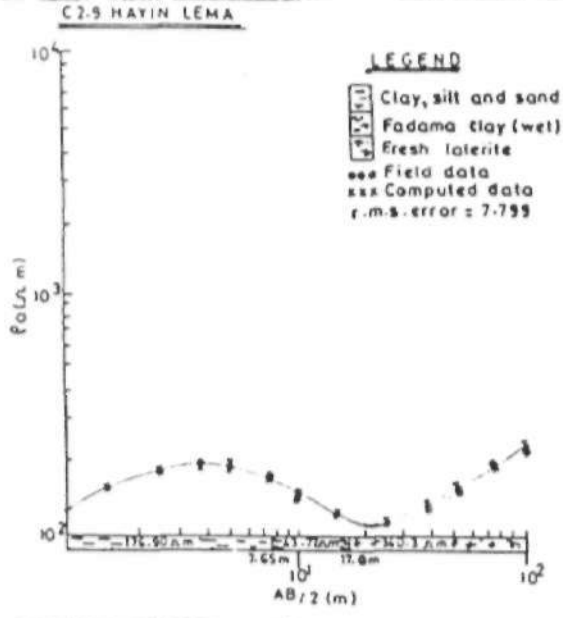
C2·7 ZANGO



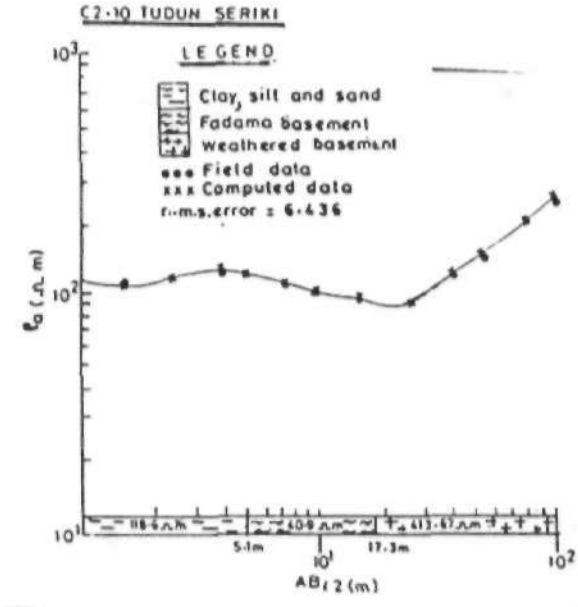
C2·8 JAMA'A KUBANNI



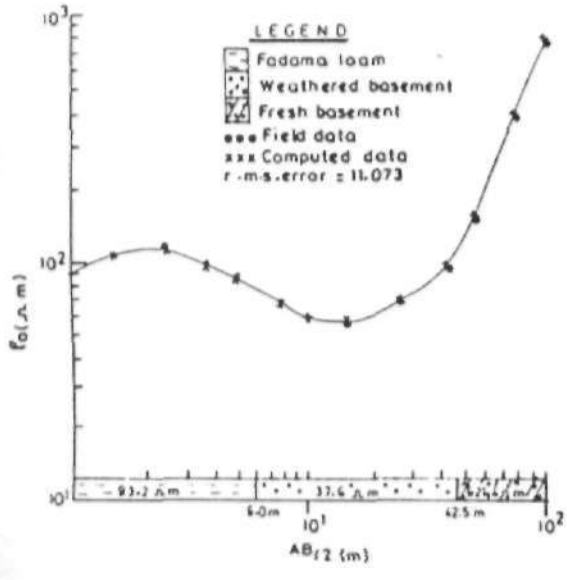
C2·9 HAYIN LEMA



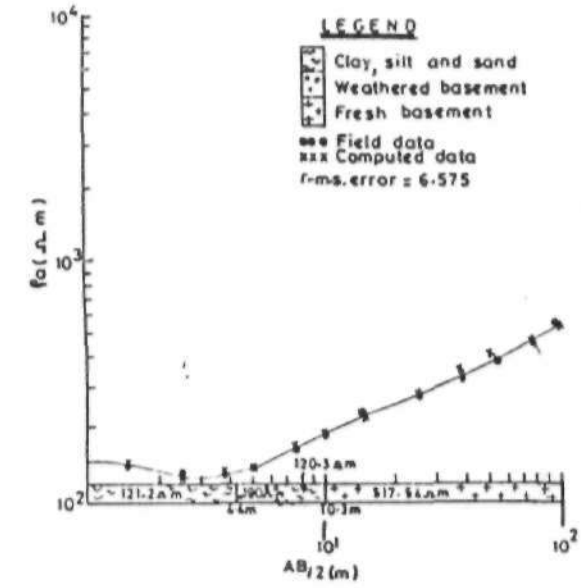
C2·10 TUDUN SERIKI



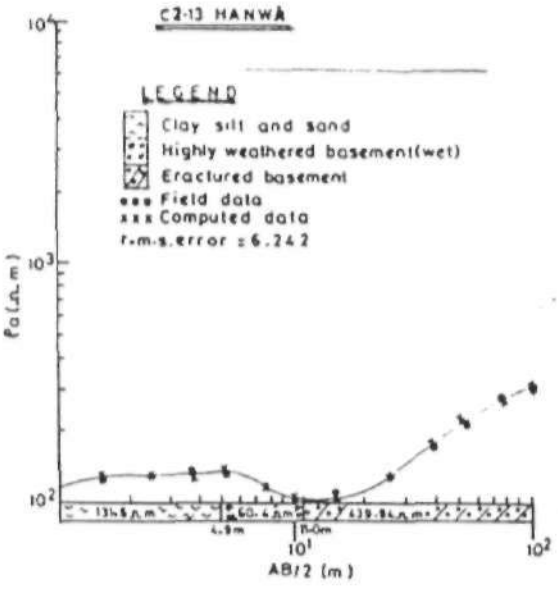
C2·11 GORUBA



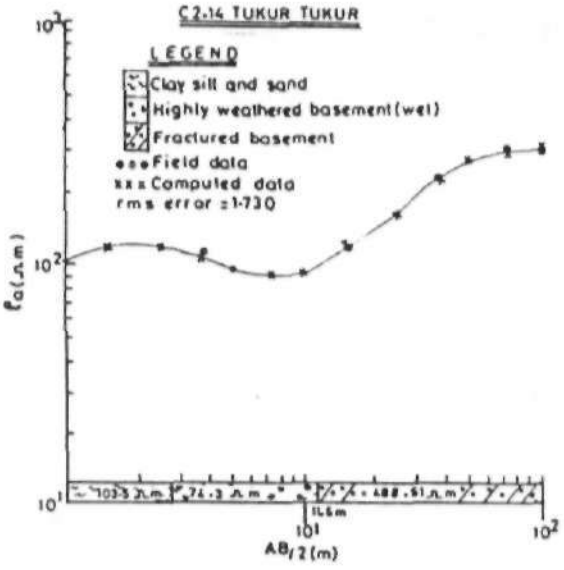
C2·12 WUSASA



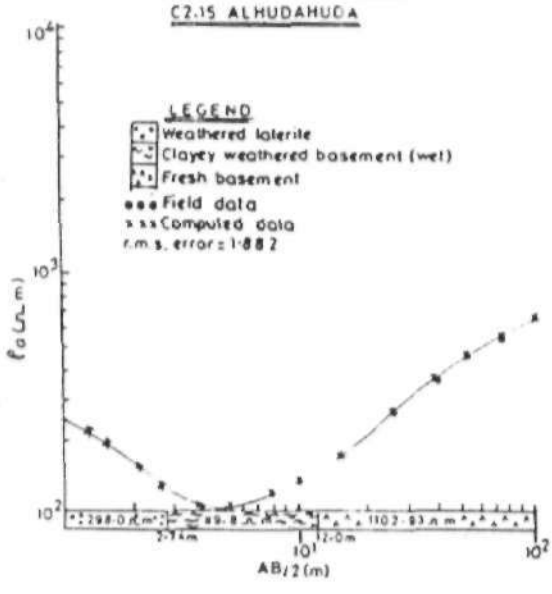
C2-13 HANWA



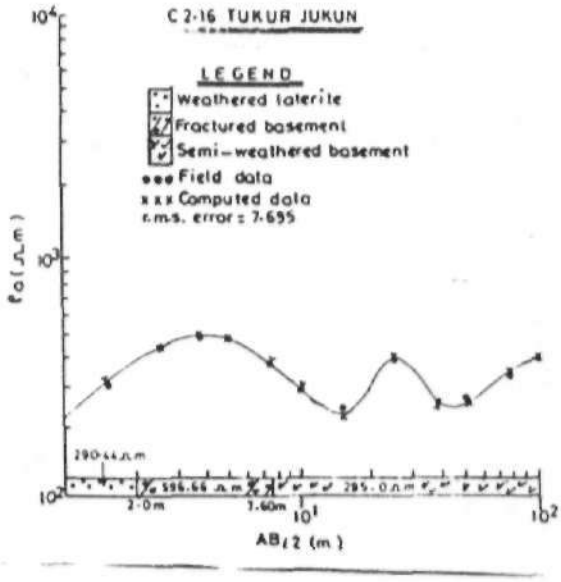
C2-14 TUKUR TUKUR



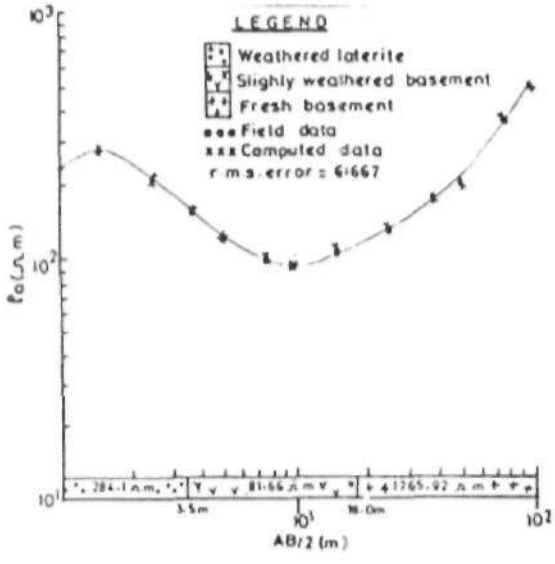
C2-15 ALHUDAHUDA



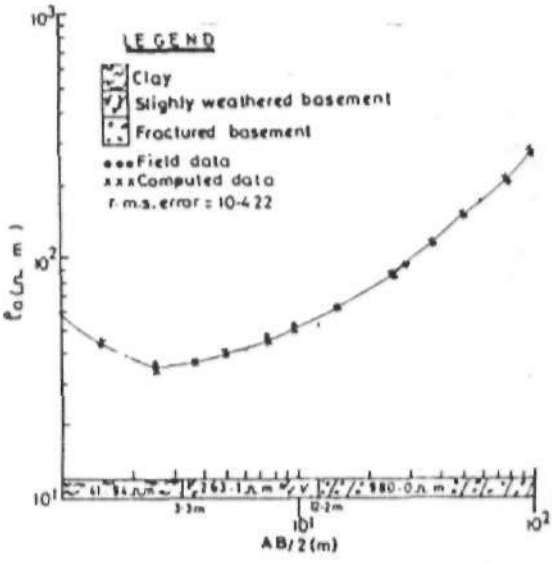
C2-16 TUKUR JUKUN



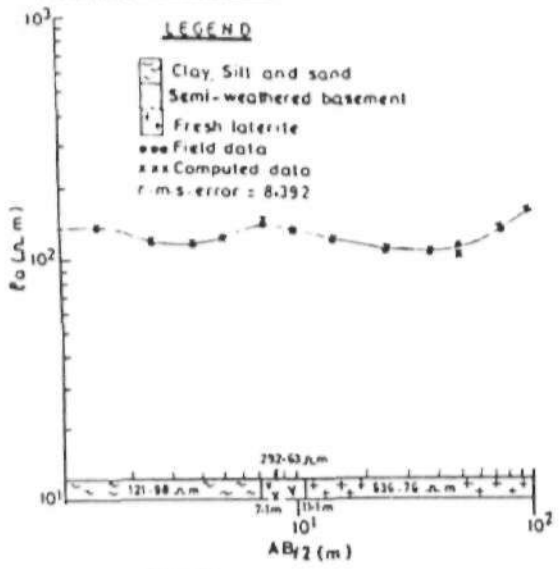
C2-17 UNGWAN SARIKI



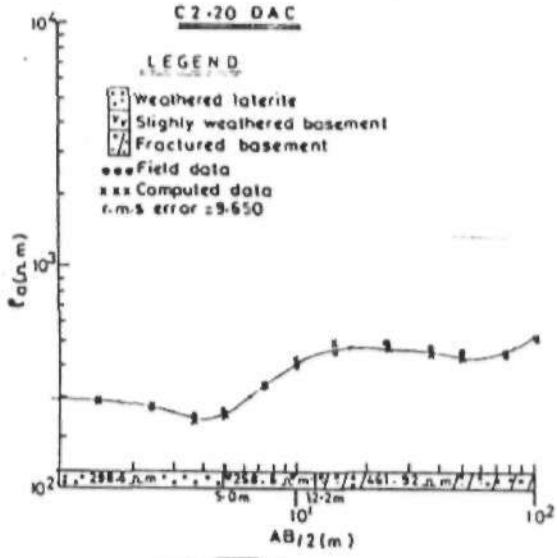
C2-18 BOMO



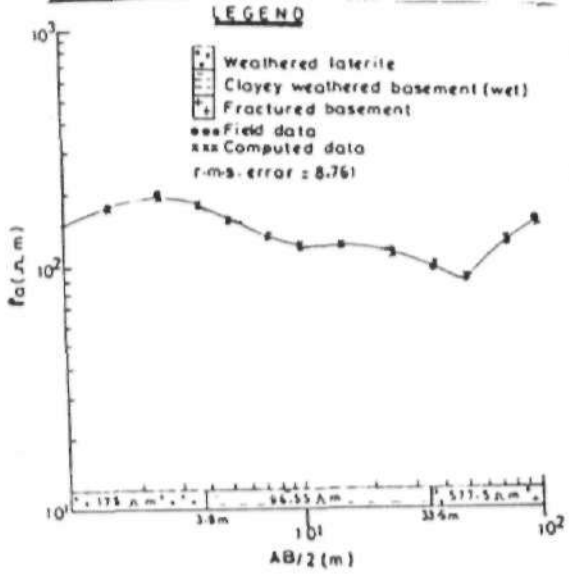
C2-19 KURRIMI BOMO



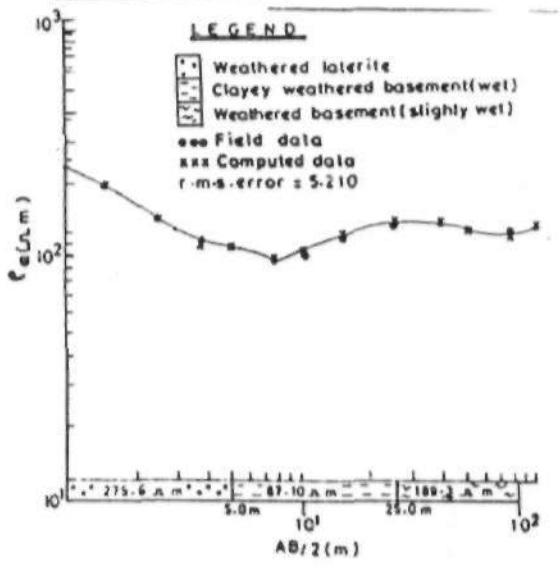
C2-20 DAC



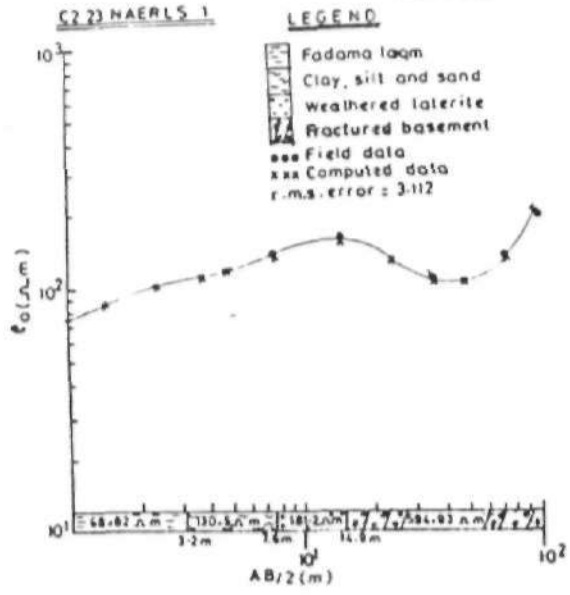
C2-21 MAIGAMO



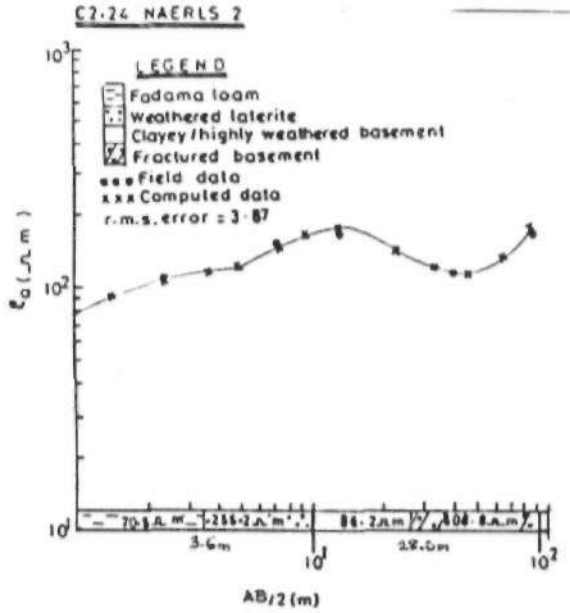
C2-22 STAFF SCHOOL



C2-23 NAERLS 1

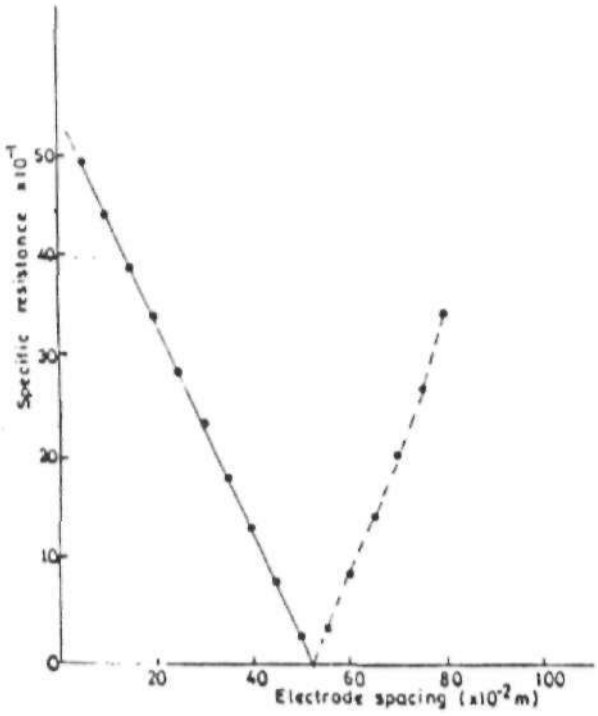


C2-24 NAERLS 2

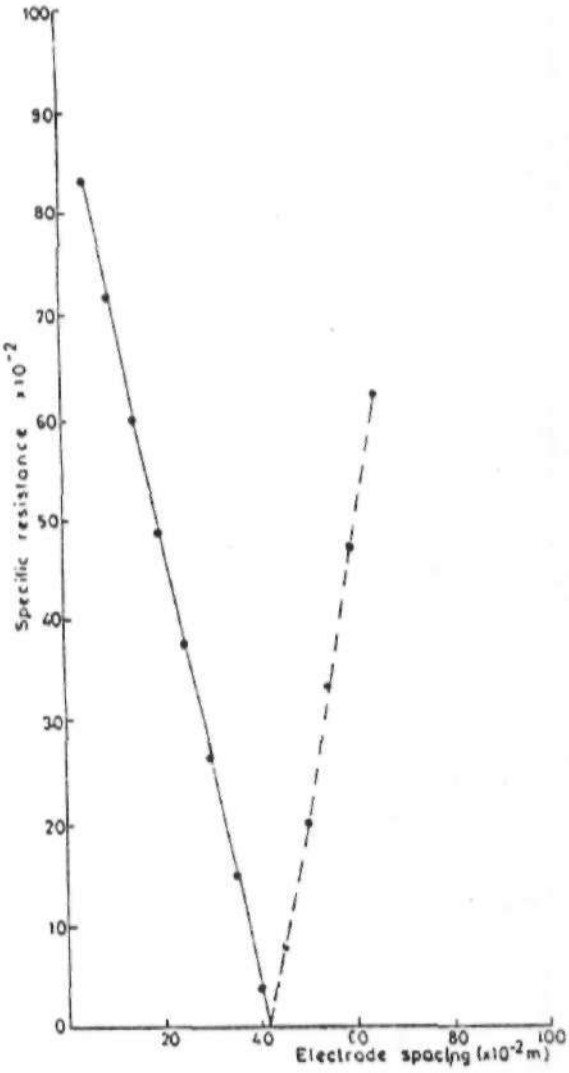


APPENDIX C3: GRAPH OF SPECIFIC RESISTANCE AGAINST ELECTRODE SPACING FOR THE LABORATORY MODELS (USING THE TWO-ELECTRODE METHOD)

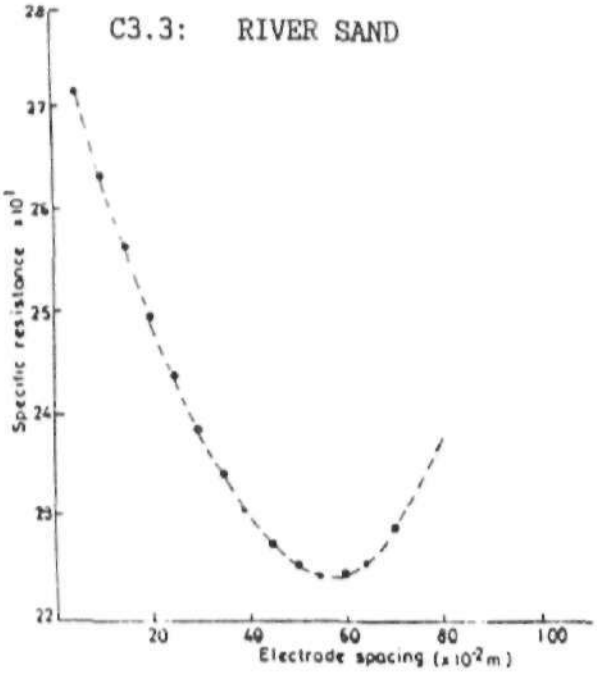
C3.1: WATER Medium



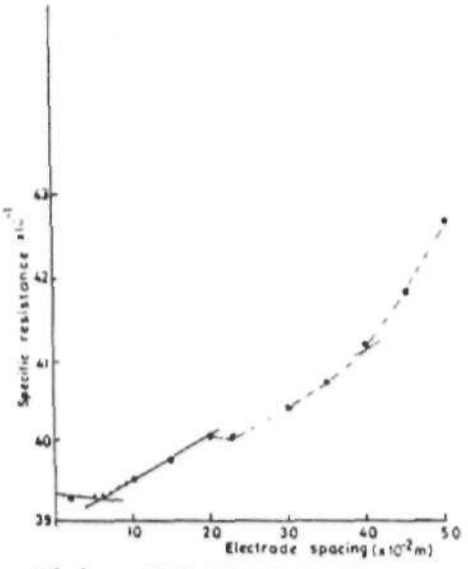
C3.2: CLAY Medium



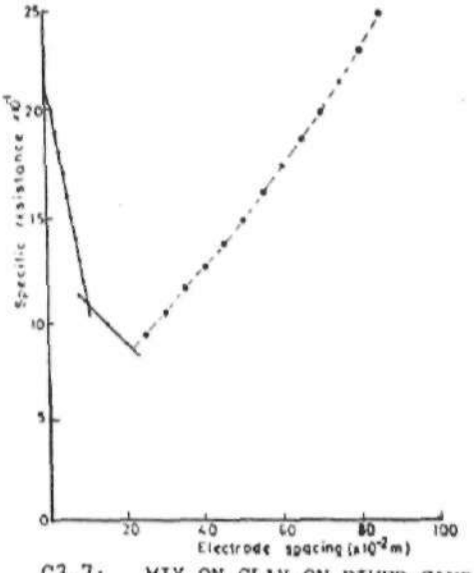
C3.3: RIVER SAND



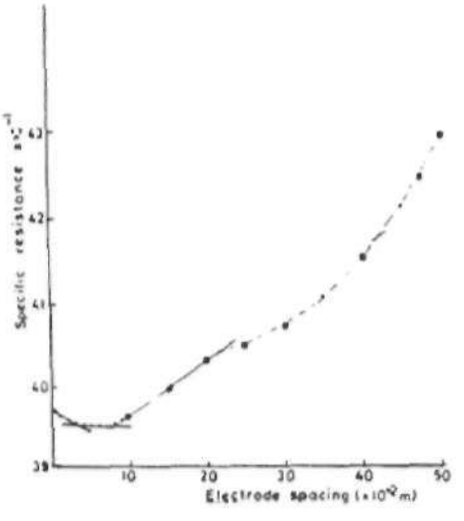
C3.4: CLAY ON RIVER SAND



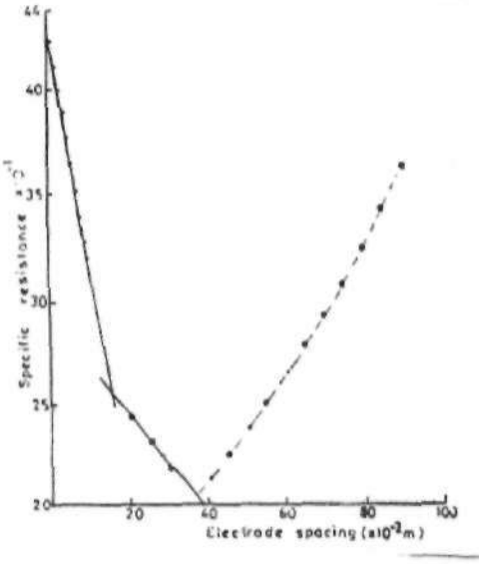
C3.5: RIVER SAND ON CLAY



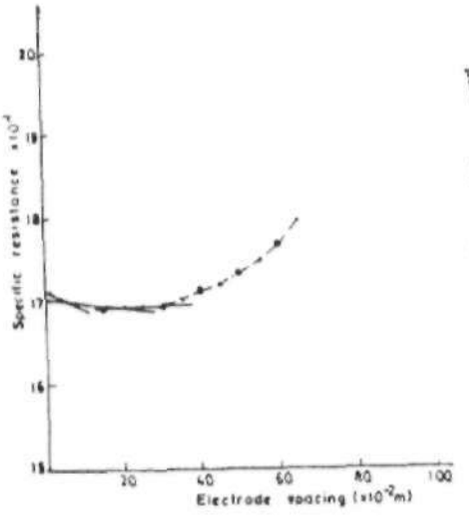
C3.6: CLAY ON MIX ON RIVER SAND



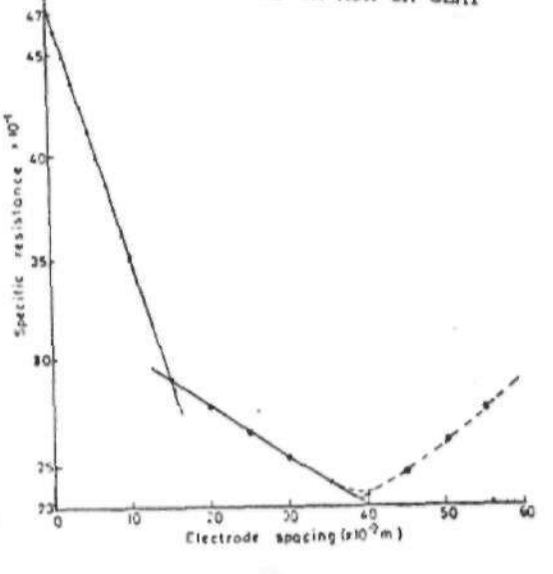
C3.7: MIX ON CLAY ON RIVER SAND



C3.8: CLAY ON RIVER SAND ON CLAY

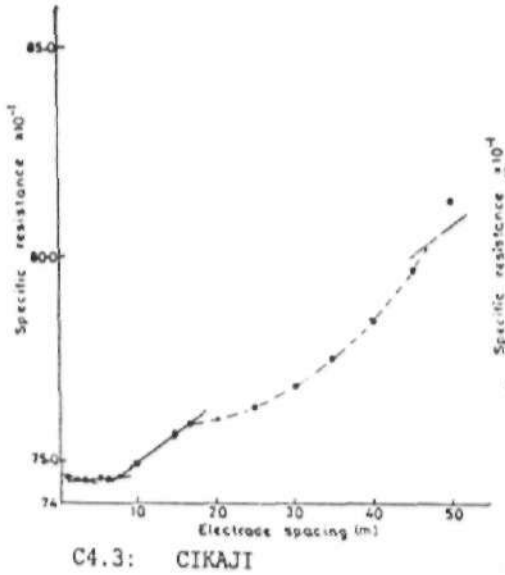


C3.9: RIVER SAND ON MIX ON CLAY

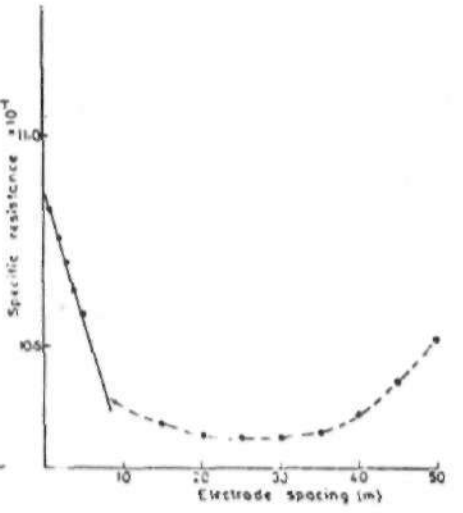


APPENDIX C4: GRAPH OF SPECIFIC RESISTANCE AGAINST ELECTRODE SPACING FOR THE FIELD STATIONS (USING THE TWO-ELECTRODE METHOD)

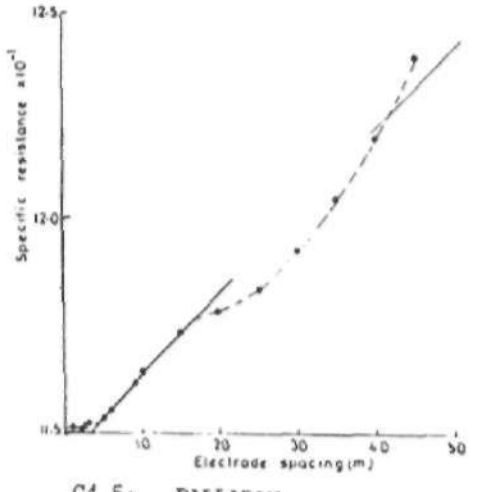
C4.1: FCE, Zaria



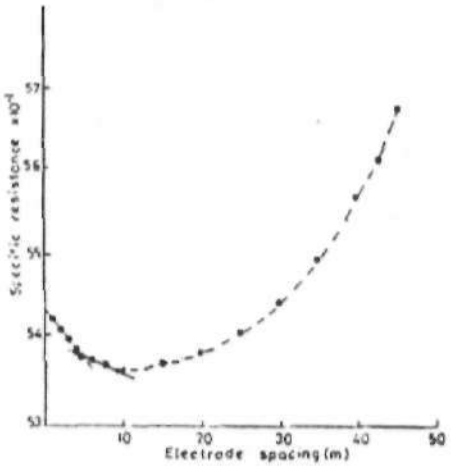
C4.2: UNGWAN KAYA (KONGO)



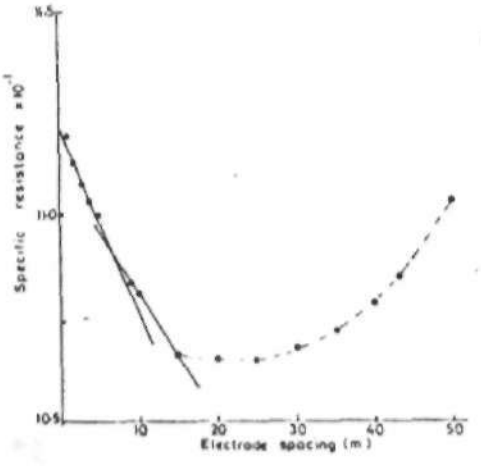
C4.3: CIKAJI



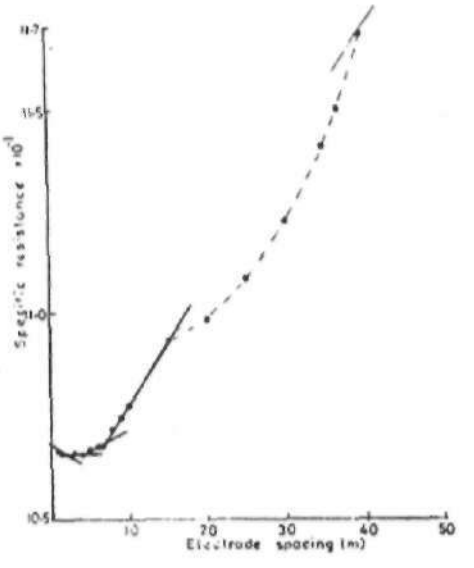
C4.4: AVIATION SITE 1



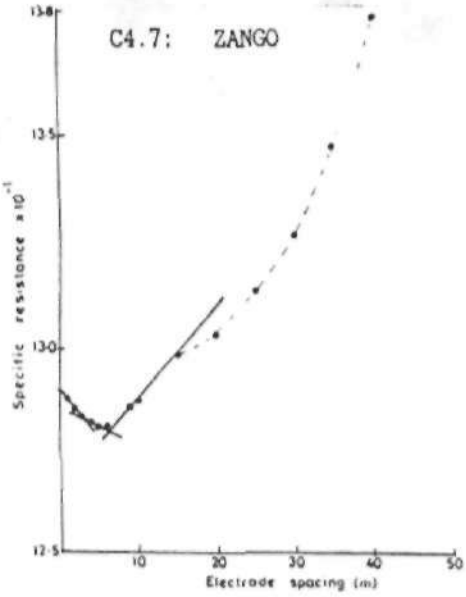
C4.5: PALLADAN



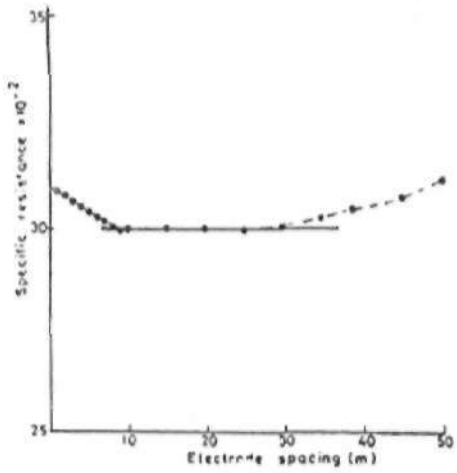
C4.6: BASSAWA



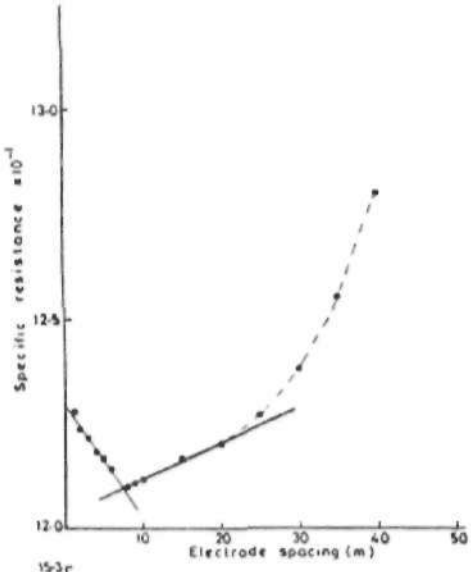
C4.7: ZANGO



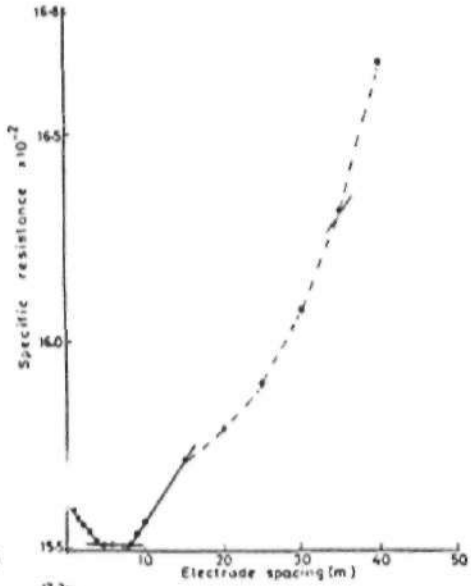
C4.8: JAMAA' KUBANNI



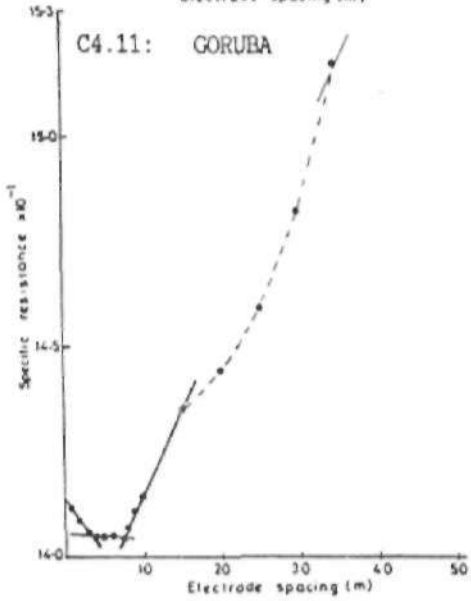
C4.9: HAYIN LEMA



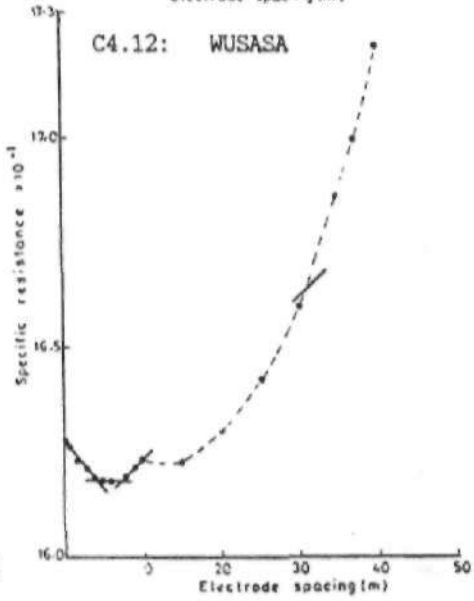
C4.10: TUDUN SARKI



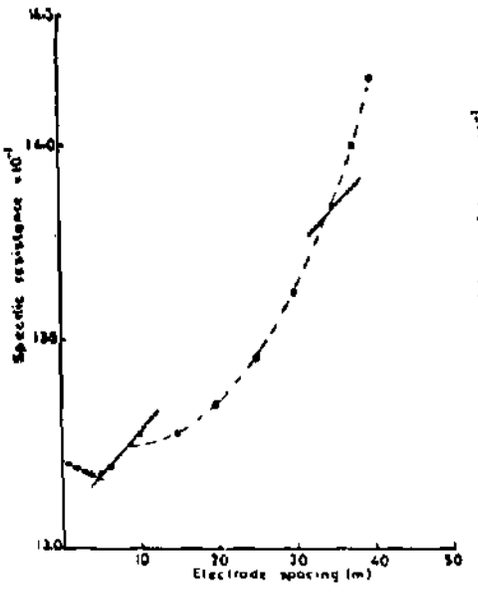
C4.11: GORUBA



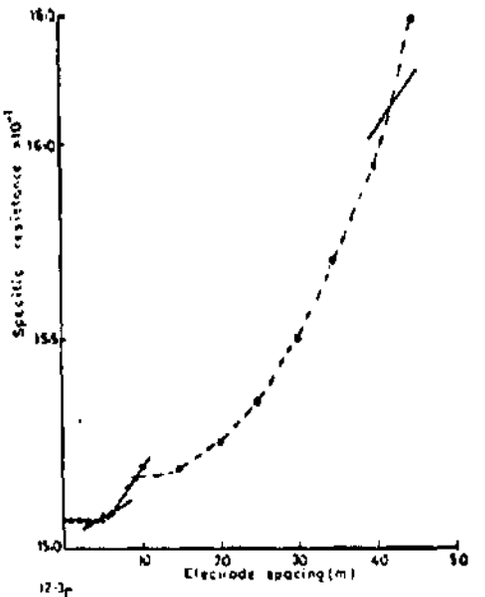
C4.12: WUSASA



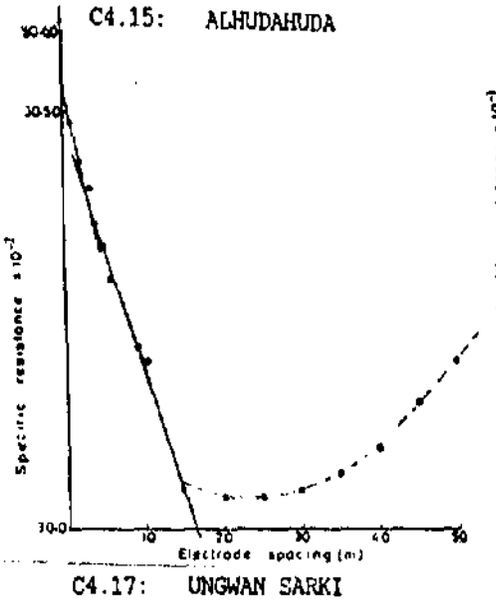
C4.13: HANWA



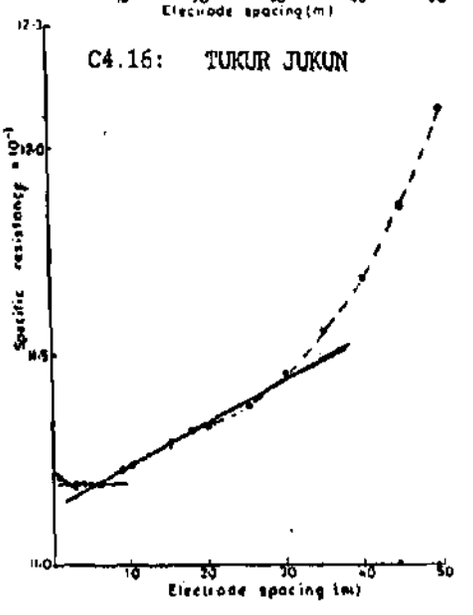
C4.14: TUKUR TUKUR



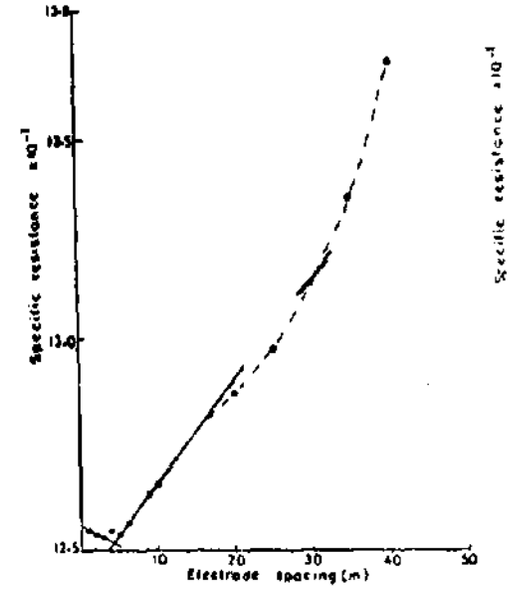
C4.15: ALHUDAHUDA



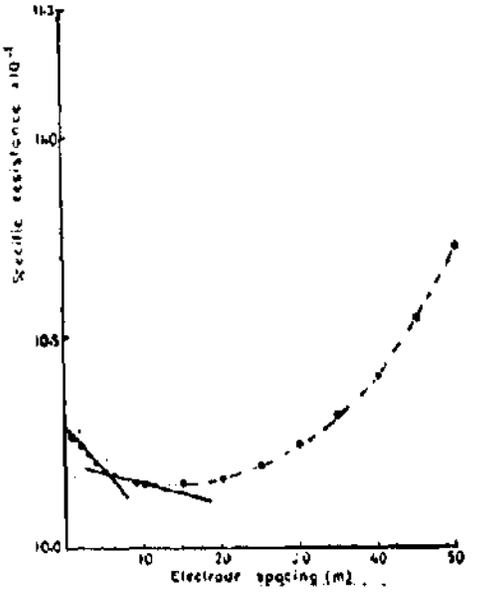
C4.16: TUKUR JUKUN



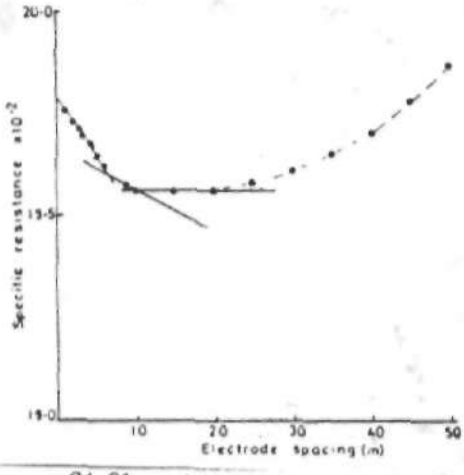
C4.17: UNGWAN SARKI



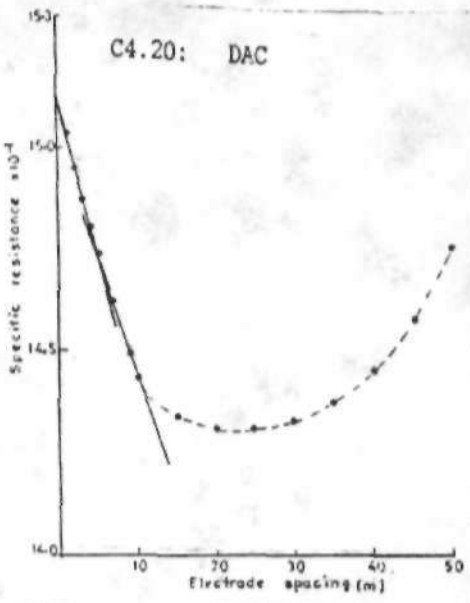
C4.18: BOMO



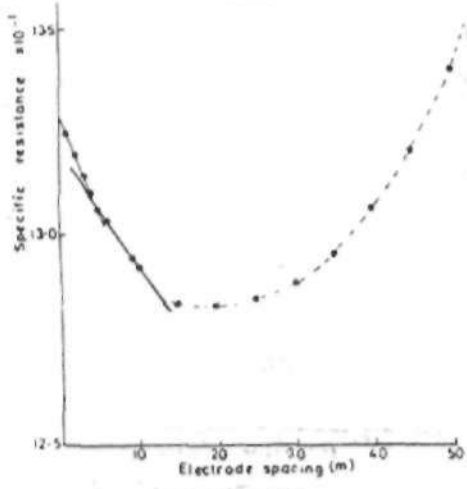
C4.19: KURRIMI BOMO



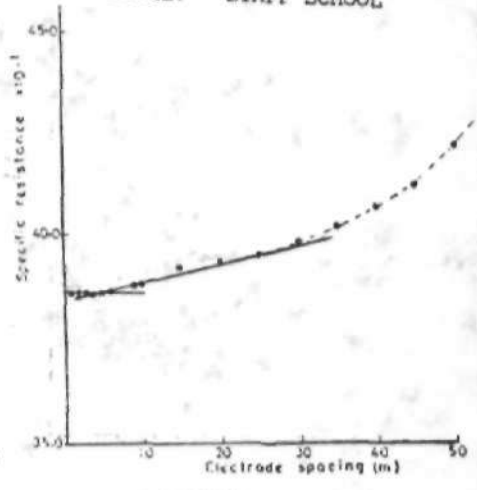
C4.20: DAC



C4.21: MAIGAMO



C4.22: STAFF SCHOOL



C4.23: NAERLS

